NASA CONTRACTOR REPORT

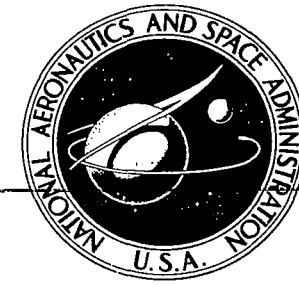

FORCE-PENETRATION CHARACTERISTICS OF A SAND HORIZONTALLY PENETRATED BY PLATES, CONES, AND SPHERICAL SEGMENTS

by Paul A. Hustad and William R. Cox

Prepared by
THE UNIVERSITY OF TEXAS AT AUSTIN
Austin, Texas
for

NATIONAL AERONAUTICS AND SPACE ADMINISTRATION • WASHINGTON, D. C. • JANUARY 1969

NASA CR-1252

FORCE-PENETRATION CHARACTERISTICS OF A SAND HORIZONTALLY PENETRATED BY PLATES, CONES, AND SPHERICAL SEGMENTS

By Paul A. Hustad and William R. Cox

Prepared under Grant No. NsG-604 by
THE UNIVERSITY OF TEXAS AT AUSTIN
Austin, Texas

for Langley Research Center

NATIONAL AERONAUTICS AND SPACE ADMINISTRATION

For sale by the Clearinghouse for Federal Scientific and Technical Information
Springfield, Virginia 22151 – CFSTI price $3.00

ABSTRACT

During this investigation, the force-penetration characteristics of a cohesionless sand were studied using several different geometrically shaped models that were penetrated into the sand in a horizontal direction. An attempt was made to determine the influence of time upon the force-penetration characteristics of the sand by varying the velocity at which the models penetrated into the backfills.

The investigation was comprised of three separate phases of laboratory testing. The first phase consisted of designing a test setup and performing pilot tests that simulated the classical plane-strain earth-pressure problem. The test setup consisted of a box in which a movable wall 1 ft high and 3 ft long was placed. The wall was penetrated into the sand backfill in a horizontal direction and the horizontal and vertical soil reactions developed on the center 1 ft section of the wall were measured. Coulomb's passive earth-pressure theory was used as a basis for evaluating the performance of the setup.

The second phase utilized much the same type of loading apparatus as that used in Phase I. Two heights of walls, 1 ft and 1.5 ft, were penetrated at various constant velocities into loose and dense backfills. For the range of velocities that were utilized, the observations showed that the time effects were negligible. The results did show that Coulomb's passive earth-pressure theory may be used to calculate the maximum developed earth pressure with a reasonable degree of accuracy. The penetration necessary to develop the maximum earth pressure was found not to be a linear function of the wall height, as is normally assumed in practice.

The third and final phase utilized two sizes of right-circular cones and spherical segments. These models were penetrated into backfills which

were horizontally supported by polyethylene membranes. The cones had apex angles of 60 degrees and base diameters of 3.54 and 7.08 inches. The spherical segments had base diameters of 4.33 and 8.66 in. and spherical diameters of 5.0 and 10.0 in. respectively. The rate and vertical depth below the soil surface at which the models penetrated the loose and dense backfills were varied during this series of tests. The same general range of velocities as were used in Phase II were utilized in this phase and it was found that the time effects were negligible. Equations are presented that provide a means of predicting the maximum horizontal and vertical soil reactions on the models that were utilized in this investigation.

PREFACE

This study was sponsored under Grant NsG-604, An Investigation of Soil Modeling Problems Related to Impact Studies, from the National Aeronautics and Space Administration, Langley Research Center, Hampton, Virginia. Mr. M. E. Hathaway of Langley Research Center was technical monitor of the Grant.

The study began in June, 1965 under the supervision of Dr. William R. Cox. C. V. Girijavallabhan was responsible for design of the testing apparatus and the conducting of tests during the period from June to September, 1965. During this time he was assisted by the author. From September, 1965 to February, 1966 Issa Oweis was assigned the prime responsibility of conducting the laboratory testing. During this time he was assisted by James F. Horadam. From February to September, 1966 James F. Horadam was responsible for the laboratory investigation.

Mr. Harold H. Dalrymple, Research Engineer Associate, and Mr. Olen L. Hudson, Technical Staff Assistant, provided much of the technical knowledge that was necessary for the design of the test setups. Dr. Clyde E. Lee of The University of Texas designed the load cells used in this investigation.

TABLE OF CONTENTS

LIST OF FIGURES

Page

LIST OF TABLES

Page

NOTATION

CD	location of center of pressure above base of wall
F	resultant force on failure surface of a wedge of soil behind a retaining wall
H	height of retaining wall
K_h	factor which depends upon developed angle of internal friction, developed angle of friction between soil and membrane, and the geometric properties of penetrating model
K_o	coefficient of earth pressure at-rest
K_p	coefficient of passive earth pressure
K_v	factor when multiplied by γZ^c yields maximum resultant vertical force
P_p	passive earth pressure
R_H	horizontal soil force
$R_{H(max)}$	maximum horizontal soil force
r_p	radius of projected contact area of model at instant maximum horizontal soil force occurs
R_v	resultant vertical soil force
$R_{v(max)}$	maximum resultant vertical soil force
W	weight of soil wedge developed behind an inwardly advancing retaining wall
Y	penetration of wall
Z	vertical distance beneath soil surface
β	angle between failure surface and horizontal
β_m	measured angle between failure surface and horizontal
β_T	theoretical angle between failure surface and horizontal, calculated using Coulomb's passive earth-pressure equation
γ	unit density of soil
δ	developed angle of wall friction
σ	normal stress

σ_p	maximum normal stress acting on a vertical plane passing through a mass of soil which has been transformed into a passive Rankine state
σ_1	major principal normal stress
σ_3	minor principal normal stress
τ	shearing stress
ϕ	developed angle of internal friction
ϕ_{max}	maximum developed angle of internal friction

CHAPTER I

INTRODUCTION

The branch of Civil Engineering known as soil mechanics is relatively young. The late development of this field can largely be attributed to man's disinterest in foundation engineering. Prior to 1900, foundations were looked upon as a necessary evil. It was not until 1923 when Karl Terzaghi published his work concerning the theory of consolidation that the problems associated with foundations began to be approached in a scientific manner. It was Terzaghi's work that brought order to and made possible the rational development of soil mechanics[1].* Since 1923 knowledge in this field has grown rapidly and many theories have evolved from laboratory experiments, full scale field tests, and observations. Although many of the now existing theories are extremely crude, they have provided a means by which the engineer can safely design structures that interact with soil masses.

Lateral earth pressures in soil is a subject about which much has been written. This subject has received a great deal of attention because of its practical value in connection with the design of retaining walls, bulkheads, buildings, and pile supported structures. The calculation of true lateral earth pressures using existing theories is often impossible and therefore it becomes necessary to perform field tests or laboratory experiments to obtain realistic values that can be used in design computations.

OBJECTIVE

This investigation was undertaken to obtain information to be utilized by the National Aeronautics and Space Administration. The primary objective of this investigation was to determine how a cohesionless soil responds to

*Superscripts refer to the list of references on p. 198.

various geometric shapes horizontally penetrating it at several constant rates of penetration.

SCOPE OF INVESTIGATION

The scope of this investigation was limited to horizontally penetrating three geometric shapes into a dry Colorado River sand at constant rates of penetration. The three geometric shapes were: (1) flat steel plates, (2) aluminum right-circular cones, and (3) aluminum spherical segments.

The plate tests were designed to simulate the classical plane-strain earth-pressure problem. Plates having heights of 12 and 18 in. were tested. The rate of penetration of the plates ranged from 0.00278 to 2.67 ips. During each test, data was recorded that permitted the evaluation of the horizontal and vertical response of the soil along with the corresponding penetrations of the plate.

The cone and spherical segment tests consisted of penetrating the soil with two sizes of cones and spherical segments. The cones had an apex angle of 60 degrees and heights of 3.06 and 6.12 inches. The spherical segments had spherical diameters of 5.0 and 10.0 inches. Prior to each test the soil was supported in a horizontal direction by a polyethylene membrane. The models penetrated the membrane and soil at rates varying from 0.533 to 4.0 ips. The depths below the soil surface at which the models penetrated were varied from 0.5 to 2.5 times the base diameter of the model. During each test, data was recorded that permitted the determination of the soil reaction in a horizontal and vertical direction. Horizontal penetrations of the models, corresponding to the force measurements, were also recorded.

Standard laboratory tests were performed to determine the engineering properties of the soil used in this investigation. The experimental results

of the penetration of the geometric shapes in sand were analyzed using existing static earth-pressure theory. Where theory was not applicable, an empirical approach was taken.

CHAPTER II

PASSIVE EARTH-PRESSURE THEORY

The scope of this chapter is limited to the discussion of ideal cohesionless soils which are subjected to lateral compression. Problems are dealt with which involve only the movement of soil in two directions, since in these cases general theory is applicable.

PLASTIC EQUILIBRIUM

Theory of plasticity, as commonly applied to soils, is based on Mohr's theory of rupture. This theory is founded on the fundamental assumption that the soil fails by shear as soon as the shearing stress on any section satisfies Coulomb's empirical equation.

$$\tau = \sigma \tan \phi \tag{1}$$

Mohr's Theory of Rupture For An Ideally Plastic and Cohesionless Soil is graphically presented in Fig. 1. The circle represents stresses (σ, τ) at a point located within a mass of soil in a state of plastic equilibrium. The following stress relationship can be derived from the Mohr diagram.

$$\sigma_1 = \sigma_3 \tan^2 (45^\circ + \phi/2) \tag{2}$$

In determining the basic behavior of an ideally cohesionless soil, it is advantageous to examine the states of stress that can exist in a semi-infinite homogeneous mass of soil. Consider a one unit square prismatic column of soil located within a semi-infinite mass. The unit weight of the soil is defined as γ and the height of the column is Z, as is shown in Fig. 2. Since every vertical section through the mass represents a plane of symmetry, the shearing stresses on any vertical and horizontal section are equal to zero.

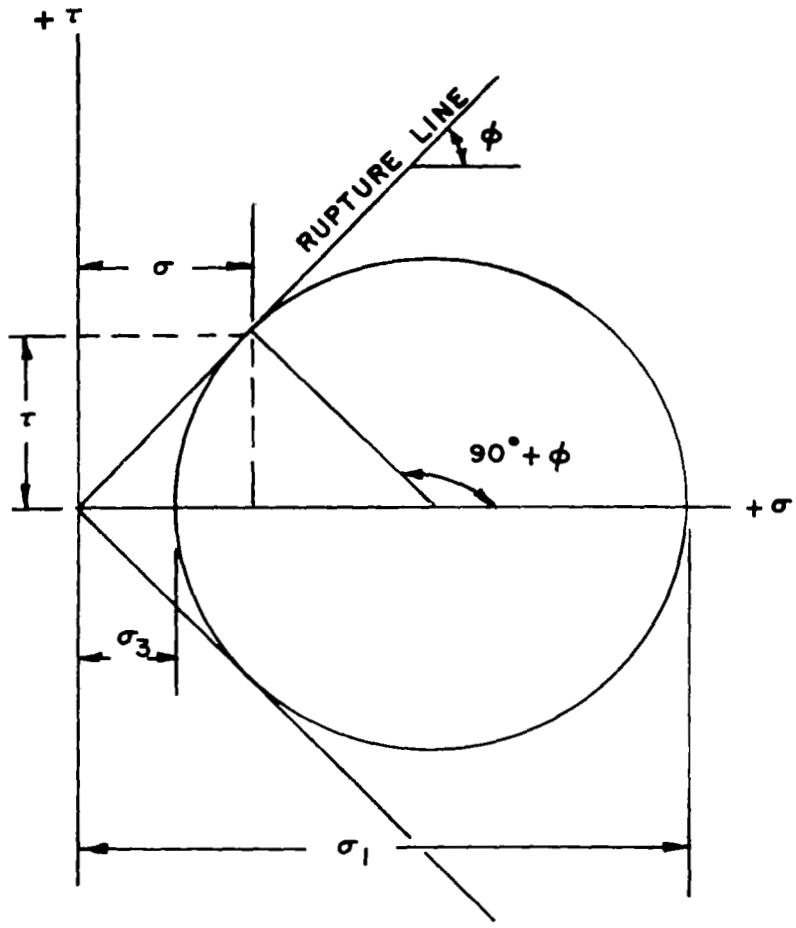

FIG. 1 MOHR'S THEORY OF RUPTURE FOR AN IDEALLY PLASTIC AND COHESIONLESS SOIL

The normal stress acting on the base of the prism is equal to the weight of the prism γZ. If the mass of soil is at rest, the ratio between the horizontal and vertical stress at any point is equal to the coefficient of earth pressure at-rest, K_o. Circle C_o in Fig. 4 represents the state of stress that exists at a point located on the base of the prism shown in Fig. 2.

If the entire soil mass is subjected to an infinitesimal amount of lateral compression, the horizontal stresses acting on the sides of the prism increase by an infinitesimal amount. The soil mass may be continuously subjected to an infinite number of lateral compressions and if none of the resulting circles of stress touch the lines of rupture, the soil mass is said to be in a state of elastic equilibrium. As the mass is compressed, the circles of stress will become larger until one circle becomes tangent to the rupture lines. When a circle of stress is tangent to the rupture line, the soil is in a state of plastic equilibrium.

The problem of determining the stresses and the orientation of the surfaces of sliding that are associated with a semi-infinite mass in a state of plastic equilibrium was first solved by Rankine in 1857[8]. The plastic state produced by compressing a semi-infinite soil mass, is called the passive Rankine state. Circle C_R in Fig. 4 represents the stresses associated with a Rankine state at a point located on the base of the soil prism shown in Fig. 3. From Fig. 4, Eq 4 may be derived which expresses the normal stress on the vertical sides of the prism at a depth Z below the surface.

$$\sigma_p = \gamma Z \tan^2 (45^\circ + \phi/2) \tag{3}$$

$$\sigma_p = \gamma Z K_p \tag{4}$$

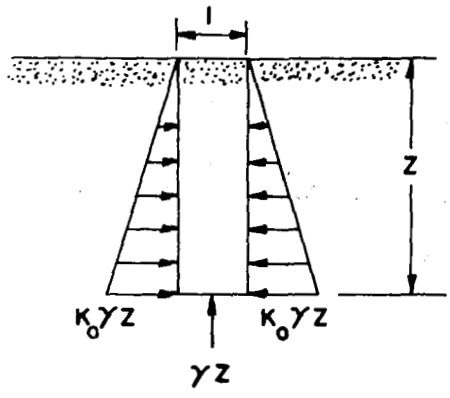

FIG. 2 STRESSES AT THE BOUNDARIES OF A PRISMATIC COLUMN OF SOIL LOCATED WITHIN A SEMI-INFINITE COHESIONLESS MASS OF SOIL IN A STATE OF REST

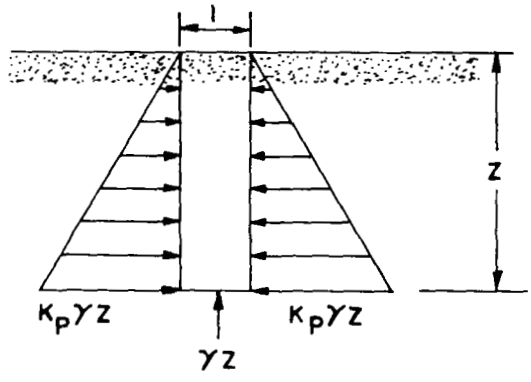

FIG. 3 STRESSES AT THE BOUNDARIES OF A COLUMN OF SOIL LOCATED WITHIN A SEMI-INFINITE COHESIONLESS MASS OF SOIL IN A RANKINE STATE

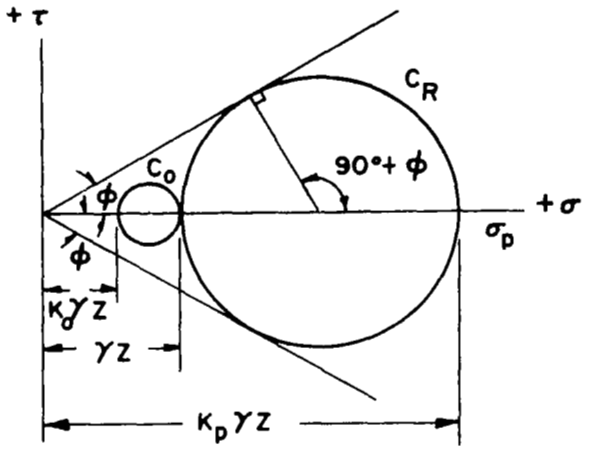

FIG. 4 GRAPHIC REPRESENTATION OF THE STATES OF STRESS ON THE BASE OF THE SOIL COLUMN IN FIG. 2 AND FIG. 3

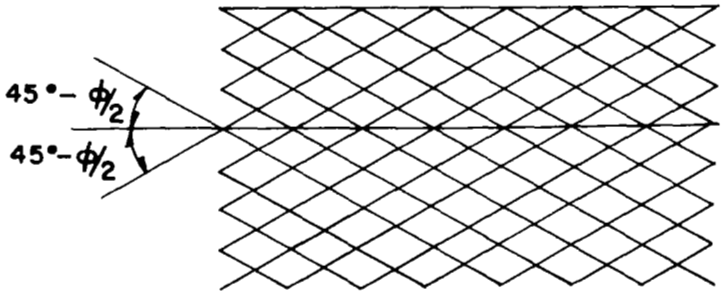

FIG. 5 ORIENTATION OF THE SURFACES OF SLIDING FOR A SEMI-INFINITE MASS OF SOIL IN A RANKINE STATE

The term K_p is the coefficient of passive earth pressure. The orientation of the surfaces of sliding that are associated with a Rankine state is shown in Fig. 5.

Rankine's Theory of Passive Earth Pressure

If the retaining wall that is shown in Fig. 6 is pushed toward the backfill, the soil resistance will increase until it reaches an upper limit. When this upper limit is reached the soil fails by plastic flow. The passive pressure per unit length of wall required to induce failure is calculated by integrating Eq 5,

$$P_p = \int_0^H \gamma Z \tan^2 (45^\circ + \phi/2)\, dZ \tag{5}$$

which yields,

$$P_p = 0.5\, \gamma H^2 \tan^2 (45^\circ + \phi/2). \tag{6}$$

Since the distribution of passive pressure on the retaining wall is triangular, the center of pressure is located at a distance of H/3 above the base of the wall. A free body diagram of the forces acting on the retaining wall in Fig. 6 is shown in Fig. 7.

Coulomb's Theory of Passive Earth Pressure

Coulomb's theory of earth pressure assumes that when the wall, which is shown in Fig. 8, is thrust into the backfill, a soil wedge is formed by a plane failure surface passing through the lower edge of the wall. The forces necessary to keep the soil wedge in equilibrium are shown in Fig. 9. The passive pressure per unit length of wall is found by summing forces in a direction perpendicular to the line of action of the force F acting on the failure surface. The summation of forces results in the following expression for the passive earth pressure.

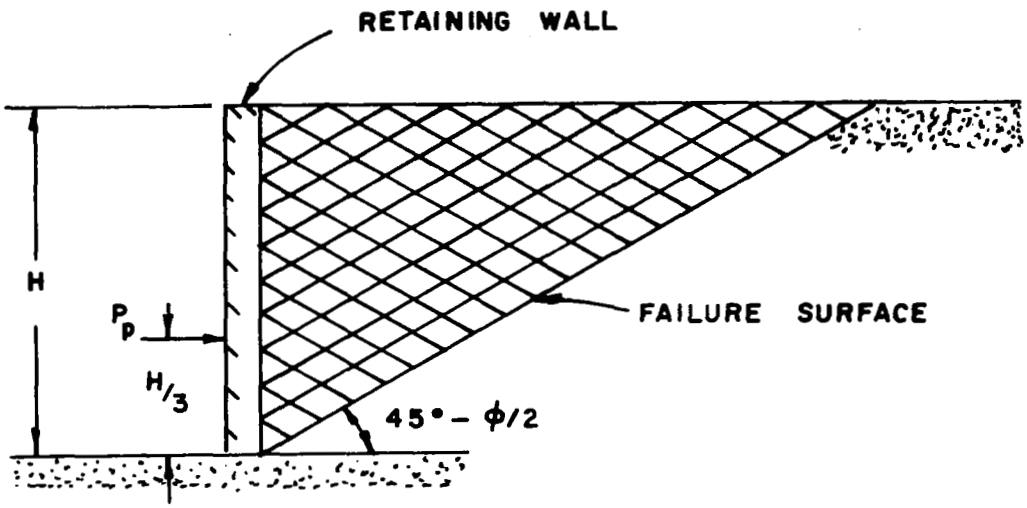

FIG. 6 PASSIVE RANKINE ZONE BEHIND AN INWARDLY ADVANCING WALL

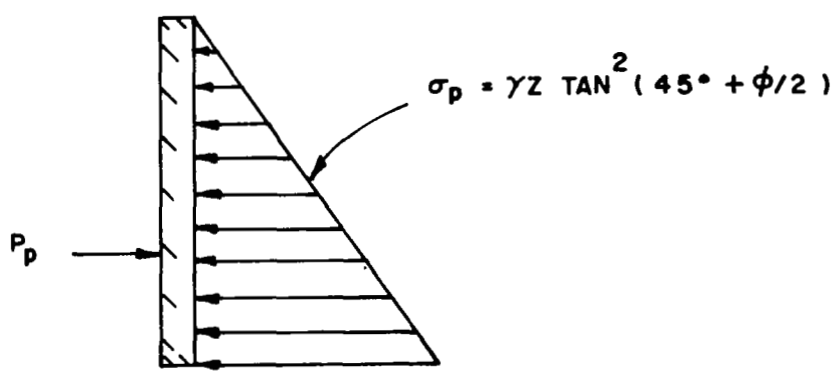

FIG. 7 DISTRIBUTION OF PASSIVE SOIL STRESSES ON THE SMOOTH, INFINITELY LONG WALL SHOWN IN FIG. 6

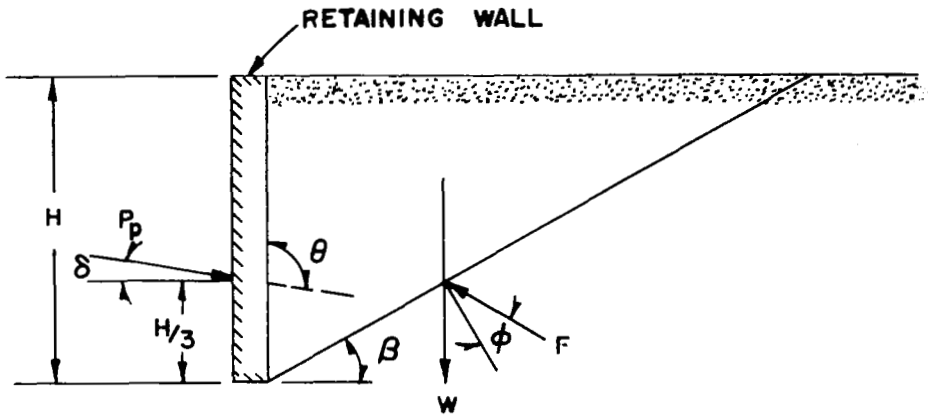

FIG. 8 FORCES ACTING ON THE WALL AND THE ASSUMED COULOMB FAILURE WEDGE

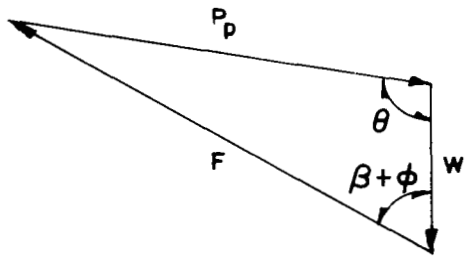

FIG. 9 EQUILIBRIUM FORCE POLYGON FOR THE ASSUMED IN FIG. 8

$$P_p = \frac{0.5\ \gamma H^2}{\cos\ \delta} \left[\frac{\cos\ \phi}{1 - \sqrt{\sin\ \phi\ (\sin\ \phi + \cos\ \phi\ \tan\ \delta)}} \right]^2 \quad (7)$$

$$P_p = 0.5\ \gamma H^2\ K_p/\cos\ \delta \quad (8)$$

If the angle of friction between the wall and the soil mass, δ, is equal to zero, the Coulomb value of passive earth pressure becomes equal to the Rankine value.

It can be seen from Eq 8 that the pressure distribution is triangular and therefore the center of pressure is located at a distance of H/3 above the bottom edge of the wall.

Wall Friction

In every practical passive earth-pressure case a frictional force will be developed at the soil-wall interface. The magnitude of the angle of wall friction depends upon the roughness of the wall, the density of the backfill material, and the amount of relative movement that takes place between the wall and the backfill. The shearing stresses at the soil-wall interface cause the failure surface to become curved in the vicinity of the wall. Large angles of wall friction cause the failure surface to be highly curved. Terzaghi[9] noted that the surface of sliding is curved as shown in Fig. 10, provided the wall tilts about its lower edge. The angle of wall friction is considered positive if the backfill material moves in an upward direction relative to the wall movement. If the backfill material moves in a downward direction relative to the movement of the wall, the surface of sliding will be as shown in Fig. 11. In either case, the distribution of passive earth pressure on the wall is triangular and the center of pressure is located at a distance of H/3 above the lower edge of the wall.

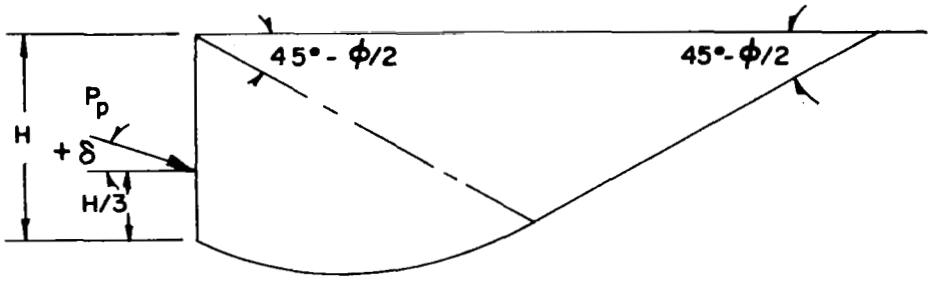

FIG. 10 SHAPE OF THE SURFACE OF SLIDING IF THE WALL FRICTION δ IS POSITIVE

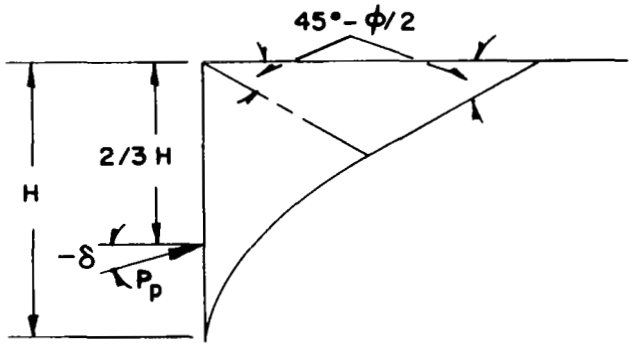

FIG. 11 SHAPE OF THE SURFACE OF SLIDING IF THE WALL FRICTION δ IS NEGATIVE

Deformation Requirements

The transformation of a backfill material, which is initially at rest, into a state of plastic equilibrium requires a definite amount of lateral compression. The magnitude of required deformation is a function of the density of the soil, the development of wall friction, the initial state of stress, and the depth Z below the surface.

Earlier in this chapter it was stated that if a semi-infinite mass of soil is laterally compressed until the circle of stress for each point in the mass is tangent to the lines of rupture, the mass of soil is in a passive Rankine state. However, when a semi-infinite mass of soil is subjected to a lateral compression produced by a body which has a finite height, only a portion of the backfill is transformed into a passive Rankine state. Figure 12 shows the portion of the backfill which is transformed into a Rankine state due to the tilting of a smooth, infinitely long, retaining wall about its inner lower edge. The remaining backfill material that is not located within the wedge, remains in a state of elastic equilibrium due to the presence of horizontal shearing stresses. These shearing stresses are developed as a consequence of the relative deformation that takes place between the soil located above and below the lower edge of the wall.

For a sand with a uniform density, the strain ϵ ($\epsilon = \Delta L/L$, in Fig. 12) required to transfer the soil from its original state of elastic equilibrium to a state of plastic equilibrium is approximately independent of depth Z[8]. Using this approximation, it can be seen that if the smooth wall tilts about its inner lower edge every element of soil located within the wedge will be simultaneously transformed into a passive Rankine state. The broken line passing through point b, Fig. 12, represents the minimum deformation required to transfer the wedge into a state of plastic equilibrium. If the wall is rotated beyond the broken line, plastic flow will occur throughout the wedge.

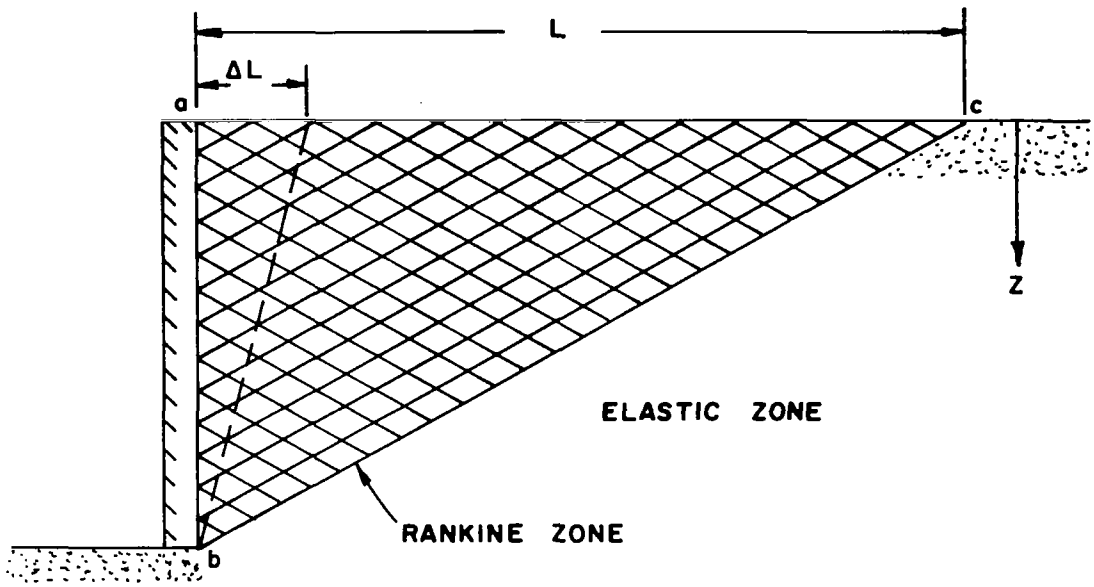

FIG. 12 PORTION OF BACKFILL TRANSFORMED INTO A RANKINE STATE, DUE TO TILTING OF A SMOOTH, INFINITELY LONG WALL ABOUT ITS LOWER INNER EDGE

ERRORS INVOLVED WITH APPLICATION OF PASSIVE EARTH-PRESSURE THEORY

The earth-pressure theories that have been previously discussed involve many simplifying assumptions which are seldom satisfied in the physical world. Although more rigorous solutions are available, they are far too complicated to be used in engineering practice. As a consequence of the complexities involved in applying more rigorous solutions to practical problem, the simpler earth-pressure theories of Coulomb and Rankine have become widely used.

Coulomb's Theory

As stated previously, Coulomb's theory of passive earth pressure is based on the simplifying assumption that the failure surface is plane. This assumption is strictly correct only if the angle of wall friction is equal to zero. The development of wall friction causes the lower portion of the failure surface to be curved. Since Coulomb's theory ignores any curvature of the failure surface, the results obtained by using this theory are in error.

Figure 13 shows a graph that has been reproduced from Wu[11]. The dashed lines in Fig. 13 represent the relationships between the angle of wall friction δ and the passive earth-pressure coefficient K_p, which was calculated using Coulomb's theory. The solid lines represent the relationships that exist between δ and K_p when K_p is calculated on the basis of a curved failure surface. Figure 13 shows that for values of δ less than $\phi/3$ the error involved in using Coulomb's theory is negligible. When δ is large, the error involved in using the same theory becomes excessive and in some cases may be 50 per cent or more[5].

The preceding discussion has been based upon the assumption that the deformation required to attain a state of plastic equilibrium has been achieved. In reality, often the deformation required to transfer the soil into a state of plastic equilibrium is not attained and in these cases the previously mentioned and discussed theories are not directly applicable.

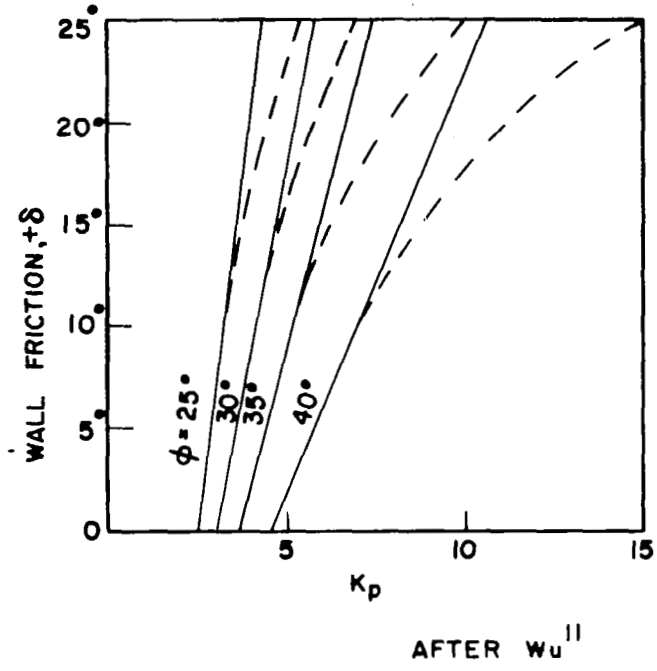

FIG. 13 EFFECT OF WALL FRICTION ON THE COEFFICIENT OF PASSIVE EARTH PRESSURE

Logarithmic Spiral Method of Calculating Passive Earth Pressure

If the value of developed wall friction δ exceeds $\phi/3$, a method of calculation that takes into account the curvature of the failure surface must be used to obtain acceptable results. Ohde has proposed a method which approximates the curved portion of the failure surface with a logarithmic spiral. The error associated with this method, when compared to more rigorous methods, is approximately 3 per cent[8]. The equilibrium forces and geometric properties associated with a logarithmic spiral solution are shown in Fig. 14.

The method consists of assuming several failure surfaces and calculating the passive earth pressure associated with each failure surface. The values of passive earth pressure are plotted as ordinates above their corresponding d points. The minimum passive earth pressure is then scaled from a curve passing through the plotted points.

The lower portion of the failure surface, be, is represented by a logarithmic spiral with the equation

$$r = r_o e^{\theta \tan \phi}, \tag{9}$$

whose center 0 is located on line af. In this equation, r represents the distance between the center 0 of the spiral and the failure surface. The angle θ is the angle between the initial vector ob and any vector which passes through the center of the spiral and also intersects the spiral portion of the failure surface. The curved portion of the failure surface becomes tangent to the plane portion of the failure surface at point e.

The passive earth pressure is found by summing moments about the center of the logarithmic spiral. The passive earth pressure acts on the wall at a distance of H/3 above the base and is expressed by the equation

$$P_p = \frac{WL_1 + P_{de} L_2}{L_3} . \tag{10}$$

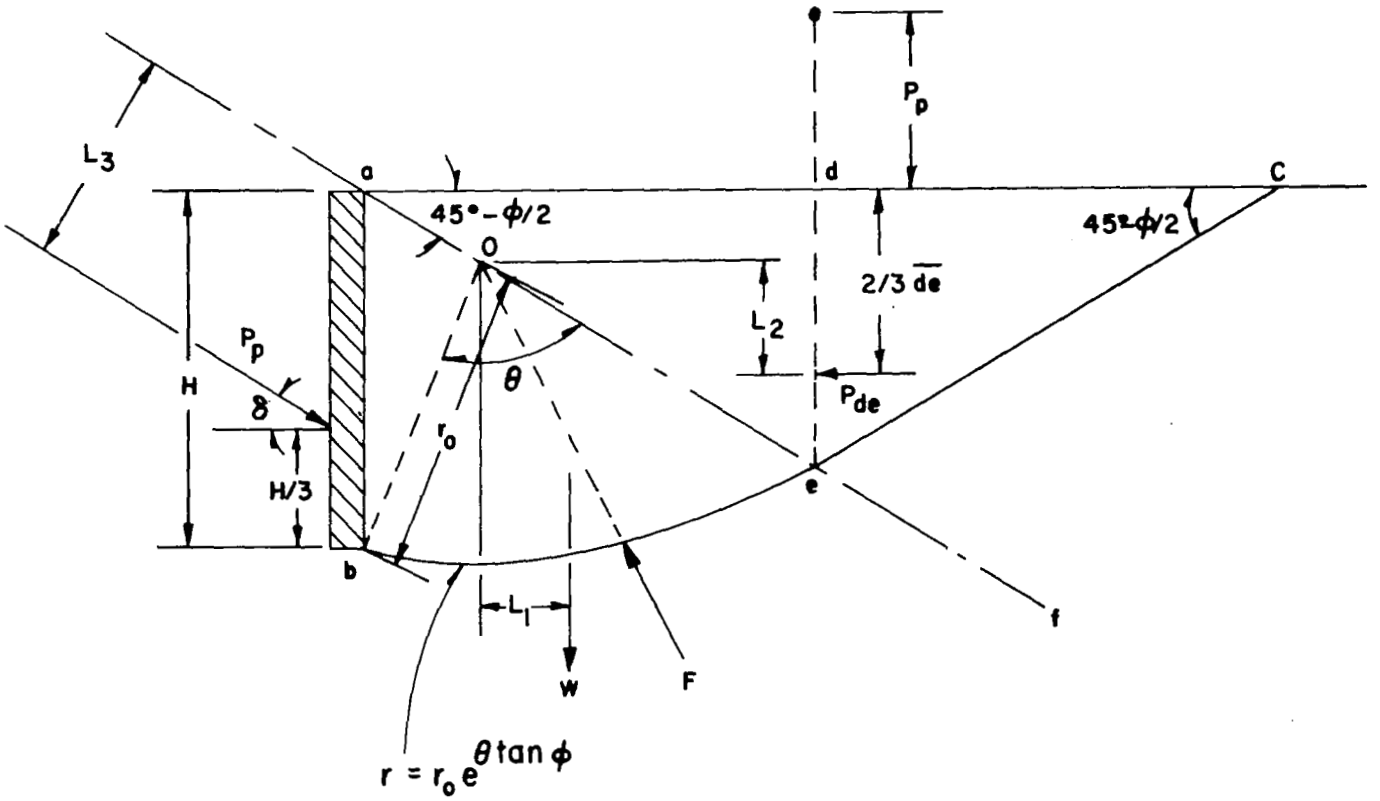

FIG. 14 LOGARITHMIC SPIRAL METHOD FOR DETERMINING PASSIVE EARTH PRESSURE

The weight and centroid location of the body of soil abed is calculated using the geometric properties of the logarithmic spiral and included triangular sections which are illustrated in Fig. 14. Since the body of soil within zone aecd is in a Rankine state, the soil in zone dec may be replaced by a pressure P_{de}. The pressure P_{de} acts at a distance of 1/3 $\overline{de}$ above point e and is equal to

$$P_{de} = 0.5\ \gamma\ (\overline{de})^2\ \tan^2\ (45^\circ + \phi/2). \qquad (11)$$

It should be noted that Eq 10 does not contain any expressions involving the forces acting on the logarithmic spiral portion of the failure surface. The properties of the spiral are such that every resultant force that acts on the failure surface passes through the center of the spiral and therefore has a moment arm of zero length.

CHAPTER III

TESTING APPARATUS

In the testing program 3 different systems of testing apparatus were designed and constructed. Three separate phases of tests were conducted using the apparatus which is discussed in this chapter.

In the first phase, flat steel plates of 12 in. height were penetrated into a dry sand backfill. Penetration of the plates was held at a constant rate of 0.00278 ips. This relatively low rate of penetration allowed all measurements to be recorded manually. Horizontal and vertical soil forces were measured with load cells and the plate penetration was measured with an Ames dial gage.

The second phase was performed using plates having heights of 12 and 18 inches. The plates were penetrated into the backfill in a direction lateral to the plane of the plates. The rate of penetration was held constant throughout a test, however, from test to test the rate was varied from 0.00667 to 2.67 ips. These higher rates of penetration necessitated the use of an oscillograph to record the continuous load cell and displacement transducer output. The soil type and the boundary conditions were identical to those used in Phase I.

The third phase consisted of horizontally penetrating cones and spherical segments into a soil identical to that used in Phases I and II. The rates of penetration and the recording equipment were similar to those used in Phase II. The horizontal soil force was measured with a load cell. Strain gages, mounted on a 0.75 in. diameter driving shaft, were used to obtain the vertical soil force. Since the models were not initially in contact with the soil, it was necessary to support the sand in a horizontal direction. A polyethylene membrane stretched over a removable frame was used to confine the sand in a horizontal direction.

PHASE I APPARATUS

The apparatus for Phase I was designed to allow the earth-pressure problem to be reduced to two dimensions. It is advantageous to reduce the problem to two dimensions because existing earth-pressure theories are applicable to studying the force-penetration characteristics of the soil. A side view of the test setup is shown in Fig. 15.

Plate Design

Each test required the use of three separate plates. The plates were pushed simultaneously in a horizontal direction. They were not allowed to rotate or freely move in a vertical direction. The plates were machined from 0.5 in. thick cold-rolled steel plate stock. Steel was chosen because of its high flexural rigidity and also because it provided a relatively smooth contact surface with the sand backfill. If the contact surface was frictionless, Coulomb's theory would yield nearly exact results when applied to the two dimensional plane-strain earth-pressure problem. When the three plates were placed in their test position, they formed a wall 1 ft high and 3 ft wide. A plan view of the wall in its test position is shown in Fig. 40 on p. 69.

Only the soil response on the center plate was measured. The main function of the two side plates was to confine the sand and to minimize three dimensional effects on the center plate. The outer edges of the side plates were milled flat to allow a smooth contact surface between the sides of the plywood box and the side plates. A 90 degree angle slot was milled in the inner vertical edge of the side plates. Ninety degree angle slots were also milled in each vertical edge of the center plate. When the three plates were placed in their test position, the slots provided an opening between the center plate and each of the side plates. Flexible rubber tubing having an outside

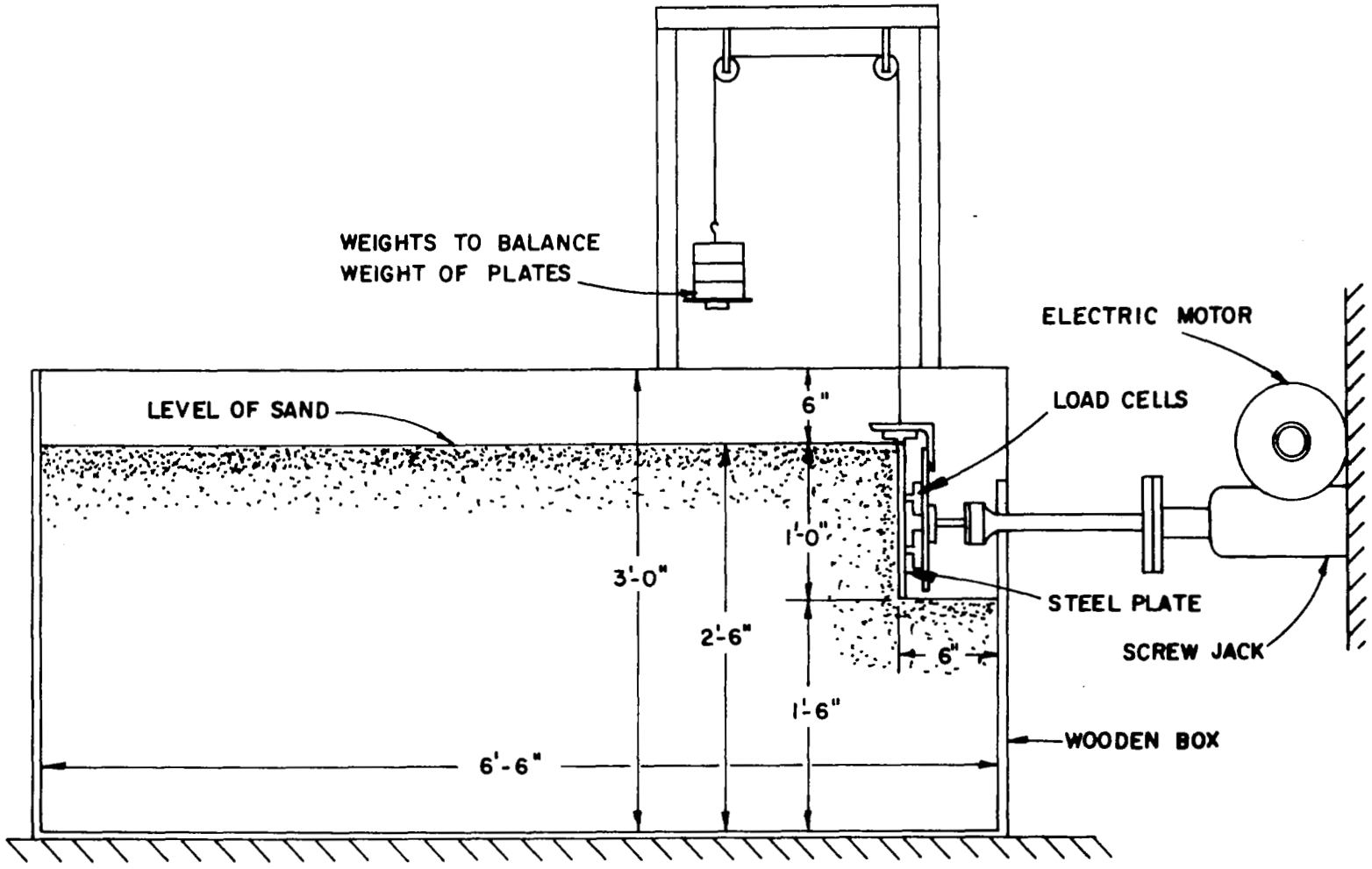

FIG. 15 SIDE VIEW OF THE TEST SETUP USED DURING PHASE I

diameter of 0.5 in. and a wall thickness of 0.125 in. was inserted in the opening. Details of the plates are shown in Figs. 16 and 17. The rubber tubing acted as a flexible connection, which served to minimize load transfer and sand leakage between the center and side plates. Petrolatum was also applied to the tubing to further reduce sand leakage during the test. The chief purpose of the above design was to simulate the boundary conditions that exist in an infinitely long 1 ft high retaining wall. The center plate represented a 1 ft wide section cut from an infinitely long wall.

Three square slots were milled in the rear face of the center plate and oil hardened precision ground tool steel inserts were cemented in the slots with Epoxy. The hardened steel inserts were intended to minimize friction between the buttons on the load cells and the center plate. Two eye bolts were threaded into the top horizontal edge of each of the plates. The eye bolt connections and counterbalance weights are shown in Fig. 18.

As the plates penetrated into the soil, the earth pressure on the sides of the sandbox increased. This caused a gap to open between the sides of the box and the outer edges of the side plates and the gap allowed sand to flow through. Thereby creating undesirable expansions of the soil mass which occur in a direction parallel to the plane of the plates. To stop this flow, additional tie rods were added to the box and aluminum angles, 1.0 in. by 0.7 in., having a thickness of 0.3125 in. were taped to the front faces of the side plates. The 0.7 in. leg of the angle rested against the plate and the 1.0 in. leg rested against the side of the box. Petrolatum was also placed between the angles and the sides of the box.

Load Cell Supports and Locations

Four load cells were used to measure the forces exerted by the sand backfill on the center plate. Three of the load cells were utilized to measure

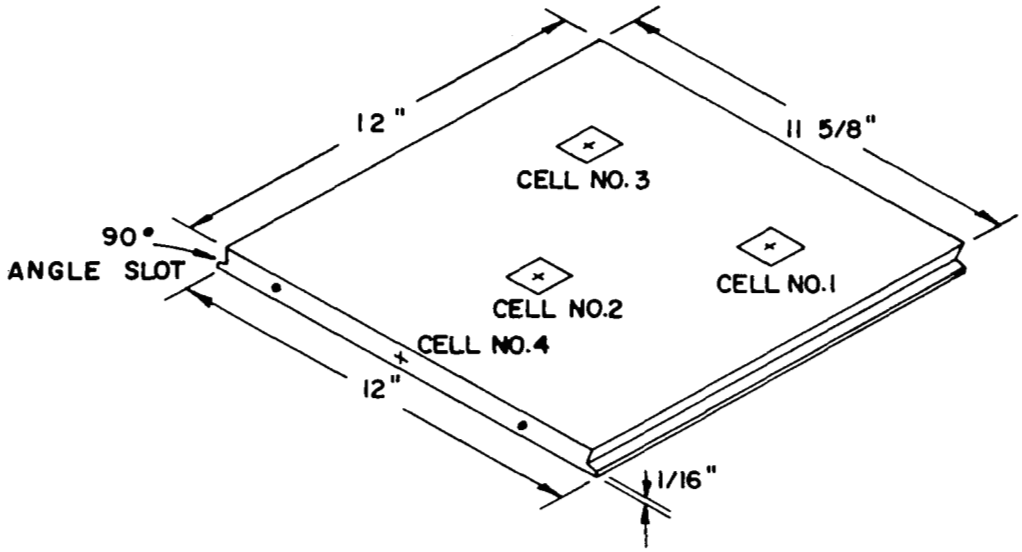

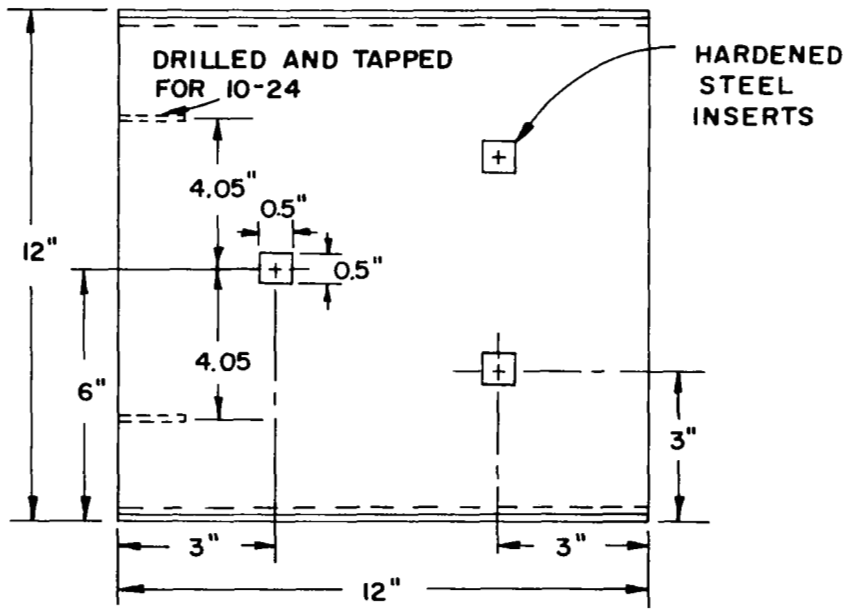

FIG.16 CENTER PLATE DESIGN — PHASE I

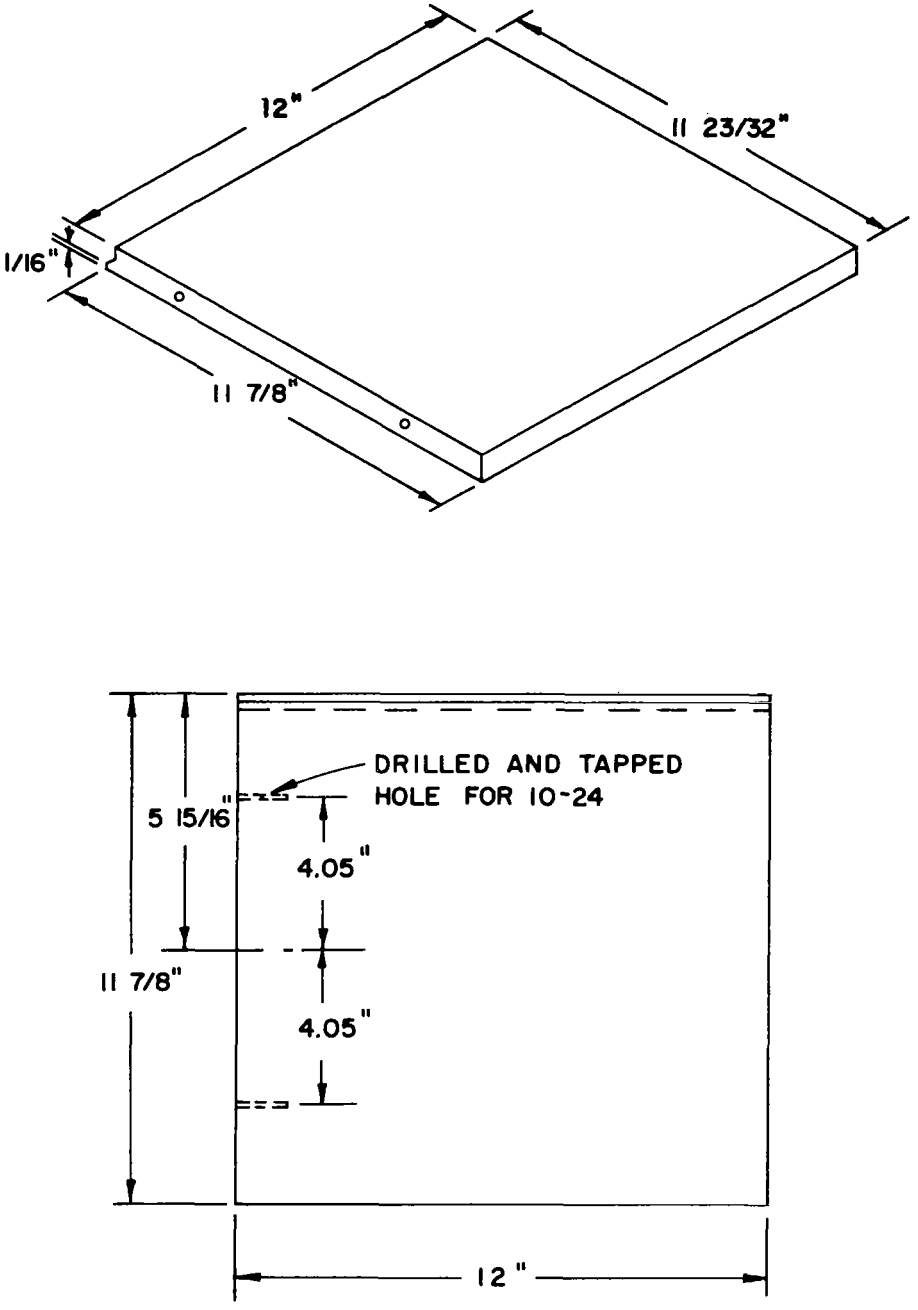

FIG.17 SIDE PLATE DESIGN — PHASE I

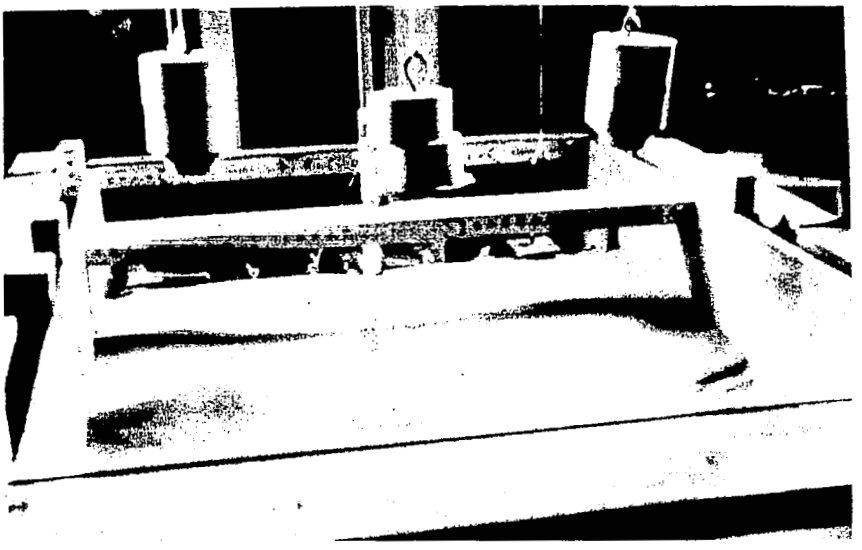

Fig. 18 View of Eye Bolt Connections and Plate Counterbalance Weights - Phase I

the horizontal soil force and the remaining cell measured the net upward frictional force on the center plate. The net frictional force is the algebraic sum of the force at the soil-plate interface and the frictional forces between the load-cell buttons and the rear face of the plate. The net frictional force is a measure of the vertical soil force on the center plate. The location of the points at which the three load cells contacted the rear side of the center plate are shown by + signs in Fig. 16. The load cell that measured a portion of the vertical soil force contacted the center of the upper edge of the center plate.

The cells that measured the horizontal soil force were held in position by plexiglas mountings which were in turn fastened to a 0.5 in. thick aluminum support plate. The aluminum plate was bolted to one flange of the 3 in. by 2.375 in. steel I-beam shown in Fig. 15. The general arrangement of load cells and the support plates will be discussed further in the Phase II Apparatus Section of this chapter. Each of the side support plates contained wing bolts for alignment of the side plates with the center plate.

Loading System

The force necessary to push the plates into the soil was furnished by a screw jack. The screw jack was powered by a single-phase 4.33 HP motor that operated at 1725 RPM. The jack pushed the plates and loading frame at a constant rate of 0.00278 ips.

Instrumentation

The basic electrical components that were utilized during the Phase I testing program consisted of a strain indicator, switch and balance unit, and 5 load cells. The strain indicator and switch and balance unit, Model Numbers P-350 and SB-1, respectively, were built by Budd Instruments Division. A block diagram of the force measurement circuit is shown in Fig. 19.

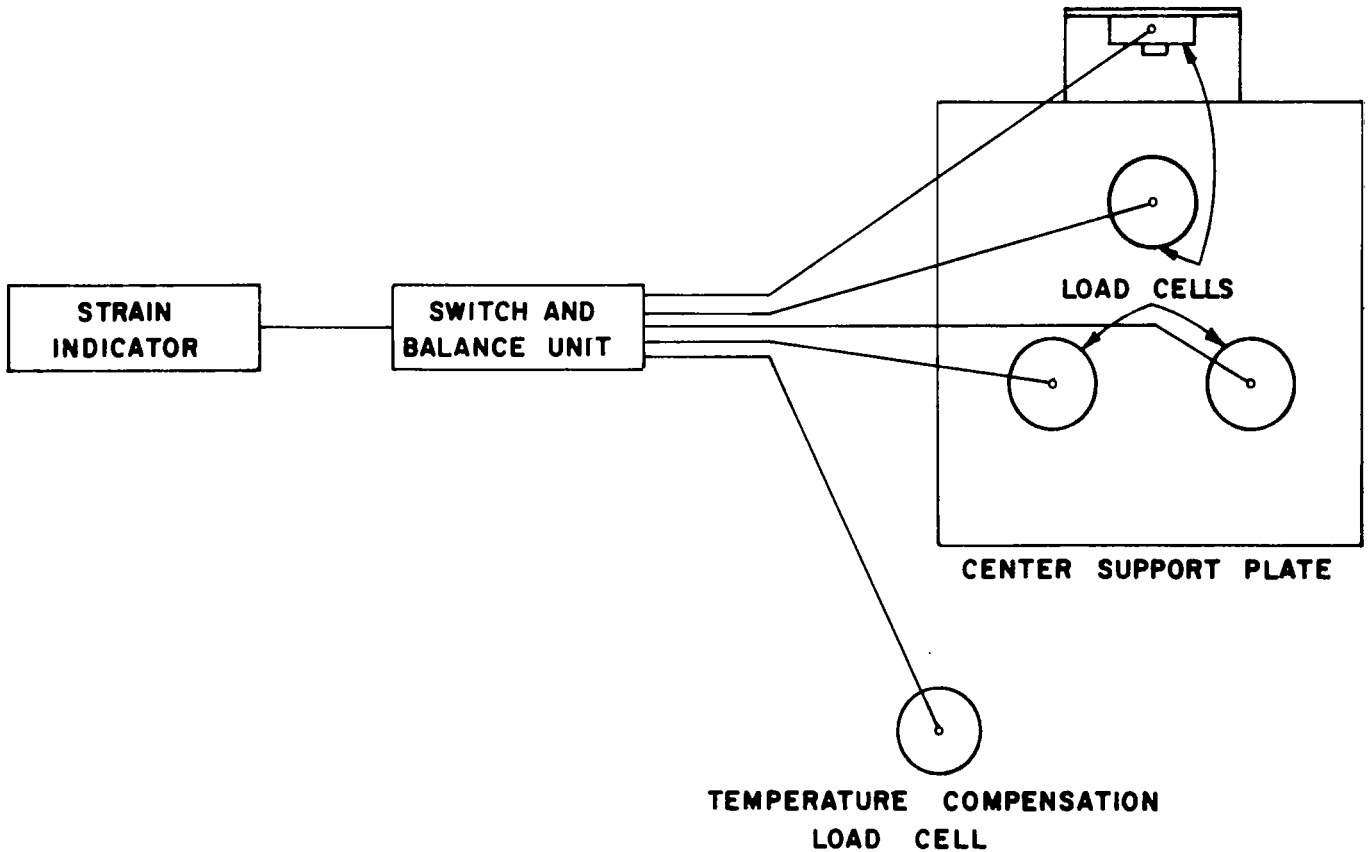

FIG. 19 BLOCK DIAGRAM OF FORCE MEASUREMENT CIRCUIT – PHASE I

Force Measurement

The purpose of Phase I was to obtain force-penetration curves for a rigid wall penetrating into cohesionless soil in a horizontal direction. Load cells were used to measure the force which varied between 5 and 800 pounds. The cells consisted of two halves. The bottom half provided a base for the top half and an outlet for strain gage wire leads. The top half consisted of a 0.130 in. thick diaphragm upon which an SR-4 spiral strain gage was bonded with Epoxy-150 cement. The strain gages were of the foil type and were manufactured by the Baldwin-Lima-Hamilton Electronics Division. The resistance of the gages were 120.0 ± 0.2 ohms and the gage factors were 2.0. A typical load cell is shown in Fig. 20.

The load cells were calibrated using a Model ULH-60 Universal Testing Machine built by the Budd Instruments Division. A Budd strain indicator that permitted strains to be recorded to the nearest microinch was also used in the calibration procedure. During calibration each cell was connected in a quarter bridge with a temperature compensating gage. Several loading and unloading cycles were performed on each load cell with readings being taken from 0 to 1,000 lbs and from 1,000 lbs to 0 pounds. The calibration curves for all the load cells were found to be linear, with the unloading curve retracing the path of the loading curve. The load cells had sensitivities that ranged from 0.64 to 1.27 lbs per microinch.

Penetration Measurement

The penetration of the top edge of the center plate, which is identical to the penetration of the bottom edge of the plate, was measured with an Ames dial gage that could be read to the nearest 0.001 inch. The procedure used in reading the dial gage and strain indicator is given in Chapter IV on p. 52.

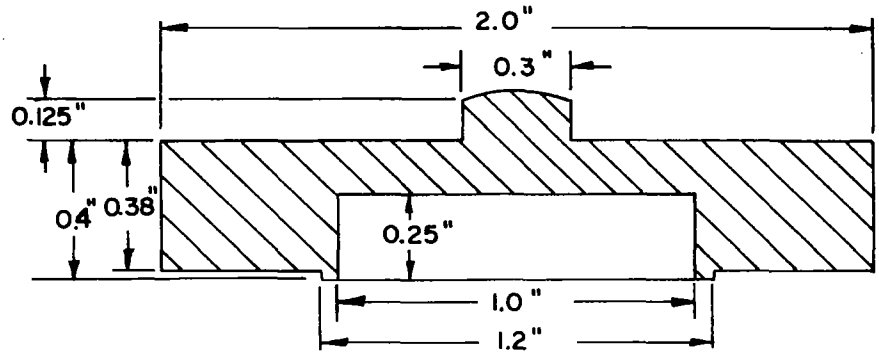

LOAD CELL – TOP HALF SECTION

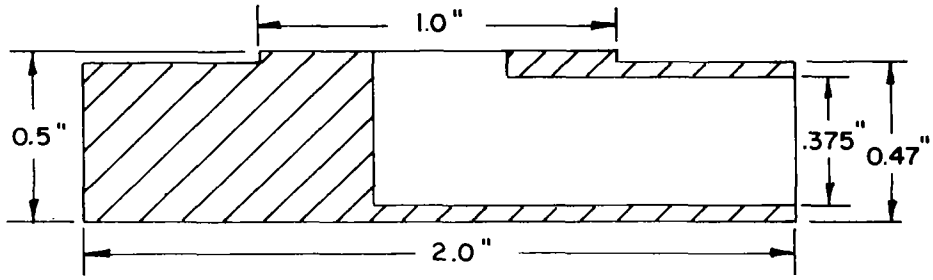

LOAD CELL – BOTTOM HALF SECTION

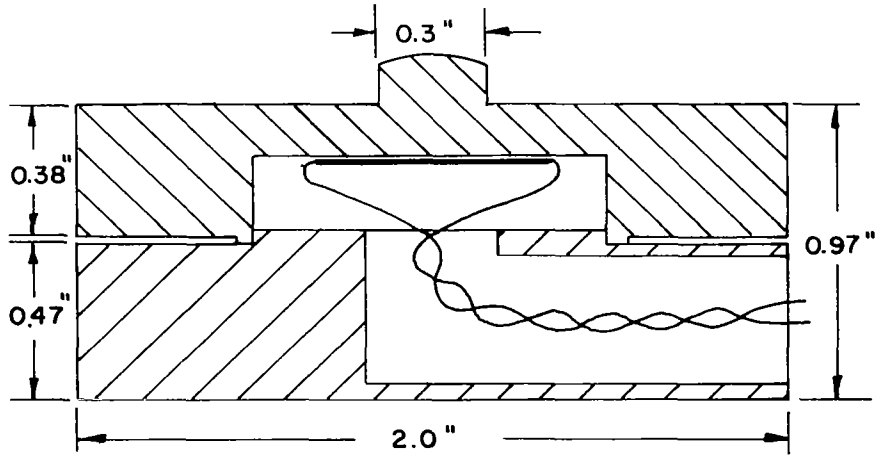

FIG. 20 DETAILS OF TYPICAL LOAD CELL

PHASE II APPARATUS

During the first phase of testing, some undesirable features were noted in the design of the testing apparatus. The foremost limitation in the apparatus was the type of restraint used to prohibit vertical movement of the loading frame. As the plates penetrated into the backfill, an upward frictional force was developed at the soil-wall interface and the upward force was in turn transferred to the loading frame. A 2 in. by 6 in. board was fastened to the sandbox so that the lower edge of the board contacted the center steel pipe portion of the loading frame. This type of restraint proved to be unsatisfactory because it did not totally eliminate the upward movement of the loading frame and plates.

Another feature of the design which was unfavorable to Phase II testing conditions, was the method used to counterbalance the weights of the plates. It should be noted that this method was satisfactory for Phase I; however, for Phase II it was not satisfactory because the higher rates of penetration caused the weights to swing.

After considering the limitations mentioned above and also that greater forces would be developed during Phase II, since higher plates would be used, it was decided to redesign the testing apparatus. A General View of the Test Setup for Phase II is shown in Fig. 21.

Plate Design

During this phase of testing, plates 12 in. wide by 12 in. high and 12 in. wide by 18 in. high were used. Figures 23 through 26 illustrate the plate designs. The basic differences between these plates and those used in Phase I are that no hardened inserts were used in the center plates and each of the side plates had a nut welded to the rear face.

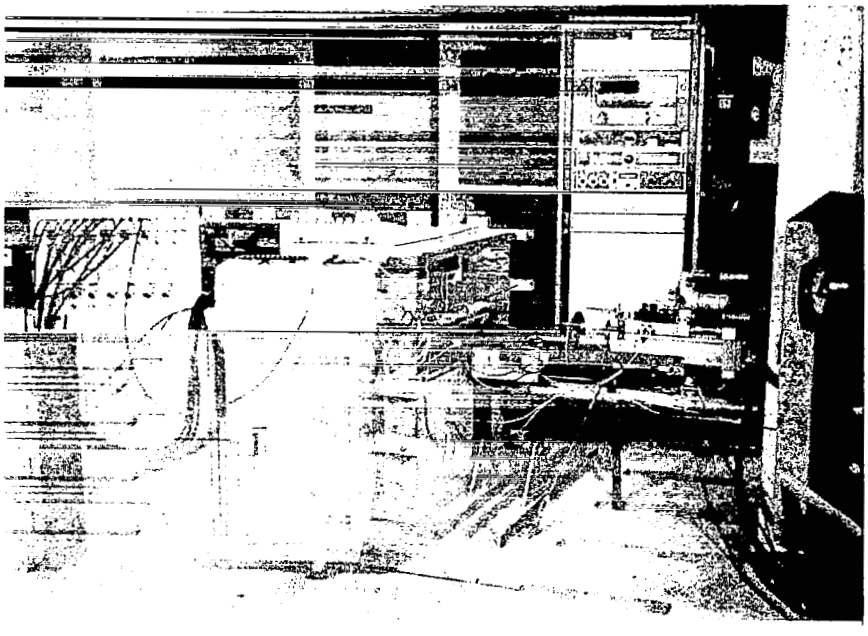

Fig. 21 A General View of Test Equipment - Phase II

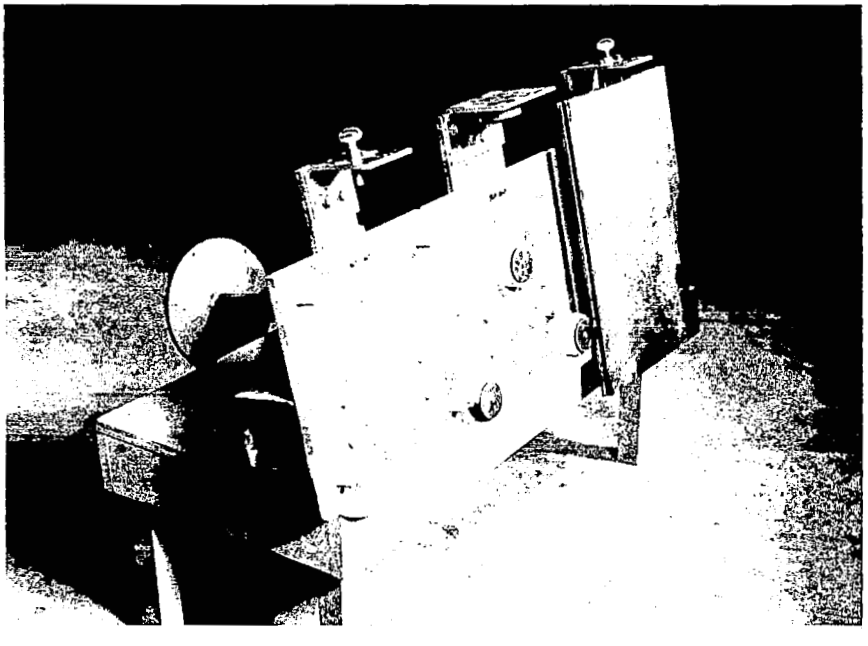

Fig. 22 View of Loading Frame and Plate Supports - Phase II

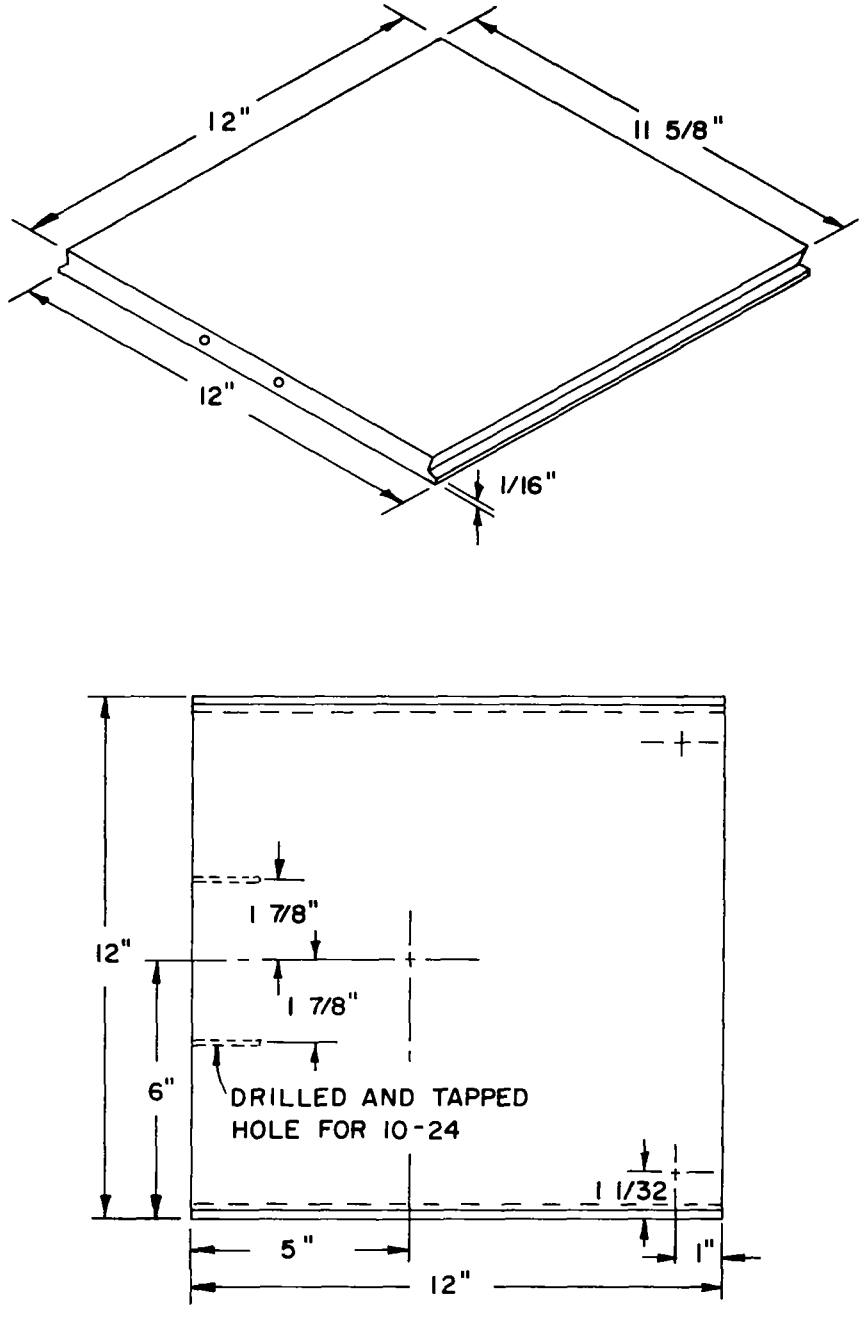

FIG.23 CENTER PLATE DESIGN, 12 IN. X 12 IN. – PHASE II

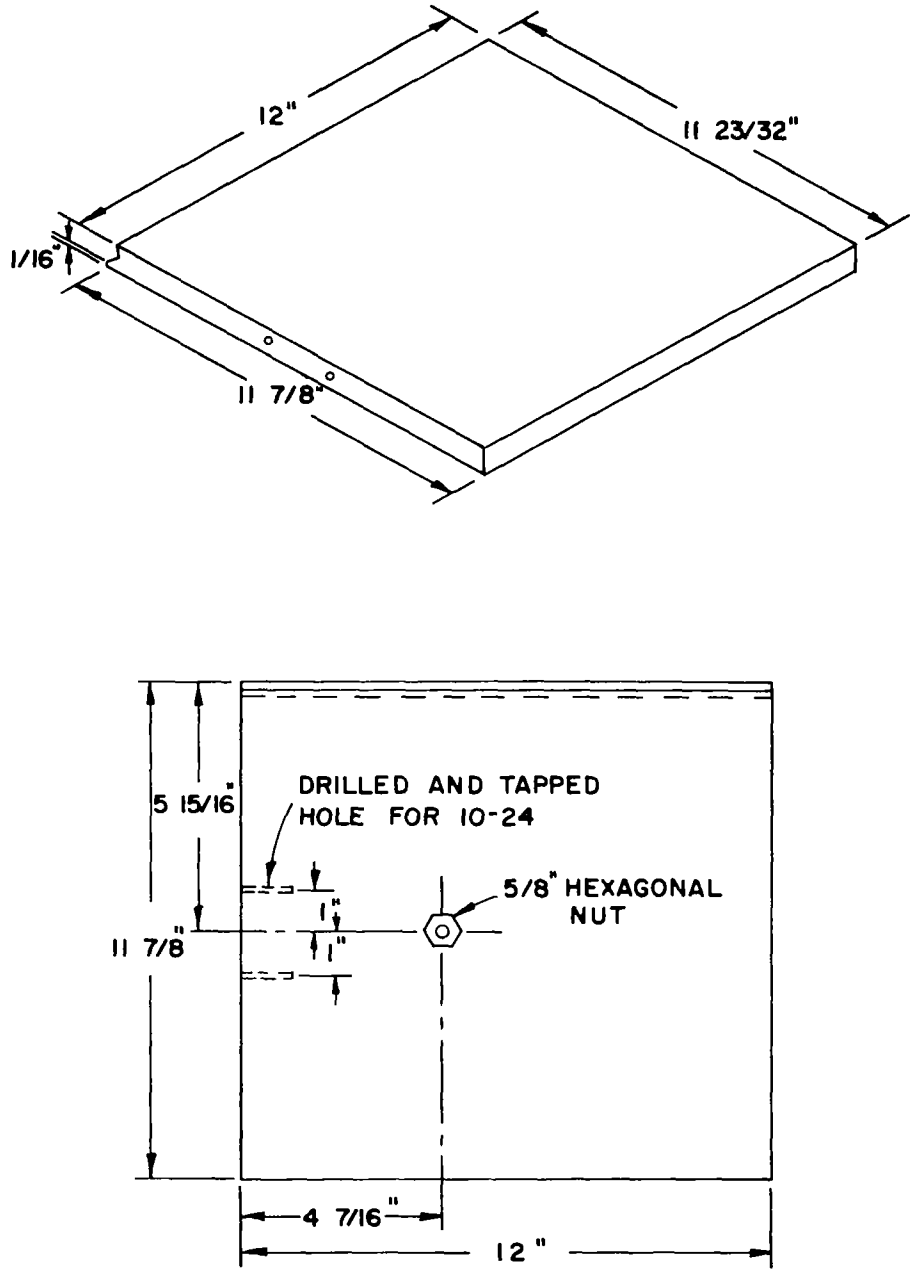

FIG. 24 SIDE PLATE DESIGN, 12 IN. X 12 IN. – PHASE II

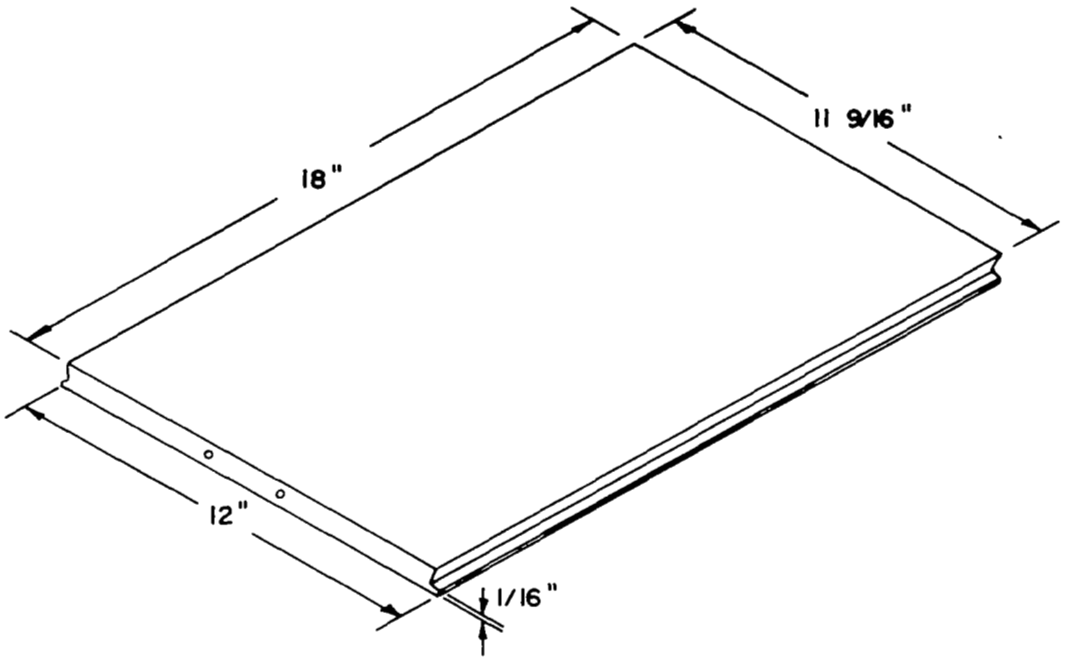

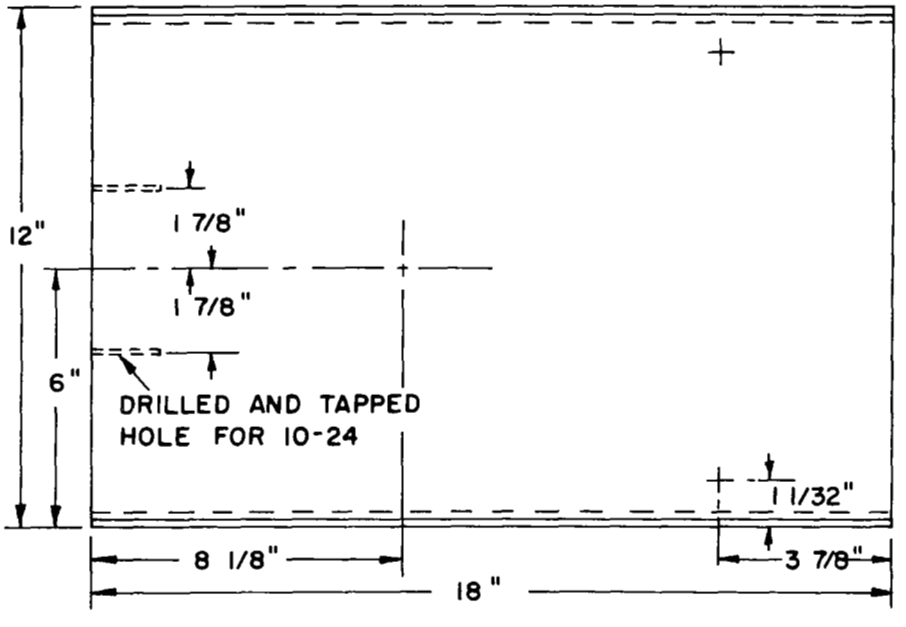

FIG. 25 CENTER PLATE DESIGN, 12 IN. X 18 IN. — PHASE II

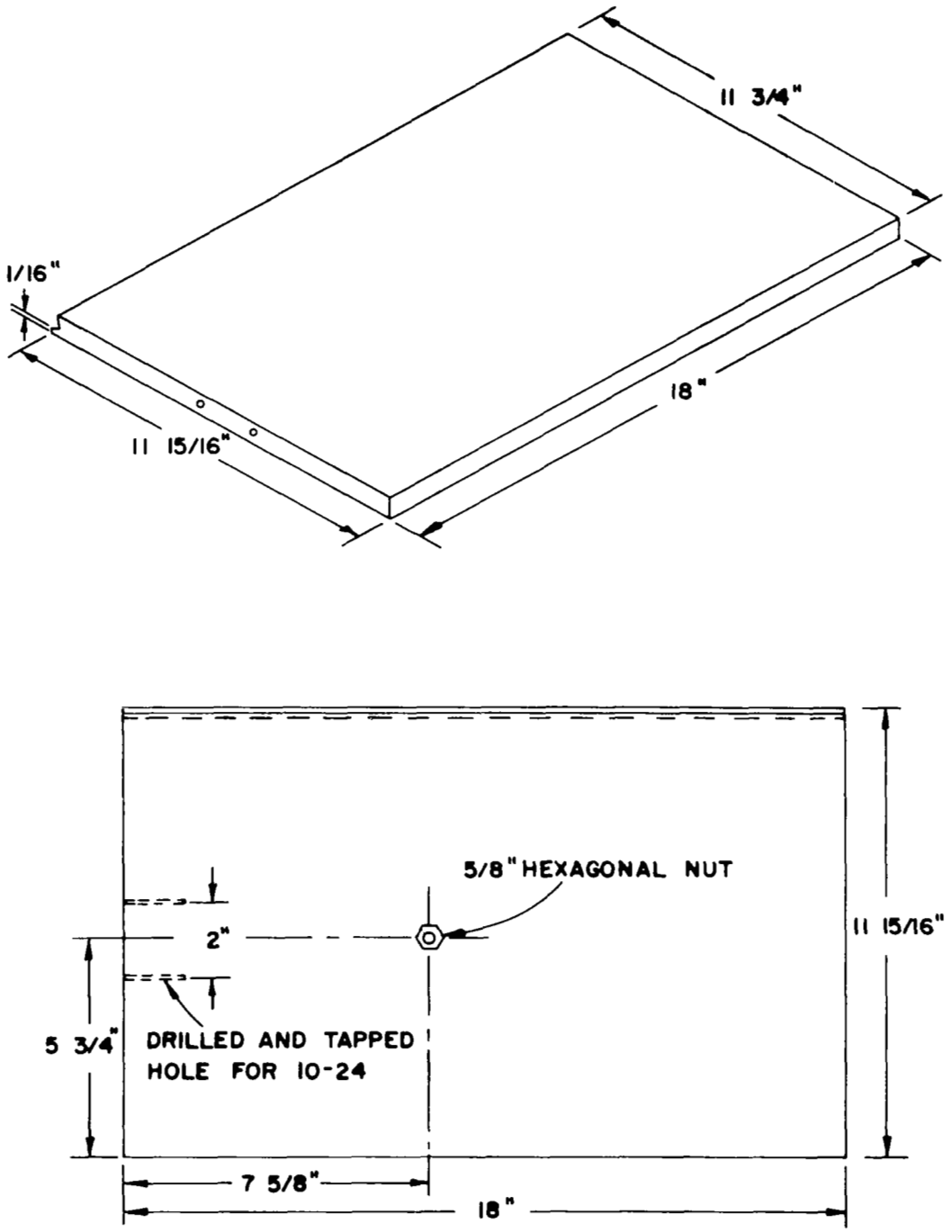

FIG. 26 SIDE PLATE DESIGN, 12 IN. X 18 IN. – PHASE II

Several tests were performed to determine the coefficient of friction between a load-cell button and a hardened steel insert. The coefficient of friction was found to be 0.10. Several tests were also performed using steel identical to that from which the plates were made, instead of the insert steel, and it was found that there was no measurable difference for the developed range of testing pressures. Therefore, it was concluded that the hardened steel inserts were unnecessary.

The nut that was welded to the rear face of each of the side plates provided a means of fastening the plates to the aluminum support plates.

Instead of using counterbalance weights as were used in Phase I, the plates were each hung by two bolts that were in turn supported by angles that were bolted to the aluminum support plates. The method used to support the plates is shown in Fig. 22. Wing bolts were used as spacers for the side plates. The two bolts that supported the center plate passed through holes that were larger than the shank but smaller than the head of the bolt. The plate was free to react against the single load cell when the frictional force at the interface of the soil and the center plate reached a value equal to the weight of the plate plus the frictional force developed between the three load cells and the rear face of the plate.

Load-Cell Supports and Locations

The load-cell support system utilized during this phase of testing was similar to that used in Phase I. In this system the aluminum support plates were connected together by a section of 4 in. by 4 in. structural tubing with a wall thickness of 0.375 inches. The loading frame and the method of restraint that was used to keep the frame from moving in an upward direction is shown in Fig. 27.

The positions at which the load cells contacted the back face of the center plates are shown by + signs in Figs. 23 and 25.

Loading System

A closed loop servo loading system, Model 900.62, manufactured by Research Incorporated, Minneapolis, Minnesota, was used to furnish the necessary horizontal thrust. The system basically consisted of a hydraulic actuator, hydraulic power supply, and a control console.

The hydraulic actuator assembly consisted of a hydraulic cylinder, an aluminum manifold and an electrohydraulic servo valve. The servo valve controlled the flow of fluid to and from the cylinder in proportion to the polarity and amplitude of the electrical signal from the electronic controller. The actuator was capable of developing 10,000 lbs and had a stroke length of 10 inches.

The hydraulic power supply was capable of delivering fluid flows at an average rate of 5 gpm under a maximum pressure of 3000 psi. The maximum stroking speed of the hydraulic cylinder was 4 ips.

The control console was composed of a Servac, control panel, counter panel, and Data-Trak system. The Data-Trak provided a means of programming the hydraulic cylinder to move at a predetermined rate. The desired rate was obtained by etching a curve on a special program chart which was in turn mounted on the program drum in the Data-Trak. The slope of the curve and the speed at which the drum revolved set the rate at which the hydraulic cylinder moved. The Servac is a solid-state electronic servo controller that was used to control the velocity of the hydraulic cylinder. The Servac received two signals: (1) the desired (programmed) signal which represented the condition of the controlled variable (velocity), and (2) the existing signal that represented

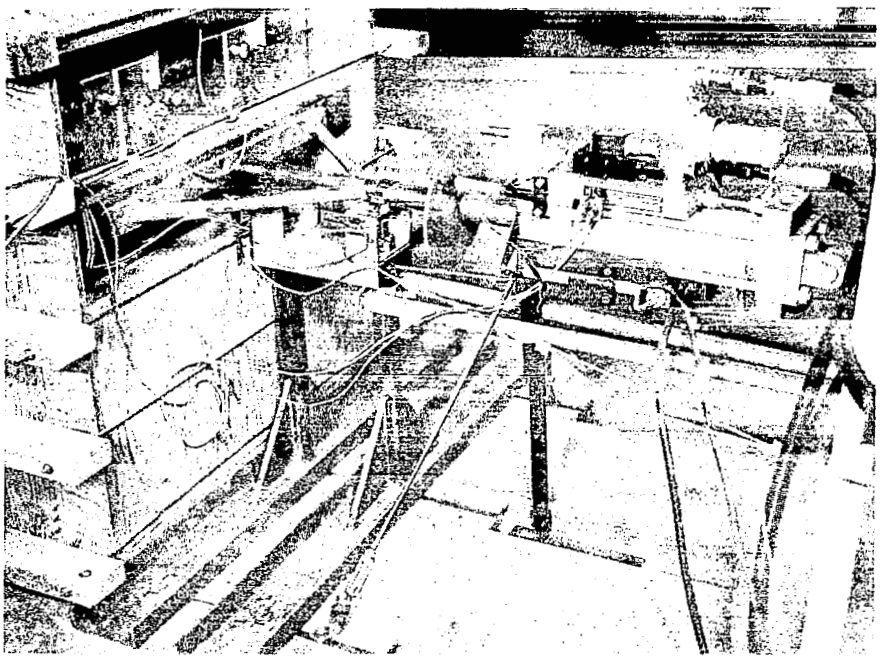

Fig. 27 Detail View of Loading Frame Restraint and Deflection Transducer Mountings

the actual condition of the controlled variable. These are the composite command and the transducer feedback signals, respectively. The feedback signal was produced by a rectilinear potentiometer that measured the displacement of the hydraulic cylinder. The Servac compares the composite command signal and the potentiometer signal, if the signals do not agree the Servac sends a signal to the servo valve which causes it to readjust and bring the system back into equilibrium.

The complete loading system is shown in Fig. 21 on p. 33.

Instrumentation

The basic electrical components used to obtain force-penetration curves, consisted of load cells, displacement transducers, a balancing and calibration unit, amplifiers, and an oscillograph. All of the external electrical wiring was shielded to prevent distortion of the oscillograph record. A block diagram of the instrumentation setup is shown in Fig. 28.

Force Measurement

The horizontal and vertical soil reaction on the center plate was measured using the same load cells that were utilized in Phase I.

Penetration Measurement

The penetration of the plates was measured by two types of displacement transducers: (1) linear variable differential transformer (LVDT), and (2) rectilinear potentiometer. It was necessary to use these two types of transducers to obtain accurate measurements during all phases of penetration.

When the sand was placed in its densest state, the ultimate horizontal load occurred well within the first 0.5 in. of penetration. These relatively small penetration values were recorded using an LVDT that had a maximum travel

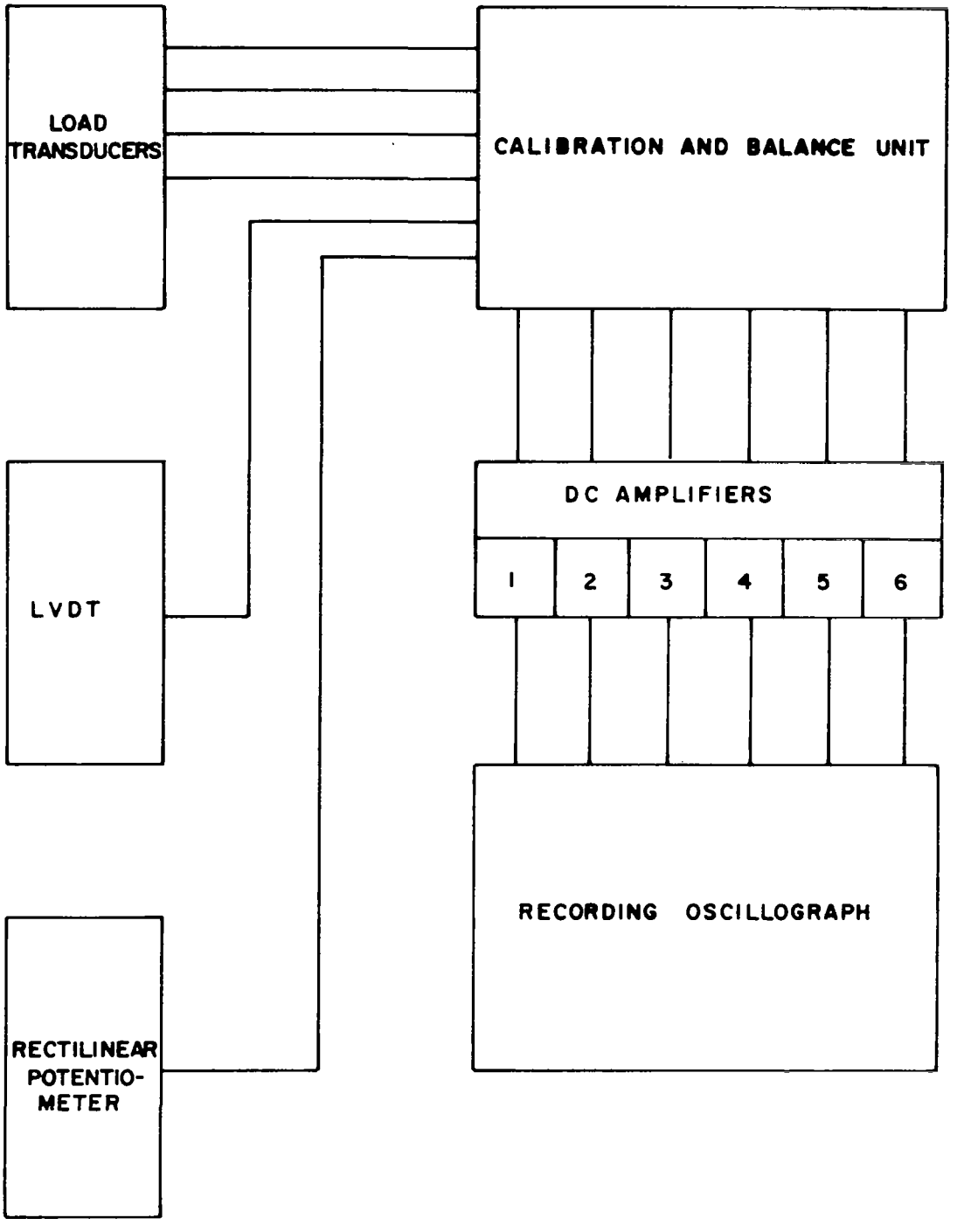

FIG. 28 BLOCK DIAGRAM OF INSTRUMENTATION SETUP – PHASE II

of ± 0.5 in. and a maximum nonlinearity of 0.5 per cent of the full-scale voltage. The transducer, Model 24DCDT-550, was built by Sanborn, a division of Hewlett-Packard, Waltham, Massachusetts.

A rectilinear potentiometer was utilized to measure penetrations greater than 0.5 inches. It was this transducer that provided the feedback signal to the Servac. When the backfill was placed in its loosest state, penetrations less than 0.5 in. were not nearly so significant and in these tests only the rectilinear potentiometer was used. The transducer had a maximum travel of 7.0 in. and a maximum nonlinearity of 0.1 per cent of the full-scale resistance. The transducer, Model L.C.-750, was manufactured by Topp Industries, Incorporated, Los Angeles, 45, California.

Balancing and Calibration Unit

Due to the physical characteristics of the system, each recording channel exhibited a different resistance. The balancing unit allowed these resistances to be balanced and thereby made it possible for all the traces to be positioned on the oscillograph.

To obtain a continuous record of the strains that occurred in the load cells, it was necessary to provide a method of obtaining calibration curves for each of the traces recorded by the oscillograph. This was accomplished by a unit that permitted known resistances to be switched into the electrical circuit which connected the load cells with the recording oscillograph. Calibration curves for the displacement transducers were obtained by moving each transducer shaft through known distances and recording the corresponding trace deflections that occurred.

Amplifiers

The electrical signals from the load cells and displacement transducers were amplified by Redcor 361404 Differential DC Amplifiers. The amplifiers permitted the voltage gain to be varied from 10 to 1,000 and their bandwidth was 100 kilocycles.

Recording Oscillograph

The output from the load cells and transducers was recorded on a Type 5-124 Recording Oscillograph, manufactured by Consolidated Electrodynamics, Pasadena, California. The oscillograph utilized light beam galvanometers, 0 to 500 cps bandwidth, that recorded the output from each trace on light sensitive paper.

PHASE III APPARATUS

This phase of testing consisted of penetrating spherical segments and cones through a flexible membrane into a sand backfill. Figures 29 through 33 show the models and the test setup that was used in this phase of testing.

Model Design

The primary purpose of this phase of the investigation was to determine the soil response to penetrating bodies of different sizes and geometric properties.

It was decided to use model sizes that could be conveniently utilized in a laboratory test setup. Spherical segments and right-circular cones were chosen because these basic geometric shapes approximate the shapes of landing gear used in the United States' space exploration program.

The spherical segments had radii of 2.5 and 5.0 inches. The cones had a 60 degree apex angle and base diameters of 3.54 and 7.08 inches.

Drawings of the small models are shown in Figs. 29 and 30. The larger models are similar to the smaller models and, therefore, are not shown.

Lateral Soil Support

During the first two phases of testing, lateral support of the backfill prior to and during each test was not a problem. The third phase of testing, however, necessitated the design of apparatus that would laterally support the backfill and at the same time permit the models to penetrate into the soil. These requirements were fulfilled by constructing a wooden frame which contained a circular opening 8.7 in. in diameter. Polyethylene, having a thickness of 1 mm, was stretched over the opening and attached to the frame. Several tests were run to determine the forces developed as a consequence of the model piercing the membrane. The findings from these tests showed that the piercing forces were negligible. There was no loss of sand through the punctured membrane until the penetration exceeded the height of the model. When tests were conducted that utilized the 5.0 in. dia spherical segment and the 3.54 in. dia cone, a 0.8 in. thick wooden ring was inserted in the circular frame opening, thus reducing the diameter of the opening to 7.0 inches. The frame was constructed so it could easily be removed from the wall of the sandbox when it was necessary to replace a punctured membrane. The wooden frame with an attached membrane is shown in Fig. 31.

Loading System

The force necessary to push the models into the backfill was furnished by the same closed loop servo loading system used in Phase II. The loading shaft to which the models were connected was restrained from moving in an upward direction by the same restraint apparatus that was used in Phase II.

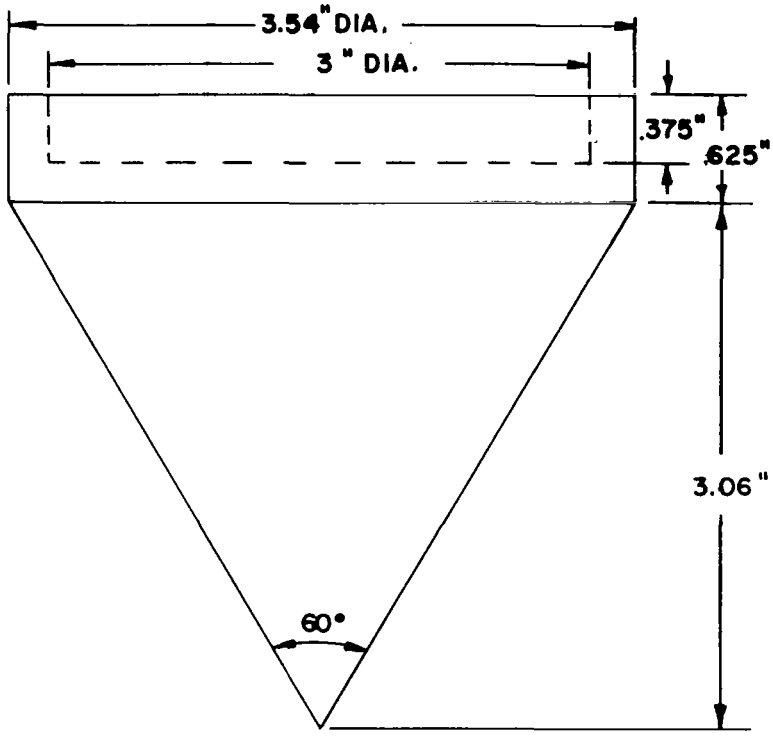

FIG. 29 ALUMINUM RIGHT-CIRCULAR CONE DESIGN — PHASE III

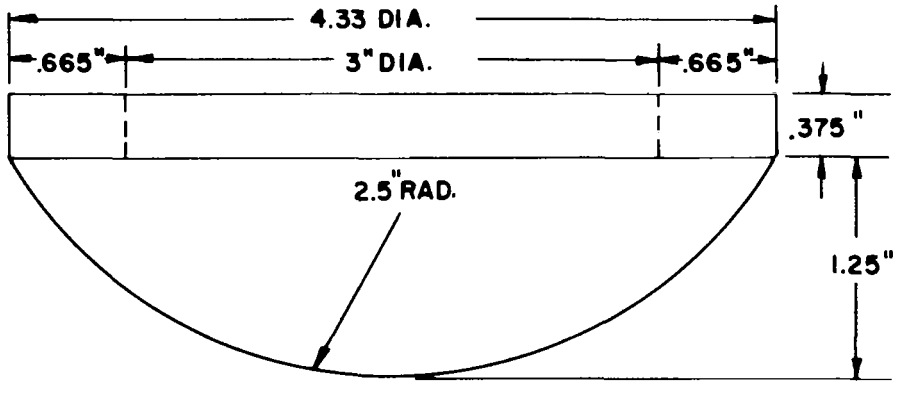

FIG. 30 ALUMINUM SPHERICAL SEGMENT DESIGN — PHASE III

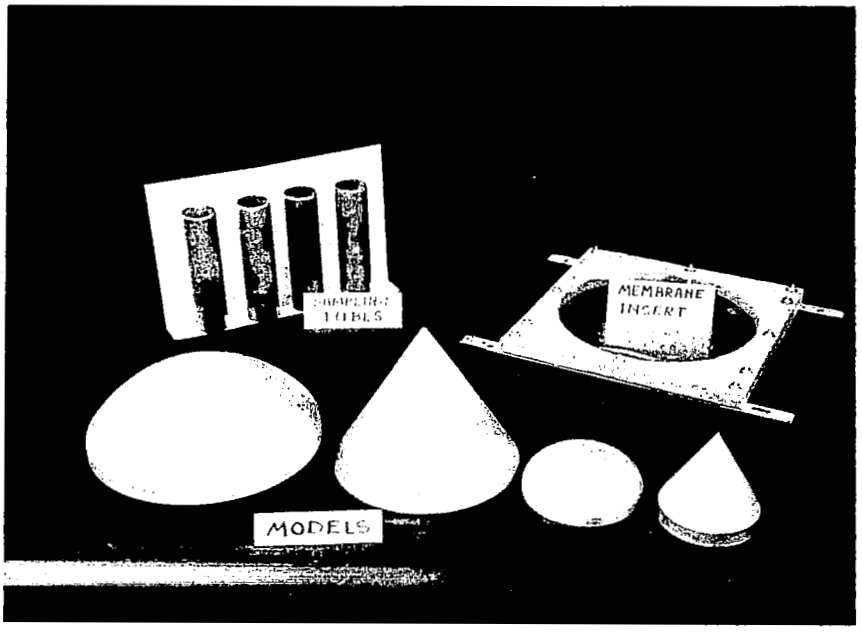

Fig. 31 View of Models, Sampling Tubes, and Lateral Soil Support - Phase III

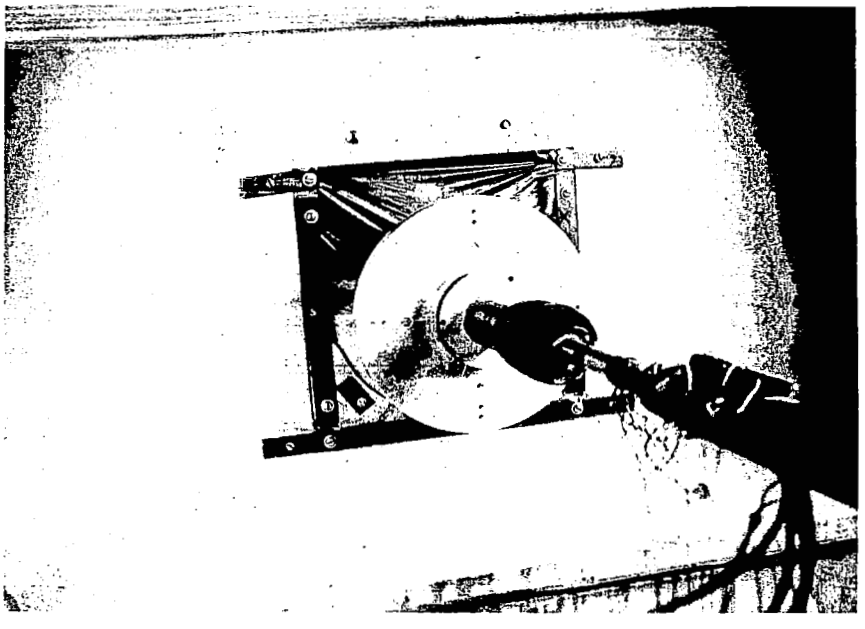

Fig. 32 Rear View of Instrumented Shaft and Spherical Segment in Initial Test Position - Phase III

Instrumentation

The electrical instrumentation consisted of a load cell, displacement transducer, bonded strain gages, and the same auxiliary recording equipment that was used in Phase II.

Force Measurements

The horizontal soil response produced by the penetration of the models into the backfill was measured using a load cell. Figure 33 illustrates the position of the load cell. This figure shows that only the top half of the load cell was used since the base of the model also served as a base for the cell. The top half of the cell is identical to the top half of the typical load cell shown in Fig. 20, with the exception of the differences in the cell buttons.

Several tests were conducted to determine the amount of friction developed between the 0.75 in. dia shaft and the two sets of ball bearings which were mounted in the shaft housing. In all tests the amount of friction was negligible.

The shaft housing was designed so it could be used, without modification, for all model testing.

To obtain a measure of the resultant vertical soil response, four equally spaced SR-4 foil strain gages were mounted on the circumference of the 0.75 in. dia shaft. Calibration curves for the four gages were obtained by applying loads in a direction normal to the axis of the shaft and recording the resulting strains. Another set of calibration curves was obtained by subjecting the shaft to axial compression loads. In every case the calibration curves were found to be linear. To increase the strain gage outputs, a 0.5 in. dia, 4.25 in. deep hole was milled in one end of the shaft.

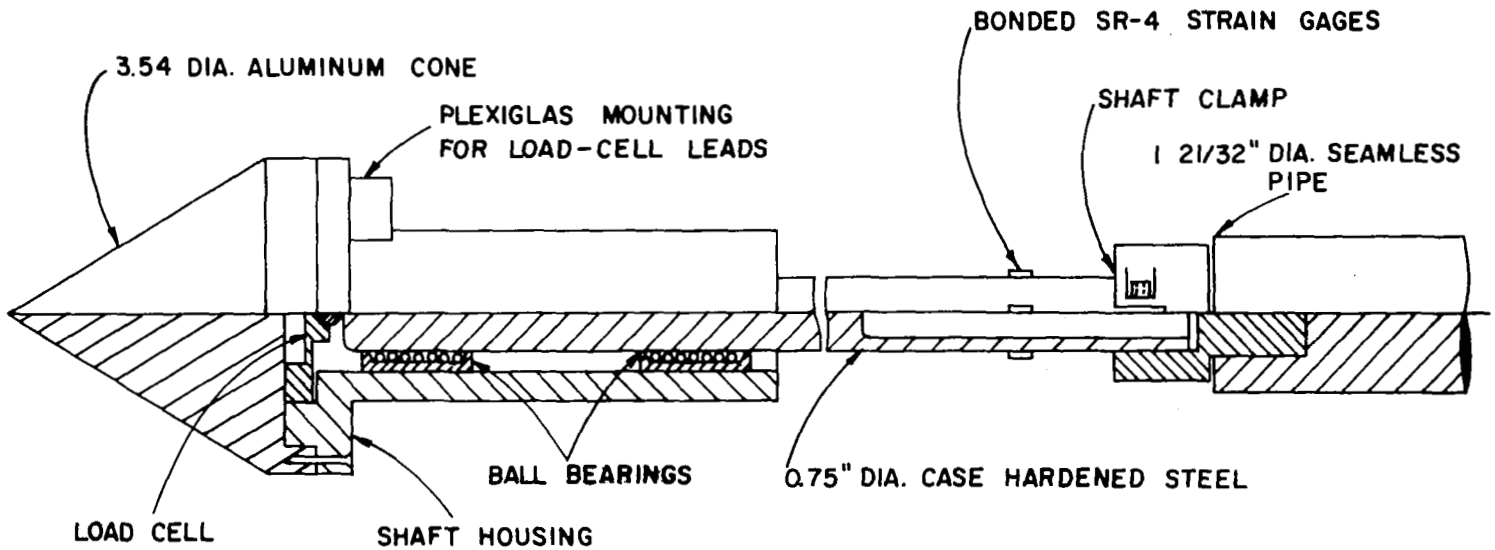

FIG. 33 DETAIL VEIW OF MODEL PENETRATION ASSEMBLY — PHASE III

Penetration Measurements

The model penetration was measured using the same rectilinear potentiometer that was utilized in Phase II. The displacement transducer was mounted on the hydraulic actuator casing and the transducer shaft was connected to the actuator's cylinder. The location of the transducer and the mounting connection was identical to the arrangement shown in Fig. 27. The distance between the point of measurement and the base of the model was approximately 4 feet. The displacement recorded from the transducer was assumed to be equal to the penetration of the model. The error involved in this assumption is negligible, since the maximum elastic shortening of the 4 ft. section of seamless pipe and steel shaft was less than 0.001 inches.

CHAPTER IV

TEST PROCEDURES AND DATA REDUCTION

The testing program was composed of three separate phases. Although each phase of testing was different from the standpoint of size and geometry of the horizontally penetrating body, the soil conditions were held constant throughout the investigation. The tests were performed using a soil bed composed of air-dry Colorado River sand that had been prepared either in its densest or loosest states.

All of the data reduction and manipulation was performed using a high speed digital computer.

PHASE I PROCEDURE

The procedure for this phase of testing consisted of:

(1) Balancing all the gages to read zero,

(2) Backfilling the sandbox,

(3) Recording initial gage readings,

(4) Recording gage readings as the plates penetrated the backfill,

(5) Recording the locations at which the failure surface intersected the surface of the backfill,

(6) Excavating the backfill,

(7) Recording the final gage readings.

Prior to backfilling the sandbox, each of the four load cells was balanced to zero on the strain indicator. The next step was to backfill the box until the surface of the sand was level with the top edge of the plates. The methods used in backfilling the box are discussed in Chapter V. Initial load cell readings were taken and a dial indicator was mounted to provide penetration measurements for the plates during the test. The sum of the

initial strain readings, from the three cells that measured the horizontal soil force represented the at-rest earth pressure acting on the center plate.

During each test, as the plates penetrated into the backfill at a constant rate of 0.00667 ips, strain readings from the four load cells were recorded for every 0.1 in. penetration up to 1.0 in. and every 0.2 in. thereafter to a maximum of 3.9 inches. Since the cell readings were recorded manually, it was impossible to record simultaneously the output from each cell for a predetermined amount of penetration of the plates. To obtain an accurate measure of the total horizontal soil force for a specified amount of penetration it was necessary to take readings in the following manner:

(1) The output from Load Cell 1 was recorded for a penetration of 0.01 in. less than the amount specified,

(2) The output from Load Cell 2 was recorded for the amount of penetration specified,

(3) The output from Load Cell 3 was recorded for a penetration of 0.01 in. greater than the amount specified.

The relative positions of the load cells are shown in Fig. 16 on p. 25. From this figure it can be seen that Cells 1 and 3 are located at equal distances from the top and side edges of the plate. Due to this symmetry, Cells 2 and 3 were subjected to nearly equal amounts of load during the test. Since Cell 1 was read prior to the specified penetration and Cell 3 was read after the specified penetration had occurred, it was assumed that the sum of the forces on Cells 1 and 3 represents an average force at the specified penetration. The output from Cell 2 represents the force Cell 2 was subjected to when the plates had penetrated the specified amount. Therefore, the total horizontal soil force acting on the center plate at a specified amount of penetration was equal to the sum of the forces on Load Cells 1, 2 and 3.

Immediately after the output from Cell 3 was recorded, the strain in Cell 4 was recorded. This strain represents a portion of the vertical soil force. It took approximately 30 sec to read and record the data output.

Measurements were made to describe the locations at which the failure surface intersected the surface of the backfill. Following the above measurements the backfill was excavated to a depth of several inches below the bottom edges of the plates and final cell readings were recorded. Details pertaining to the placement of backfill material and measurement of the *in situ* soil density are given in Chapter V.

PHASE I DATA REDUCTION

A computer program, designated as PASSIV, was written to reduce and convert the raw load-cell data to a usable form. The program also calculated values for the passive earth pressure on the center plate and other significant quantities. The above values were calculated using Coulomb's theory of passive earth pressure.

A listing of program PASSIV along with examples of input and output data are given in Appendix A.

PHASE II PROCEDURE

The execution of each test in Phase II consisted of the following operations:

(1) Backfilling the sandbox,

(2) Adjusting the closed loop Servo loading system,

(3) Positioning each trace on the oscillograph chart,

(4) Calibrating each trace,

(5) Recording the load cell and displacement transducer output with the oscillograph,

(6) Recording the locations at which the failure surface intersected the surface of the backfill,

(7) Taking density samples,

(8) Recalibrating each trace,

(9) Excavating the backfill.

Operations 1, 6 and 9 were performed in accordance with the methods outlined for Procedures 2, 5 and 6 in Phase I. Adjusting the loading system consisted of: (1) setting the fluid pressure and (2) programming the Data-Trak system to obtain the desired rates of penetration.

Each trace was positioned on the oscillograph chart by adjusting the resistance of each channel. Calibration data for each load-cell channel was obtained by switching known resistances into each channel and recording the corresponding trace deflections. Calibration data for the displacement transducers was obtained by moving the transducer shafts through known distances and recording the corresponding trace deflections. Figure 34 illustrates typical calibration data output. Each step on the load-cell portion of the calibration chart represents a certain number of microinches of strain. Calibration curves for the load-cell channels were obtained by plotting strain versus trace deflection. Calibration curves for the displacement transducers were obtained by plotting displacement versus trace deflection.

Activation of the loading system caused the plates to penetrate into the backfill. During penetration, the output from each channel was recorded. A typical example of the output is shown in Fig. 35.

The methods used for measuring the in situ density of the backfill are discussed in Chapter V. Prior to excavation of the backfill material, each recording channel was recalibrated to check the calibration stability. In all cases, the two sets of calibration curves were linear and in close agreement.

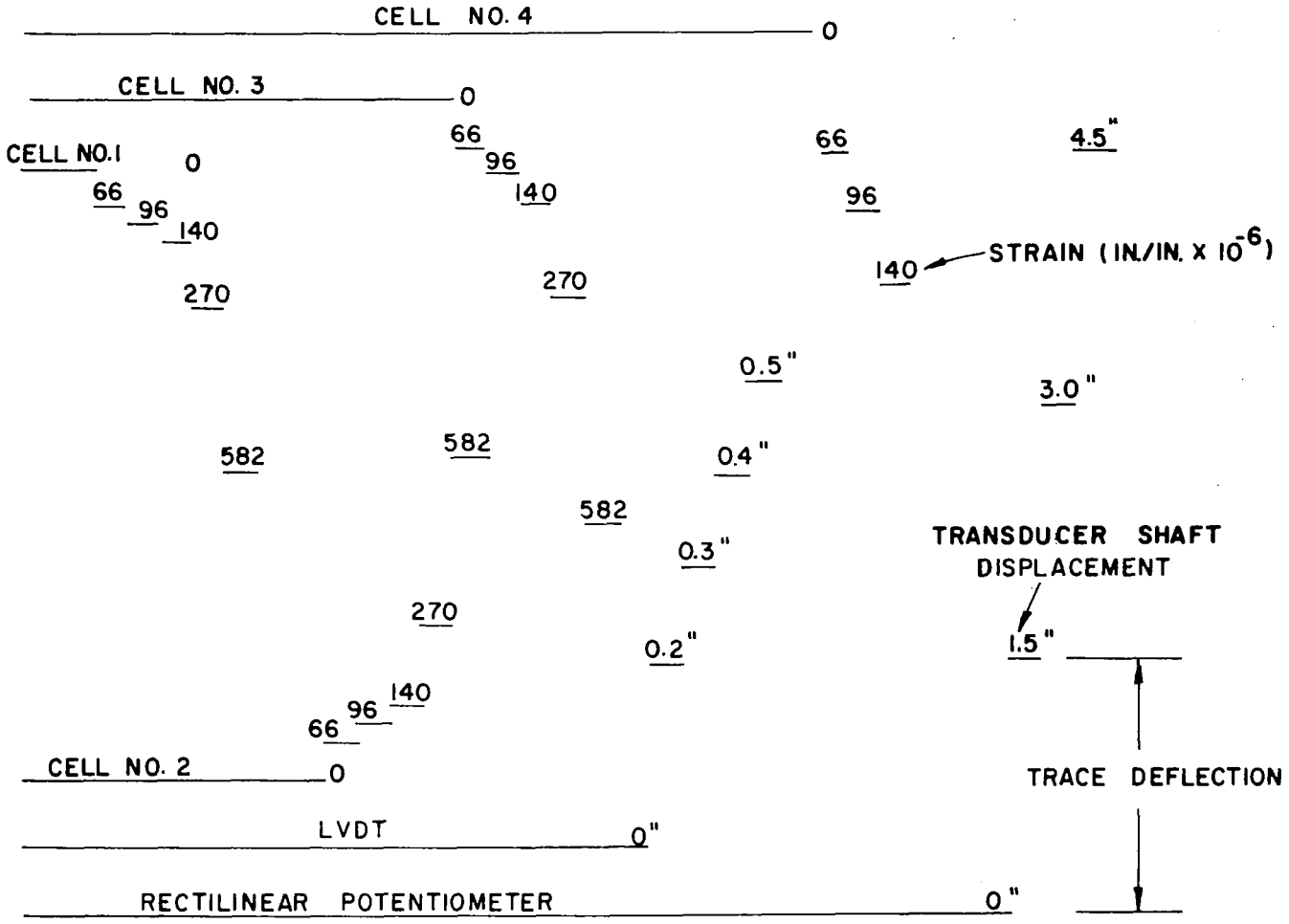

FIG.34 TYPICAL CALIBRATION DATA OUTPUT - PHASE II

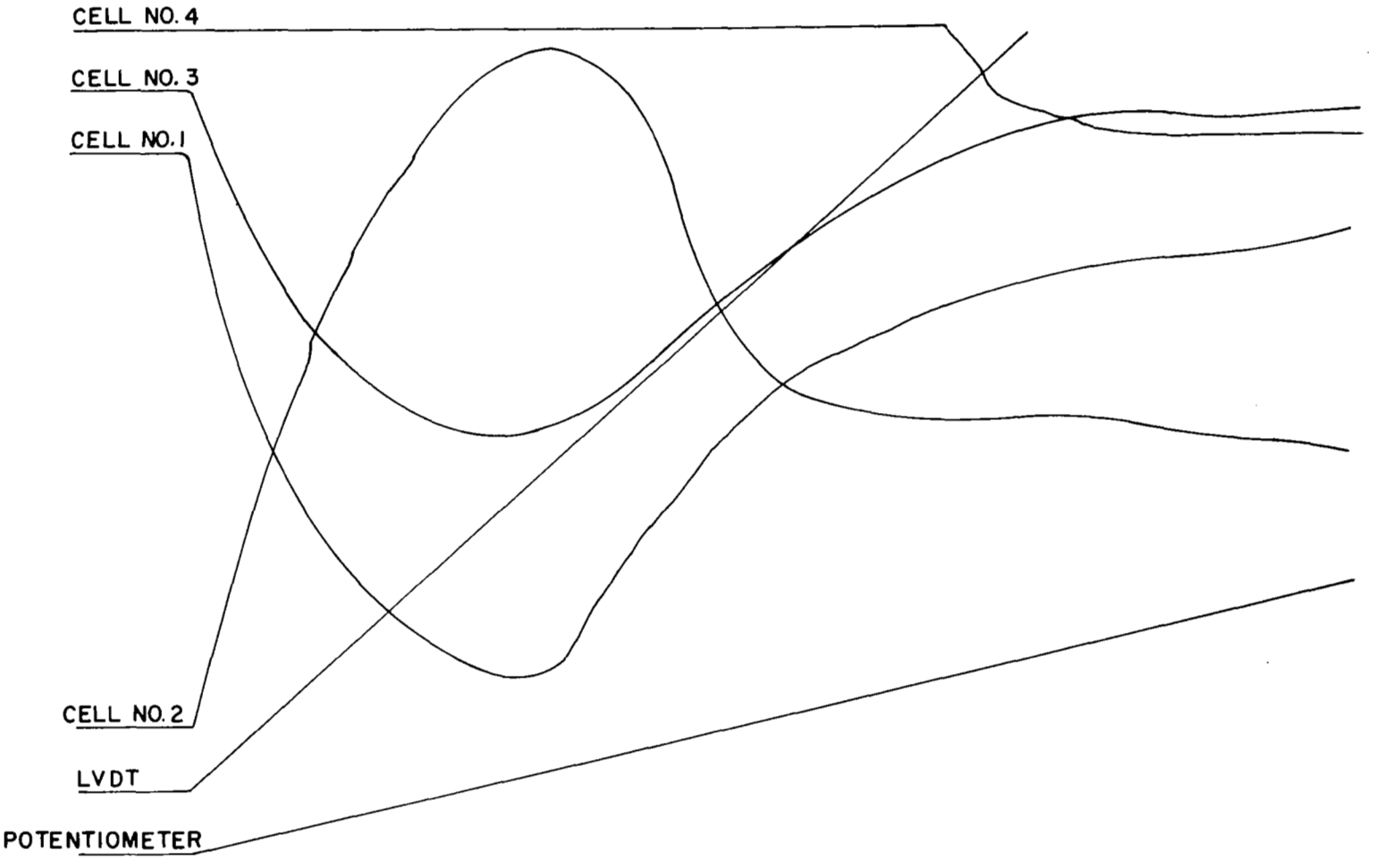

FIG. 35 TYPICAL LOAD CELL AND DISPLACEMENT TRANSDUCER OUTPUT – PHASE II

PHASE II DATA REDUCTION

The reduction and manipulation of the raw data was accomplished using a computer program which was similar to the program utilized during Phase I. The basic differences in the programs were the methods used to calculate the magnitude of load carried by each load cell and the amount of penetration of the plates. In the Phase II program loads were calculated using

$$\text{Horizontal Load} = (TD)\ (SC)\ (SL) \tag{12}$$

where,

TD = Trace Deflection (in.),

SC = Slope of calibration curve for load cells; obtained from oscillograph chart (microinches/in. of trace deflection),

SL = Slope of calibration curve for load cells (lbs/microinch).

The penetrations were calculated using

$$\text{Penetration} = (TD)\ (SC) \tag{13}$$

where,

TD = Trace Deflection (in.),

SC = Slope of calibration curve for displacement transducers; obtained from oscillograph chart (in./in. of trace deflection).

PHASE III PROCEDURE

The basic procedures necessary for the completion of a test during Phase III were similar to those outlined for Phase II. During Phase III, the locations at which the failure surfaces intersected the surface of the backfill were not recorded.

The depth below the backfill surface at which the models penetrated was varied by changing the elevation of the backfill surface. Tests were conducted with the surface of the sand located at elevations of 1, 2, 3, and 5 times the base radius of each model. The elevation of the surface of the sand was measured with reference to the lower edge of the base of each model. A sketch illustrating the elevation of the sand surface with reference to the position of a model is shown in Fig. 36.

PHASE III DATA REDUCTION

A computer program was used for converting into usable information the trace deflection readings which were taken off the oscillograph record. The usable information consisted of:

(1) Model penetration,

(2) Horizontal soil reaction on the model (R_H),

(3) Resultant vertical soil reaction on the model (R_V).

The horizontal soil reaction R_H and penetration values were calculated using Eqs 12 and 13. The bending moment, caused by the resultant vertical soil reaction R_V, was calculated using

$$\text{Bending Moment} = \left[(\text{TD})\ (\text{SC}) \pm \text{Load/SR4} \right] (\text{SBM}) \qquad (14)$$

where

TD = Trace Deflection (in.),

SC = Slope of calibration curve for load cell; obtained from oscillograph chart (microinches/in. of trace deflection),

Load = Horizontal Load as determined by Eq 12 (lbs),

SR4 = Slope of calibration curve for SR-4 strain gage when the rod is subjected to axial compression (lbs/microinch),

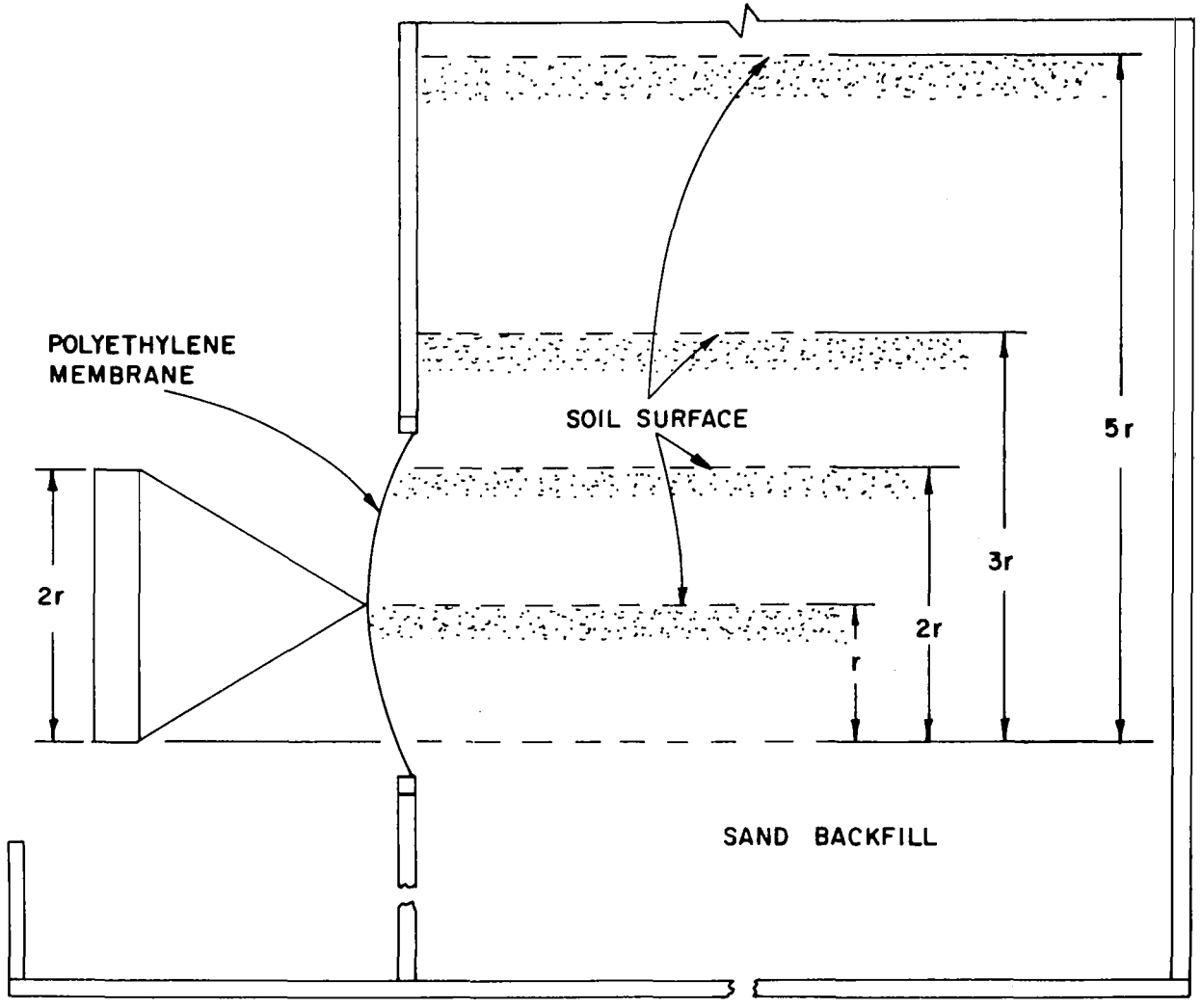

FIG.36 SKETCH SHOWING THE DEPTHS OF SOIL USED IN MODEL TESTS - PHASE III

SBM = Slope of calibration curve for SR-4 strain gage when the rod is subjected to bending (in.-lbs/microinch).

The minus sign in Eq 14 is used when the bending moment is calculated using the output from Gage 1 (Fig. 37) and the plus sign is used when the output from Gage 3 is utilized. The resultant vertical soil reaction was calculated using

$$R_V = \frac{(\text{Bending Moment})_1 + (\text{Bending Moment})_3}{2D} \qquad (15)$$

where,

$(\text{Bending Moment})_1$ = Bending moment calculated using output from Gage 1,

$(\text{Bending Moment})_3$ = Bending moment calculated using output from Gage 3,

D = Distance between SR-4 strain gages and resultant vertical soil reaction.

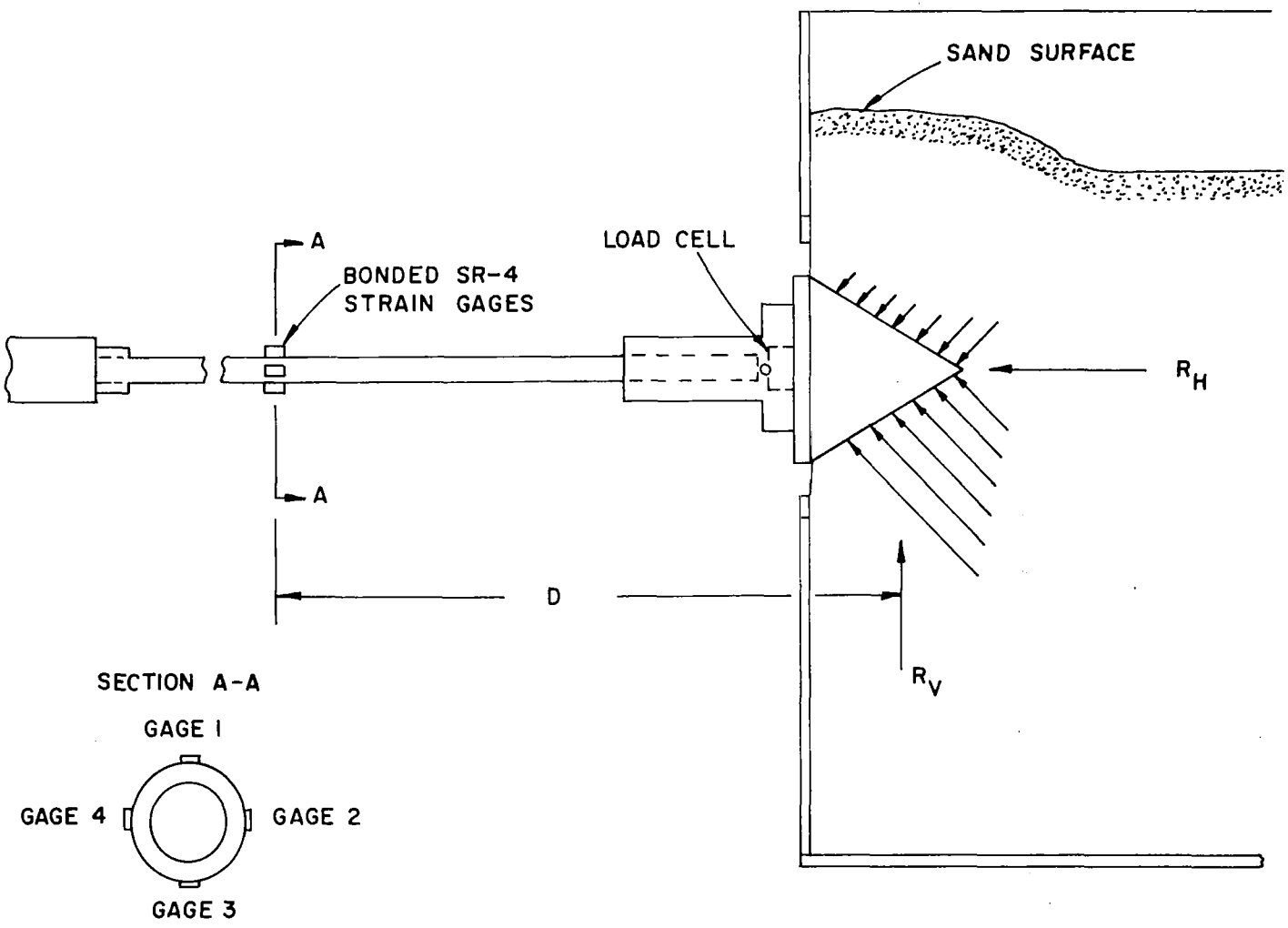

FIG. 37 SKETCH SHOWING THE NOTATION USED IN CALCULATING SOIL REACTIONS – PHASE III

CHAPTER V

SOIL PROPERTIES

Throughout the investigation one soil type was used for testing purposes. A sand was chosen, rather than a silt or clay, because a soil bed composed of sand is much easier to prepare and at the same time maintain a close control on the significant engineering properties.

The soil was a clean, air-dry Colorado River sand. The sand was obtained locally from Capitol Aggregates, Inc. It is light reddish brown in color and composed of subangular grains. A mechanical analysis was performed to determine the grain size distribution and the sand was found to be of a medium, uniform nature. A semilogarithmic plot of the grain size distribution curve is shown in Fig. 38.

The maximum and minimum dry densities were found to be 102.5 and 88.0 pcf, respectively. Using a value of 2.67 for the specific gravity of the sand, the maximum and minimum void ratios were calculated to be 0.94 and 0.63, respectively. The specific gravity value was obtained from the previous work of Ghazzaly[4].

Angle of Internal Friction Measurement

Standard triaxial compression tests were conducted on 1.4 in. dia samples to determine the angle of internal friction. Each of the samples was prepared with a height-diameter ratio of 2.0 or greater. The tests were performed with the sand in its densest and loosest states. The triaxial test results are shown in Table 1.

The desired density for each sample was obtained by using two set procedures.

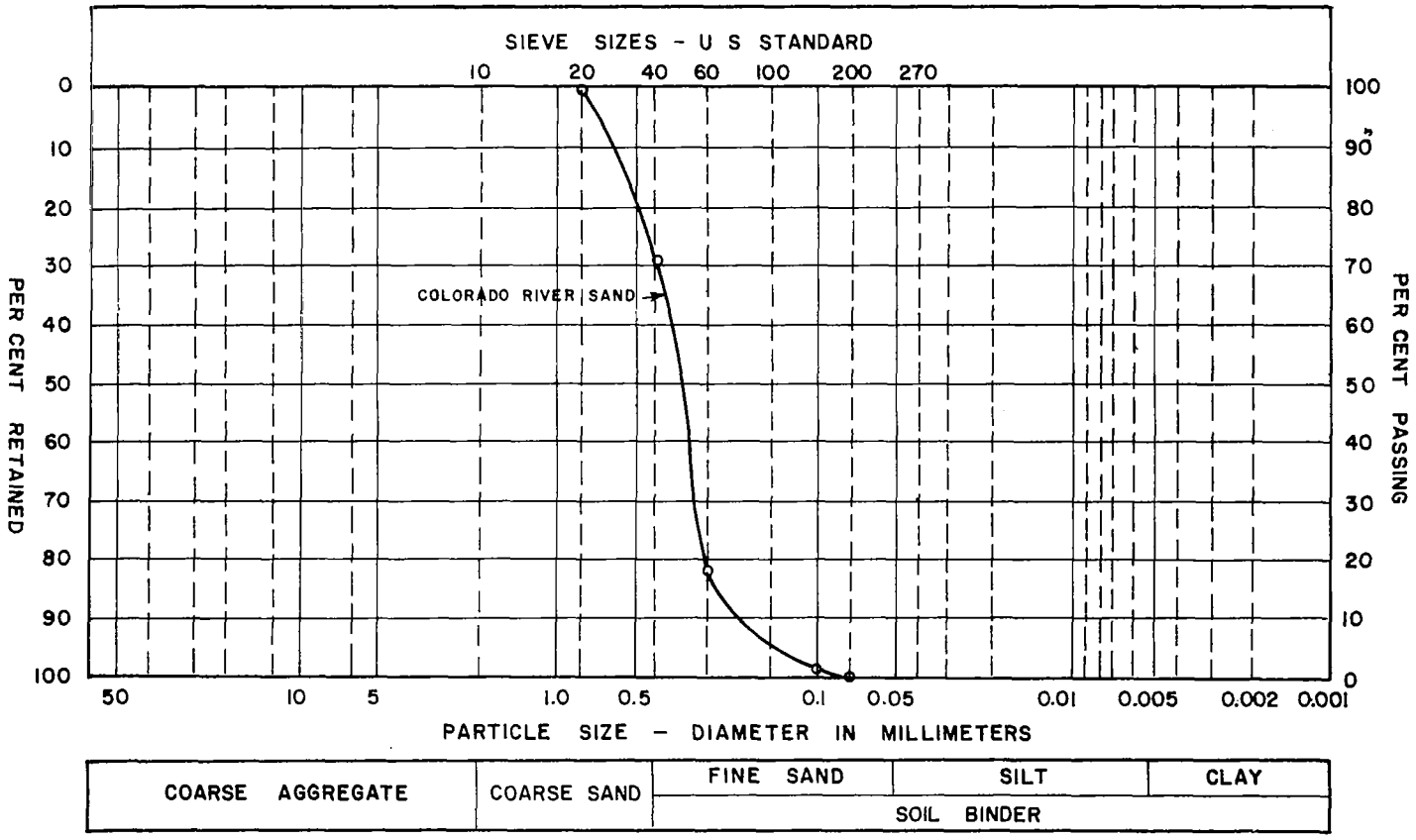

FIG.38 MECHANICAL ANALYSIS GRAIN SIZE ACCUMULATIVE CURVE

TABLE 1

TRIAXIAL TEST RESULTS

Major Principal Stress σ_1 (psi)	Minor Principal Stress σ_3 (psi)	Angle of Internal Friction ϕ (Degrees)	Average Angle of Internal Friction ϕ (Degrees)	Density γ (pcf)
40.0	5.0	51.2	51.7	102.5
10.7	1.26	52.2		102.5
23.0	5.0	40.1	39.5	88.0
5.5	1.26	38.8		88.0

The first procedure consisted of pouring the sand through a small funnel into a standard removable mold that was lined with a thin rubber membrane. By this procedure, samples were prepared at the minimum dry density. The remaining steps in preparing the apparatus for a triaxial test were performed in accordance with procedures recommended by Dawson[3].

The maximum density was obtained by pouring the sand into the mold in five equal height layers. The triaxial cell base was placed on a small table vibrator and each successive layer was vibrated for 2 minutes. The soil was also tamped during vibration. The remaining steps were performed in accordance with Dawson's[3] recommendations.

Angle of Wall Friction

Phase I and Phase II testing consisted of penetrating flat plates into Colorado River sand in a horizontal direction. As the plates penetrated into the soil a frictional force was developed at the soil-plate interface. This frictional force has previously been defined in Chapter I as the vertical soil response. The developed angle of friction, or angle of wall friction as it is more commonly called, can be calculated by taking the arctangent of the ratio of the vertical soil force to the horizontal soil force.

The maximum angle of wall friction that could be developed at the soil-plate interface was measured using a direct shear box. The shear box consisted of a top and bottom frame. The inside dimensions of each frame were 1.0 in. deep by 2.36 in. wide by 2.36 in. long. The bottom frame was partially filled with sand and wax. This material provided a firm base for a 0.125 in. thick steel plate insert which occupied the remaining portion of the section. The top half of this box was filled with Colorado River sand. The method of sand placement was similar to that used in preparing samples for the triaxial compression tests.

Several tests were performed in which the applied normal stress was varied over the range of values that existed in the flat-plate earth-pressure tests. The maximum shear stress corresponding to each applied normal stress is plotted in Fig. 39. The slopes of the straight lines passing through the plotted points represent the maximum coefficients of friction developed at the steel-sand interface.

Density Determination

The accurate determination of the *in situ* density of a dry cohesionless soil is a difficult task. Any method that requires the use of sampling tubes involves a disturbance effect which alters the density of the soil. Other techniques that do not involve sampling tubes are costly and time consuming.

Phase I Density

During the first phase of testing the *in situ* soil density was determined by an indirect method. This method involved the use of a standard proctor mold which had a volume of one-thirtieth of a cubic foot. To obtain a measure of the minimum density, the sand was poured through a funnel whose spout was maintained 2 in. above the surface of the sand in the mold. This method of placement is identical to the procedure used in backfilling the sandbox prior to each test conducted with the sand at its minimum density. The unit density of the sand in the box was assumed to be equal to the weight of the sand in the mold multiplied by thirty. The values of unit density obtained using this procedure varied between 86 and 90 pcf. A value of 88 pcf was chosen to represent the minimum density of the sand in the box.

The maximum density was also estimated using a proctor mold. The sand was placed in the mold in five equal height layers. As the sand was

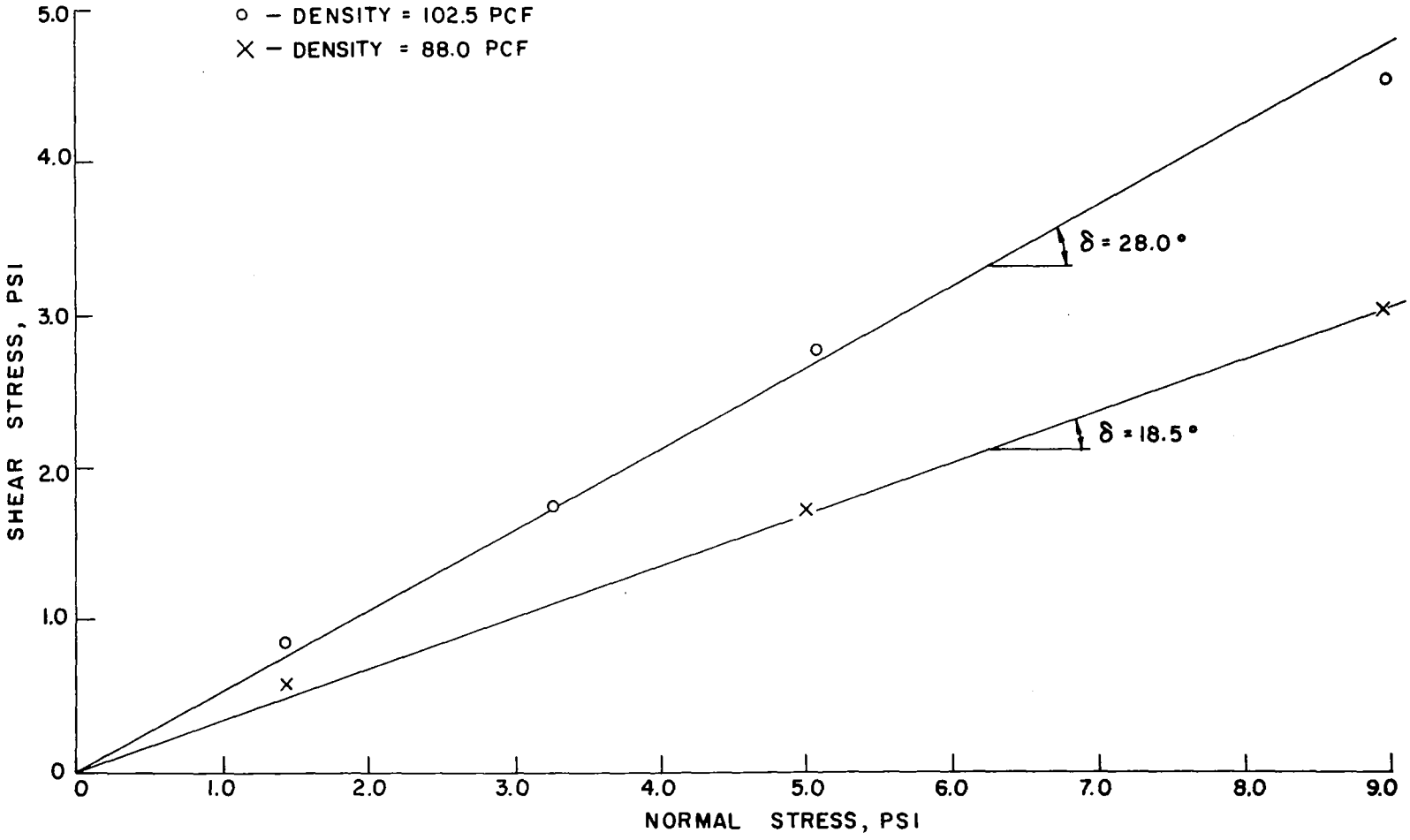

FIG.39 ANGLES OF SLIDING FRICTION FOR COLORADO RIVER SAND ON STEEL

placed in the mold each successive layer was vibrated for 2 min using a table vibrator. This method of placement is not identical to the procedure used in backfilling the sandbox. Prior to each test the box was backfilled by placing the sand in layers approximately 3 in. in height. Each successive layer was vibrated with a hand concrete vibrator for approximately 10 minutes. The results from the proctor mold determinations revealed that the maximum density varied between 102 and 103 pcf. A value of 102.5 pcf was chosen to represent the maximum density of the sand in the box.

Phase II Density

Two methods were used to determine the in situ soil bed density during the second phase of testing.

The first method consisted of weighing the sand placed in the sandbox during backfilling. The average density was then calculated by dividing the total weight of sand in the box by the volume that it occupied. The backfilling procedures used in this phase of testing were identical to the procedures used in Phase I. The results from this method showed the average density to be approximately 102.5 pcf when the sand was vibrated during backfilling. Using the same method the average density of the backfill was found to be approximately 88.0 pcf when the sand was placed using a funnel.

The second method utilized sampling tubes to determine the in situ soil density. After the completion of each plate-penetration test four density samples were taken using brass sampling tubes that were 6 in. in length and had inside and outside diameters of 1.4 and 1.5 in. respectively. Figure 31 on p. 47 shows the sampling tubes used in this investigation. The locations at which the samples were taken are shown in Fig. 40. The sampling locations marked 1 and 2 are in a zone that is not affected by the penetration of the plates and therefore these samples provide results that

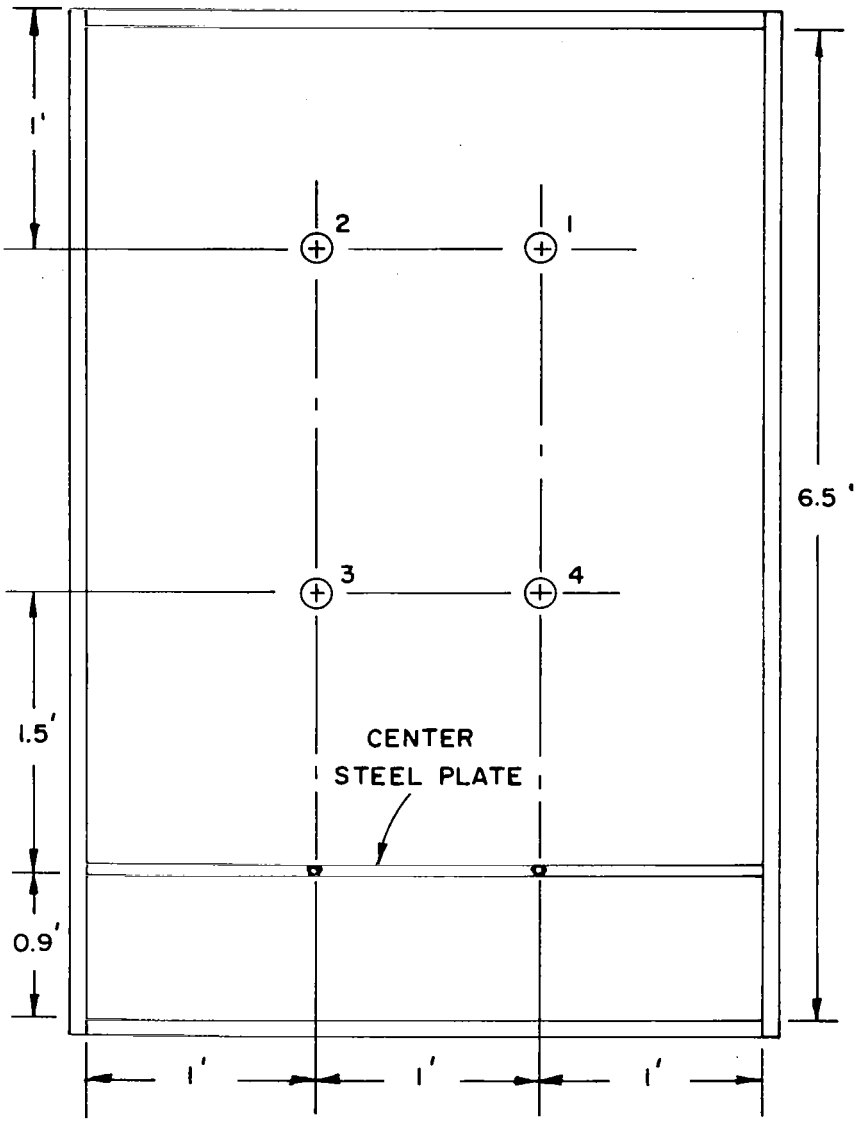

FIG.40 PLAN VIEW OF THE SANDBOX SHOWING THE LOCATIONS AT WHICH DENSITY SAMPLES WERE TAKEN - PHASE II

can be used in determining the pre-test soil density. The samples taken from locations 3 and 4 provide data that can be used in the determination of the post-test soil density within the failure wedge.

As stated earlier, the use of sampling tubes causes disturbances in the soil which tend to alter the density. Several tests were performed to evaluate the effect of sampling tube disturbances on the in situ soil density. Each test consisted of preparing a soil sample in a proctor mold either by using a funnel or by vibrating the sample. The density of the sample was then calculated. A sampling tube was then pushed into the soil sample and the density of the soil within the tube was calculated. The difference between the density of the soil in the proctor mold and the sampling tube represents the change in density due to the sampling procedure.

The results obtained from the tests described above show the change in soil density to be approximately 3.0 pcf when the in situ density is 88.0 pcf and 2.0 pcf when the in situ is 102.5 pcf. The tube disturbance caused the sand in the loose state (88.0 pcf) to become denser and the sand in the dense state (102.5 pcf) to become less dense.

Phase III Density

During the third phase of testing, sampling tubes were used to measure the in situ density of the soil bed. The sampling tubes were the same as those used during Phase II. Three samples were taken at the completion of each test. The samples were taken in that portion of the soil bed that was not affected by the penetration of the cones and spherical segments and they therefore represented the pre-test in situ soil density.

CHAPTER VI

PHASE I TEST RESULTS AND DISCUSSION

The main purpose of Phase I was to evaluate the performance of the testing apparatus. The test setup was designed to model the classical plane-strain earth-pressure problem. The earth pressure-penetration curves that were obtained from the load-cell data were used as basis for evaluating the apparatus.

EARTH-PRESSURE DEVELOPMENT

Fourteen passive earth-pressure tests were conducted. In each test the penetration of the wall was held at a constant rate of 0.00278 ips. Four tests were conducted with the backfill in a loose state and 10 tests were performed with the backfill in a dense state. Passive earth pressure as a function of wall penetration and backfill density is plotted in Fig. 41 for 2 tests. Terzaghi[10] observed, that for wall penetrations less than or equal to the penetration necessary to develop the maximum earth pressure, the earth pressure-penetartion curve was parabolic in shape. A parabola was fitted through the first and last data point of Test L1 and is represented by the solid line which closely fits the lower set of observations shown in Fig. 41. A parabola was also fitted through the first data point and the maximum measured earth-pressure point for the upper curve. The slope of the parabola, dY/dP_p, is equal to zero at the first point on each curve. The figure also demonstrates the large influence the density of the backfill has upon the shape of the earth pressure-penetration curve. The curves are similar in shape to those obtained by plotting stress-strain values from triaxial compression tests conducted on loose and dense sands.

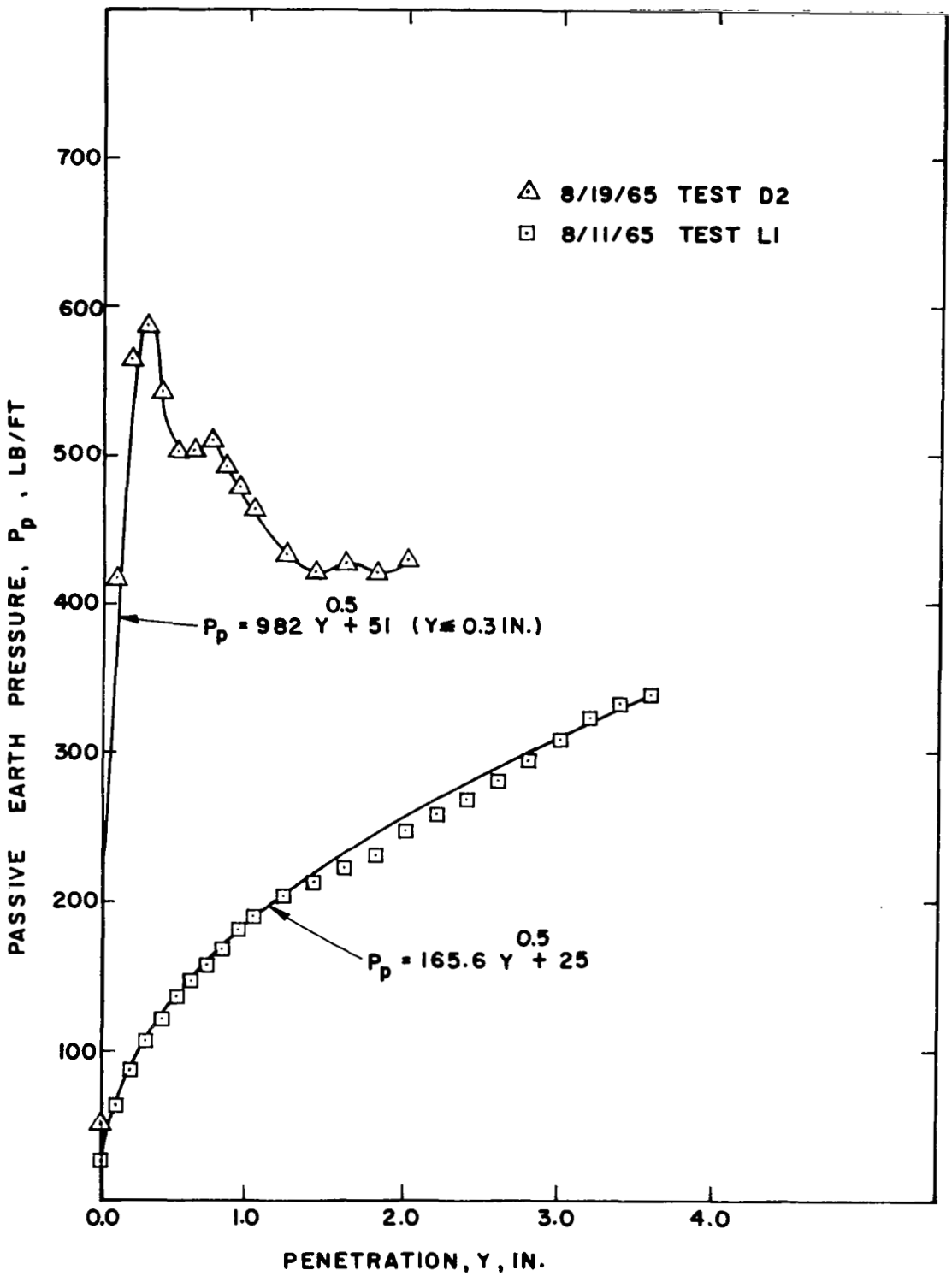

FIG. 41 PASSIVE EARTH PRESSURE VERSUS PENETRATION

WALL FRICTION ANALYSIS

The main purpose of this series of tests was to determine how well the test setup approximated plane-strain loading conditions. One method of evaluating the performance of the apparatus is to compare the measured results with those predicted by existing plane-strain earth-pressure theory. As a comparison, Coulomb's equation (7) was used to calculate passive earth pressure. One of the variables appearing in this equation is δ, the angle of wall friction.

Test data expressing the development of the angle of friction at the soil-wall interface is plotted in Figs. 42 through 44. Average curves have been drawn through the data points in Figs. 42 and 43 which indicate a definite trend in the development of wall friction. The wall friction data from the loose tests (Fig. 44) was much more erratic than that for the dense tests and therefore no pronounced trend was found to exist. The data points represent only a portion of the angle of friction developed at the soil-wall interface. The apparatus was designed so the frictional force at the soil-wall interface minus the frictional force developed between the wall and the three load cells was measured.

Several tests were performed to determine the angle of friction between the 3 load-cell buttons and the steel plate. The angle of friction was observed to be 5.9 degrees for the entire range of horizontal test-pressures.

Although the curves for dense backfill tests (Figs. 42 and 43) do have a similarity in shape, it can be seen that for a given penetration the differences in the indicated values of wall friction are great. These differences can largely be attributed to the inadequate method used to restrain the loading frame from moving in a vertical direction. A wall friction-penetration curve was constructed for the dense backfill case assuming the early portion

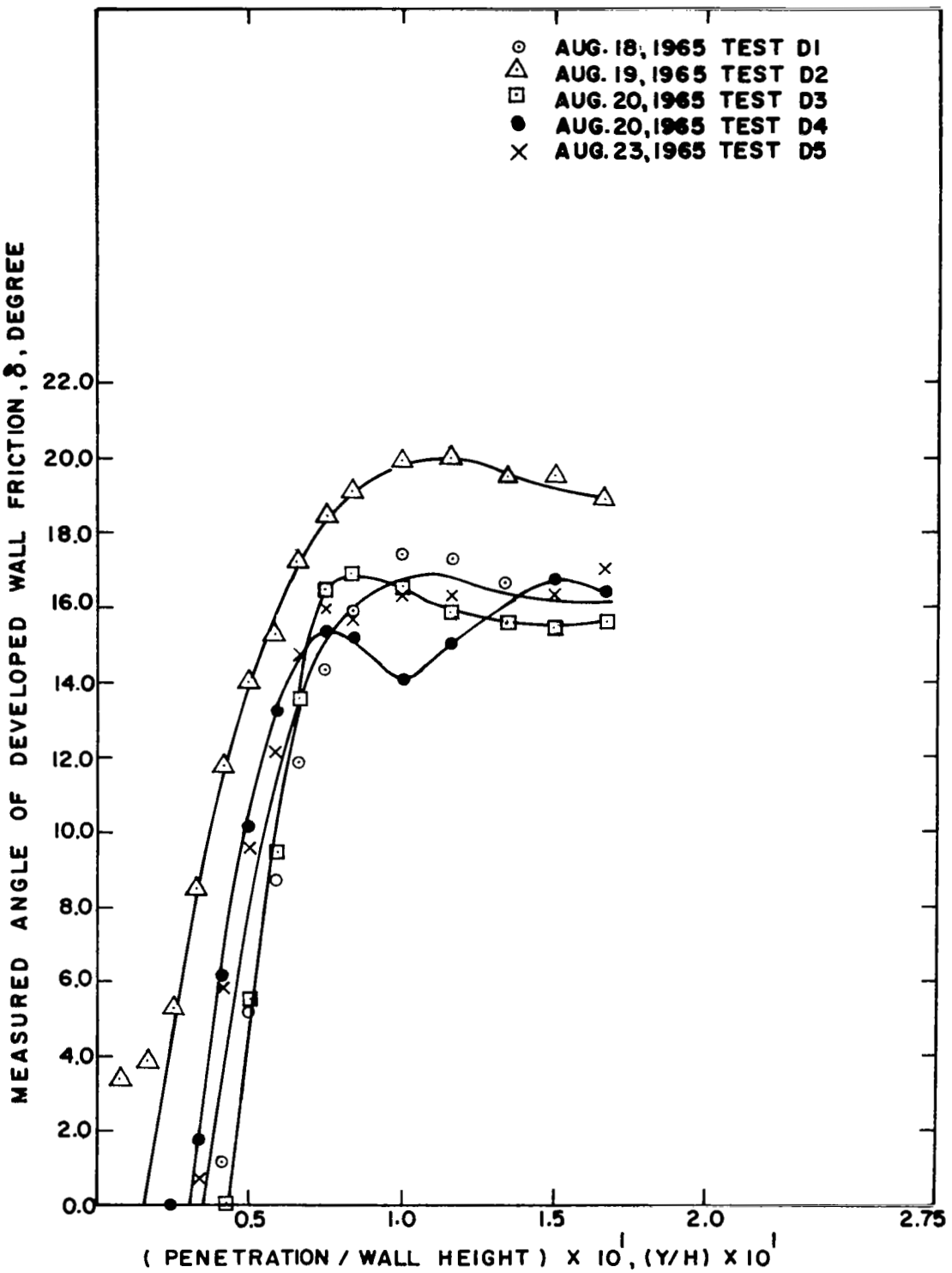

FIG.42 WALL FRICTION DEVELOPMENT CURVES—DENSE CASE

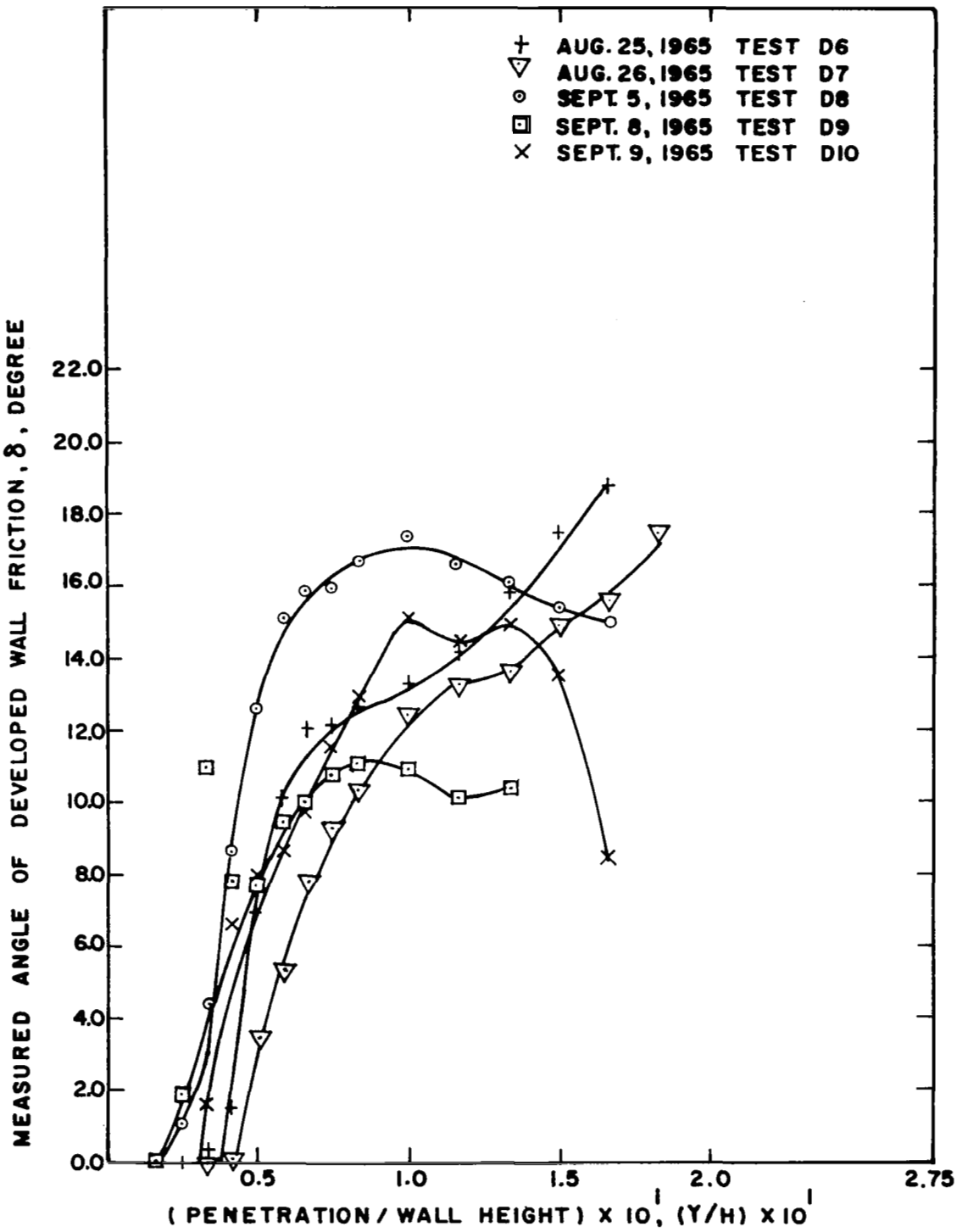

FIG. 43 WALL FRICTION DEVELOPMENT CURVES - DENSE CASE

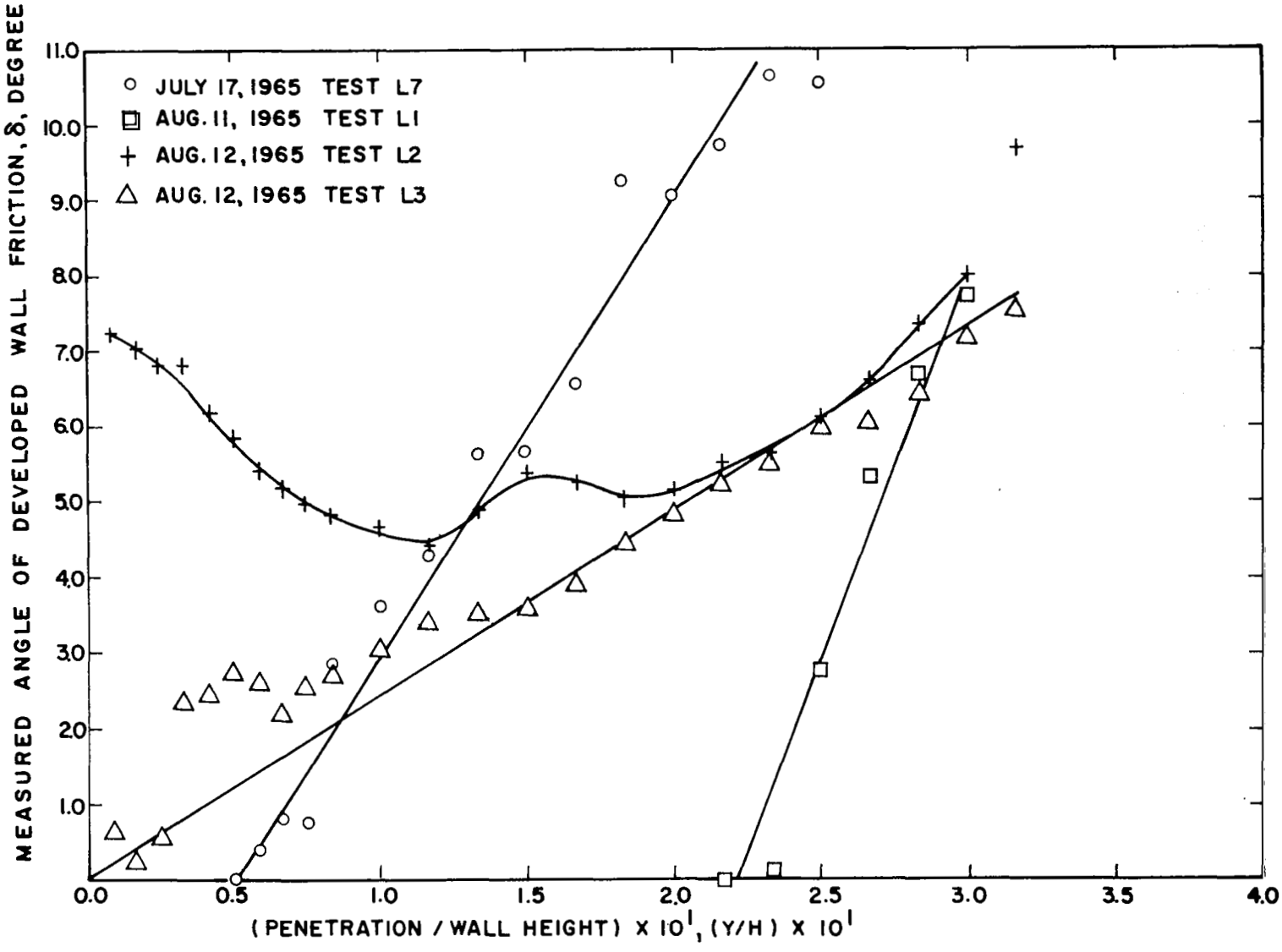

FIG. 44 WALL FRICTION DEVELOPMENT CURVES – LOOSE CASE

of the curve could be represented by a straight line, the intermediate portion by a parabola, and the final portion by another straight line. A bilinear curve was used to represent the development of wall friction when the backfill was in a loose state. The configurations of the constructed curves are illustrated in Fig. 45.

The test data in Figs. 42 through 44 was used as a basis for developing the constructed wall friction-penetration curve. Dense test data indicates that for developed angles of wall friction less than 13 degrees the data points may be closely approximated by a straight line. Using a straight line approximation, the average slope was found to be 444 degrees/in. penetration/in. of wall height.

It can be seen from Fig. 45 that the initial straight line portion of the constructed curve extends to a wall friction development of 18.9 degrees. The value of 18.9 degrees was obtained by adding the 5.9 degree angle of friction, which was developed between the load cells and the plate, to the 13 degrees that was actually measured by the single load cell. This, of course, is an approximation since the tangent of the sum of two quantities is not equal to the sum of the tangents of each quantity. However, the error created by this approximation was not significant in this investigation.

Figure 45 shows that the slope of the early portion of the curve has been reduced from 444 to 360 degrees/in. penetration/in. of wall height. The slope was reduced so the location of the parabolic section would agree closer with the position observed from the test results. The equation for the parabolic section was derived using three sets of conditions: (1) the beginning point on the curve is (0.0525, 18.9 degrees), (2) the slope of the parabola at the beginning point is 360 degrees/in. penetration/in. of wall ht., and (3) the final point on the parabola is (0.0858, 22.9 degrees). The ultimate value of

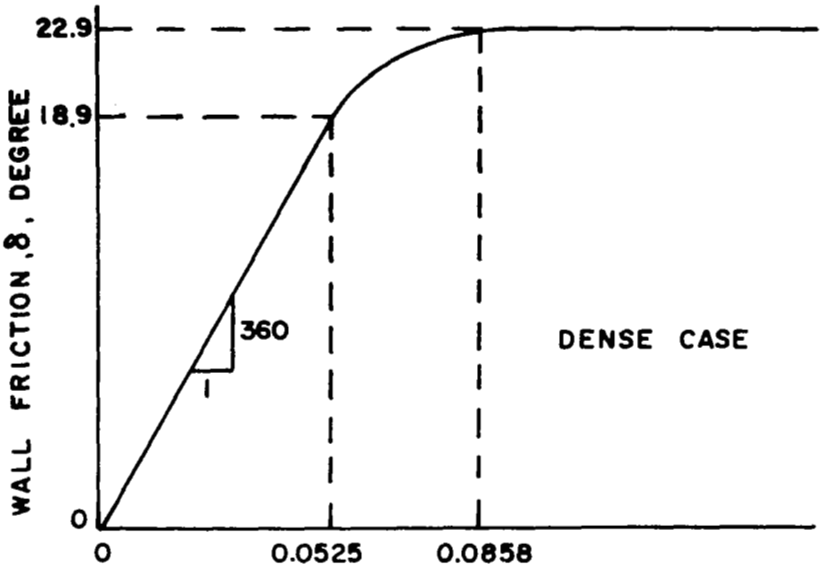

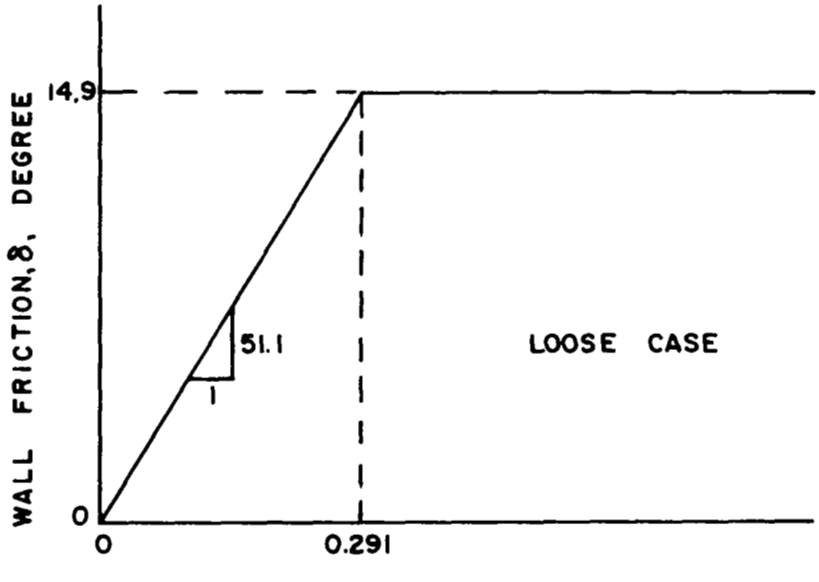

FIG. 45 CONSTRUCTED WALL FRICTION CURVES FOR LOOSE AND DENSE CASES

wall friction was obtained by adding 5.9 degrees to an average test value of 17 degrees. The length of the parabolic section and the value of ultimate wall friction were determined from the test data shown in Figs. 42 and 43.

The development of wall friction was more erratic when the backfill was placed in a loose state. The scatter in the test data prevented the rational development of a constructed wall friction-penetration curve.

COMPARISON BETWEEN MEASURED AND CALCULATED EARTH-PRESSURE FACTORS

Table 2 lists some of the results used in evaluating the performance of the test apparatus. The table shows that the loose test values of measured and calculated earth-pressure factors agree well, while the dense test agreement is poor in most cases. In every instance the calculated earth-pressure factor is greater than the measured quantity. The measured earth-pressure factor is expressed by Eq 24 on p. 170. The calculated earth-pressure factors were found using Eqs 26 and 24. The developed angle of wall friction corresponding to the dimensionless ratio, Penetration/Wall Height, listed in Table 2 was found using the appropriate curve in Fig. 45, the choice of curve depending upon the density of the backfill. The developed angle of internal friction that corresponded to the maximum measured earth-pressure factor was calculated using Coulomb's Eq 28 appearing on p.172.

The amount of wall penetration required to develop the maximum measured earth-pressure factors for the dense tests varied greatly, as can be seen from the dimensionless term, Penetration/Wall Height in Table 2. The wide variation of wall penetration necessary to cause failure was created by the inadequate method used to restrain the loading frame from moving in a vertical direction. The wooden vertical restraint and its connections to the sandbox were rigid enough to keep the loading frame moving in a horizontal plane when the backfill was in a loose state. However, after the completion of several dense tests the wooden vertical restraint shifted upward. This movement

TABLE 2

COMPARISON BETWEEN MAXIMUM MEASURED EARTH-PRESSURE FACTORS

AND CALCULATED EARTH-PRESSURE FACTORS

Test Identification	Penet./Ht. of Wall Y/H (in./in.)	Earth-Pressure Factors		Ratio Calc./ Meas.	Developed Angle		Density γ (pcf)
		Measured $K_p/\cos\delta$	Calculated $K_p/\cos\delta$		Internal Friction ϕ (Degrees)	Wall Friction δ (Degrees)	
7/17/65 - L7	0.250	7.7	7.7	1.0	39.4	12.8	88.0
8/11/65 - L1	0.300	7.7	8.6	1.1	37.8	14.9	88.0
8/12/65 - L2	0.317	7.1	8.6	1.2	36.3	14.9	88.0
8/12/65 - L3	0.317	7.0	8.6	1.2	36.3	14.9	88.0
8/18/65 - D1	0.0250	12.1	13.9	1.2	49.7	9.0	102.5
8/19/65 - D2	0.0250	11.5	13.9	1.2	49.0	9.0	102.5
8/20/65 - D3	0.133	11.0	47.6	4.3	36.7	22.9	102.5
8/20/65 - D4	0.100	12.1	47.6	3.9	37.9	22.9	102.5
8/23/65 - D5	0.0833	10.9	46.4	4.3	36.7	22.7	102.5
8/25/65 - D6	0.0167	11.4	11.5	1.0	51.5	6.0	102.5
8/26/65 - D7	0.0250	11.7	13.9	1.2	49.2	9.0	102.5
9/5/65 - D8	0.0250	11.4	13.9	1.2	48.8	9.0	102.5
9/8/65 - D9	0.0500	14.5	27.9	1.9	44.4	18.0	102.5
9/9/65 - D10	0.0500	13.6	27.9	2.1	43.5	18.0	102.5

caused a gap to occur between the loading frame and vertical restraint. The gap permitted the wall and loading frame to move vertically, thereby reducing the development of wall friction and horizontal pressures during the early stages of wall penetration. The vertical movement caused the maximum earth pressure to develop at values of wall penetration much larger than those normally occurring under the condition of no vertical movement.

Although the penetration necessary to develop the maximum measured earth-pressure factor varied greatly between tests, the maximum measured earth-pressure factor remained essentially constant. Two offsetting variables, δ, and ϕ, are responsible for the development of nearly constant earth-pressure factors. Relatively small wall displacements are required for development of the maximum angle of internal friction. When displacements larger than those necessary to develop the maximum angle of internal friction occur, the value of internal friction decreases because the density of the backfill material decreases as it undergoes increased shearing strains. As can be seen from Figs. 42 through 44, the angle of wall friction increases with wall penetration.

Five of the tests tabulated in Table 2 have calculated earth-pressure factors much greater than the measured earth-pressure factors. The angle of wall friction that developed in these cases was approximately 20 degrees. As stated previously in Chapter II, the error associated with the plane failure surface assumption may be as large as 50 per cent in cases where the angle of developed wall friction is large. The value of the calculated earth-pressure factor is also based upon the maximum developed value of internal friction ϕ as measured from a triaxial test and, for reasons explained previously, the maximum developed earth pressure and maximum developed angle of internal friction may not occur at the same instant.

The development of the earth-pressure factor ($K_p/\cos \delta$) as the wall penetrated into the backfill is shown in Figs. 46 through 49. Only the values of $K_p/\cos \delta$ up to and including the maximum value have been plotted for the dense tests. The data obtained from the loose tests is less erratic than that obtained from the dense tests.

DEVELOPED ANGLE OF INTERNAL FRICTION

The development of internal friction as the wall penetrated into the backfill is shown in Fig. 50 and 51. The curves for the loose and dense tests are similar in shape to the passive earth-pressure curves that are shown in Fig. 41. The angle of developed internal friction was calculated using Coulomb's Eq 28 on p. 172.

CENTER OF PRESSURE LOCATIONS

The distribution of horizontal soil pressure on a semi-infinite retaining wall depends upon the method in which the backfill was placed and also upon the amount and type of wall movement. If a wall moves towards a cohesionless backfill by tilting around its inner lower edge the pressure distribution is approximately triangular. The testing apparatus was designed so the wall moved only in a horizontal direction. Therefore, it is expected that the pressure distribution during the early stages of penetration may be something other than triangular.

The variation in the location of the center of pressure as the wall penetrated into loose backfill is shown in Fig. 52. Although the at-rest locations of the center of pressures differ, the agreement between tests is good after a small amount of wall penetration has taken place. The average location of the center of pressure throughout the four loose tests is approximately 0.39H above the base of the wall.

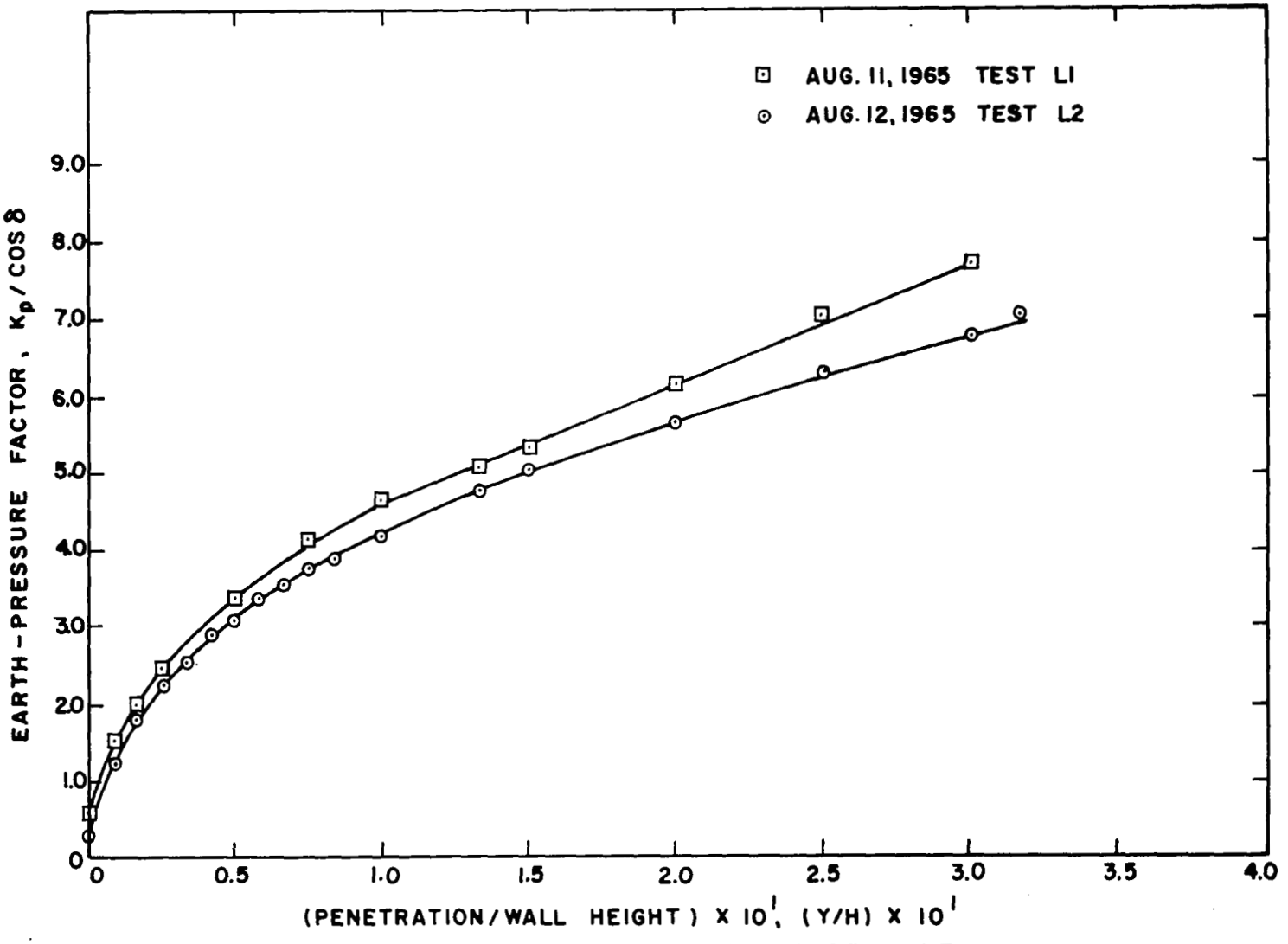

FIG. 46 EARTH-PRESSURE FACTOR CURVES – LOOSE CASE

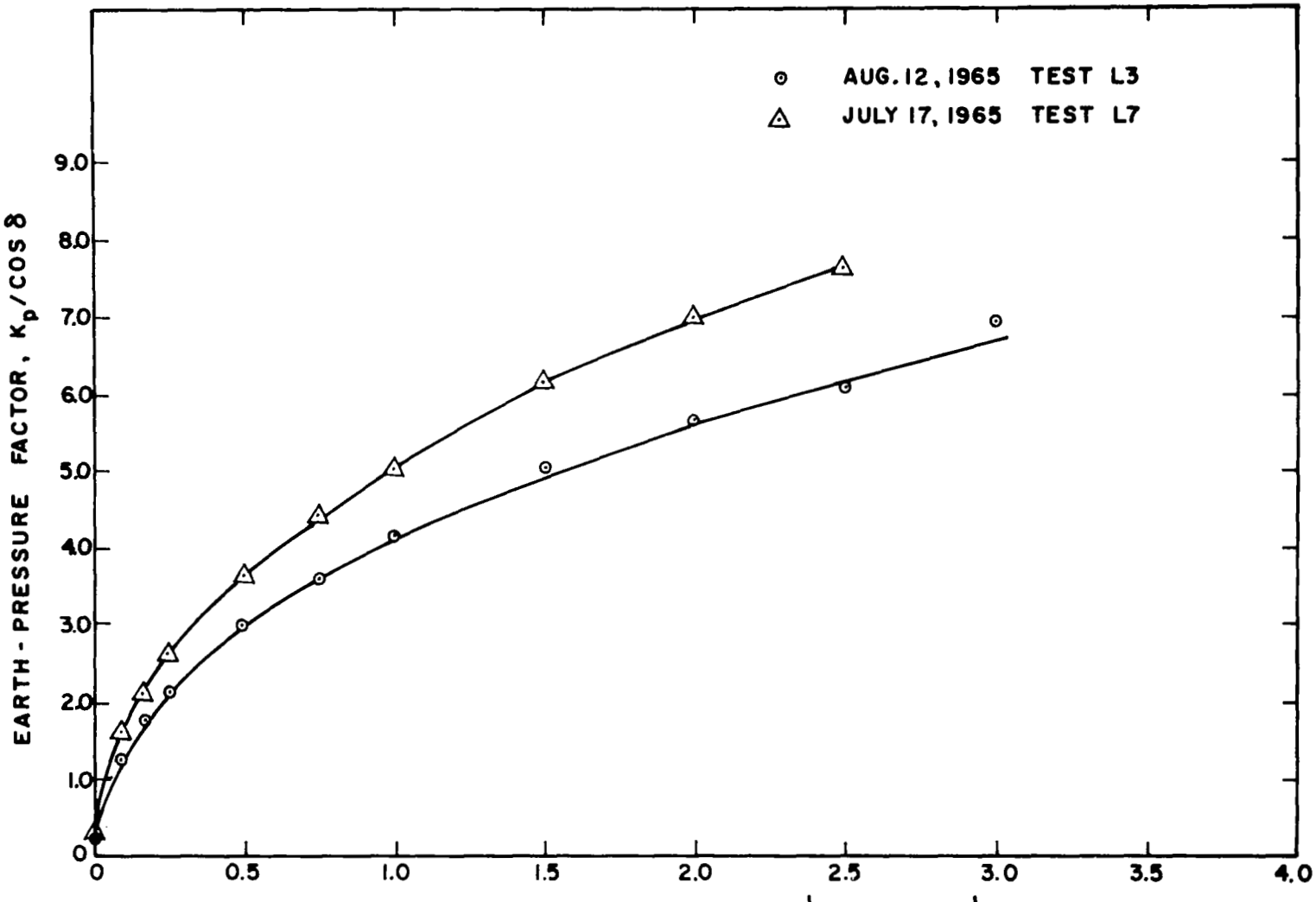

FIG. 47 EARTH - PRESSURE FACTOR CURVES — LOOSE CASE

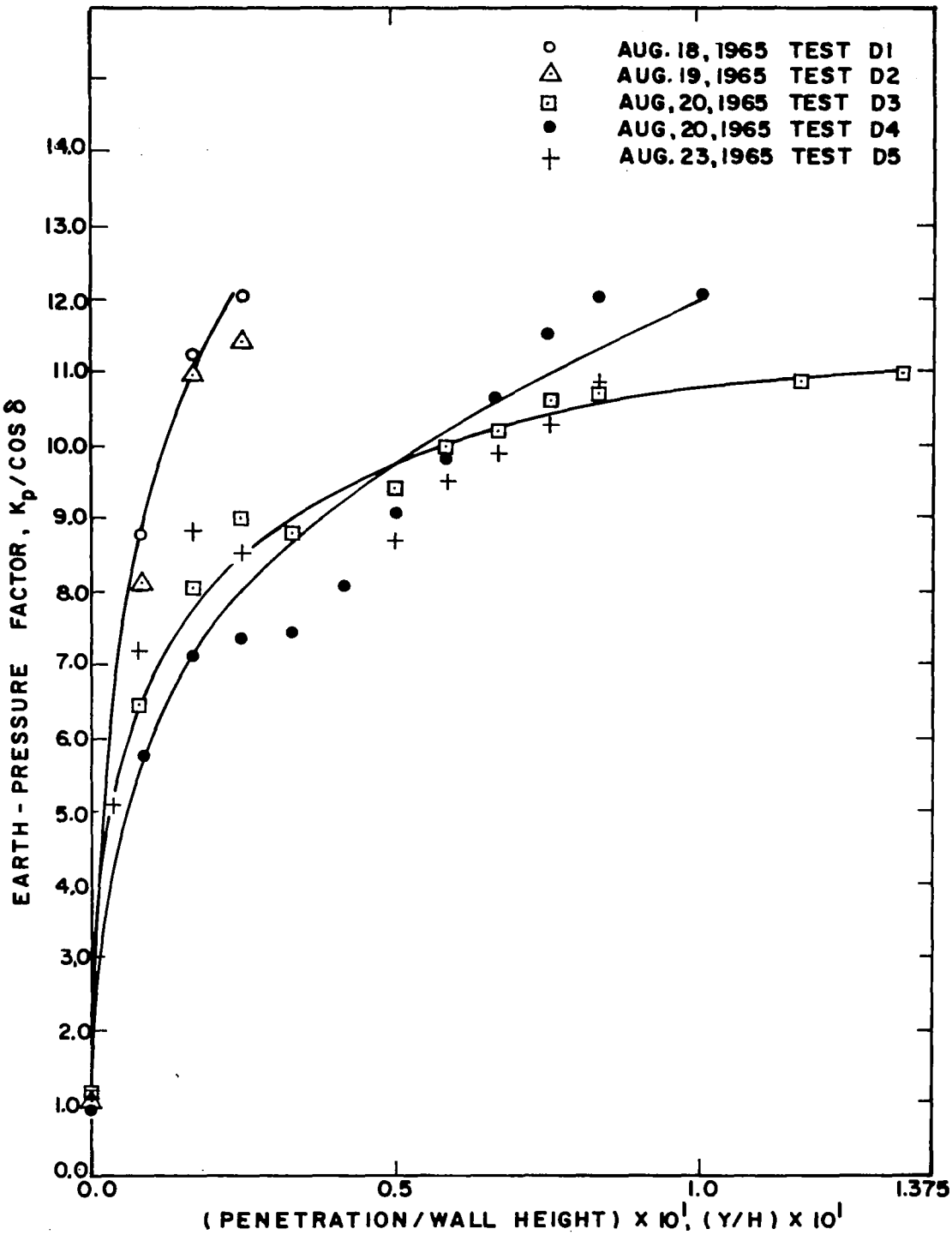

FIG. 48 EARTH-PRESSURE FACTOR CURVES - DENSE CASE

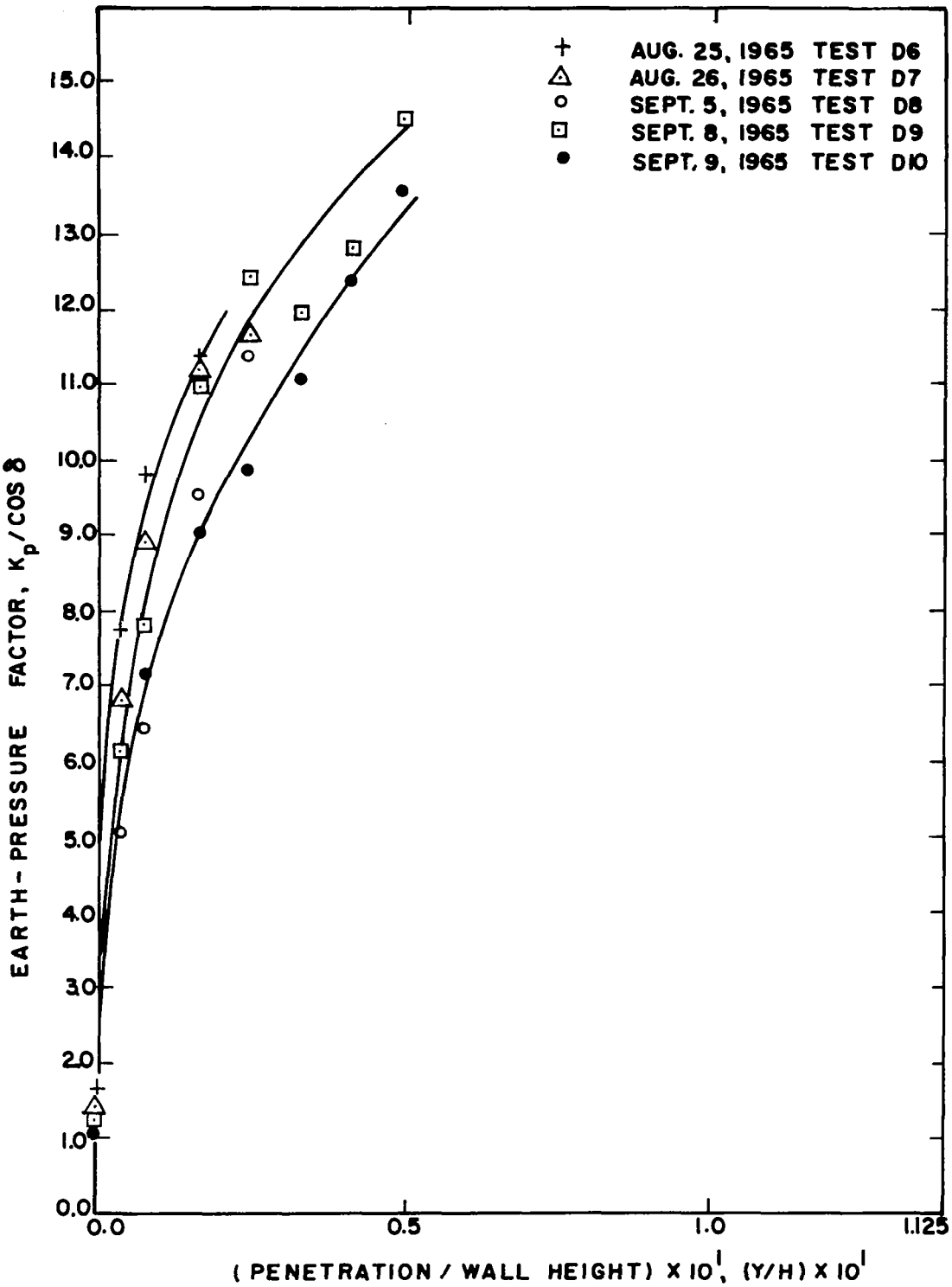

FIG. 49 EARTH-PRESSURE FACTOR CURVES - DENSE CASE

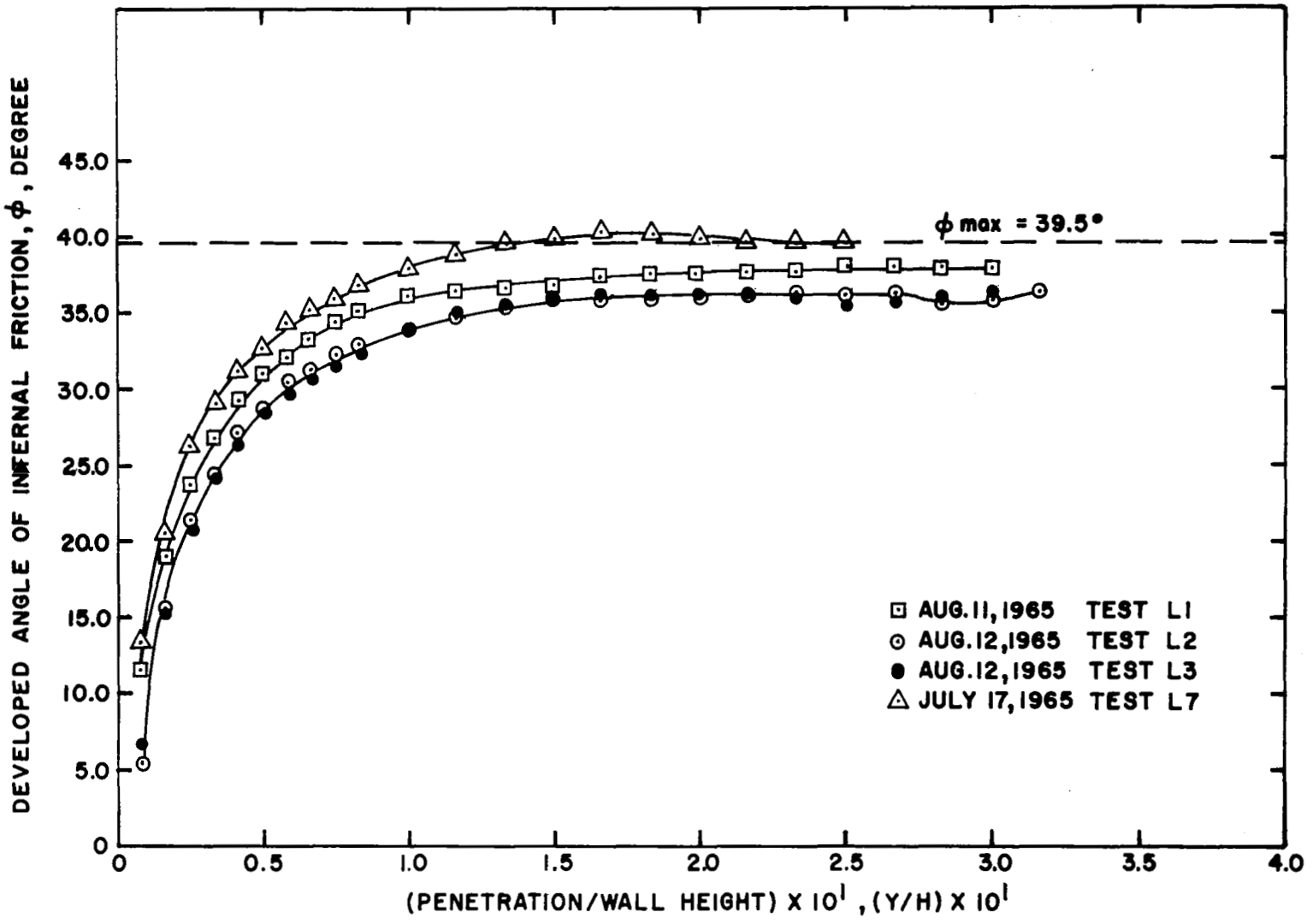

FIG. 50 INTERNAL FRICTION DEVELOPMENT CURVES — LOOSE CASE

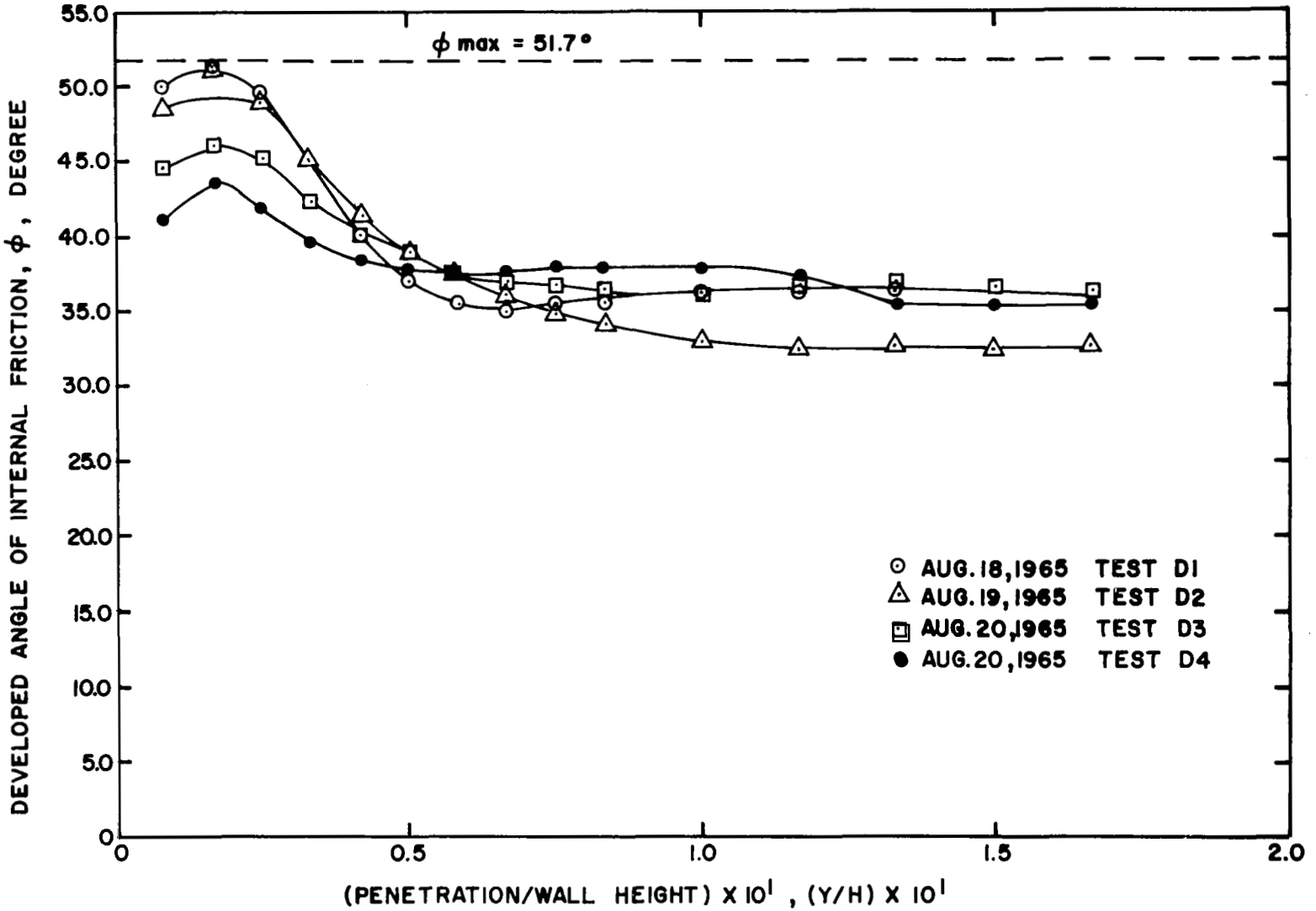

FIG. 51 INTERNAL FRICTION DEVELOPMENT CURVES — DENSE CASE

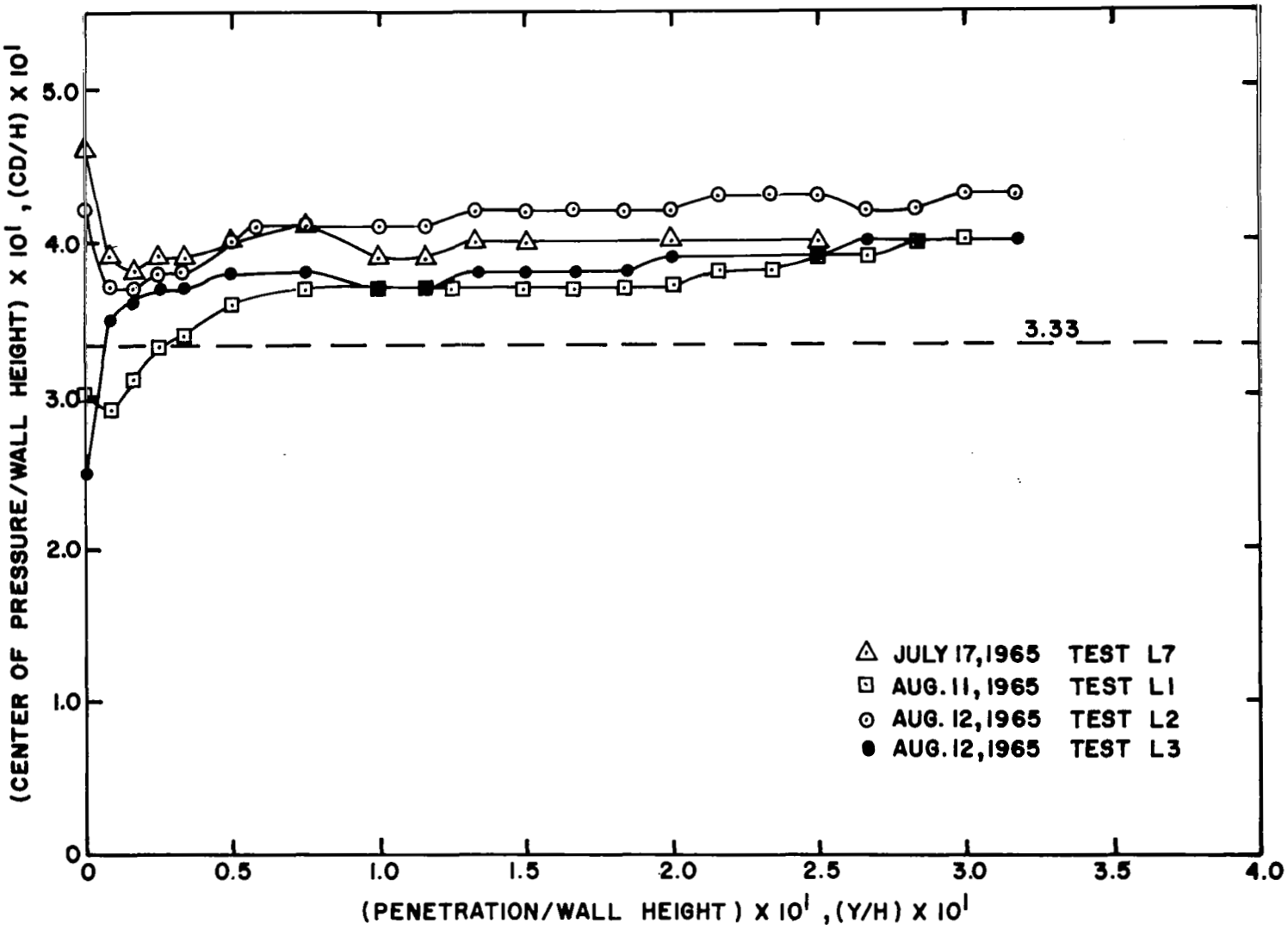

FIG. 52 VARIATIONS IN THE LOCATION OF THE CENTER OF PRESSURE — LOOSE CASE

The data relating to the location of the center of earth pressure for the dense tests is shown in Figs. 53 through 55. All of the tests, except D3, exhibit a sharp initial upward shift in the location of the center of pressure. This initial shift is followed by a downward shift which is in turn followed by a slight increase in the location of the center of pressure. The initial upward shift was produced by vertical movement of the wall and loading frame. The upward movement of the wall greatly reduced the horizontal earth pressure near the base of the wall, thus producing an upward shift of the center of pressure. Once the loading frame made contact with the wooden restraint, the wall moved approximately in a horizontal direction. This horizontal movement caused the center of pressure to shift downward. The gradual rise in the location of the center of pressure near the final stages of each test may have been caused by the increased depth of backfill material located within the plastic failure region. The increase of soil depth in the vicinity of the wall is shown in Fig. 18 on p. 27. The final stages of Test D9 are represented by the broken line in Fig. 55. The final portion of the curve is represented differently because the load cells were positioned so center of pressure locations below 0.25H could not be measured. Hence, this portion of the curve may not reflect the true location. The method that was used to calculate the location of the center of pressure is described on p. 170.

Values of at-rest coefficients of earth pressure K_o and corresponding locations of the center of pressures are shown in Table 3. Average values of at-rest coefficients, K_o, for loose and dense states are 0.35 and 1.17 respectively. The corresponding average locations of the center of pressure for the loose and dense states are 0.36 and 0.33 respectively.

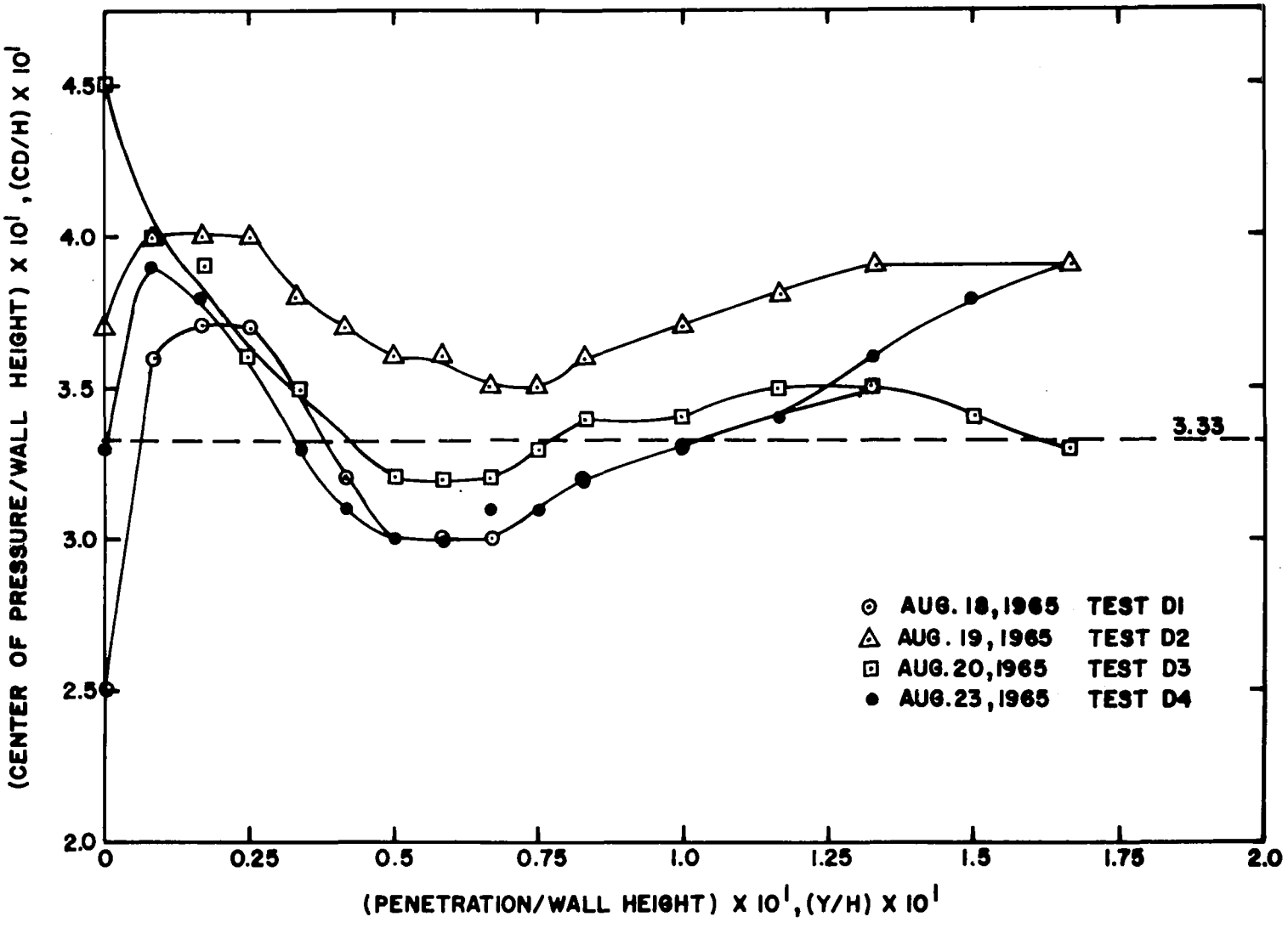

FIG. 53 VARIATIONS IN THE LOCATION OF THE CENTER OF PRESSURE — DENSE CASE

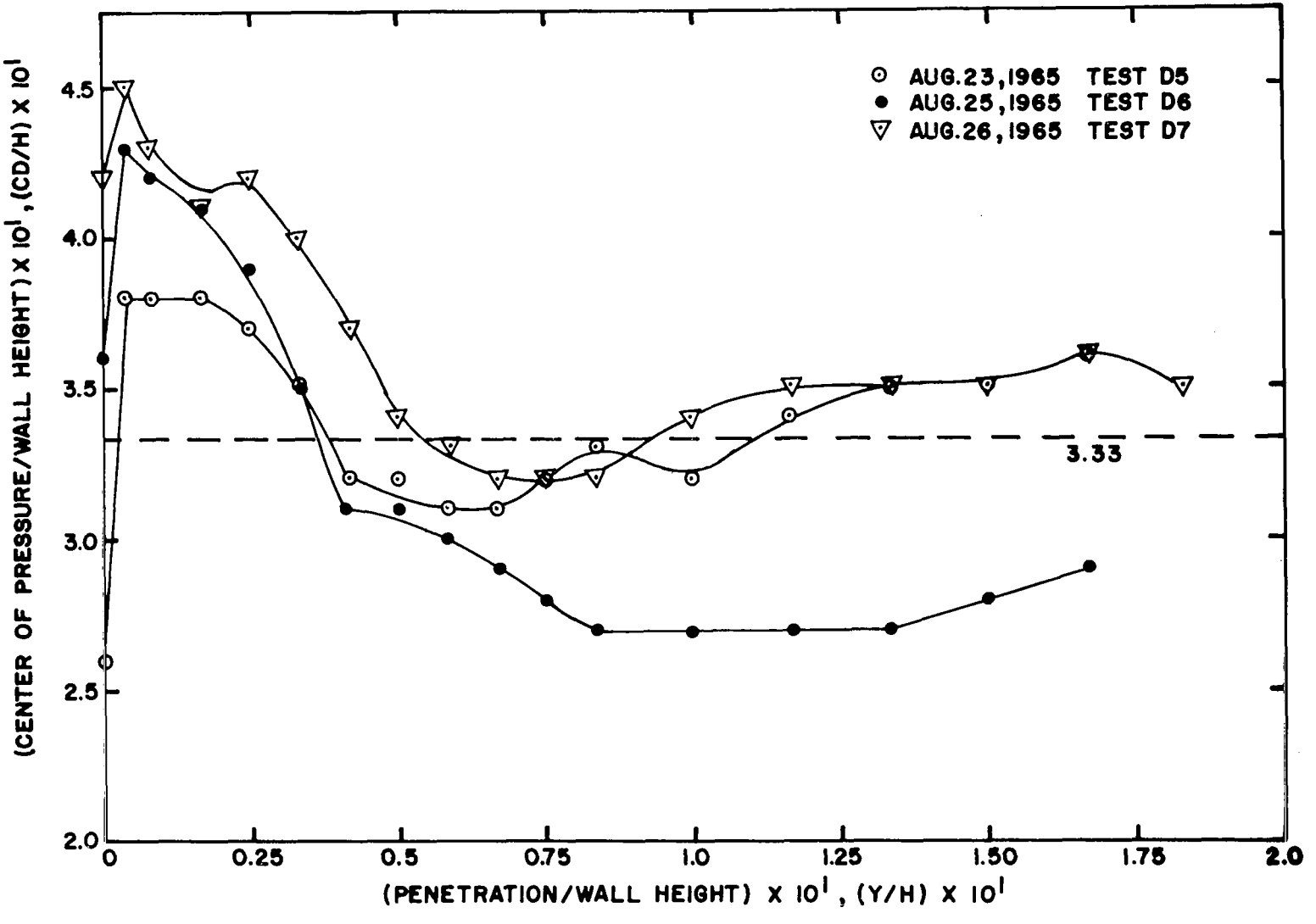

FIG.54 VARIATIONS IN THE LOCATION OF THE CENTER OF PRESSURE — DENSE CASE

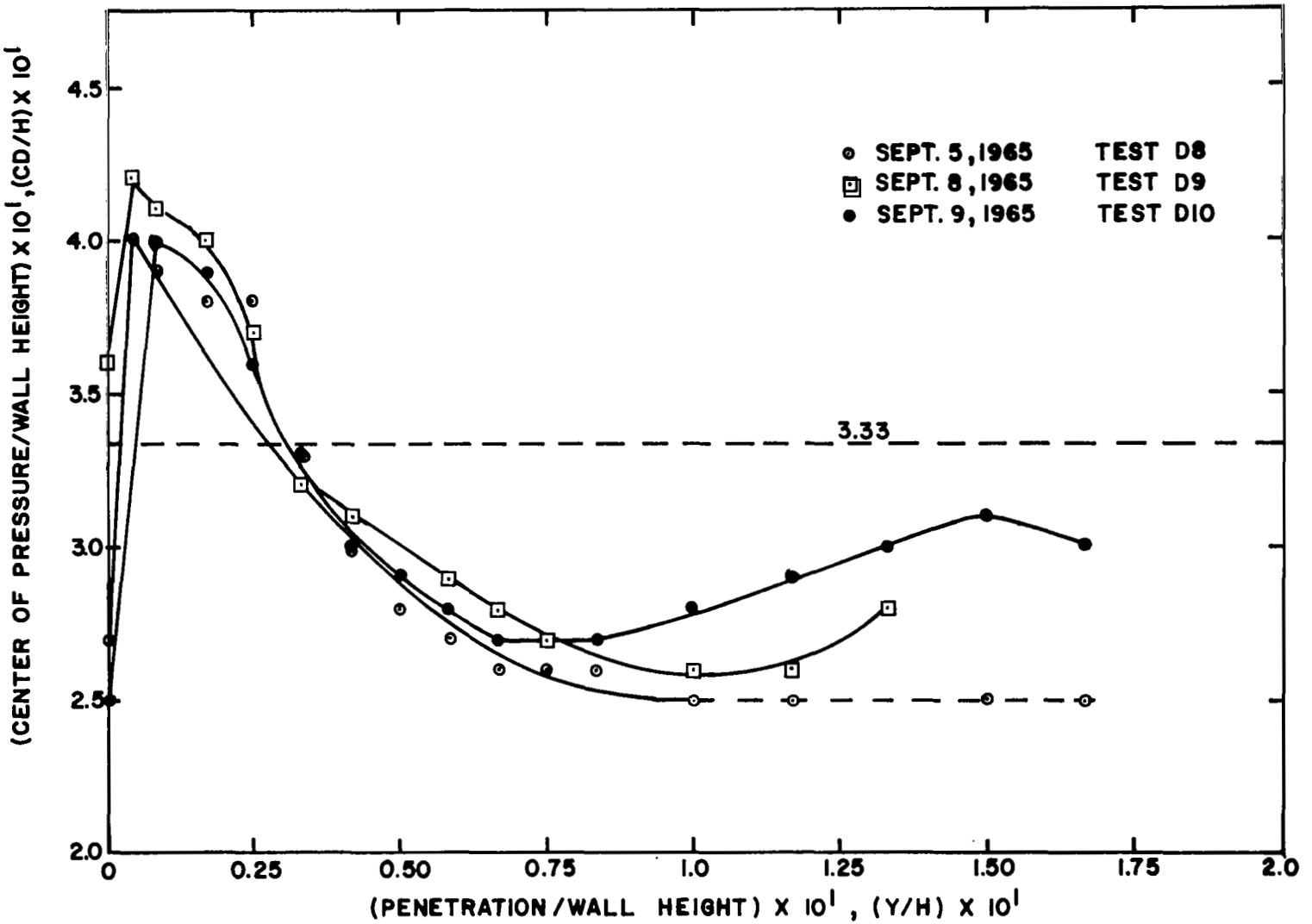

FIG. 55 VARIATIONS IN THE LOCATION OF THE CENTER OF PRESSURE – DENSE CASE

TABLE 3

VALUES OF THE EARTH PRESSURE AT-REST COEFFICIENT

AND THE CORRESPONDING CENTER OF PRESSURES

Test Identification	Earth Pressure At-Rest Coefficient K_o	Center of Pressure/ Height of Wall CD/H (in./in.)
7/17/65 - L7	0.31	0.46
8/11/67 - L1	0.57	0.30
8/12/65 - L2	0.27	0.42
8/12/65 - L3	0.24	0.25
8/18/65 - D1	0.99	0.25
8/19/65 - D2	1.00	0.37
8/20/65 - D3	1.11	0.45
8/20/65 - D4	0.89	0.33
8/23/65 - D5	1.01	0.26
8/25/65 - D6	1.78	0.38
8/26/65 - D7	1.50	0.42
9/5/65 - D8	1.07	0.27
9/8/65 - D9	1.30	0.36
9/9/65 - D10	1.08	0.25

FAILURE SURFACE ORIENTATION

The measured and calculated orientation of the failure surface for each test are listed in Table 4. The orientation of the failure surface was assumed to be plane in all cases. The measured orientation of the failure plane, β_m (Fig. 8, p. 11), was found using

$$\beta_m = \tan^{-1} (H/DM), \tag{16}$$

where,

H = Wall Height,

DM = Measured horizontal distance between the upper inner edge of the wall and the intersection of the failure surface and the surface of the backfill.

Calculated orientations were found using Eq 26 on p. 172. In every instance the measured angle was greater than the calculated angle. If the wall were perfectly smooth the calculated angle would be equal to $(45^{\circ} - \phi/2)$, or 25.3 degrees for the loose state and 19.2 degrees for the dense state.

TABLE 4

COMPARISON BETWEEN MEASURED AND CALCULATED ORIENTATIONS

OF THE FAILURE SURFACE AT MAXIMUM MEASURED EARTH PRESSURES

Test Identification	Penetration/ Ht. of Wall Y/H (in./in.)	Failure Surface Orientations		Ratio Calc./Meas.
		Meas. Angle β_m (Degree)	Calc. Angle β_T (Degree)	
7/17/65 - L7	0.250	25.7	18.0	0.7
8/11/65 - L1	0.300	24.8	17.0	0.7
8/12/65 - L2	0.317	21.8	16.9	0.8
8/12/65 - L3	0.317	23.0	16.9	0.7
8/18/65 - D1	0.0250	24.5	14.2	0.6
8/19/65 - D2	0.0250	23.3	14.2	0.6
8/20/65 - D3	0.133	21.8	7.0	0.3
8/20/65 - D4	0.100	22.5	7.0	0.3
8/23/65 - D5	0.0833	21.3	7.5	0.4
8/25/65 - D6	0.0167	--	15.9	-
8/26/65 - D7	0.0250	21.3	14.2	0.7
9/5/65 - D8	0.0250	18.0	14.2	0.8
9/8/65 - D9	0.0500	--	9.8	-
9/9/65 - D10	0.0500	20.0	9.8	0.5

CHAPTER VII

PHASE II TEST RESULTS AND DISCUSSION

This phase of testing utilized 12 and 18 in. high plates. Unlike Phase I the rate of wall penetration was varied from test to test, although, the rate was held constant during any one test. As previously noted, the loading apparatus used during Phase I contained several undesirable features which had to be corrected before the second phase of testing could be undertaken. The changes that were made are discussed in Chapter III. Since the rates of penetration used during this phase of testing were greater than the rate of penetration used in Phase I, another method was utilized to support the plates in a vertical direction. However, this method retarded the measurement of developed wall friction. Before a frictional force was indicated by the load cell, the upward force on the front face of the wall had to overcome the weight of the center plate and the frictional force developed between the three horizontal load measuring cells and the rear face of the plate. Therefore, it was necessary to use the wall friction data that was obtained during Phase I.

The data presented in Fig. 44 indicates that the measured development of wall friction, when the backfill was placed in a loose state, was erratic. Hence, a curve identical to the constructed curve shown in Fig. 45 was used for the analysis of the loose test data for Phase II. The dense test data presented in Figs. 42 and 43 indicates that the average slope of the early portion of the curve is 444 degrees /in. penetration/in. of wall height. The small amount of wall friction data obtained from the Phase II dense tests indicated that the maximum value of developed wall friction was approximately 28 degrees. Using the above information the wall friction-penetration curves shown in Fig. 56 were constructed. The curve consists of two linear portions

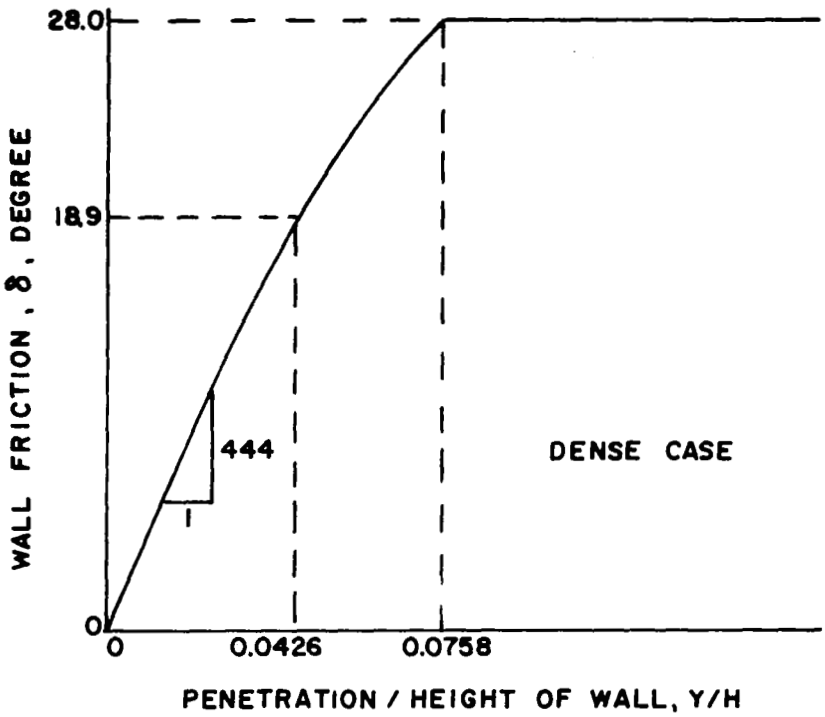

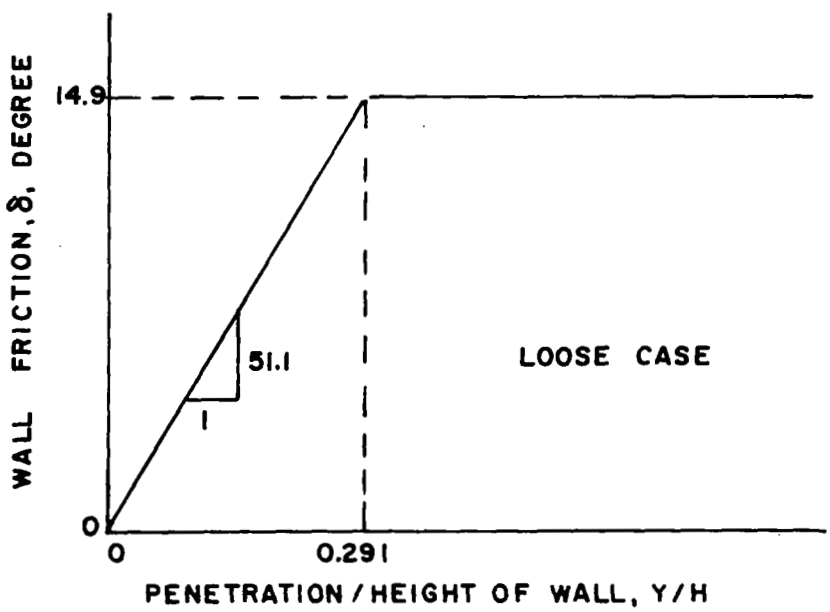

FIG. 56 CONSTRUCTED WALL FRICTION CURVES FOR LOOSE AND DENSE CASES

and an intermediate parabolic portion.

During this phase of testing, at-rest earth pressure measurements were not recorded. The at-rest coefficients listed in Table 3 were used as a basis for selecting at-rest coefficients for the backfill in its loose and dense states. A value of 0.27 was chosen for the loose state and a value of 1.0 for the dense state.

The principal purpose of this phase of testing was to determine the relation between the rate of wall penetration and the maximum developed passive earth pressure. Typical earth pressure-penetration curves for loose and dense tests are shown in Figs. 57 and 58 respectively. The upper curve in each figure was obtained using an 18 in. wall and the lower curves represent data plotted from 12 in. wall tests.

EFFECT OF WALL PENETRATION VELOCITY ON EARTH PRESSURE

Tests were conducted using wall penetration velocities of 0.00667, 0.0133, 0.0333, 0.133, 0.533, and 2.67 ips. Semilogarithmic plots of the Maximum Earth-Pressure Factor versus Velocity are shown in Figs. 59 and 60 for the loose and dense states respectively. The plots indicate that this range of wall penetration velocities has a negligible influence upon the maximum developed earth pressure. However, the exact nature of the relationship has been obscured by the scatter in the experimental data. Examination of complete earth pressure-penetration curves showed once again that the relationship between the rate of wall penetration and developed earth pressure was obscured by scatter in the data.

COMPARISON BETWEEN MEASURED AND CALCULATED EARTH-PRESSURE FACTORS

Since the rate of wall penetration did not have a significant effect upon the developed earth pressure, the measured earth-pressure results were

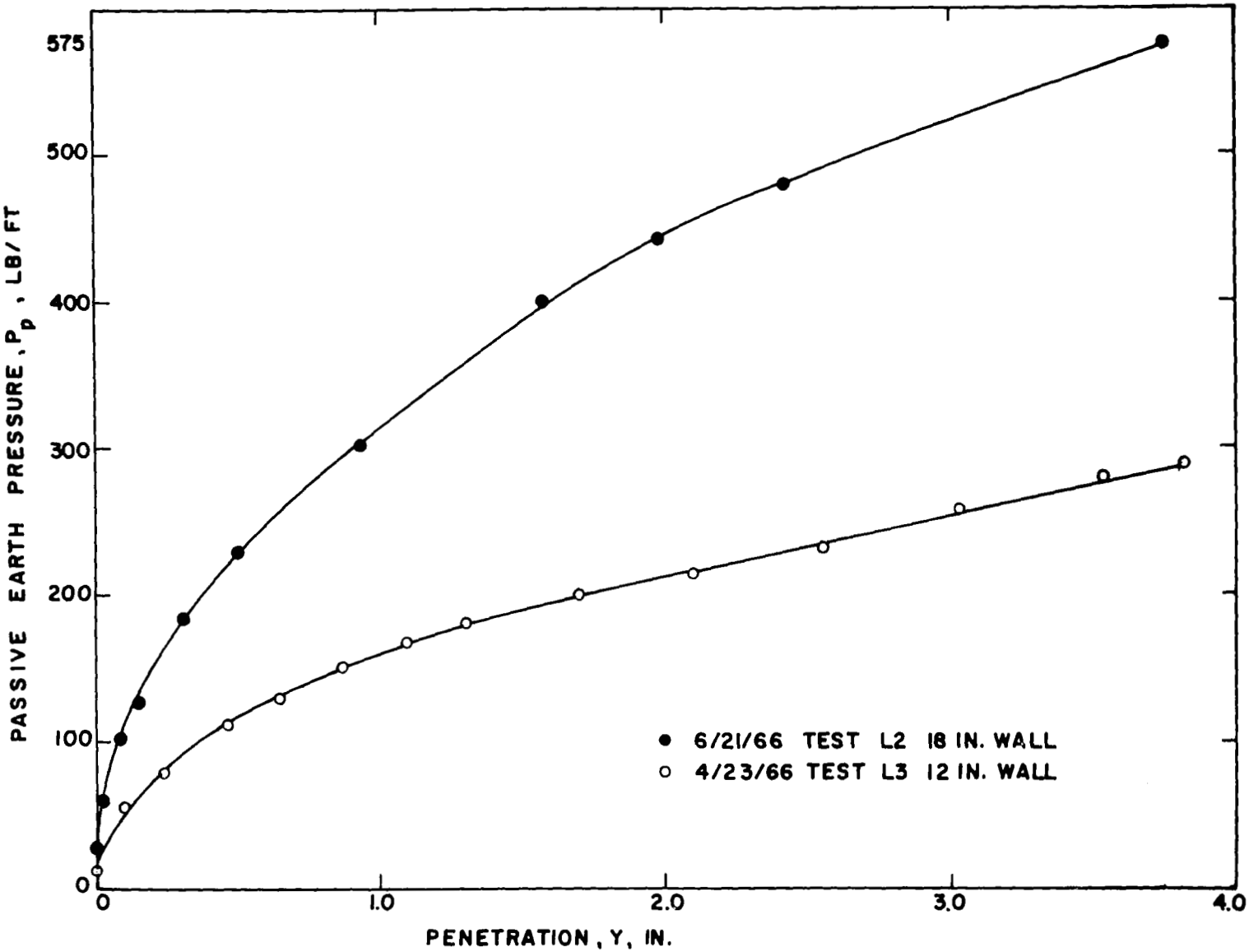

FIG. 57 TYPICAL PASSIVE EARTH PRESSURE DEVELOPMENT FOR 12 IN. AND 18 IN. WALLS – LOOSE CASE

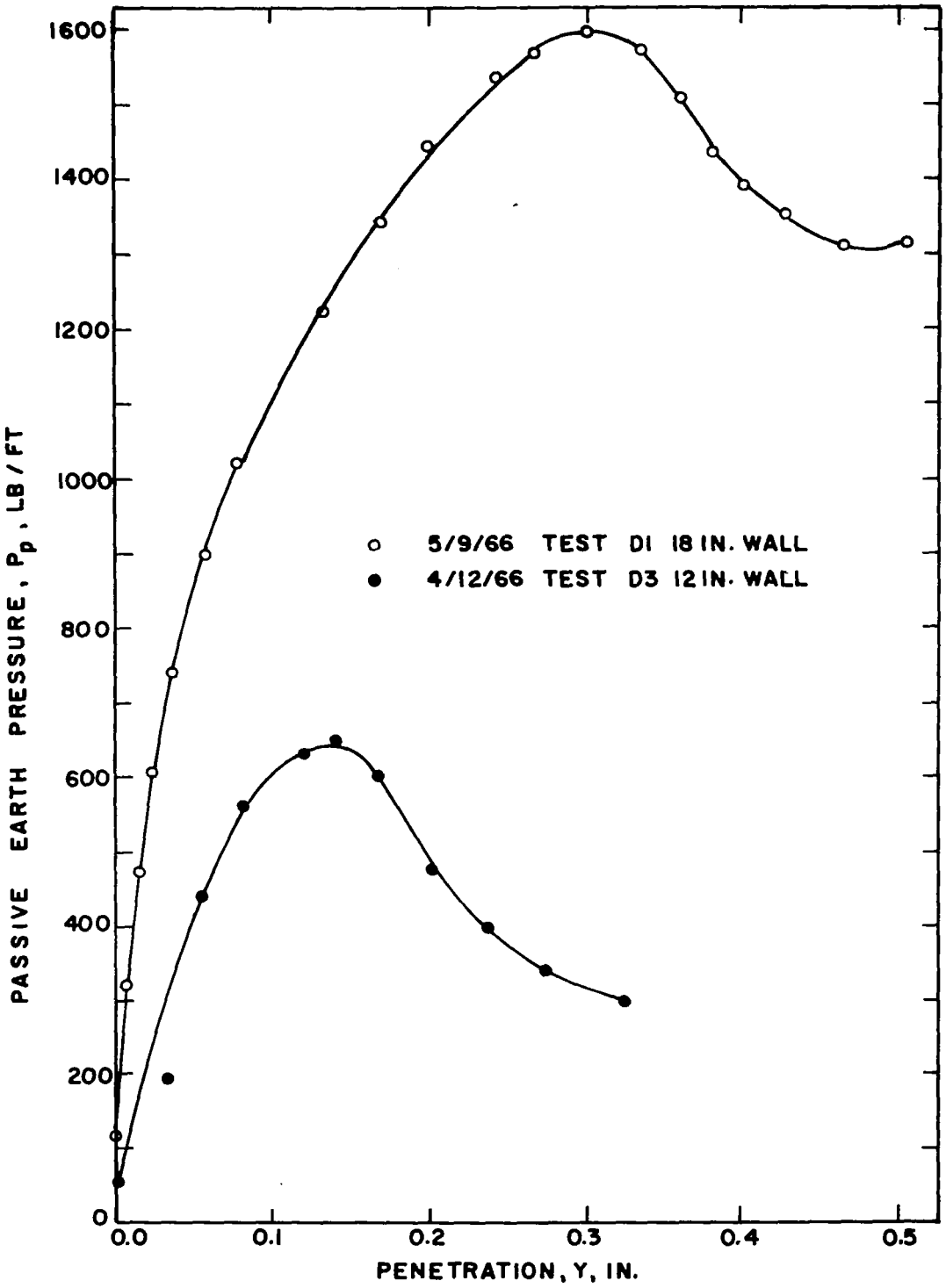

FIG. 58 TYPICAL PASSIVE EARTH PRESSURE VERSUS PENETRATION FOR 12 AND 18 IN. WALLS — DENSE CASE

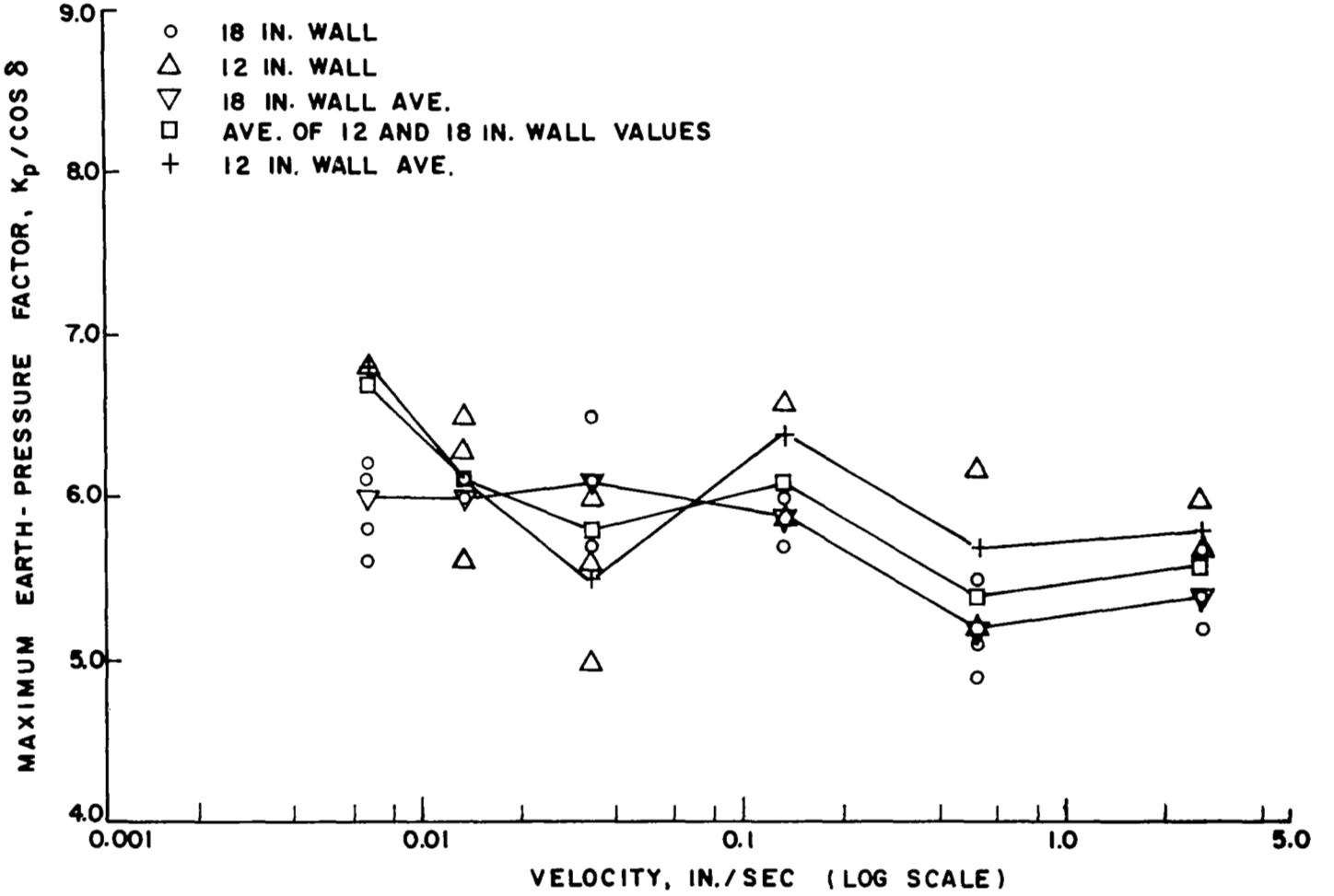

FIG. 59 MAXIMUM EARTH-PRESSURE FACTOR VERSUS VELOCITY-LOOSE CASE

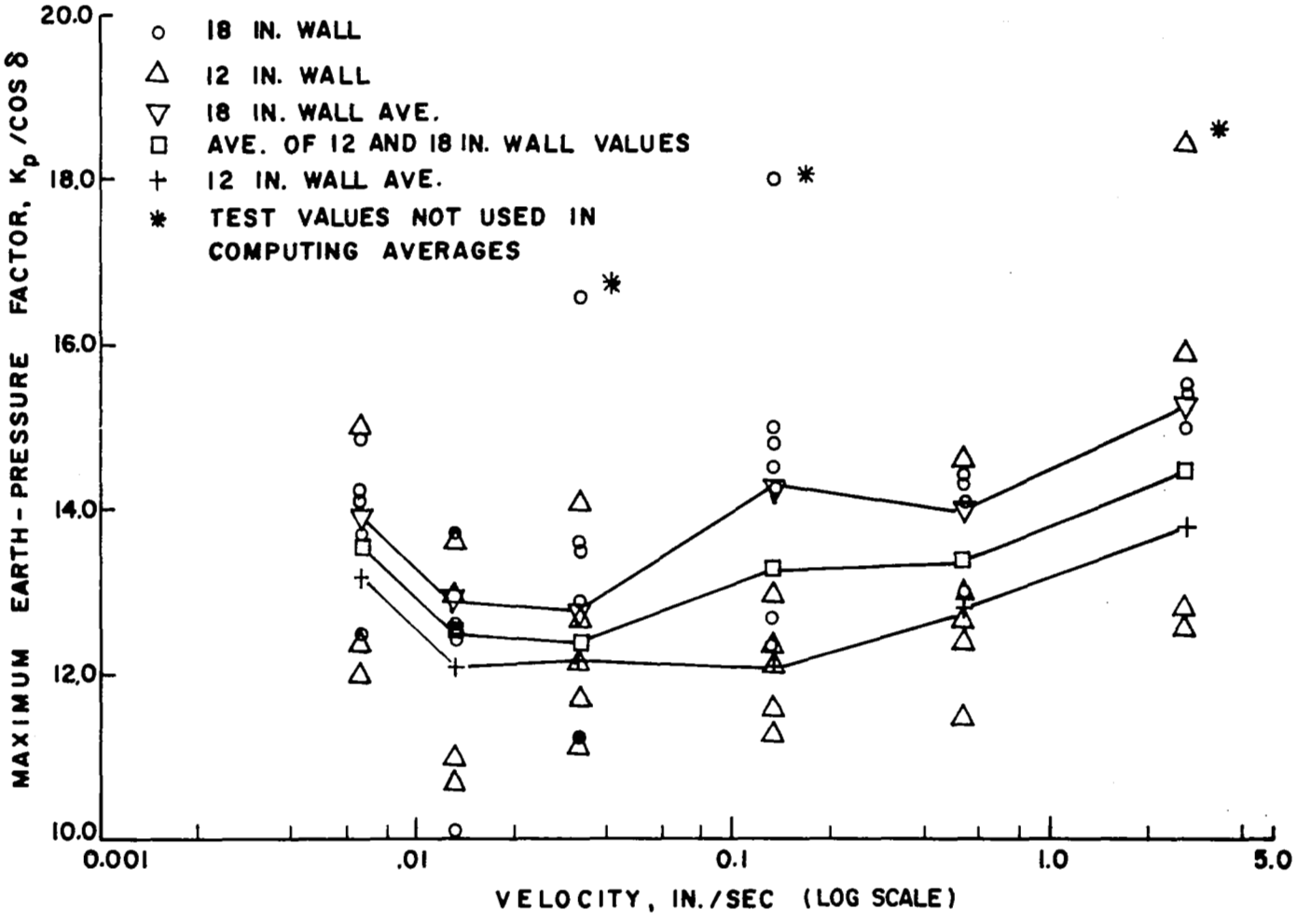

FIG. 60 MAXIMUM EARTH-PRESSURE FACTOR VERSUS VELOCITY-DENSE CASE

once again compared with Coulomb's theory of passive earth pressure. All of the terms that are presented in this section are defined in Chapter VI.

Twelve Inch Wall (Loose Tests)

The results obtained from the loose tests with the 12 in. wall are listed in Table 5. The listing indicates the calculated earth-pressure factors are greater than the measured factors. The difference in values stems mainly from the method used to evaluate the developed angle of wall friction. The prediction of passive earth pressure using Coulomb's equation is extremely sensitive to variations in the angle of wall friction. It was not possible to use a rational approach in constructing a wall friction-penetration curve for a backfill placed in a loose state and it is, therefore, expected that some error would exist.

Table 5 also indicates that the developed angles of internal friction are much below the 39.5 degrees obtained from triaxial tests. This discrepancy is associated with the error involved in using the wall friction-penetration curve for the loose case shown in Fig. 56 on p. 98. The developed angle of internal friction is calculated using the measured earth pressure and the corresponding developed angle of wall friction as predicted by the constructed curve. These values are inserted in Coulomb's equation and the value of internal friction ϕ is varied until a value of ϕ is found which satisfies the equation.

Twelve Inch Wall (Dense Tests)

The results from this series of tests are tabulated in Table 6. In every instance the measured earth-pressure factors are greater than the calculated factors. Although there is some discrepancy, the agreement is good. Since all the measured earth-pressure factors are greater than the calculated

TABLE 5

COMPARISON BETWEEN MAXIMUM MEASURED EARTH-PRESSURE FACTORS AND CALCULATED EARTH-PRESSURE FACTORS FOR 12 IN. WALL - LOOSE CASE

Test Identification	Penet./Ht. of Wall Y/H (in./in.)	Earth-Pressure Factors		Ratio Calc./ Meas.	Developed Angle		Velocity (in./sec)
		Measured $K_p/\cos\delta$	Calculated $K_p/\cos\delta$		Internal Friction ϕ (Degrees)	Wall Friction δ (Degrees)	
4/23/66 - L3	0.288	6.0	8.5	1.4	33.6	14.7	2.667
4/23/66 - L4	0.291	5.7	8.5	1.5	32.7	14.9	2.667
4/25/66 - L1	0.273	5.9	8.2	1.4	33.9	14.0	2.667
4/21/66 - L2	0.312	6.2	8.6	1.4	34.0	14.9	0.533
4/22/66 - L1	0.298	5.2	8.6	1.7	31.0	14.9	0.533
4/22/66 - L2	0.316	6.6	8.6	1.3	35.1	14.9	0.133
4/23/66 - L1	0.315	5.9	8.6	1.5	33.2	14.9	0.133
4/23/66 - L2	0.318	6.6	8.6	1.3	35.1	14.9	0.133
4/19/66 - L1	0.295	5.0	8.6	1.7	30.2	14.9	0.0333
4/21/66 - L1	0.287	6.0	8.4	1.4	33.7	14.6	0.0333
4/25/66 - L2	0.319	5.6	8.6	1.5	32.3	14.9	0.0333
6/30/66 - L1	0.324	5.6	8.6	1.5	32.3	14.9	0.0133
6/30/66 - L2	0.320	6.5	8.6	1.3	35.0	14.9	0.0133
6/30/66 - L3	0.324	6.3	8.6	1.4	34.3	14.9	0.0133
6/29/66 - L4	0.320	10.4	8.6	0.8	42.4	14.9	0.00667
7/1/66 - L1	0.328	6.8	8.6	1.3	35.6	14.9	0.00667
7/1/66 - L2	0.323	6.8	8.6	1.3	35.5	14.9	0.00667

TABLE 6

COMPARISON BETWEEN MAXIMUM MEASURED EARTH-PRESSURE FACTORS AND CALCULATED EARTH-PRESSURE FACTORS FOR 12 IN. WALL - DENSE CASE

Test Identification	Penet./Ht. of Wall Y/H (in./in.)	Earth-Pressure Factors		Ratio Calc./ Meas.	Developed Angle		Velocity (in./sec)
		Measured $K_p/\cos\delta$	Calculated $K_p/\cos\delta$		Internal Friction ϕ (Degrees)	Wall Friction δ (Degrees)	
6/29/66 - D1	0.0177	18.4	12.9	0.7	56.3	7.9	2.667
6/29/66 - D2	0.0180	15.9	13.0	0.8	54.4	8.0	2.667
4/13/66 - D1	0.00692	12.8	9.7	0.8	55.9	3.7	2.667
4/14/66 - D1	0.0117	12.6	11.0	0.9	53.8	5.2	2.667
4/6/66 - D1	0.00992	12.4	10.5	0.8	54.2	4.4	0.533
4/12/66 - D2	0.00920	11.5	10.3	0.9	53.4	4.1	0.533
4/12/66 - D3	0.0115	12.7	10.9	0.9	53.9	5.1	0.533
6/24/66 - D2	0.0184	14.6	13.1	0.9	53.1	8.2	0.533
6/28/66 - D1	0.0163	13.0	12.4	1.0	52.4	7.2	0.533
4/4/66 - D1	0.0107	12.4	10.7	0.9	53.8	4.8	0.133
4/26/66 - D1	0.00833	11.6	10.0	0.9	53.9	3.7	0.133
4/26/66 - D2	0.00833	11.3	10.0	0.9	53.4	3.7	0.133
6/24/66 - D1	0.00790	13.0	10.0	0.8	55.7	3.5	0.133
6/24/66 - D3	0.00795	12.1	10.0	0.9	54.6	3.5	0.133
3/29/66 - D1	0.00960	12.7	10.4	0.8	54.7	4.3	0.0333
3/29/66 - D2	0.00710	11.3	9.8	0.9	54.0	3.2	0.0333
3/30/66 - D1	0.00749	12.2	9.9	0.8	54.9	3.3	0.0333
6/23/66 - D2	0.0110	11.7	10.8	0.9	52.9	4.9	0.0333
6/23/66 - D3	0.0103	11.2	10.6	0.9	52.5	4.6	0.0333
6/23/66 - D4	0.0194	14.1	13.5	1.0	52.3	8.6	0.0333
4/4/66 - D2	0.00940	10.7	10.4	1.0	52.2	4.2	0.0133
4/5/66 - D2	0.00817	11.0	10.0	0.9	53.1	3.6	0.0133
6/22/66 - D2	0.0100	13.7	10.5	0.8	55.7	4.4	0.0133
6/22/66 - D3	0.0129	13.0	11.3	0.9	53.7	5.7	0.0133
4/5/66 - D3	0.00805	12.0	10.0	0.8	54.5	3.6	0.00667
6/22/66 - D1	0.0137	15.0	11.6	0.8	55.4	6.1	0.00667
6/23/66 - D1	0.00836	12.4	10.1	0.8	54.8	3.7	0.00667

factors, the developed angle of internal friction ϕ was found to be greater than the 51.7 degree value obtained from triaxial tests. However, it has been shown by Cornforth[2] that the maximum value of ϕ obtained from a triaxial test is 0.5 to 4.0 degrees less than that obtained in a plane strain test. The above statement pertains to results obtained from tests using Brasted sand. The 0.5 degree value corresponds to a loose sand condition and the 4.0 degree value corresponds to a dense sand condition. If the triaxial value of ϕ were adjusted to conform to a plain strain ϕ value, the calculated earth-pressure factors for dense tests would most likely agree better with the majority of the measured values.

The developed angle of wall friction, δ, is in every case much less than $\phi/3$. It can also be seen, by comparing the dimensionless quantities (Penetration/Height of Wall) listed in Tables 2 and 6, that the amount of penetration required to develop the maximum earth-pressure factors are much less for the Phase II series of tests. The differences in the dimensionless quantities is attributed to the vertical wall movement which took place in the Phase I series of tests. The upward movement caused the horizontal earth pressures to be reduced in early stages of penetration. Once the wall stopped moving in a vertical direction the pressures began to increase more rapidly. However, this increase in pressure occurred at penetrations greater than the penetration required to produce failure in the backfill when penetrated by the wall moving strictly in a horizontal direction.

Eighteen Inch Wall (Loose Tests)

This series of tests is similar to the loose tests conducted using the 12 in. wall. The basic differences in the two series of tests were the height and location of the wall. The top and bottom edges of the 18 in. wall were

located 3 in. above and below the top and bottom of the 12 in. wall. Although the bottom edge of 18 in. wall was 3 in. closer to the bottom of the sandbox, it is felt that this change in distance does not significantly change the boundary conditions.

The results listed in Table 7 agree well with the results obtained from the 12 in. wall tests. The measured and calculated 18 in. wall earth-pressure factors are generally lower than the 12 in. wall values. The results would have agreed closer had the dimensionless ratio (Penetration/Height of Wall) values been equal for each series of tests. It should be noted that the same constructed wall friction curve was used for the 12 and 18 in. wall tests.

Eighteen Inch Wall (Dense Tests)

Test results for this series of tests are similar to the values listed in Table 6. The measured and calculated earth-pressure factors listed in Table 8 are both generally higher than those from the 12 in. wall tests. Comparison of the two tables also indicates that the dimensionless ratio (Penetration/Height of Wall) values obtained from the 18 in. wall tests are larger than the 12 in. wall values. Hence, the developed angles of wall friction are also larger, since the same constructed wall friction curve was used for both series of tests.

COMPARISON BETWEEN MEASURED AND CALCULATED ORIENTATIONS OF THE FAILURE SURFACE

The measured and calculated orientations of the failure surface for each series of tests are listed in Tables 9 through 12. The methods used in measuring and calculating the orientations of the failure surfaces are similar to those used in obtaining the Phase I results. These methods are discussed in Chapter VI and Appendix A. Examination of each table shows that in every case the calculated angle β_T is smaller than the measured angle β_m. Nearly all the

TABLE 7

COMPARISON BETWEEN MAXIMUM MEASURED EARTH-PRESSURE FACTORS AND CALCULATED EARTH-PRESSURE FACTORS FOR 18 IN. WALL - LOOSE CASE

Test Identification	Penet./Ht. of Wall Y/H (in./in.)	Earth-Pressure Factors		Ratio Calc./ Meas.	Developed Angle		Velocity (in./sec)
		Measured $K_p/\cos\delta$	Calculated $K_p/\cos\delta$		Internal Friction ϕ (Degrees)	Wall Friction δ (Degrees)	
6/15/66 - L1	0.196	5.2	6.8	1.3	34.7	10.0	2.667
6/15/66 - L2	0.207	5.4	6.9	1.3	34.8	10.6	2.667
6/16/66 - L1	0.210	5.7	7.0	1.2	35.8	10.7	2.667
6/8/66 - L1	0.209	4.9	7.0	1.4	33.0	10.7	0.533
6/8/66 - L2	0.199	5.1	6.8	1.3	33.9	10.2	0.533
6/8/66 - L3	0.228	5.5	7.3	1.3	34.5	11.6	0.533
6/16/66 - L2	0.199	5.7	6.8	1.2	36.2	10.1	0.133
6/16/66 - L3	0.216	6.0	7.1	1.2	36.5	11.0	0.133
6/16/66 - L4	0.212	6.0	7.0	1.2	36.8	10.8	0.133
6/20/66 - L3	0.216	6.5	7.1	1.1	38.0	11.0	0.0333
6/20/66 - L4	0.208	5.7	6.9	1.2	35.7	10.6	0.0333
6/20/66 - L5	0.223	6.1	7.2	1.2	36.5	11.4	0.0333
6/17/66 - L1	0.215	6.0	7.1	1.2	36.5	11.0	0.0133
6/17/66 - L2	0.214	6.1	7.0	1.1	36.9	10.9	0.0133
6/21/66 - L2	0.208	5.8	6.9	1.2	36.2	10.6	0.00667
6/17/66 - L3	0.210	6.1	7.0	1.1	37.0	10.7	0.00667
6/20/66 - L1	0.212	6.1	7.0	1.1	36.8	10.8	0.00667
6/20/66 - L2	0.215	6.2	7.1	1.1	37.1	11.0	0.00667
6/21/66 - L3	0.211	5.6	7.0	1.3	35.5	10.8	0.00667

TABLE 8

COMPARISON BETWEEN MAXIMUM MEASURED EARTH-PRESSURE FACTORS AND CALCULATED EARTH-PRESSURE FACTORS FOR 18 IN. WALL - DENSE CASE

Test Identification	Penet./Ht. of Wall Y/H (in./in.)	Earth-Pressure Factors		Ratio Calc./ Meas.	Developed Angle		Velocity (in./sec)
		Measured $K_p \cos \delta$	Calculated $K_p/\cos \delta$		Internal Friction ϕ (Degrees)	Wall Friction δ (Degrees)	
5/17/66 - D3	0.0161	15.0	12.3	0.8	54.4	7.1	2.667
5/17/66 - D4	0.0172	15.5	12.7	0.8	54.3	7.6	2.667
5/17/66 - D5	0.0179	15.4	13.0	0.8	54.0	7.9	2.667
5/16/66 - D1	0.0141	14.1	11.7	0.8	54.4	6.2	0.533
5/16/66 - D2	0.0159	14.4	12.3	0.9	53.9	7.1	0.533
5/17/66 - D1	0.0165	14.1	12.5	0.9	53.4	7.3	0.533
5/17/66 - D2	0.0178	14.5	12.9	0.9	53.2	7.9	0.533
6/7/66 - D1	0.0193	13.0	13.5	1.0	51.1	8.6	0.533
5/2/66 - D1	0.0149	12.7	11.9	0.9	52.6	6.6	0.133
5/3/66 - D1	0.0132	12.4	11.4	0.9	52.9	5.8	0.133
5/3/66 - D2	0.0158	14.3	12.2	0.9	53.9	7.0	0.133
7/8/66 - D2	0.0230	14.5	15.0	1.0	51.2	10.2	0.133
7/9/66 - D2	0.0161	15.0	12.3	0.8	54.4	7.1	0.133
7/12/66 - D1	0.0214	14.8	14.3	1.0	52.1	9.5	0.133
7/12/66 - D2	0.0241	18.0	15.5	0.9	53.5	10.7	0.133
4/29/66 - D1	0.0193	12.9	13.5	1.0	51.1	8.5	0.0333
5/4/66 - D1	0.0158	13.5	12.2	0.9	53.1	7.0	0.0333
5/5/66 - D1	0.0174	11.3	12.8	1.1	49.9	7.7	0.0333
7/7/66 - D4	0.0234	16.6	15.2	0.9	52.8	10.4	0.0333
7/8/66 - D1	0.0168	13.6	12.6	0.9	52.7	7.5	0.0333
5/9/66 - D1	0.0167	13.8	12.5	0.9	53.1	7.4	0.0133
5/10/66 - D1	0.0162	12.6	12.4	1.0	52.0	7.2	0.0133
5/10/66 - D2	0.0187	12.4	13.2	1.1	50.7	8.3	0.0133
7/7/66 - D2	0.0145	10.1	11.8	1.2	49.2	6.4	0.0133
5/10/66 - D3	0.0158	14.1	12.2	0.9	53.7	7.0	0.00667
5/10/66 - D4	0.0250	14.2	16.0	1.1	50.1	11.1	0.00667
5/11/66 - D1	0.0137	13.7	11.6	0.8	54.2	6.1	0.00667
5/11/66 - D2	0.0136	12.5	11.5	0.9	52.9	6.0	0.00667

TABLE 9

COMPARISON BETWEEN MEASURED AND CALCULATED ORIENTATIONS

OF THE FAILURE SURFACE FOR 12 IN. WALL - LOOSE CASE

Test Identification	Penetration/ Ht. of Wall Y/H (in./in.)	Failure Surface Orientations Meas. Angle β_m (Degree)	Calc. Angle β_T (Degree)	Ratio Calc./Meas.
4/23/66 - L3	0.288	21.8	17.0	0.8
4/23/66 - L4	0.291	21.8	16.9	0.8
4/25/66 - L1	0.273	24.8	17.3	0.7
4/21/66 - L2	0.312	21.4	16.9	0.8
4/22/66 - L1	0.298	--	16.9	-
4/22/66 - L2	0.316	22.8	16.9	0.7
4/23/66 - L1	0.315	24.0	16.9	0.7
4/23/66 - L2	0.318	--	16.9	-
4/19/66 - L1	0.295	26.1	16.9	0.6
4/21/66 - L1	0.287	24.4	17.0	0.7
4/25/66 - L2	0.319	24.0	16.9	0.7
6/30/66 - L1	0.324	20.6	16.9	0.8
6/30/66 - L2	0.320	22.1	16.9	0.8
6/30/66 - L3	0.324	20.6	16.9	0.8
6/29/66 - L4	0.320	21.8	16.9	0.8
7/1/66 - L1	0.328	21.8	16.9	0.8
7/1/66 - L2	0.323	21.8	16.9	0.8

TABLE 10

COMPARISON BETWEEN MEASURED AND CALCULATED ORIENTATIONS

OF THE FAILURE SURFACE FOR 12 IN. WALL - DENSE CASE

Test Identification	Penetration/ Ht. of Wall Y/H (in./in.)	Failure Surface Orientations: Meas. Angle β_m (Degree)	Failure Surface Orientations: Calc. Angle β_T (Degree)	Ratio Calc./Meas.
6/29/66 - D1	0.0177	19.4	14.9	0.8
6/29/66 - D2	0.0180	20.6	14.9	0.7
4/13/66 - D1	0.00692	20.0	17.2	0.9
4/14/66 - D1	0.0117	19.2	16.2	0.8
4/6/66 - D1	0.00992	—	16.8	-
4/12/66 - D2	0.00920	19.4	16.9	0.9
4/12/66 - D3	0.0148	21.4	16.2	0.8
6/24/66 - D2	0.0184	21.8	14.8	0.7
6/28/66 - D1	0.0163	20.0	15.2	0.8
4/4/66 - D1	0.0107	21.4	16.2	0.8
4/26/66 - D1	0.00833	21.4	17.1	0.8
4/26/66 - D2	0.00833	18.4	17.1	0.9
6/24/66 - D1	0.00790	23.2	17.2	0.7
6/24/66 - D3	0.00795	18.4	17.2	0.9
3/29/66 - D1	0.00960	—	16.8	-
3/29/66 - D2	0.00710	—	17.2	-
3/30/66 - D1	0.00749	—	17.2	-
6/23/66 - D2	0.0110	18.4	16.2	0.9
6/23/66 - D3	0.0103	21.2	16.2	0.8
6/23/66 - D4	0.0194	22.1	14.2	0.6
4/4/66 - D2	0.00940	18.4	16.9	0.9
4/5/66 - D2	0.00817	19.4	17.2	0.9
6/22/66 - D2	0.0100	20.6	16.7	0.8
6/22/66 - D3	0.0129	23.5	16.1	0.7
4/5/66 - D3	0.00805	17.3	17.2	1.0
6/22/66 - D1	0.0137	17.6	15.9	0.9
6/23/66 - D1	0.0130	18.9	16.0	0.8

TABLE 11

COMPARISON BETWEEN MEASURED AND CALCULATED ORIENTATIONS

OF THE FAILURE SURFACE FOR 18 IN. WALL - LOOSE CASE

Test Identification	Penetration/ Ht. of Wall Y/H (in./in.)	Failure Surface Orientations Meas. Angle β_m (Degree)	Calc. Angle β_T (Degree)	Ratio Calc./Meas.
6/15/66 - L1	0.196	25.1	19.3	0.8
6/15/66 - L2	0.207	24.8	19.1	0.8
6/16/66 - L1	0.210	--	19.0	-
6/8/66 - L1	0.209	--	19.1	-
6/8/66 - L2	0.199	--	19.3	-
6/8/66 - L3	0.228	--	18.3	-
6/16/66 - L2	0.199	24.2	19.3	0.8
6/16/66 - L3	0.216	24.8	18.9	0.8
6/16/66 - L4	0.212	24.2	19.0	0.8
6/20/66 - L3	0.216	--	18.9	-
6/20/66 - L4	0.208	22.7	19.1	0.8
6/20/66 - L5	0.223	23.8	18.3	0.8
6/17/66 - L1	0.215	--	18.9	-
6/17/66 - L2	0.214	--	18.9	-
6/21/66 - L2	0.208	--	19.1	-
6/17/66 - L3	0.210	--	19.0	-
6/20/66 - L1	0.212	--	19.0	-
6/20/66 - L2	0.215	--	19.0	-
6/21/66 - L3	0.211	--	19.0	-

TABLE 12

COMPARISON BETWEEN MEASURED AND CALCULATED ORIENTATIONS

OF THE FAILURE SURFACE FOR 18 IN. WALL - DENSE CASE

Test Identification	Penetration/ Ht. of Wall Y/H (in./in.)	Failure Surface Orientations Meas. Angle β_m (Degree)	Calc. Angle β_T (Degree)	Ratio Calc./Meas.
5/17/66 - D3	0.0161	18.8	15.2	0.8
5/17/66 - D4	0.0172	18.8	15.1	0.8
5/17/66 - D5	0.0179	17.9	14.9	0.8
5/16/66 - D1	0.0141	19.1	15.8	0.8
5/16/66 - D2	0.0159	20.2	15.2	0.8
5/17/66 - D1	0.0165	18.5	15.2	0.8
5/17/66 - D2	0.0178	18.5	14.9	0.8
6/7/66 - D1	0.0193	19.5	14.2	0.7
5/2/66 - D1	0.0149	21.4	15.2	0.7
5/3/66 - D1	0.0132	21.8	16.0	0.7
5/3/66 - D2	0.0158	21.8	15.2	0.7
4/29/66 - D1	0.0193	20.8	14.2	0.7
7/8/66 - D2	0.0230	17.9	13.7	0.8
7/9/66 - D2	0.0161	20.2	15.2	0.8
7/12/66 - D1	0.0214	19.1	14.0	0.7
7/12/66 - D2	0.0241	19.8	13.2	0.7
5/4/66 - D1	0.0158	20.0	15.2	0.8
5/5/66 - D1	0.0174	22.5	15.0	0.7
7/7/66 - D4	0.0234	21.0	14.9	0.7
7/8/66 - D1	0.0168	21.4	15.2	0.7
5/9/66 - D1	0.0164	22.3	15.2	0.7
5/10/66 - D1	0.0162	19.5	15.2	0.8
5/10/66 - D2	0.0187	21.2	14.7	0.7
7/7/66 - D2	0.0145	20.6	15.2	0.7
5/10/66 - D3	0.0158	19.8	15.2	0.8
5/10/66 - D4	0.0250	18.8	13.2	0.7
5/11/66 - D1	0.0137	21.4	15.9	0.7
5/11/66 - D2	0.0136	20.2	15.9	0.8
7/7/66 - D1	0.0177	21.0	14.9	0.7

values of β_m agree well with theoretical values of β_T which were calculated for the zero wall friction case. These values of β_T are 25.3 degrees for the loose state and 19.2 degrees for the dense state.

The discrepancy between measured and calculated angles can basically be attributed to two factors, the first factor being the inherent error involved in the method used to obtain the calculated and measured angles. These methods are based upon Coulomb's assumption of a plane failure surface, whereas, in reality the failure surface is curved near the base of the wall. However, Rowe[6] has shown that the curvature is slight for developed wall friction values less than 10 degrees. It can be seen from the previous tables that the majority of developed wall friction values at failure, for the dense states, are less than 10 degrees. Although the actual orientation of the failure surface is not greatly influenced by small angles of wall friction, the calculated orientation of the failure surface is comparatively sensitive to developed values of wall friction. It should also be noted that the measured orientations of the failure surfaces have not been recorded at the instant the maximum passive earth pressure was developed, but immediately upon completion of the test. This approximation does not involve significant error, since the orientation of the measured angle depends on the distance, DM, between the inner edge of the wall and the failure surface outcrop and this distance was found to remain essentially constant throughout a test, once a surface outcrop has developed.

The second factor has been discussed by Taylor[7] in connection with triaxial compression tests. The theoretical angle between the failure surface and the minor principal plane, of a cylindrical triaxial sample, is equal to $(45^\circ - \phi/2)$. Taylor stated that it has been found by observation that the measured angle is, in the majority of cases, greater than the theoretical angle. Failure along planes other than those predicted by theory, may be

due to stress concentrations. It seems rational to assume that the failure conditions existing in a triaxial specimen may approximate the failure conditions which exist in a horizontally compressed backfill; since the triaxial compression test is nothing more than a passive type of earth-pressure test.

It was not possible to obtain the measured orientation of the failure surface in many of the 18 in. wall loose tests because the intersection of the failure surface with the backfill surface was not clearly defined. Figures 61 and 62 show the raised portion of the backfill which has failed due to penetration of the retaining wall.

CENTER OF PRESSURE LOCATIONS

Variations in the location of the center of pressure as the wall penetrated into the backfill are shown in Figs. 63 and 64. The test data shown in these figures is representative of all the data that was obtained from the 12 and 18 in. wall tests. It should be noted that for small penetrations, the data obtained during Phases I and II differ significantly. The results differ since the vertical restraint that was used during Phase II performed much more satisfactorily than the restraint used during Phase I. These results, like those of Phase I, show higher center of pressure locations when the backfill is placed in a loose state.

AVERAGE EARTH-PRESSURE DATA

A summary of significant earth-pressure data obtained during the second phase of testing is tabulated in Table 13. The numerical values listed in Table 13, except for those appearing in the Center of Pressure Column, represent values obtained by averaging the data listed in previous tables. The values in the Center of Pressure Column are average values obtained from each series of tests. The location of the center of pressure for each test

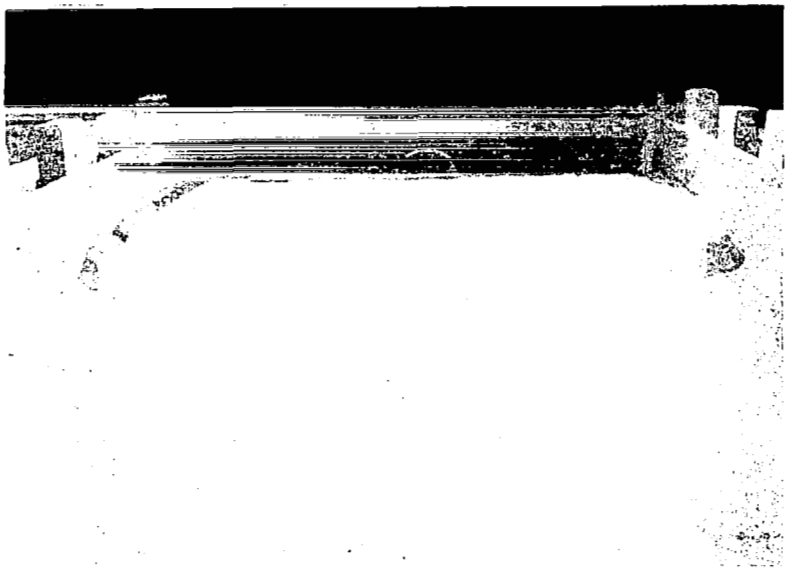

Fig. 61 View of Intersection of Failure Surface with Surface of Backfill - 12 in. High Wall, Dense Test

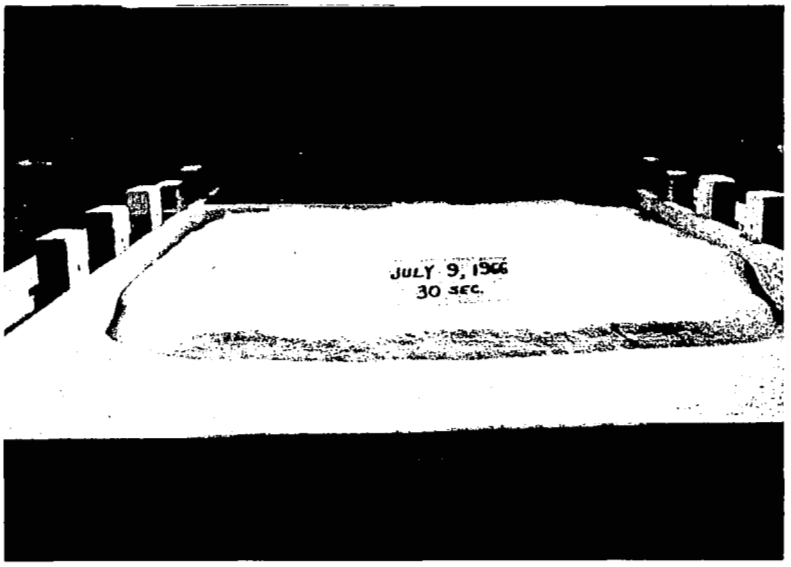

Fig. 62 View of Intersection of Failure Surface with Surface of Backfill - 18 in. High Wall, Dense Test

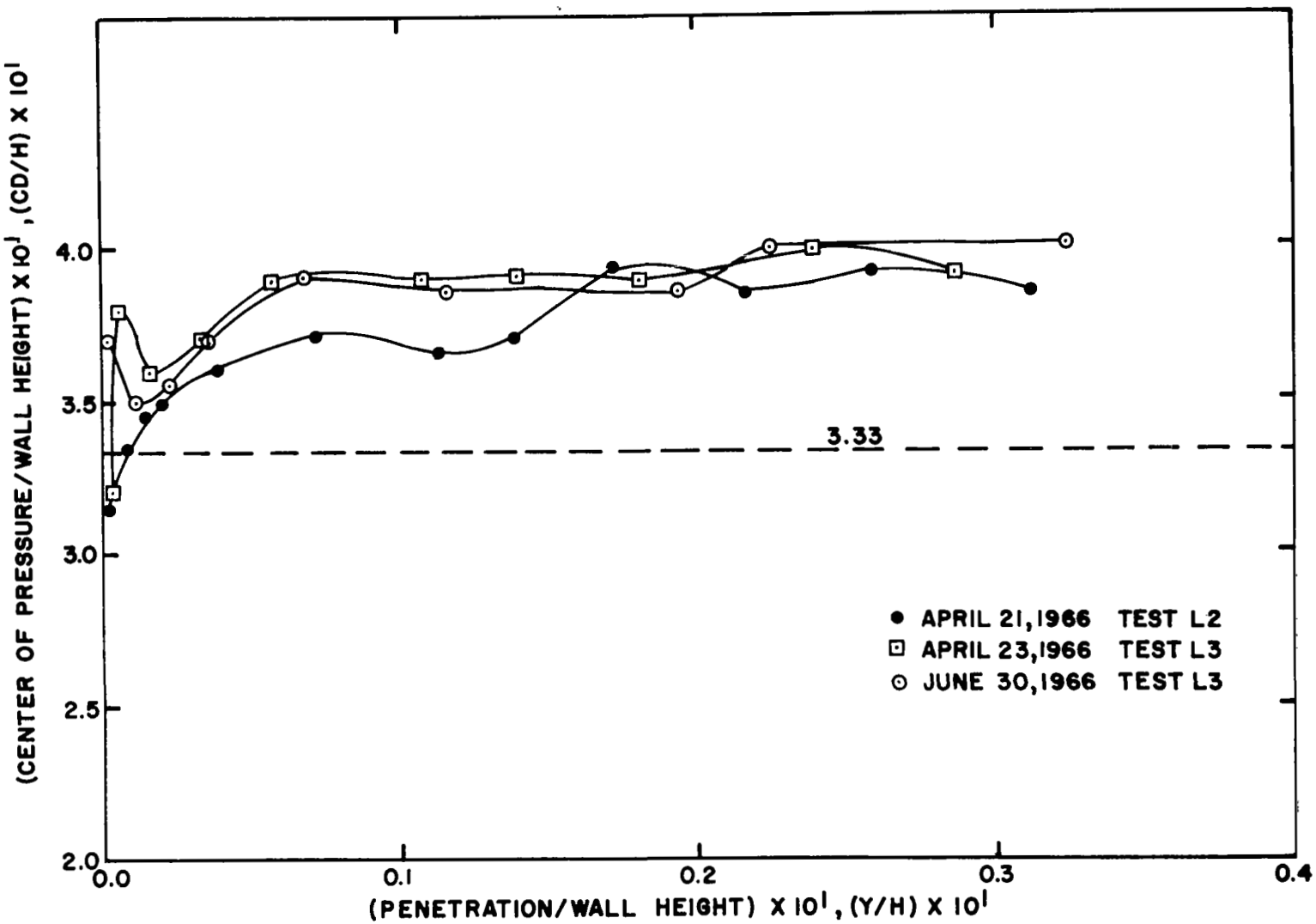

FIG. 63 EFFECT OF WALL PENETRATION ON THE LOCATION OF THE CENTER OF PRESSURE - 12 IN. WALL, LOOSE CASE

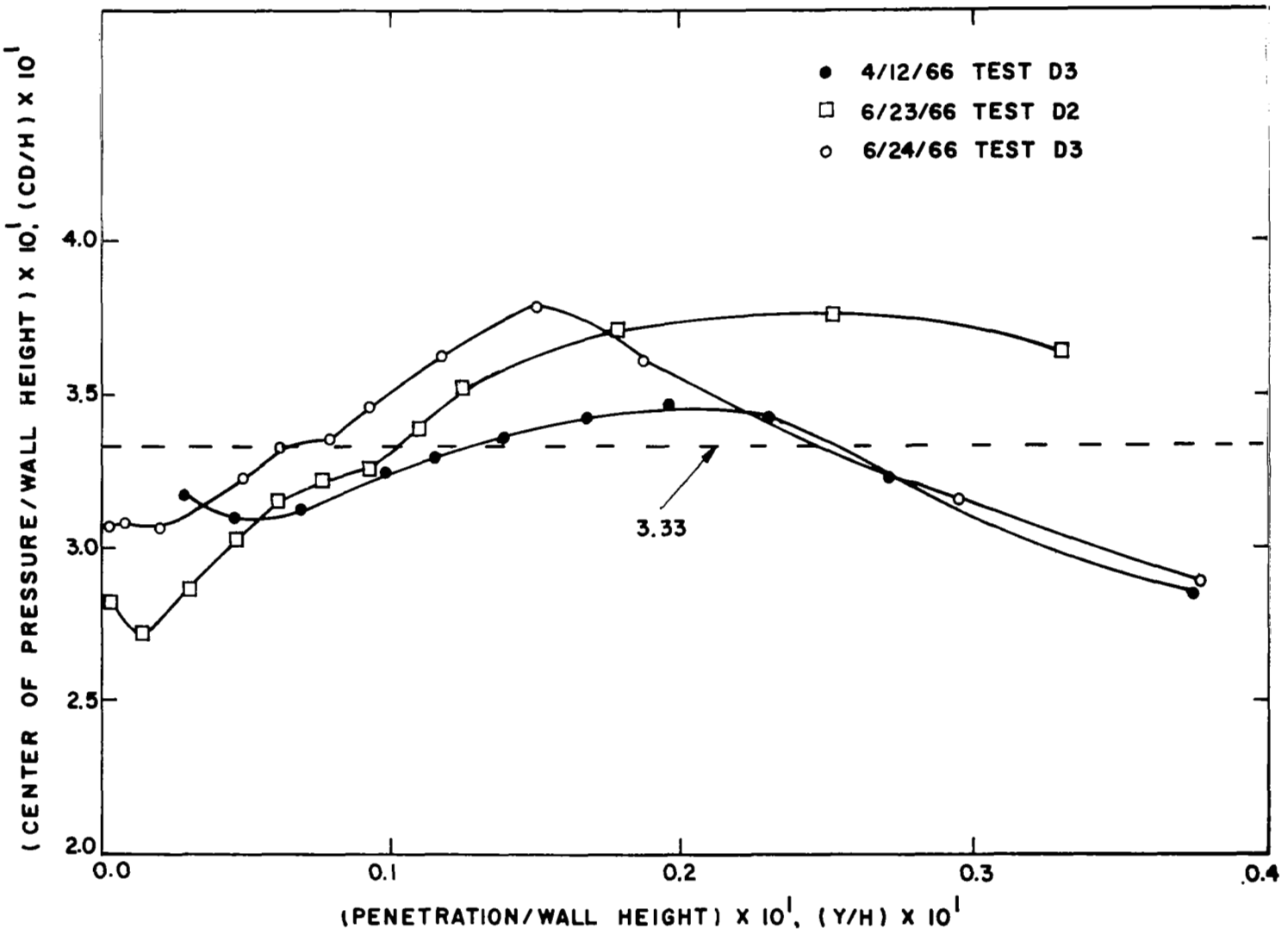

FIG. 64 EFFECT OF WALL PENETRATION ON THE LOCATION OF THE CENTER OF PRESSURE - 12 IN. WALL, DENSE CASE

TABLE 13

COMPARISON OF AVERAGE MEASURED AND CALCULATED

EARTH-PRESSURE FACTORS

Test Conditions	Penet./Ht. of Wall Y/H (in./in.)	Earth-Pressure Factor		Developed Internal Friction ϕ (Degrees)	Measured Failure Pl. Orient. β_m (Degrees)	Calculated Failure Pl. Orient. β_T (Degrees)	Center of Pressure CD/H (in./in.)
		Measured $K_p/\cos\delta$	Calculated $K_p/\cos\delta$				
12 in. Wall Dense Backfill	0.0113	12.6	10.9	54.1	20.1	16.4	0.332
18 in. Wall Dense Backfill	0.0175	13.8	12.9	52.7	20.1	14.9	0.332
12 in. Wall Loose Backfill	0.309	6.0	8.6	33.6	22.7	16.9	0.396
18 in. Wall Loose Backfill	0.211	5.8	7.0	35.9	24.2	19.0	0.388

has not been reported. The listed values represent the average locations of the center of earth pressure at the time of failure, which is defined by development of the maximum earth pressure.

Table 13 illustrates the good agreement obtained between the 12 and 18 in. wall tests. The average orientation of the failure surface for the dense 12 and 18 in. wall tests indicates that the geometrics of the highly stressed soil masses are similar. In other words, the distances from the face of the 18 in. wall to the failure surface were approximately 1.5 times greater than the corresponding distances in the 12 in. wall tests. Therefore, assuming that uniform soil conditions exist between the 12 and 18 in. wall tests, the amount of penetration required to produce failure in the 18 in. wall tests, should be approximately 1.5 times greater than the 12 in. wall penetration that is required to produce a similar state of failure. If the above is true, the dimensionless ratio (Penetration/Height of Wall) should have the same value for the 12 and 18 in. wall tests. Inspection of Table 13 shows that the value of the dimension ratio (Penetration/Height of Wall) required to produce failure within a dense backfill is larger for the 18 in. wall tests. For any particular set of soil and boundary conditions, the passive earth pressure is a function of the developed internal friction and the developed wall friction. The development of these two parameters, at any point within the backfill, is a function of the overburden pressure. The increased confining pressures that existed in the 18 in. wall tests may have caused the discrepancy in the dimensionless ratio (Penetration/Height of Wall) values.

Comparison of the dimensionless ratio, Y/H, values for the two series of loose tests indicates that the 18 in. wall ratio is less than the 12 in. wall ratio. The discrepancy exists because of the manner in which the tests were conducted. Each of the walls was penetrated into the backfill approximately

3.8 in. The shape of developed earth pressure-penetration curve for a loose backfill, was such that the maximum earth pressure nearly always occurred at the maximum amount of penetration. Therefore, had the 18 in. wall penetrated into the backfill a distance of 5.5 in. the ratio Y/H would have been nearly the same and the measured earth-pressure factors may have agreed closer.

CHAPTER VIII

PHASE III TEST RESULTS AND DISCUSSION

Phase III utilized conical and spherical models. Two sizes of each model were tested. The rate and vertical depth beneath the backfill surface at which the models penetrated were also varied. Details pertaining to the model designs and the test setup are shown in Chapters III and IV. Over 200 usable tests were obtained during this phase.

EFFECT OF MODEL PENETRATION VELOCITY ON EARTH PRESSURE

The models penetrated the backfill at the constant rates of 4.0, 2.667 and 0.533 ips. As found in Phase II, the scatter in the data from these tests obscured any force-velocity relationships which may have existed. Several force-penetration plots for various representative tests are shown in Appendix B. It can be seen from these plots that the scatter is not abnormal for tests conducted using soil as a penetration medium. Only the force-penetration curves for the 4.0 ips tests have been presented, since no additional information is attained from the tests at other rates.

It should be pointed out that it was known prior to the beginning of this study, that for low rates of penetration the strain rate effects would be small. However, it was felt that the test data would reflect some trends that would be more pronounced at higher penetration velocities.

HORIZONTAL FORCE-PENETRATION CURVES

The magnitude of the horizontal force that is developed, during model penetration, is a function of the following parameters:

(1) Geometry of the contact surface between the backfill and the penetrating model,

(2) Rate of penetration,

(3) Amount of penetration,

(4) Vertical depth at which the model penetrates the backfill,

(5) Angle of internal friction of the backfill,

(6) Angle of friction between soil and polyethylene membrane,

(7) Backfill density.

During each test that utilized a spherical segment model, all of these parameters, except 2, varied simultaneously. Only parameters 3, 4, 5, 6 and 7 varied during a cone test, since the contact geometry of the cones remained constant. Although the vertical distance between the geometric center of the model and the initial surface of the backfill remained constant, the effect of the overburden depth is continuously changing as the contact area between the model and the soil increases. The simultaneous variations in parameters creates a complex situation to which there is no existing rigorous solution.

Cone Tests

It is essential that the above discussion be kept in mind when observing the force-penetration curves that are shown on the following pages. The force-penetration curves which were obtained from the tests that utilized cone shaped models are shown in Figs. 65 through 68. Each graph contains a family of curves which were obtained by drawing average curves through sets of data points obtained from three or more identical tests. Appendix B contains representative plots of the data points, through which the average curves were drawn. Each of the average curves is denoted by a Z value, which indicates the vertical distance between the lowest point on the model and the surface of the backfill. Examples of the vertical distances, Z, are shown in Fig. 36 on p. 59. Figure 36 expresses the Z distances in terms of the base radius r of the model. The backfill material was placed either in its densest state (102.0 pcf) or loosest state (88.0 pcf).

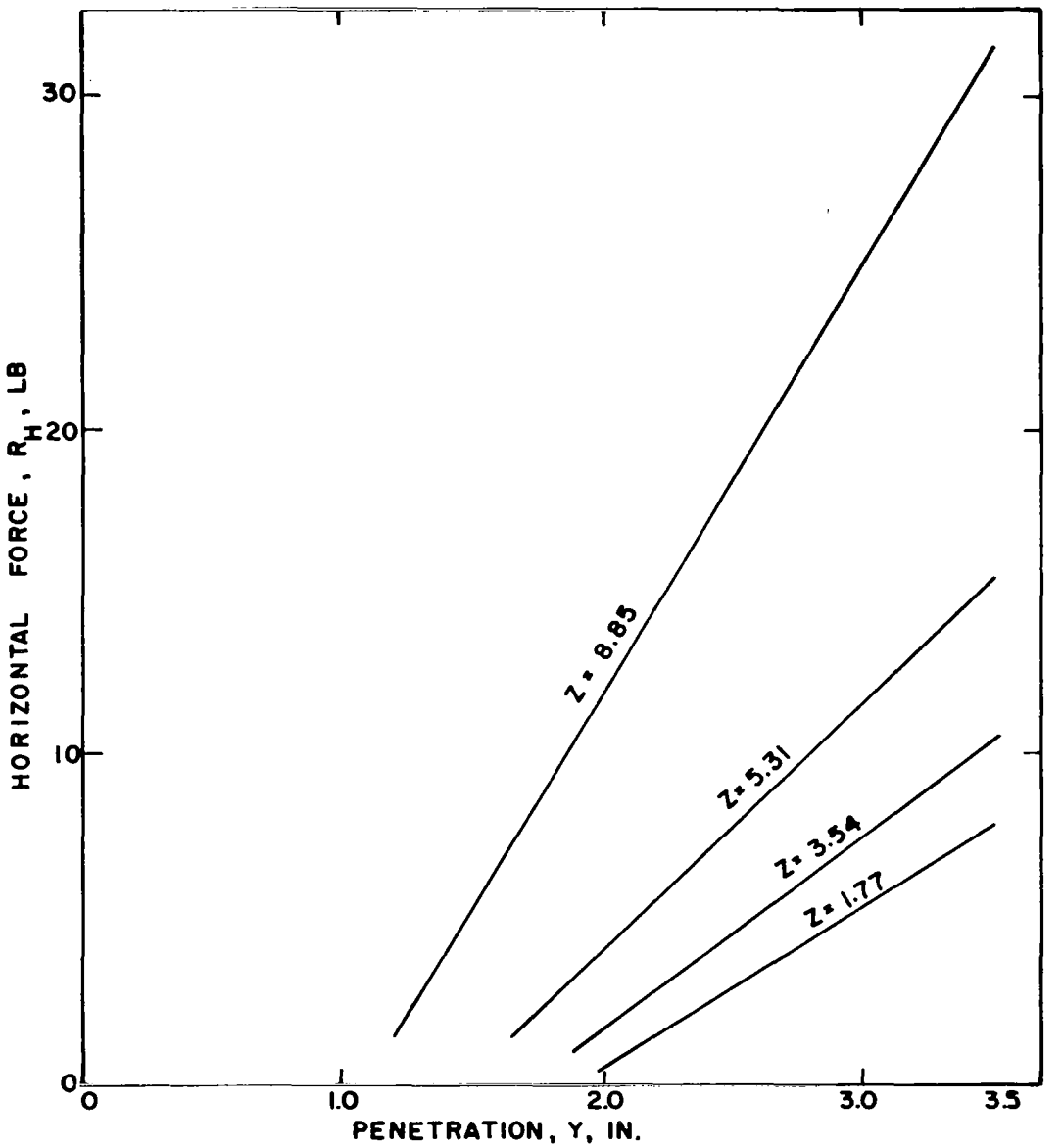

FIG.65 HORIZONTAL FORCE VERSUS PENETRATION FOR MULTIPLE OVERBURDEN DEPTHS-3.54 IN. DIA CONE, LOOSE CASE

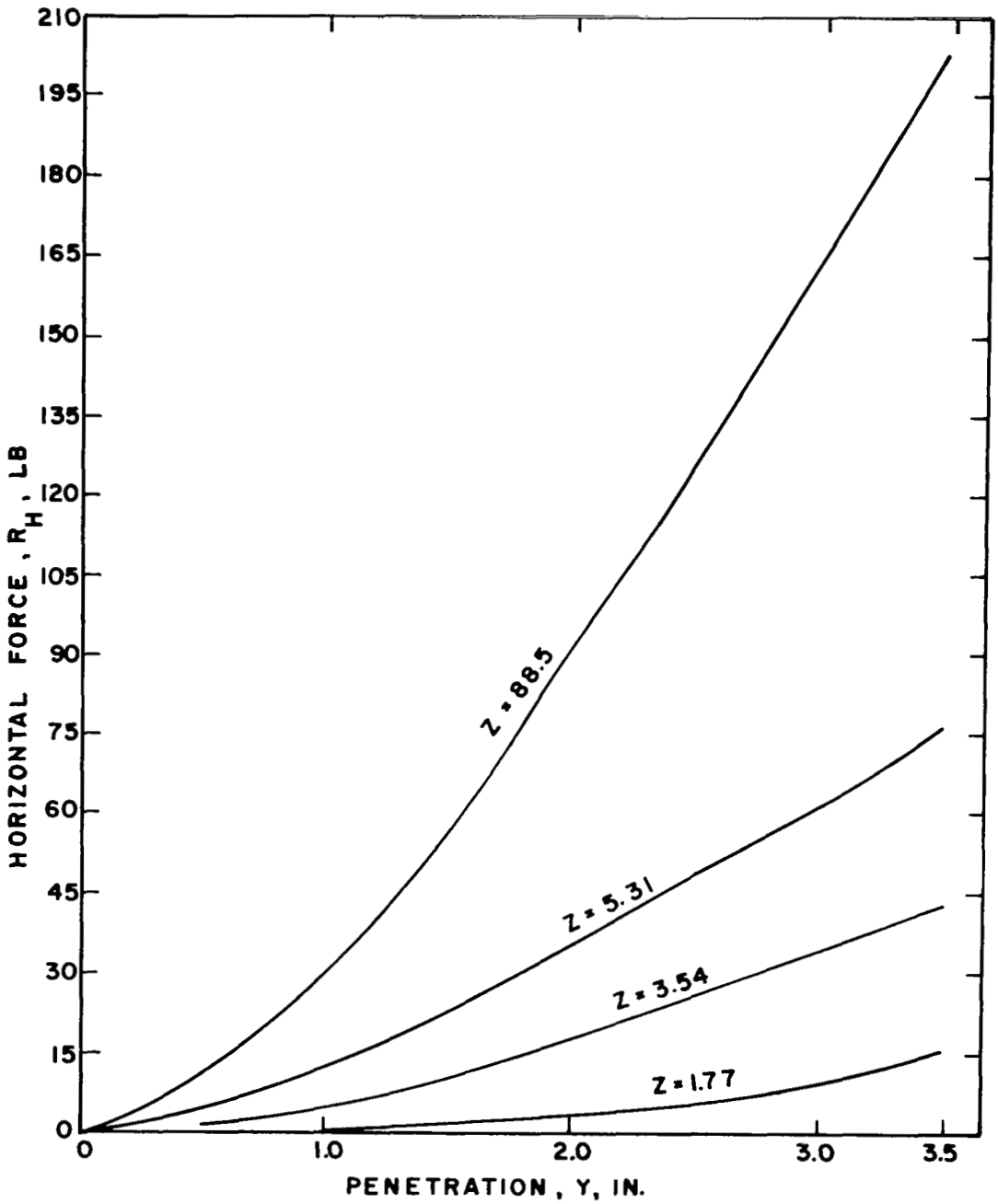

FIG. 66 HORIZONTAL FORCE VERSUS PENETRATION FOR MULTIPLE OVERBURDEN DEPTHS – 3.54 IN. DIA CONE, DENSE CASE

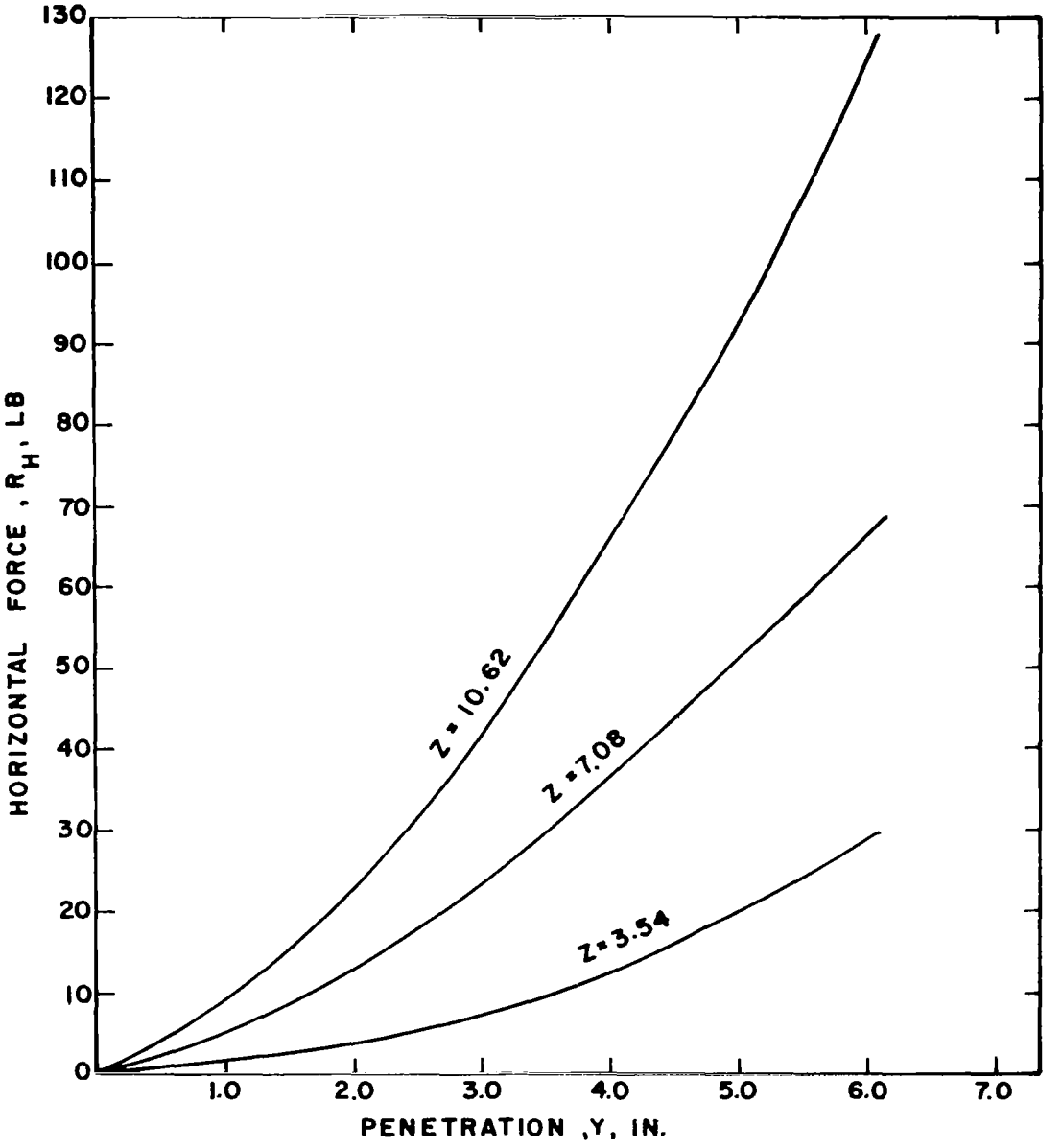

FIG. 67 HORIZONTAL FORCE VERSUS PENETRATION FOR MULTIPLE OVERBURDEN DEPTHS—7.08 IN. DIA CONE, LOOSE CASE

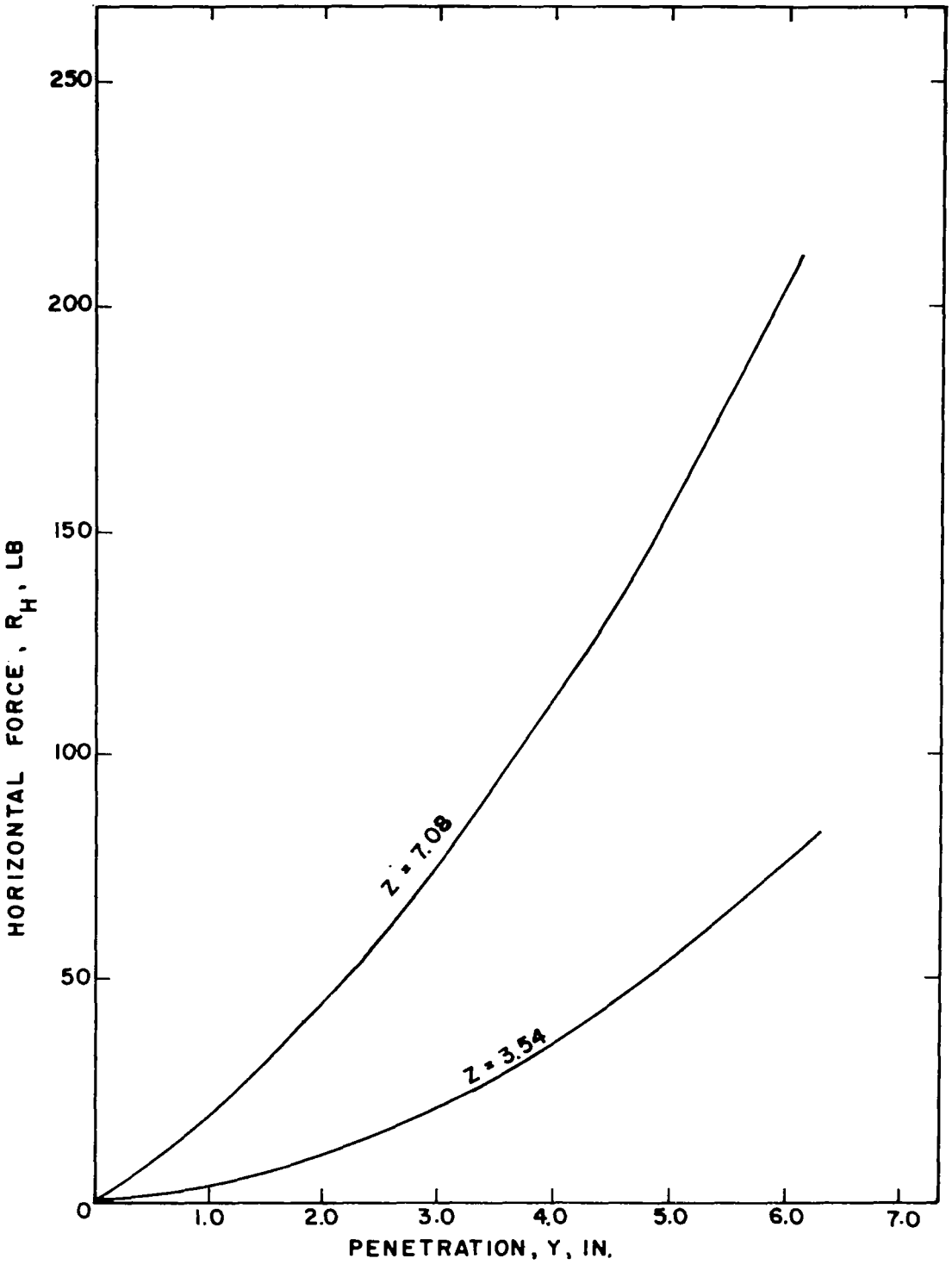

FIG. 68 HORIZONTAL FORCE VERSUS PENETRATION FOR MULTIPLE OVERBURDEN DEPTHS - 7.08 IN. DIA CONE, DENSE CASE

All of the average curves, except those obtained from the 3.54 in. dia cone loose-test data, are concave upward, This shape is to be expected since the increasing contact area of the cone as it penetrates into the backfill is described by an equation which is also concave upward when plotted. These graphs demonstrate the large influence the density of the backfill material has upon the horizontal forces developed on the penetrating cone. The early portion of the family of curves shown in Fig. 65 was not obtained because the measuring load cell was not sensitive enough to provide recordable output for this developed range of loads.

Sphere Tests

Figures 69 through 72 illustrate the average force-penetration curves obtained for the 4.33 and 8.66 in. dia spherical segments. From these figures it can be seen that the test conditions have an appreciable effect upon the shape of the curves. The curves obtained from the 4.33 in. dia spherical segment, loose tests are similar in shape to those obtained from the 3.54 in. dia cone, loose tests. The curves in Fig. 70 are similar in shape to the passive earth pressure-penetration curves obtained from Phase I or II test results. The test date for the 8.66 in. dia spherical segment indicates that for low overburden depths and loose backfill conditions the curves are similar in shape to those obtained from the cone data.

Only the portions of the curve which correspond to penetrations approximately equal to and less than the penetration required to completely bury the model have been presented. Information concerning the developed horizontal forces which correspond to penetrations greater than the height of the models is desirable; however, the behavior of the membrane precluded meaningful force measurements. As the model penetrated into the backfill the membrane

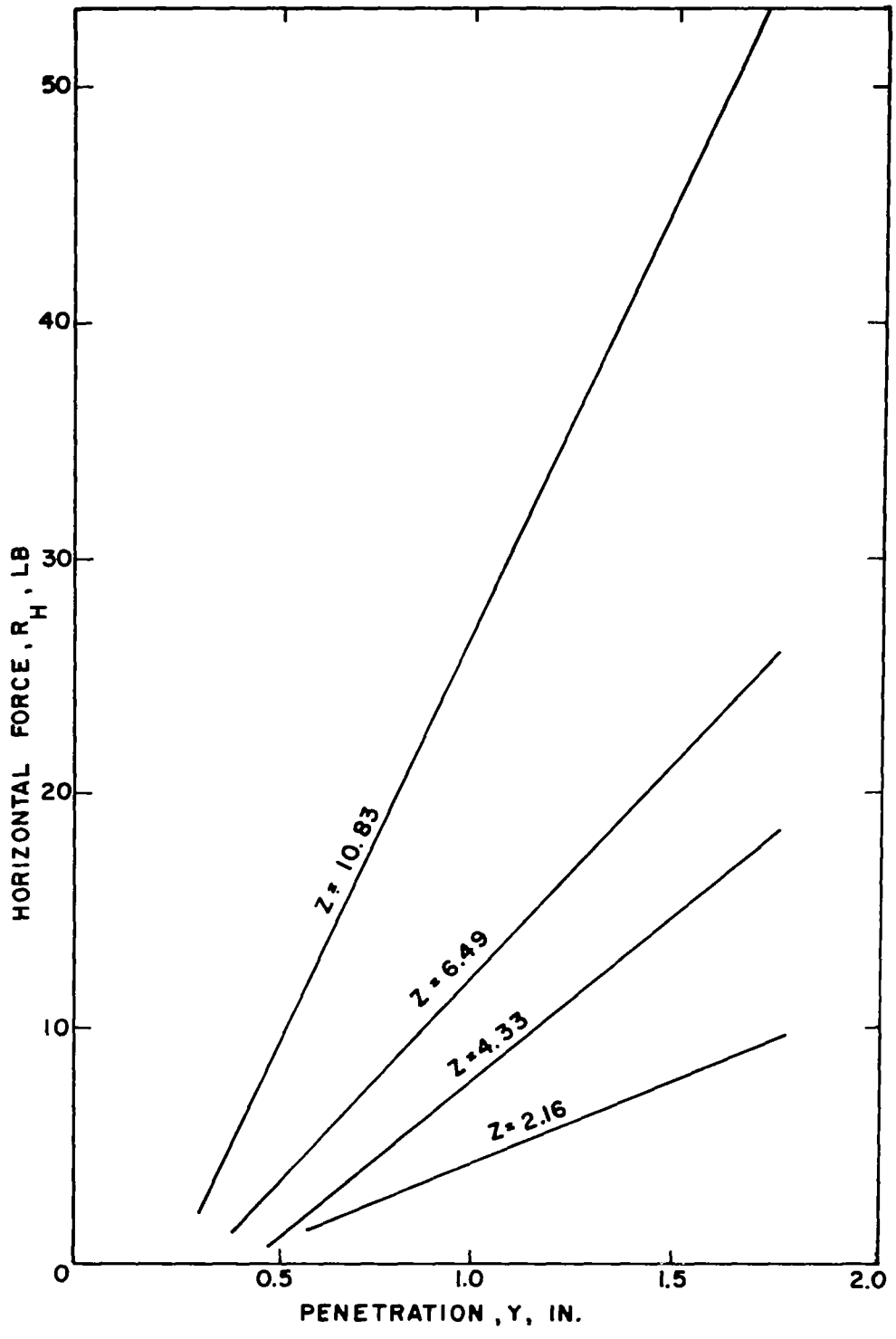

FIG. 69 HORIZONTAL FORCE VERSUS PENETRATION FOR MULTIPLE OVERBURDEN DEPTHS — 4.33 IN. DIA SPHERICAL SEGMENT, LOOSE CASE

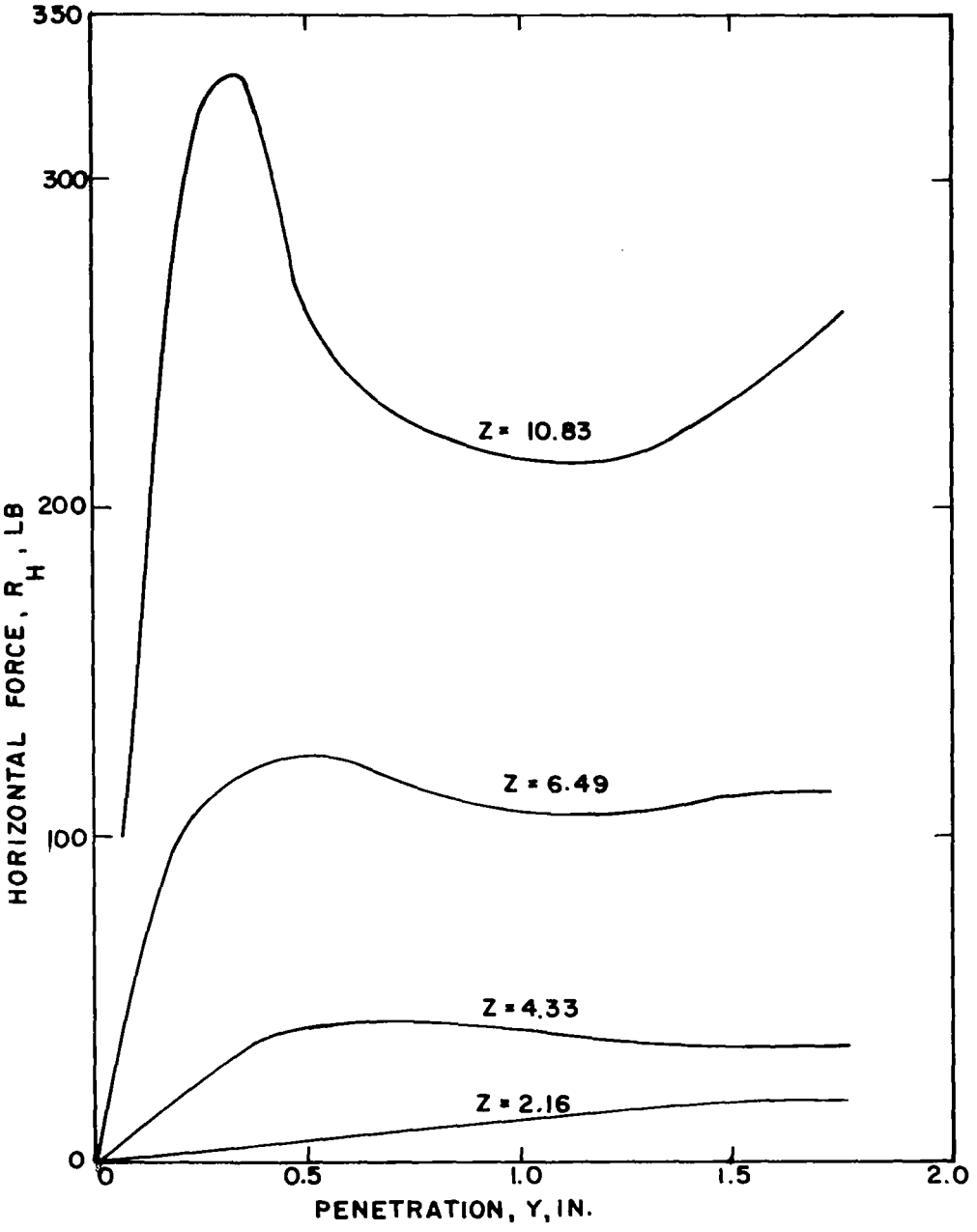

FIG. 70 HORIZONTAL FORCE VERSUS PENETRATION FOR MULTIPLE OVERBURDEN DEPTHS - 4.33 IN. DIA SPHERICAL SEGMENT, DENSE CASE

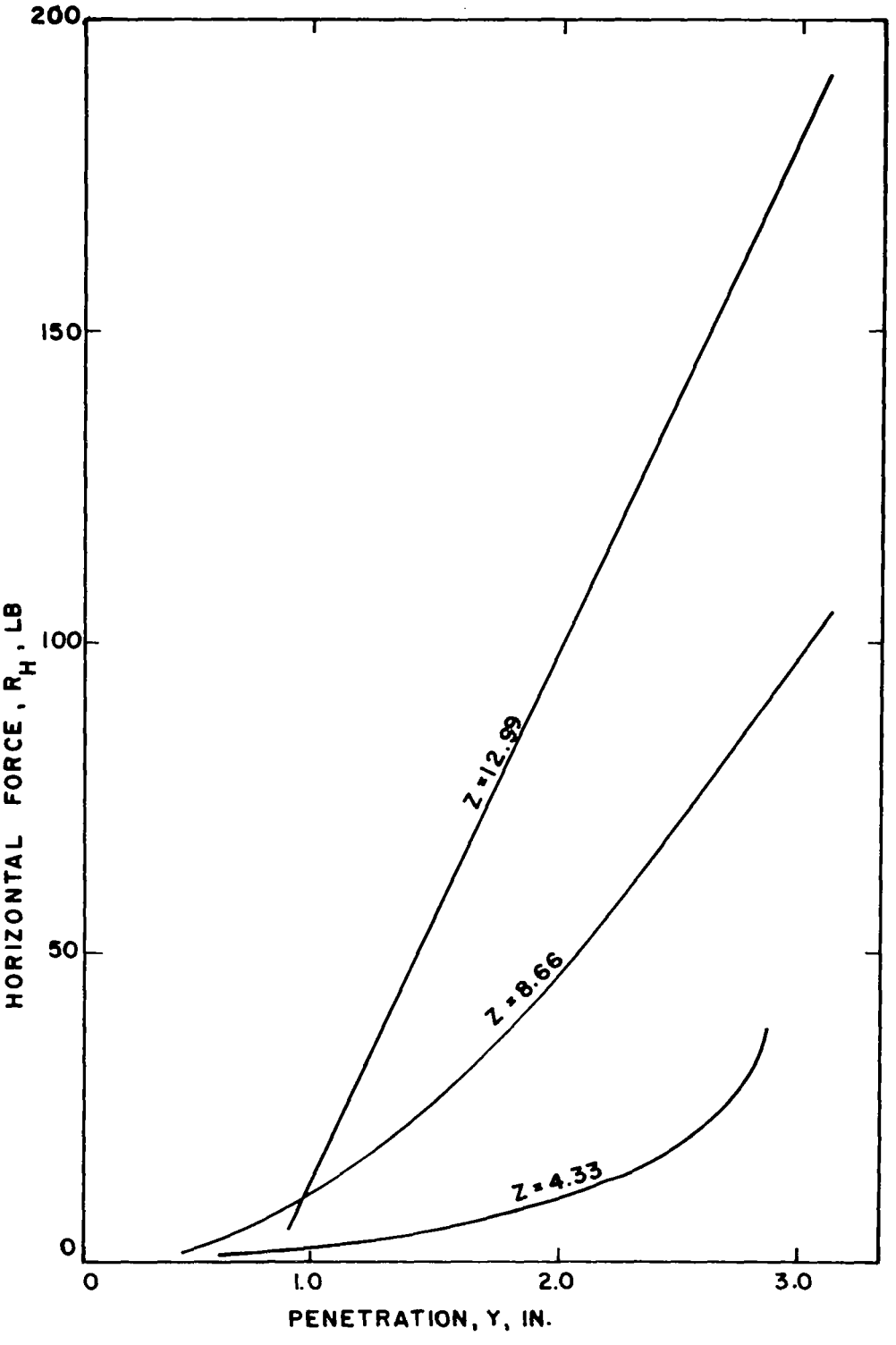

FIG. 71 HORIZONTAL FORCE VERSUS PENETRATION FOR MULTIPLE OVERBURDEN DEPTHS – 8.66 IN. DIA SPHERICAL SEGMENT, LOOSE CASE

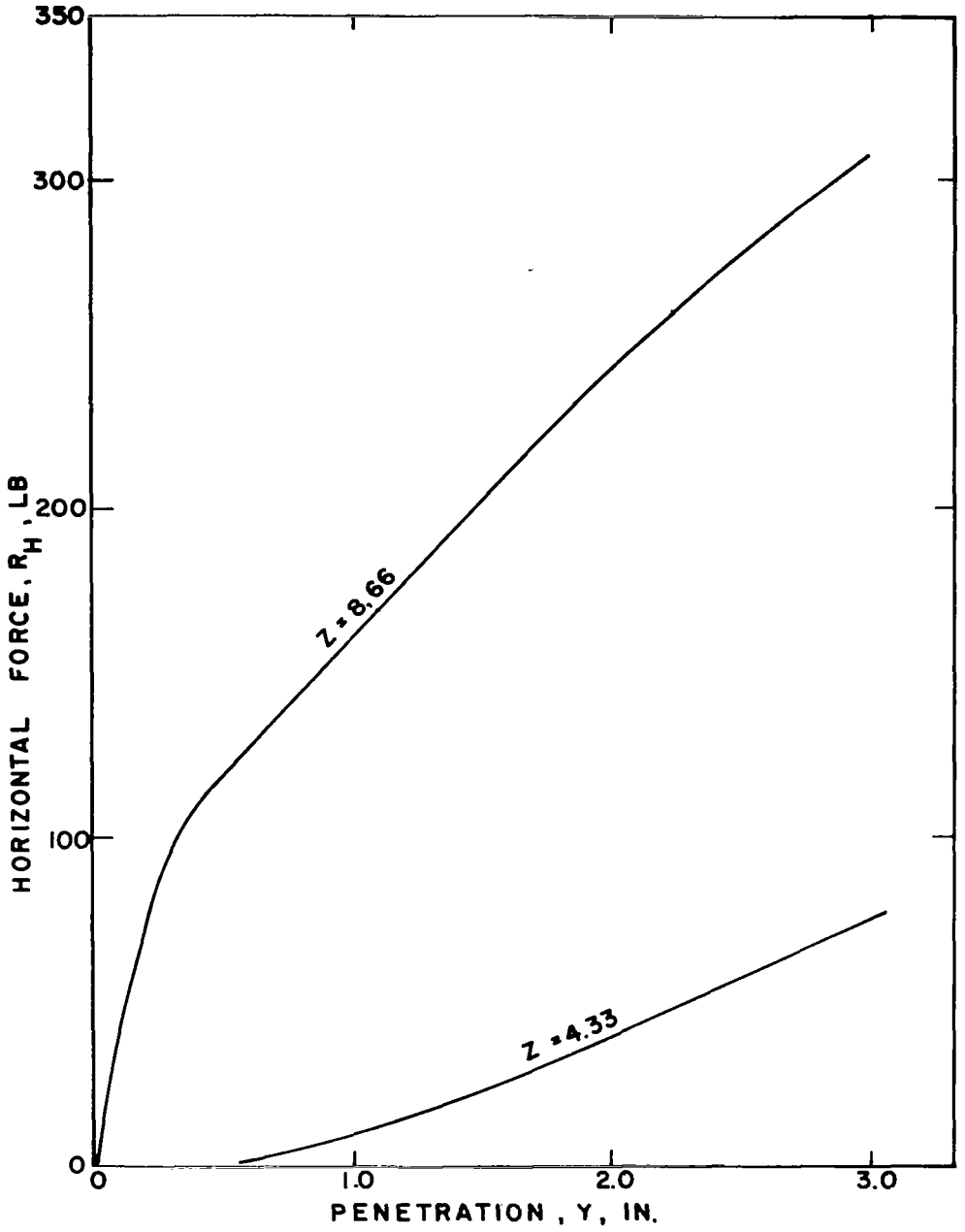

FIG.72 HORIZONTAL FORCE VERSUS PENETRATION FOR MULTIPLE OVERBURDEN DEPTHS - 8.66 IN. DIA SPHERICAL SEGMENT, DENSE CASE

deformed to accommodate the geometry of the model. However, when the model penetrated a distance greater than its height, the membrane allowed sand to flow through the hole in the membrane which was created by the previous penetration. This sand leakage caused the horizontal forces to be greatly reduced, thereby making the forces recorded meaningless.

MAXIMUM HORIZONTAL FORCE ANALYSIS

Generally, the force-penetration curves that were presented previously indicate that the horizontal force continues to increase with increasing penetration. This is true for all tests, except the 4.33 in. dia spherical segment, dense tests. Since insufficient data was obtained for penetration values greater than the heights of the models, the maximum horizontal force was defined as the force which occurred at the instant the model penetration was equal to the height of the model. If the maximum force occurred before the model had penetrated its full height, this force was recorded as the maximum.

Table 14 lists maximum force values obtained from the force-penetration curves. Plots of $R_{H(max)}$ versus Z^2 are shown in Figs. 73 through 75. The plots show that the maximum horizontal force is approximately a linear function of the overburden depth squared. The straight line drawn through the data points in Fig. 73 has a force intercept. This intercept is due to membrane resistance which was created during model penetration. Since developed forces for this case were relatively small, the membrane resistance cannot be considered negligible. The membrane resistance can be eliminated from Fig. 73 by constructing a straight line which passes through the origin and is parallel to the existing straight line. Although the geometrics of the two models differ vastly, the maximum horizontal forces may be represented by the same relationship.

TABLE 14

MAXIMUM DEVELOPED HORIZONTAL FORCES

Model Type	Penetration (in.)	Maximum Horizontal Force (lb)	Depth of Overburden (in.)	Density (pcf)
3.54 in. dia cone	3.06	5.5	1.77	88.0
	3.06	7.5	3.54	88.0
	3.06	12.0	5.31	88.0
	3.06	25.0	8.85	88.0
	3.06	10.5	1.77	102.5
	3.06	36.0	3.54	102.5
	3.06	63.0	5.31	102.5
	3.06	165.0	8.85	102.5
7.08 in. dia cone	6.12	30.0	3.54	88.0
	6.12	69.0	7.08	88.0
	6.12	127.5	10.62	88.0
	6.12	79.0	3.54	102.5
	6.12	211.5	7.08	102.5
4.33 in. dia spherical segment	1.25	6.0	2.16	88.0
	1.25	11.5	4.33	88.0
	1.25	17.0	6.49	88.0
	1.25	36.5	10.83	88.0
	1.25	16.0	2.16	102.5
	0.80	43.0	4.33	102.5
	0.50	125.0	6.49	102.5
	0.35	326.0	10.83	102.5
8.66 in. dia spherical segment	2.50	18.0	4.33	88.0
	2.50	71.0	8.66	88.0
	2.50	41.0	12.99	88.0
	2.50	57.5	4.33	102.5
	2.50	277.5	8.66	102.5

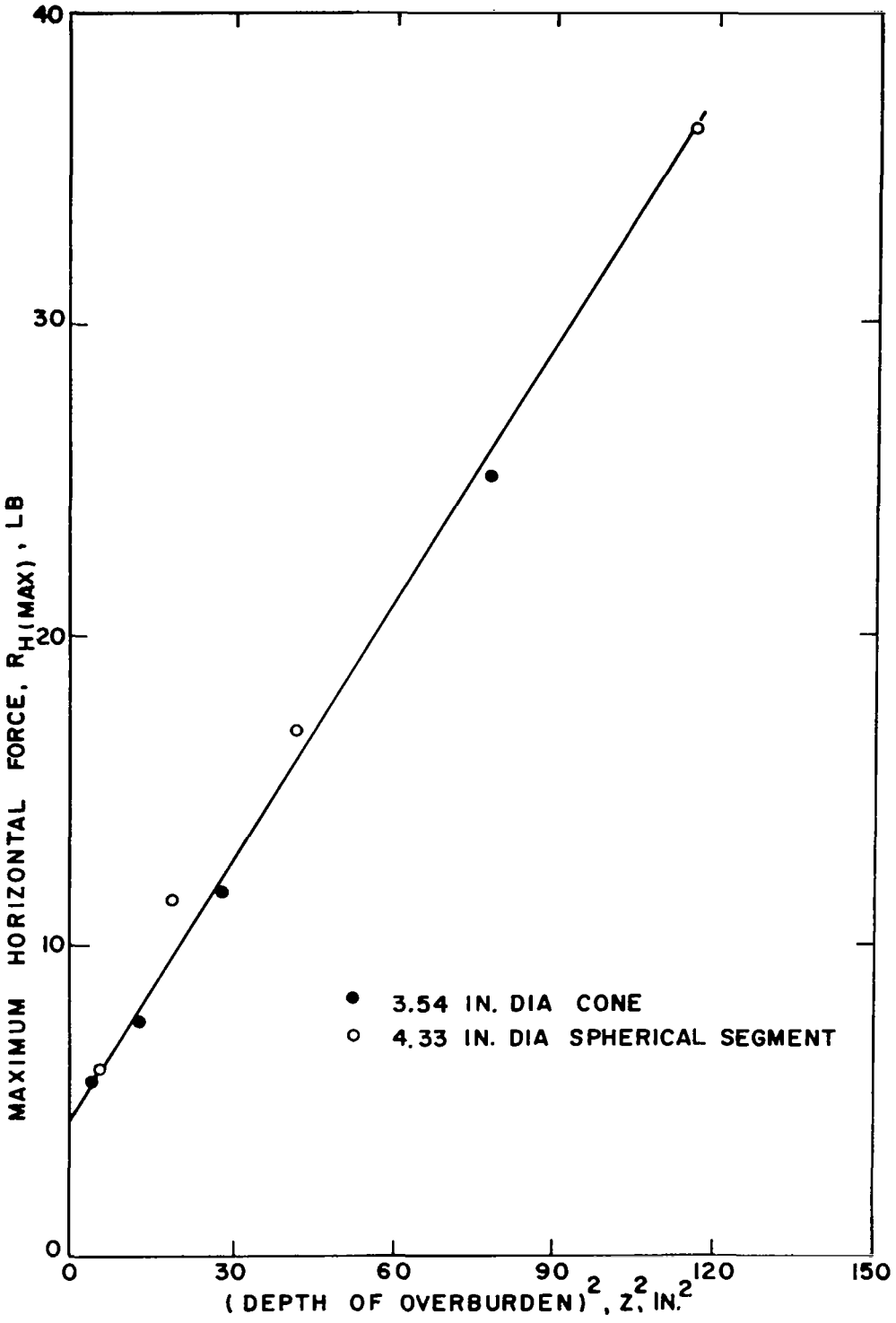

FIG. 73 EFFECT OF OVERBURDEN DEPTH ON THE MAXIMUM DEVELOPED HORIZONTAL FORCE - LOOSE CASE

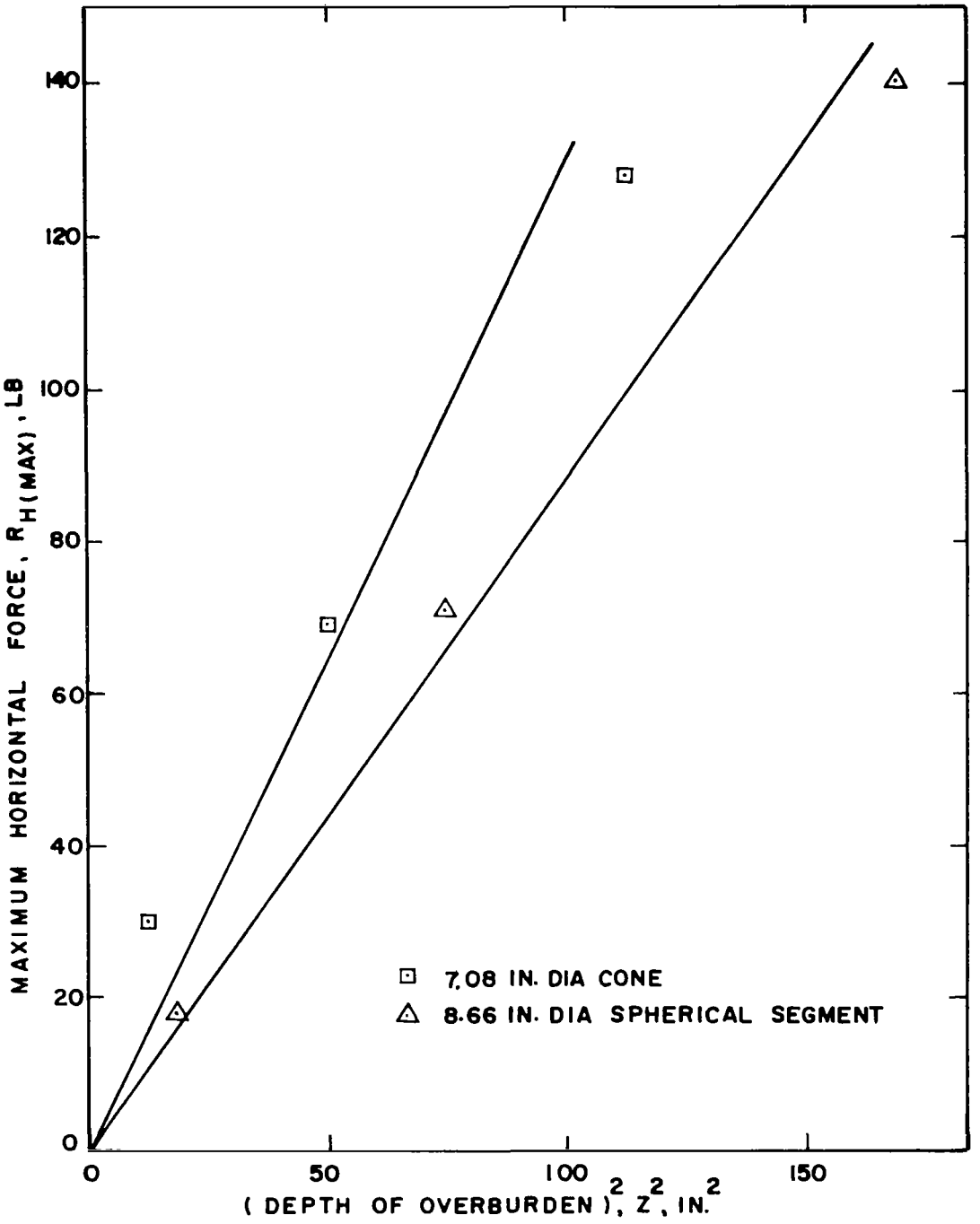

FIG.74 EFFECT OF OVERBURDEN DEPTH ON THE MAXIMUM DEVELOPED HORIZONTAL FORCE - LOOSE CASE

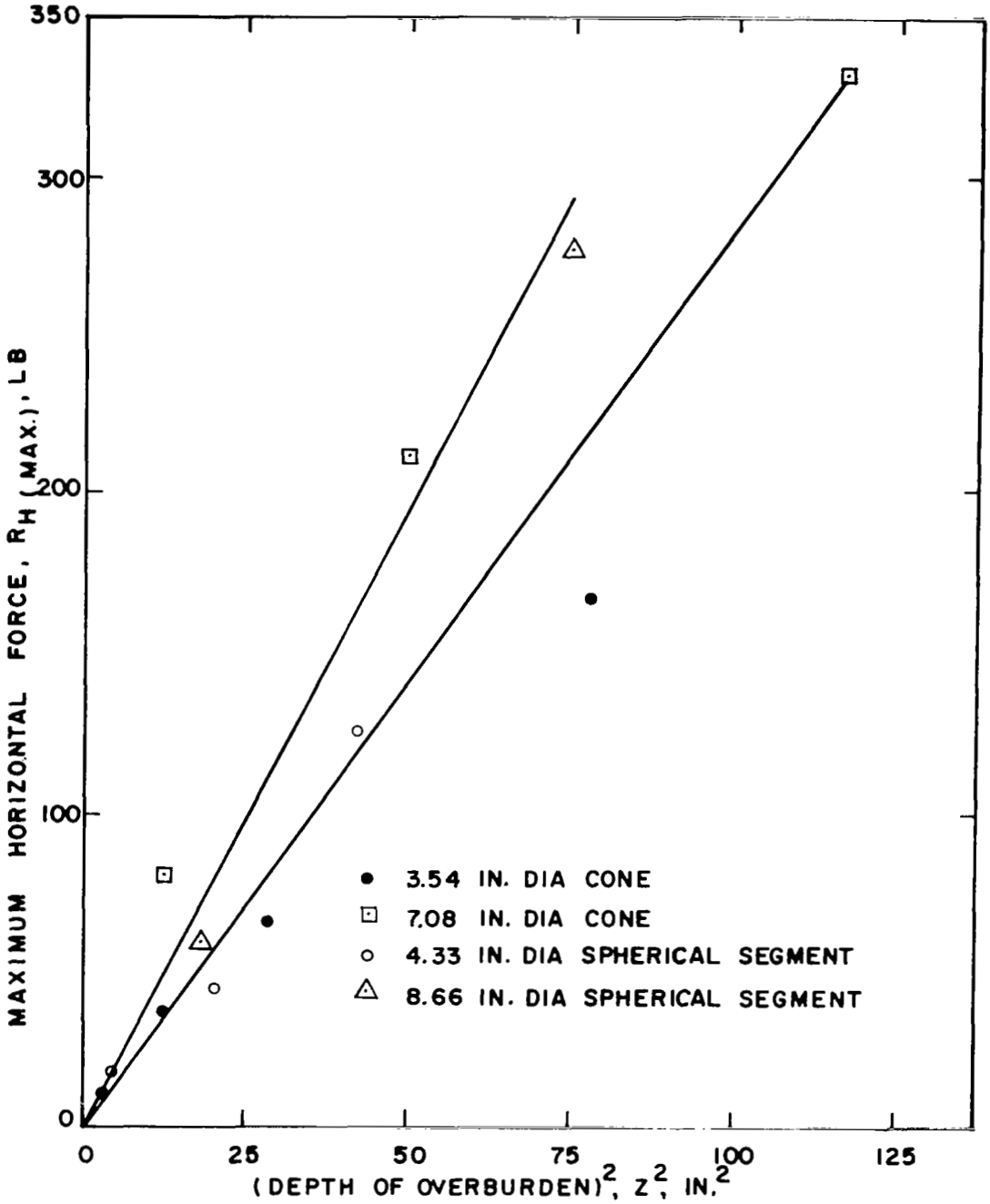

FIG. 75 EFFECT OF OVERBURDEN DEPTH ON THE MAXIMUM DEVELOPED HORIZONTAL FORCE - DENSE CASE

Two relationships are required to represent the maximum forces developed on the large cone and large spherical segment when they are penetrated into a backfill in a loose state. The developed horizontal soil forces on the cone were higher than the soil forces acting on the spherical segment.

The maximum horizontal force data obtained from the tests conducted when the backfill was placed in a dense state is plotted in Fig. 75. The maximum forces developed on the large models are greater than the forces developed on the small models, which is to be expected.

Maximum Force Prediction

It has been shown that the maximum developed force is a linear function of the overburden depth squared. The existing passive earth-pressure equations which were derived assuming that plane-strain earth-pressure conditions existed, also indicate the same relationship. It is desirable to write an expression for $R_{H(max)}$ which involves the geometry of the model and the engineering properties of the soil.

Equation 18 is proposed to fulfill these desirable requirements.

$$R_{H(max)} = \gamma r_p^2 K_h \int_0^Z Z dZ \tag{17}$$

$$R_{H(max)} = 0.5 \gamma Z^2 r_p^2 K_h \tag{18}$$

The terms appearing in the above equation are defined as follows:

$R_{H(max)}$ = Maximum horizontal force,

γ = Unit density of the backfill material,

r_p = The radius of the projected contact area at the instant the maximum horizontal force occurs,

Z = Vertical depth beneath the backfill surface,

K_h = Factor which depends upon the developed angle of internal friction, the developed angle of friction between the soil and the membrane, and the geometric properties of the penetrating model.

The quantity $0.5 \gamma Z^2$ may be thought of as an equivalent fluid pressure acting over a depth Z. Values of K_h were calculated using Eq 18. These values along with other significant information are listed in Table 15. The table shows that the K_h values obtained for the large model tests (7.08 in. dia cone and 8.66 in. dia spherical segment) on loose sand are approximately equal to the small model tests on loose sand. The family of curves on p. 131 shows that the maximum developed force, for each of the curves, occurs at varying amounts of penetration. The value of K_h for the 4.33 in. dia spherical segment was calculated using an r_p value of 1.5 inches. This value of r_p corresponds to a penetration of 0.5 inches. The 4.33 in. dia spherical segment tests on dense backfills were the only series of tests in which it was necessary to use an approximate value of r_p. Comparison of the values obtained from the dense tests shows that the small models (3.54 in. dia cone and 4.33 in. dia spherical segment) have K_h values which are approximately 3 and 6 times greater than the large models respectively.

Figures 76 and 77 show the 8.66 in. dia spherical segment prior to, and following a dense test. The overburden depth for this test was 4.33 inches. Figure 77 shows the displacement of the sand caused by model penetration. Several failure surface intersections are visible within the displaced portion of the backfill. The increasing contact area of the model caused

TABLE 15

COMPARISON OF K_h VALUES

Model Type	K_h ($in.^{-1}$)	Ratio of K_h Values for Dense and Loose States	Density γ (pcf)
3.54 in. dia cone	3.3	9.3	88.0
3.54 in. dia cone	30.5		102.5
7.08 in. dia cone	4.1	2.6	88.0
7.08 in. dia cone	10.5		102.5
4.33 in. dia spherical segment	2.2	19.3	88.0
4.33 in. dia spherical segment	42.5		102.5
8.66 in. dia spherical segment	1.9	3.7	88.0
8.66 in. dia spherical segment	7.0		102.5

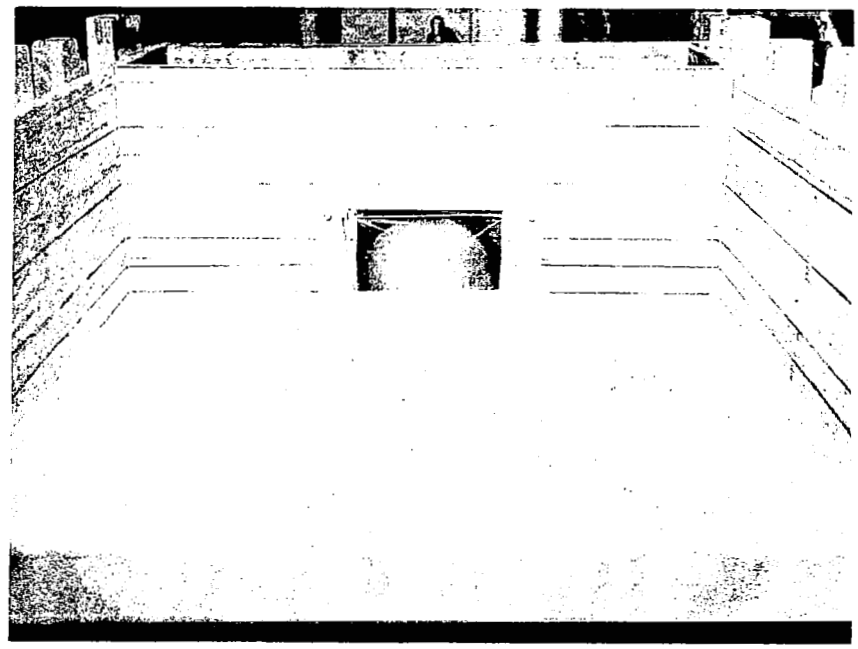

Fig. 76 Front View of Test Setup Before Model Penetration

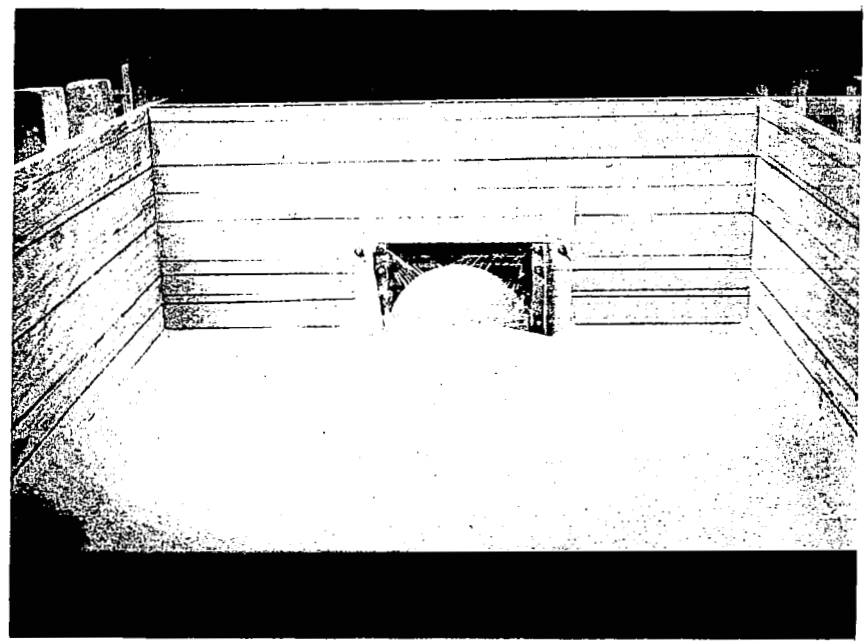

Fig. 77 Front View of Test Setup After Model Penetration

several well defined failure intersections to occur during each test. Therefore, unlike the earlier tests in which the depth of the penetrating wall remained constant and only one well defined failure surface occurred, the cone and spherical segment tests indicate that several major slip surfaces occur.

RESULTANT VERTICAL FORCE-PENETRATION CURVES

The resultant vertical force R_v and the method of calculation are defined on p. 60 and 61. As can be seen from Eq 15 on p. 60, the value of R_v depends upon the magnitude of the measured bending moment data and the moment arm D. Since the soil pressure distribution on the model was unknown, it was necessary to make some assumptions concerning the location of R_v. A uniform pressure distribution was assumed to act over the projected area of the cone. The projected area of a cone on a horizontal plane is triangular in shape. Therefore, D was calculated using

$$D = D_o - 2/3\ Y \tag{19}$$

where,

D = Moment arm,

D_o = Distance between the model tip and the center of the bonded SR-4 strain gages,

Y = Model Penetration.

Equation 19 was also used to calculate D values when the spherical segment models were utilized. Although this is a further approximation, the error is thought to be negligible when compared to the error involved in the previous assumptions.

Plots of the development of the resultant vertical force as the model penetrated into the backfill are illustrated in Figs. 78 through 83. Each graph contains a family of curves which were obtained by drawing average curves through sets of data points taken from three or more identical tests. Appendix C contains representative plots of the data points, through which the average curves were drawn.

Cone Tests

The resultant vertical force-penetration curves are similar in shape to the horizontal force-penetration curves that were presented previously in this chapter. Examination of the upper graph in Fig. 78 shows that the measured resultant vertical force is independent of the depth of overburden Z. This curve was obtained from test results that were acquired from the penetration of the 3.54 in. dia cone into a loose backfill. The curves shown in the lower graph were obtained from the penetration of the same cone into a dense backfill. However, the lower graph demonstrates that the resultant vertical force is a function of the overburden depth Z. When the model penetrated into the backfill a portion of the soil was displaced to accommodate the model. The displacement can occur, either by the model forcing the soil to be displaced at the surface of the backfill or by local densification of the soil in the vicinity of the model.

When the backfill is initially in a dense state the major portion of the soil displacement occurs at the surface of the backfill. This displacement is illustrated in Fig. 37 on p. 61. Displacement of the soil is resisted by downward forces which are due to the weight of the soil above the model and shear forces which are developed at the boundaries between the displaced soil and the surrounding backfill material. The upward force on the

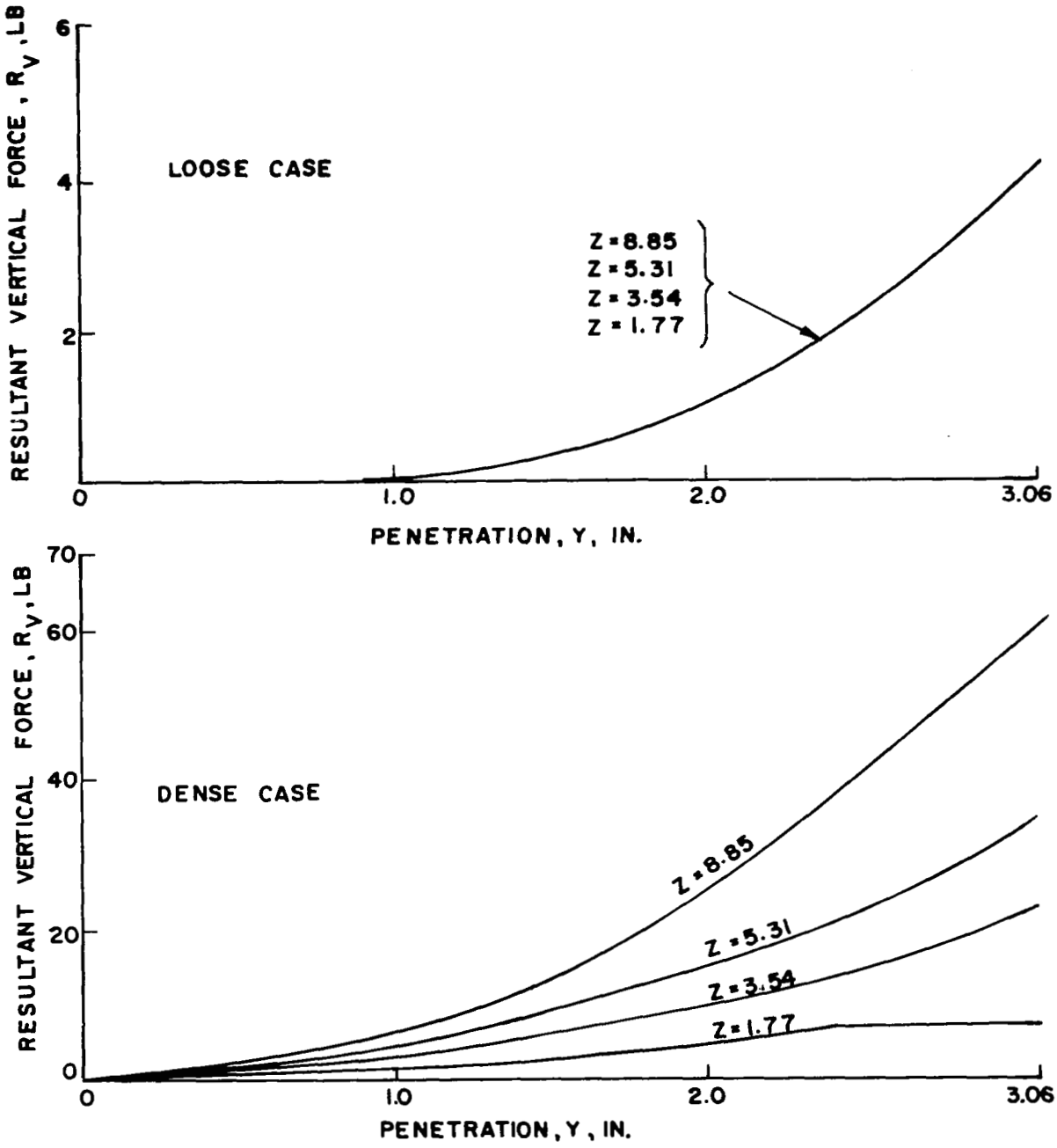

FIG. 78 RESULTANT VERTICAL FORCE VERSUS PENETRATION FOR MULTIPLE OVERBURDEN DEPTHS - 3.54 IN. DIA CONE, LOOSE, AND DENSE CASES

model is created by the soil which is confined beneath the lower side of the model. Since the soil is initially in its densest possible state practically no displacement of the soil occurs in the downward direction, but the soil is forced to flow in an upward direction. The lower graph in Fig. 78 shows that as the depth of overburden increases, the upward forces on the model increase at a faster rate than do the resisting downward forces.

Penetration of the model into a loose backfill causes the soil to densify in the vicinity of the model, thereby creating additional space to accommodate the penetrated portion of the model. The backfill material was placed by allowing the soil to fall through a funnel. This type of placement creates an overall unstable condition throughout the backfill. Slight vibrations or minor disturbances will cause the backfill to densify to a more stable condition. The upward displacement of the loose-backfill surface, due to model penetration, was slight when compared to the displacement which took place when the backfill was in a dense state.

Both test results and visual observations confirm that there is a significant difference between the behavior of the backfill in a loose and dense state. The large cone test results are shown in Figs. 79 and 80. The large cone, loose-backfill tests show that the resultant vertical force is a function of the overburden depth for depths less than 7.08 inches. The tests that were performed at a Z depth of 10.62 in. indicate that the resultant vertical forces are of the same magnitudes as those obtained from the tests conducted at a Z depth of 7.08 inches. This indicates that the increased upward vertical forces were nullified by the increased downward resistance that was afforded by the 3.54 in. of added backfill material.

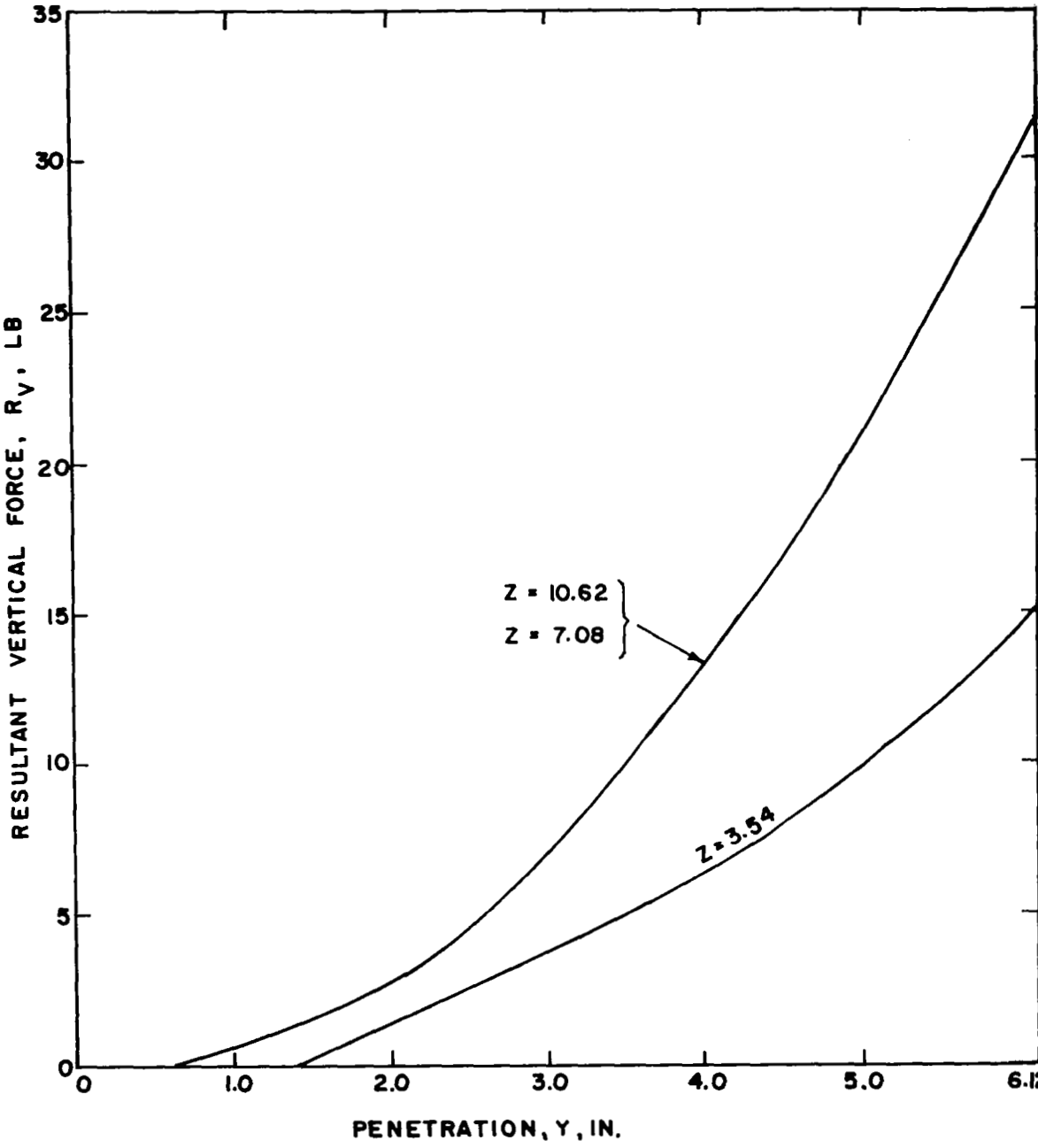

FIG. 79 RESULTANT VERTICAL FORCE VERSUS PENETRATION FOR MULTIPLE OVERBURDEN DEPTHS - 7.08 IN. DIA CONE, LOOSE CASE

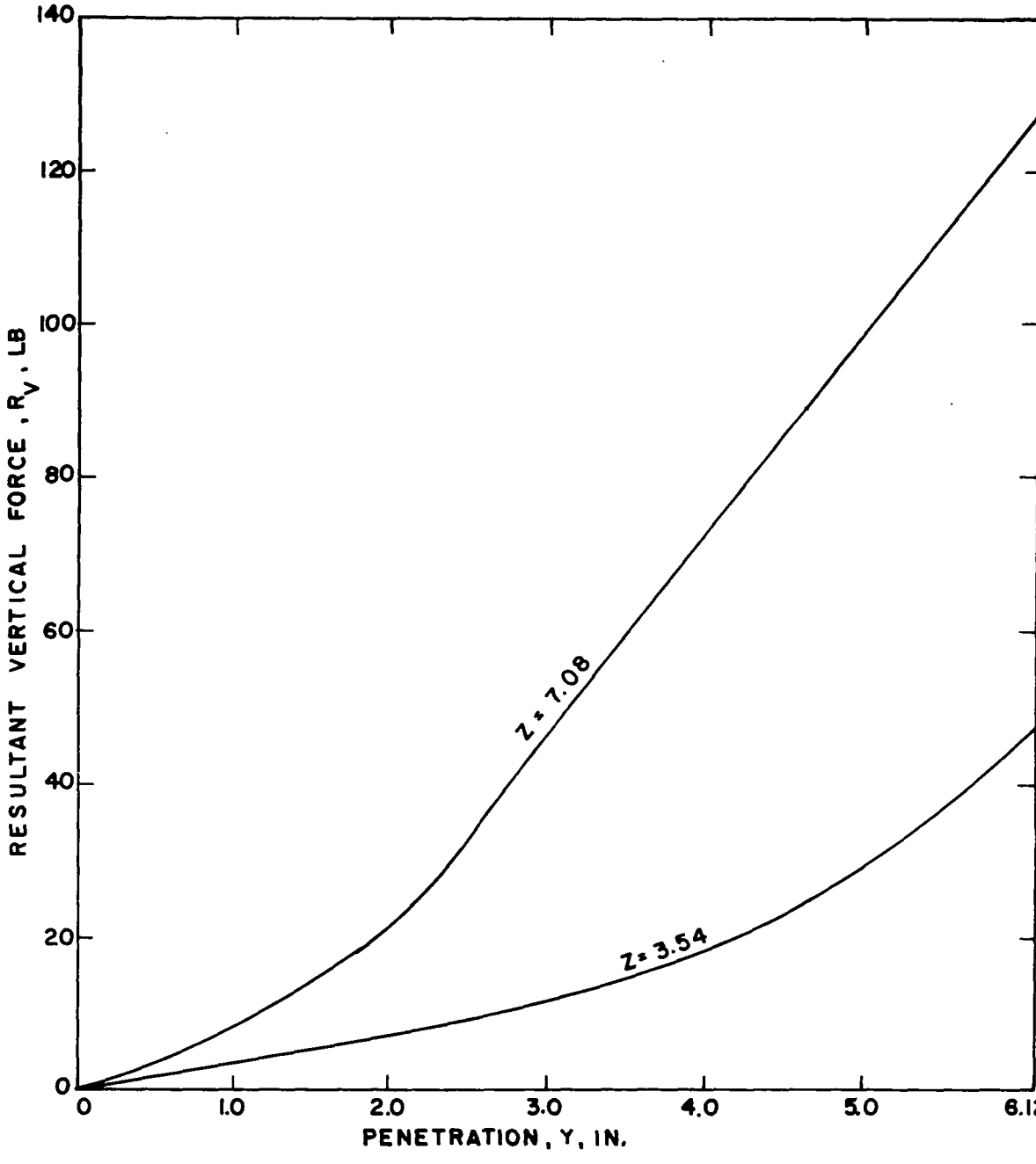

FIG. 80 RESULTANT VERTICAL FORCE VERSUS PENETRATION FOR MULTIPLE OVERBURDEN DEPTHS - 7.08 IN. DIA CONE, DENSE CASE

Sphere Tests

The resultant vertical force-penetration curves that were obtained from the sphere tests are shown in Figs. 81 through 83. The 4.33 in. dia spherical segment tests on loose sand show that the resultant vertical force R_v is not a function of the overburden depth. Identical tests were performed on dense backfills and these tests revealed that R_v is a function of the overburden depth. These findings agree with the 3.54 in. dia cone results. The previous discussion of the small cone test results also applies to the small spherical segment test results.

The small and large spherical segment tests on dense backfills indicate that R_v is a linear function of penetration. The test results indicate that the development of vertical forces on the models is governed by the complex behavior of the soil which is a function of the geometry of the penetrating body, the overburden depth, and the engineering properties of the backfill.

MAXIMUM RESULTANT VERTICAL FORCE ANALYSIS

All of the tests, except the small model tests on loose backfills, indicate that the resultant vertical force R_v is a function of the overburden depth Z. The purpose of this analysis is to provide a means of predicting the maximum resultant vertical soil response, $R_{v(max)}$, that occurred during the previous tests, Since $R_{v(max)}$ in the majority of the tests was found to be a function of the overburden depth Z it was convenient and logical to express $R_{v(max)}$ in terms of Z.

Plots of $R_{v(max)}$ versus Z^c are shown in Figs. 84 through 88. The $R_{v(max)}$ value was defined as the resultant vertical force which occurred at the instant the model penetration was equal to the height of the model. The overburden exponent c is a constant whose value depends on the type of model

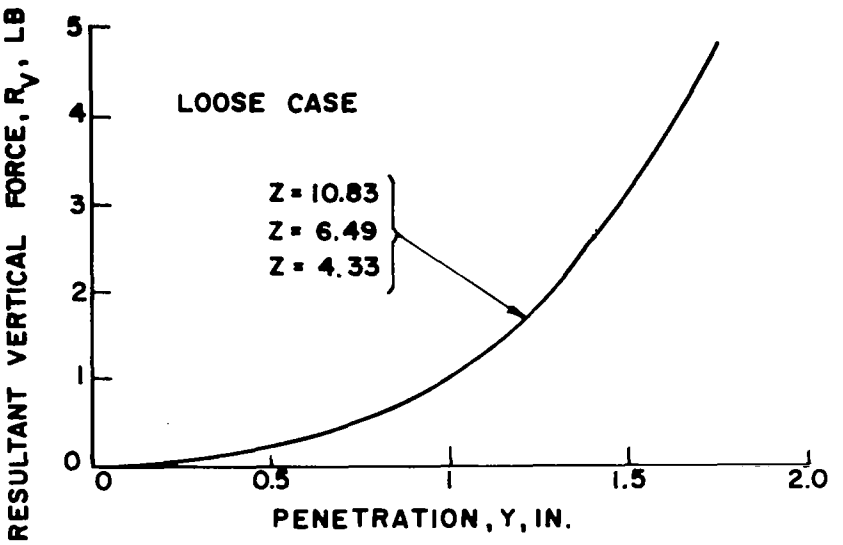

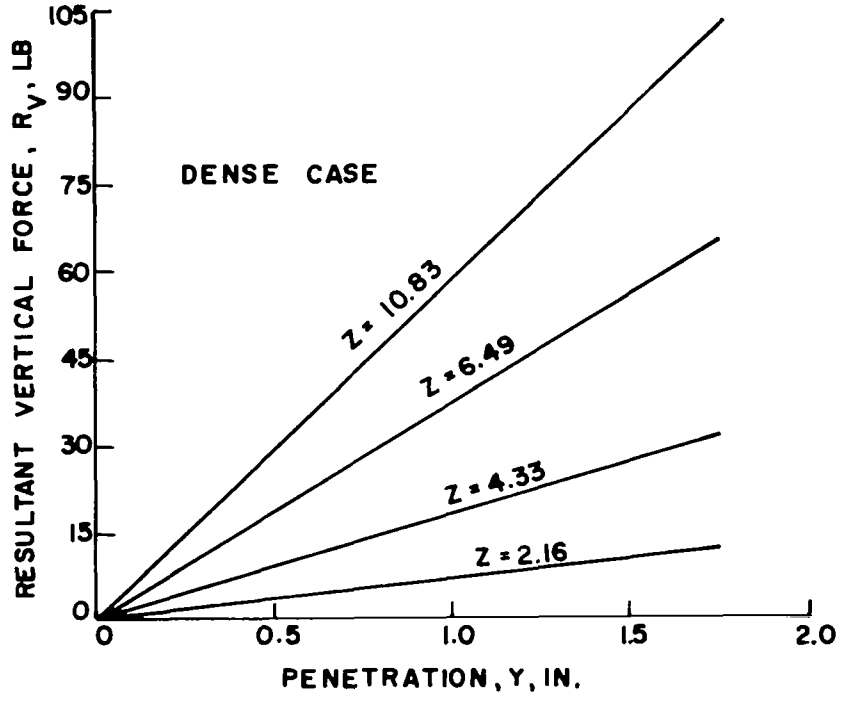

FIG. 81 RESULTANT VERTICAL FORCE VERSUS PENETRATION FOR MULTIPLE OVER-BURDEN DEPTHS - 4.33 IN. DIA SPHERICAL SEGMENT, LOOSE AND DENSE CASES

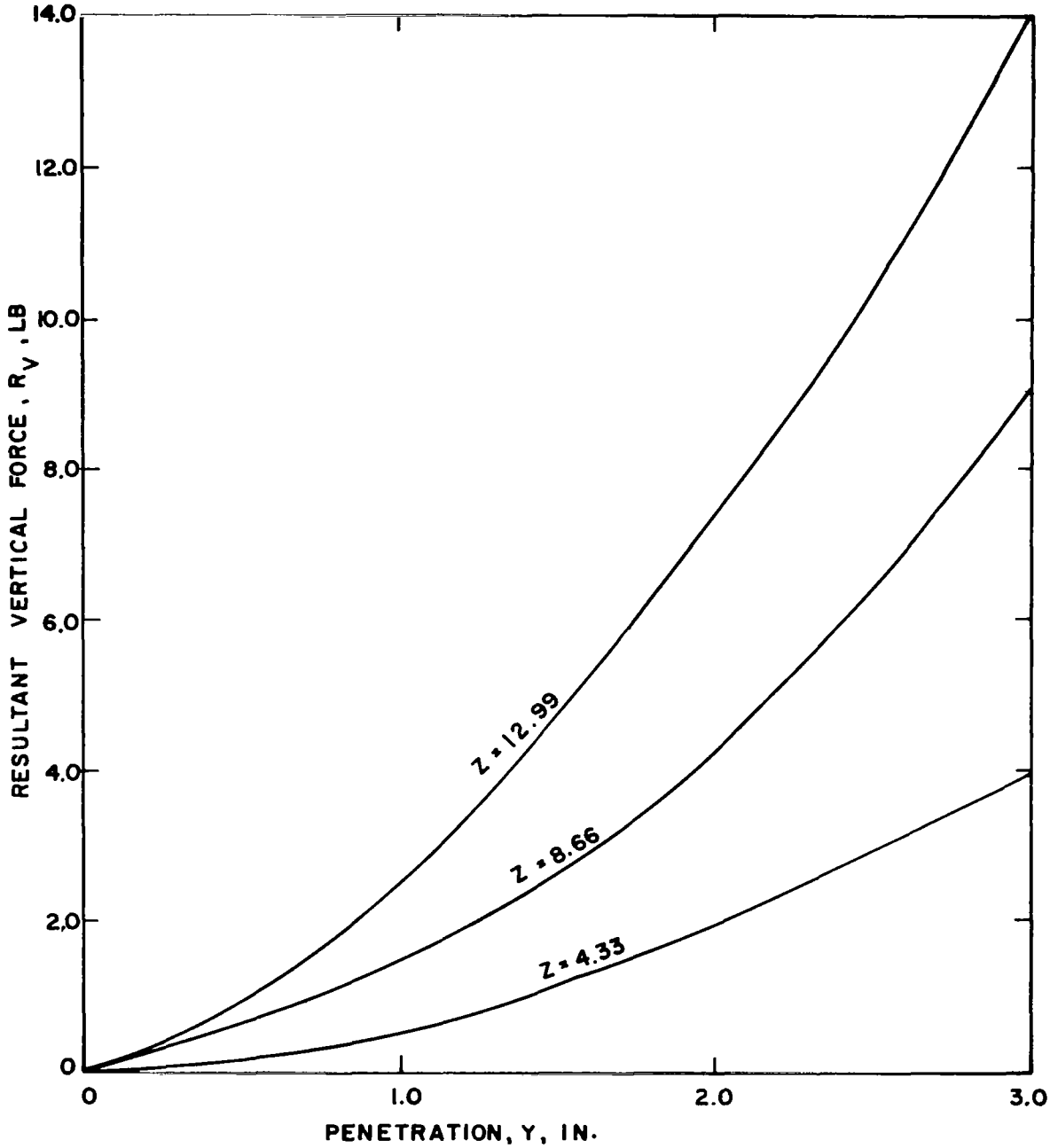

FIG. 82 RESULTANT VERTICAL FORCE VERSUS PENETRATION FOR MULTIPLE OVERBURDEN DEPTHS—8.66 IN. DIA SPHERICAL SEGMENT, LOOSE CASE

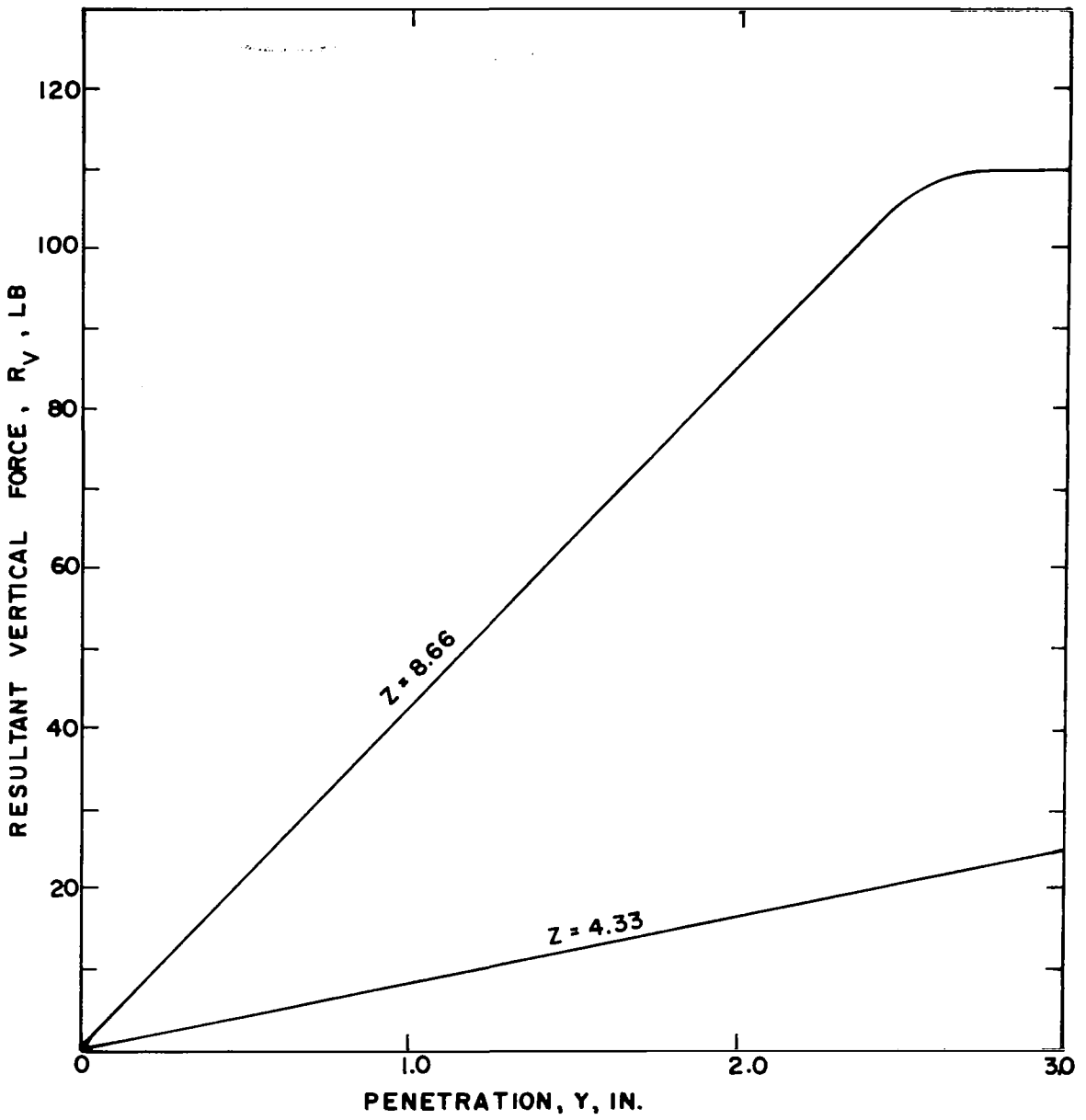

FIG.83 RESULTANT VERTICAL FORCE VERSUS PENETRATION FOR MULTIPLE OVERBURDEN DEPTHS – 8.66 IN. DIA SPHERICAL SEGMENT, DENSE CASE

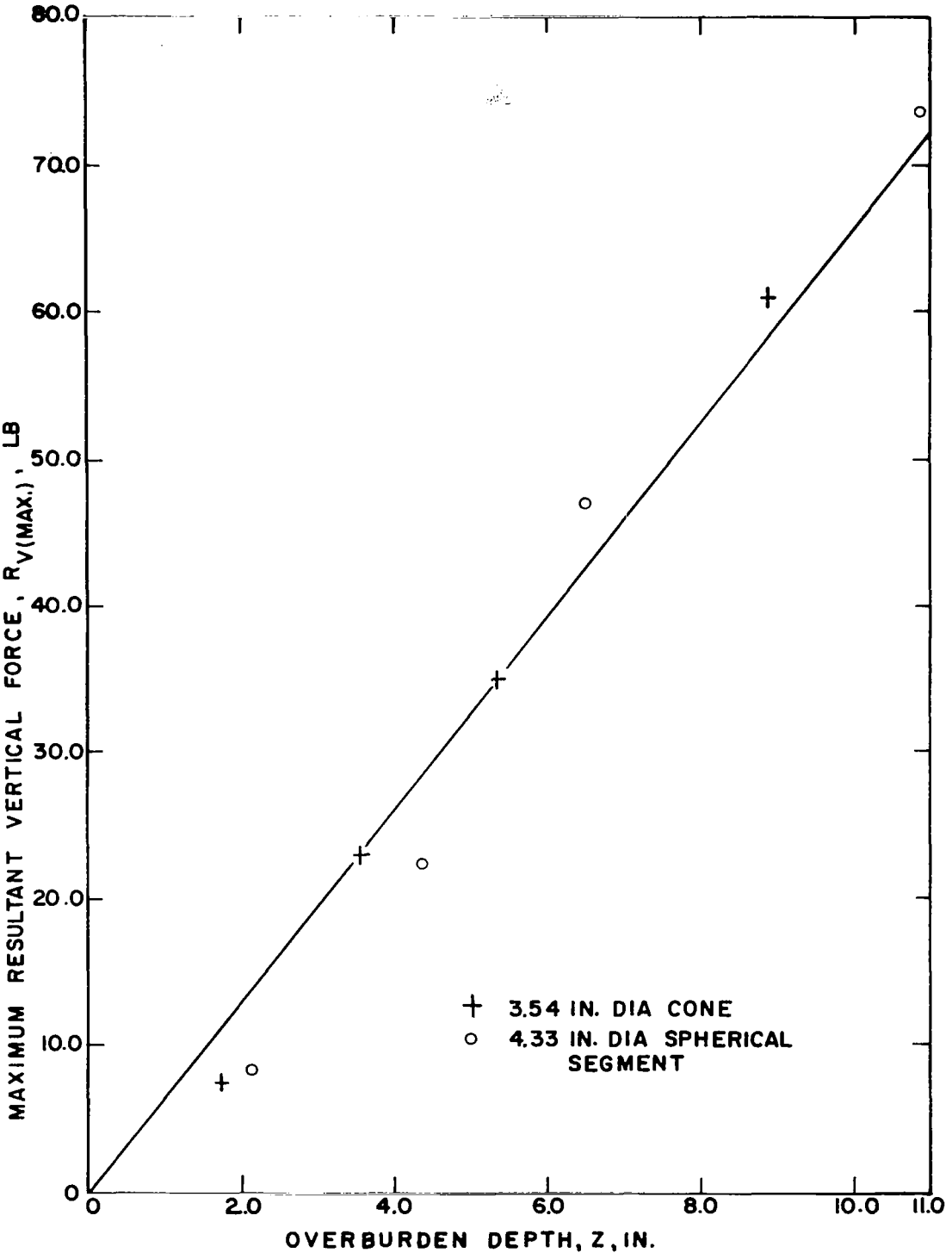

FIG. 84 EFFECT OF OVERBURDEN DEPTH ON THE MAXIMUM DEVELOPED RESULTANT VERTICAL FORCE-DENSE CASE

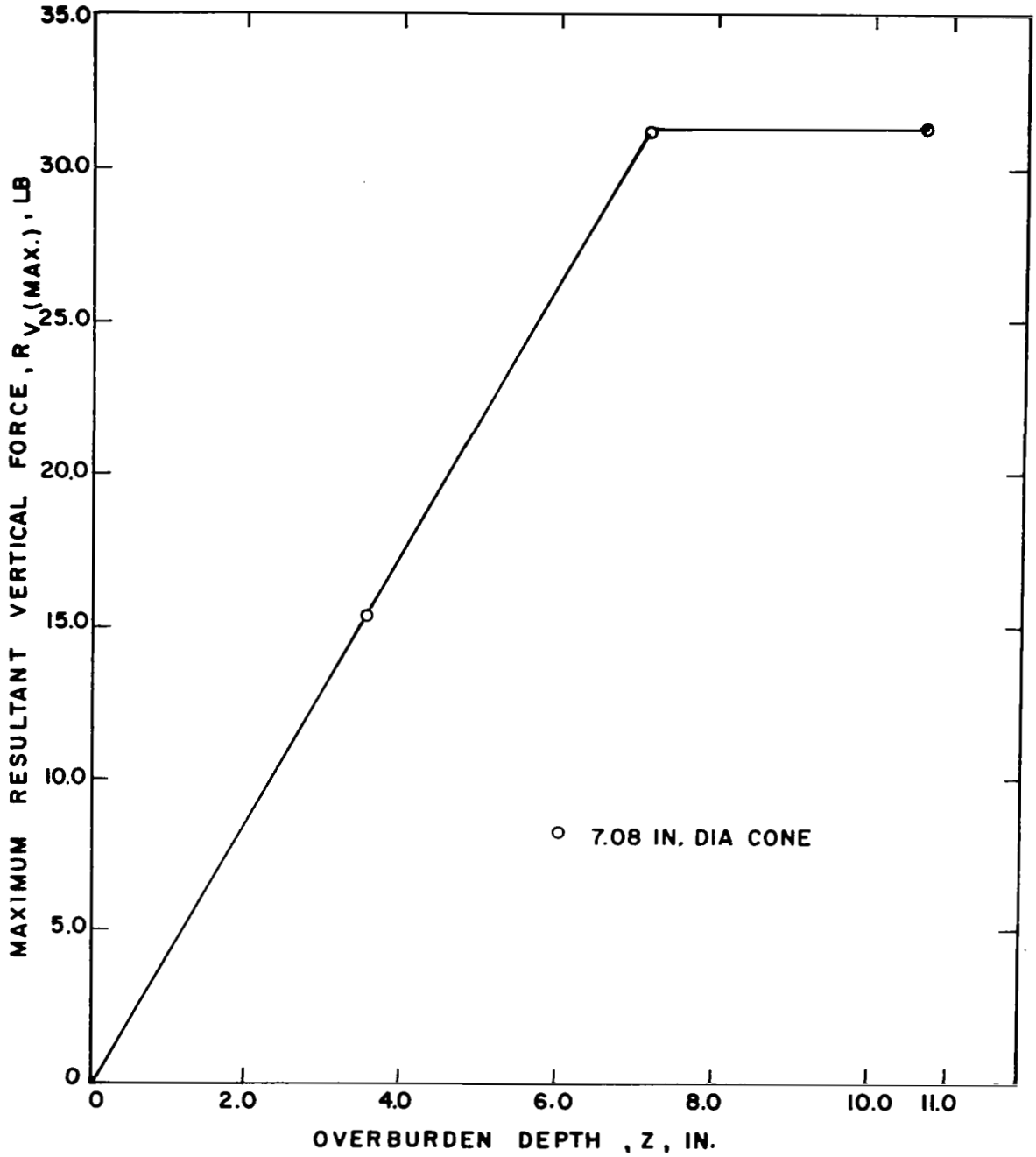

FIG. 85 EFFECT OF OVERBURDEN DEPTH ON THE MAXIMUM DEVELOPED RESULTANT VERTICAL FORCE-LOOSE CASE

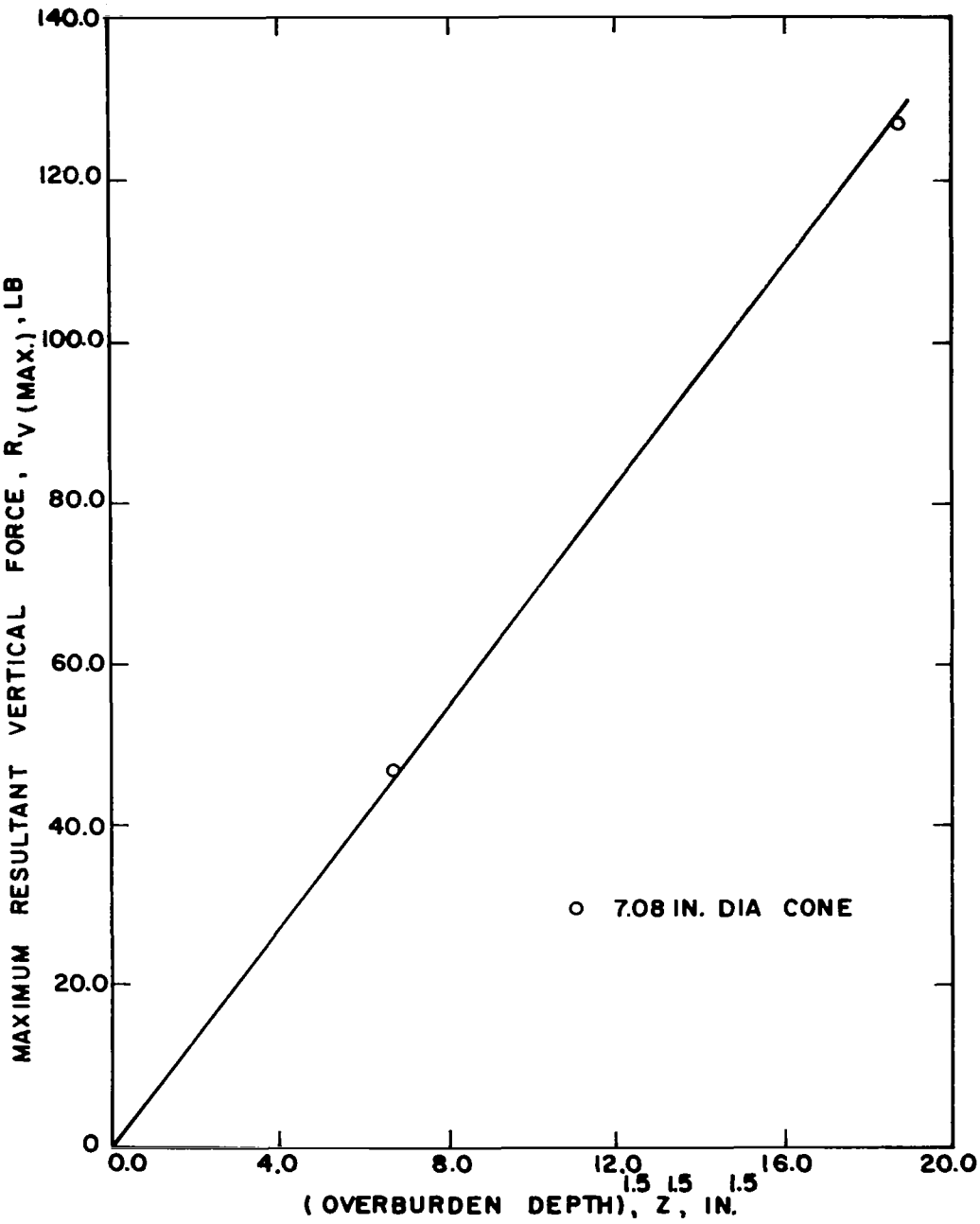

FIG. 86 EFFECT OF OVERBURDEN DEPTH ON THE MAXIMUM DEVELOPED RESULTANT VERTICAL FORCE - DENSE CASE

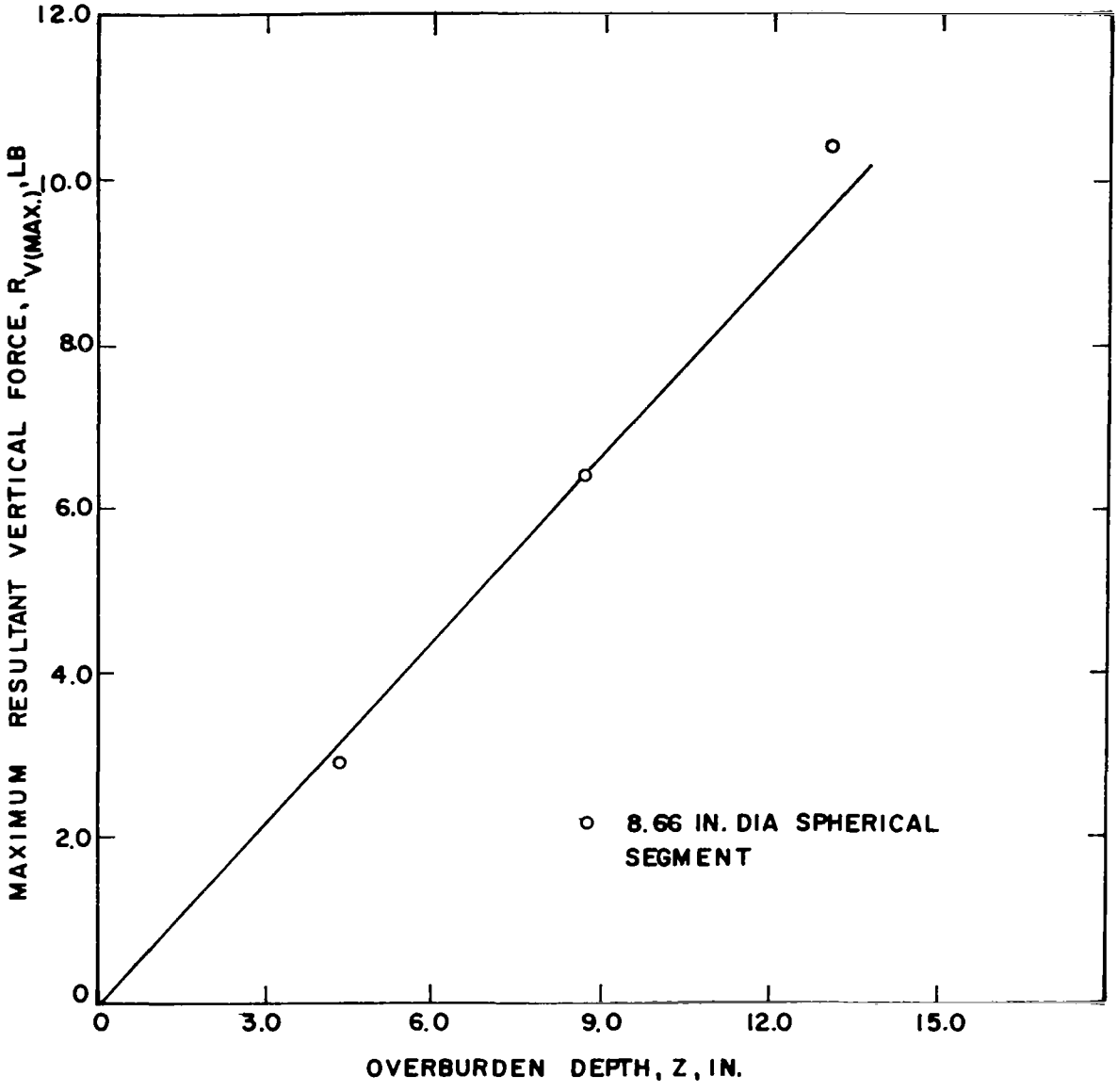

FIG. 87 EFFECT OF OVERBURDEN DEPTH ON THE MAXIMUM DEVELOPED RESULTANT VERTICAL FORCE - LOOSE CASE

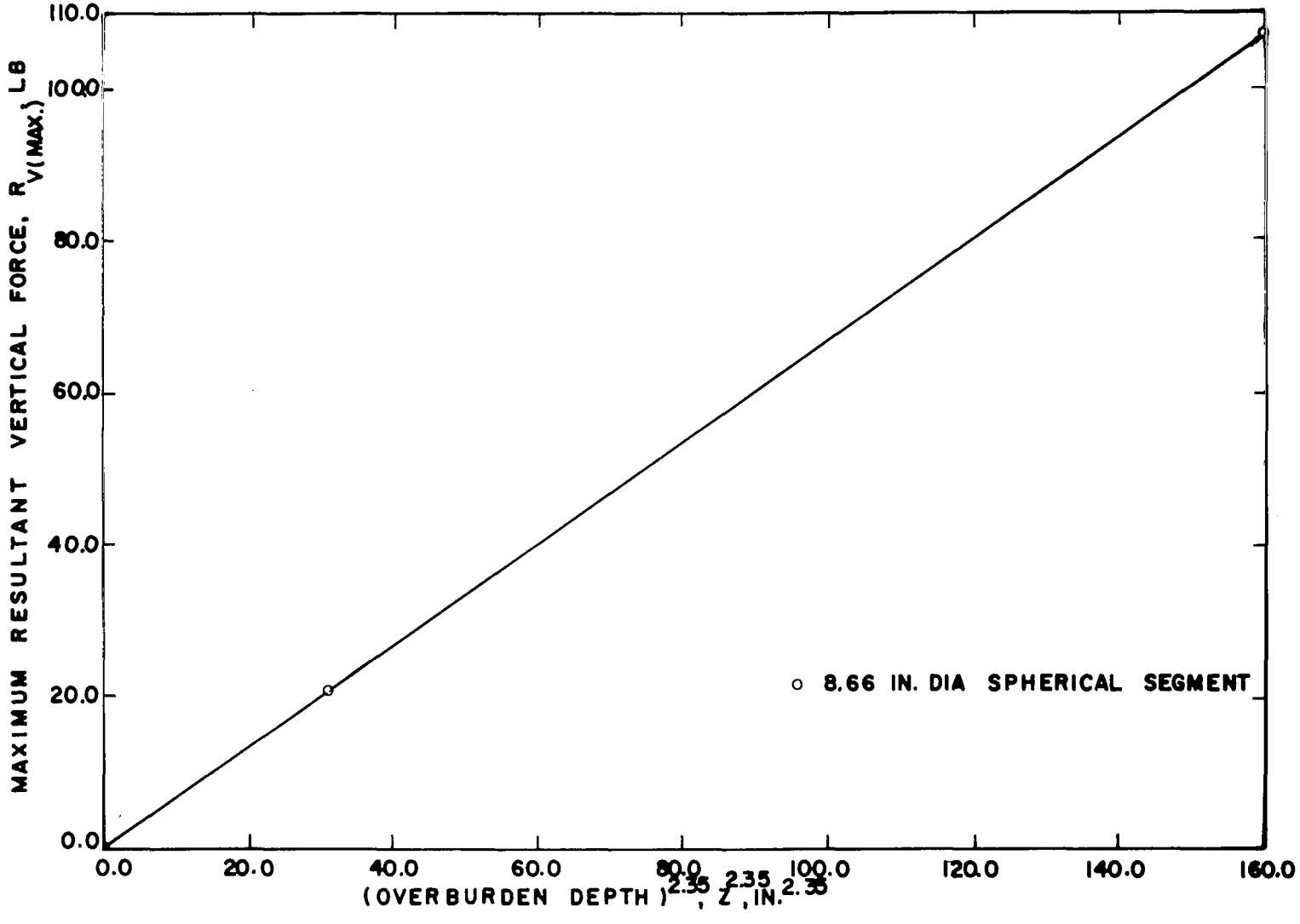

FIG.88 EFFECT OF OVERBURDEN DEPTH ON THE MAXIMUM DEVELOPED RESULTANT VERTICAL FORCE - DENSE CASE

TABLE 16

MAXIMUM DEVELOPED RESULTANT VERTICAL FORCES

Model Type	Penetration (in.)	Maximum Resultant Vertical Force (lb)	Depth of Overburden (in.)	Density (pcf)
	3.06	4.2	1.77	88.0
	3.06	4.2	3.54	88.0
	3.06	4.2	5.31	88.0
3.54 in. dia	3.06	4.2	8.85	88.0
cone	3.06	7.5	1.77	102.5
	3.06	23.0	3.54	102.5
	3.06	35.0	5.31	102.5
	3.06	61.0	8.85	102.5
	6.12	15.3	3.54	88.0
7.08 in. dia	6.12	31.3	7.08	88.0
cone	6.12	31.3	10.62	88.0
	6.12	47.0	3.54	102.5
	6.12	127.0	7.08	102.5
	1.25	1.8	4.33	88.0
	1.25	1.8	6.49	88.0
4.33 in. dia	1.25	1.8	10.83	88.0
spherical	1.25	8.3	2.16	102.5
segment	1.25	22.5	4.33	102.5
	1.25	47.0	6.49	102.5
	1.25	73.5	10.83	102.5
	2.5	2.9	4.33	88.0
8.66 in. dia	2.5	6.4	8.66	88.0
spherical	2.5	10.4	12.99	88.0
segment	2.5	21.0	4.33	102.5
	2.5	107.0	8.66	102.5

and soil conditions. Table 16 lists the $R_{v(max)}$ values that were obtained from Figs. 78 through 83. Figure 84 shows that development of maximum resultant vertical forces on the 3.54 in. dia cone and the 4.33 in. dia spherical segment may be represented by a single linear relationship. It is interesting to note that for the same series of tests the developed $R_{H(max)}$ values were also closely approximated by a single relationship.

The large model test results, which are plotted in Figs. 85 through 88, indicate that the loose-case test results may be represented by linear approximations that relate $R_{v(max)}$ and Z. The dense test results indicate that a simple linear relationship between $R_{v(max)}$ and Z does not exist. In Figs. 86 and 88 $R_{v(max)}$ was plotted as a linear function of the overburden depth Z raised to some constant power c. Since test results from only two overburden depths were obtained, the validity of an exponential relationship existing between $R_{v(max)}$ and Z is not confirmed by the test data. This mode of representation was chosen because it is consistent with previous modes.

Maximum Force Prediction

Figures 85 through 88 indicate that it is possible to write a single expression to calculate the approximate value of the maximum developed resultant vertical soil force $R_{v(max)}$. Equation 20 is proposed as a method for calculating $R_{v(max)}$.

$$R_{v(max)} = \gamma Z^{c} K_{v} \tag{20}$$

The terms appearing in the above equation are defined as follows:

$R_{v(max)}$ = Maximum resultant vertical force,

γ = Unit density of the backfill material,

Z = Vertical depth beneath the backfill surface,

c = Overburden depth exponent,

K_v = A factor which when multiplied by γZ^c yields the maximum resultant vertical force.

Values of K_v were calculated using Eq 20. These values along with other significant information are listed in Table 17. It should be noted that the K_v values appearing in this table are valid for only the test conditions under which they were obtained.

TABLE 17

COMPARISON OF K_v VALUES

Model Type	K_v	Overburden Depth Exponent c	Density γ (pcf)
3.54 in. dia cone	82.5 in^3	0	88.0
	110.0 in^2	1.0	102.5
7.08 in. dia cone	87.4 in^2*	1.0	88.0
	115.5 $in^{1.5}$	1.5	102.5
4.33 in. dia spherical segment	35.4 in^3	0	88.0
	110.0 in^2	1.0	102.5
8.66 in. dia spherical segment	14.7 in^2	1.0	88.0
	11.3 $in^{0.65}$	2.35	102.5

*This K_v value is valid for overburden depths less than 7.08 inches. See Fig. 85.

CHAPTER IX

SUMMARY OF CONCLUSIONS AND RECOMMENDATIONS

The purpose of this chapter is to present a brief summary of the pertinent information obtained from this investigation.

PHASE I CONCLUSIONS

1. The earth pressure-penetration curves obtained from the tests on loose backfills are parabolic in shape. The tests on dense backfills indicate that, for penetration values less than, or equal to, the penetration necessary to obtain failure, the earth pressure-penetration curve is also parabolic.
2. The density of the backfill material has a large influence upon the passive earth pressure developed. The measured earth-pressure factor ($K_p / \cos \delta$) was approximately 7 for tests performed on loose backfills and 12 for tests on dense backfills.
3. The rate and magnitude of the development of passive earth pressure is extremely sensitive to the type of wall movement which occurs. Purely horizontal penetration of the wall causes maximum earth pressures to be developed at minimum penetration; for walls which undergo both horizontal and upward vertical movement lesser earth pressures are developed at greater penetrations.
4. Combined horizontal and upward movement of the wall caused the center of earth pressure to shift sharply upward.
5. The center of earth pressure at failure was approximately 0.39H for tests on loose backfills and 0.33H for tests on dense backfills.

6. The coefficient of earth pressure at-rest K_o was approximately 0.3 When the backfill was placed in a loose state and 1.0 with the backfill in a dense state. Vigorous vibration of the backfill may cause the at-rest coefficient to be as large as 1.78.
7. The measured angle β_m that the failure surface made with the horizontal was in every instance greater than the β_T value calculated using Coulomb's equation for passive earth pressure.
8. The amount and rate of wall friction development is a function of the density of the backfill material.
9. The test setup adequately simulated the classical plane strain earth-pressure problem, although, the wall was not completely restricted from moving in a vertical direction.

PHASE I RECOMMENDATIONS

1. The wooden vertical restraint that was used to constrain the loading apparatus from moving in a vertical direction did not function properly. A rigidly mounted steel restraint would be more satisfactory.
2. The measurement of wall friction using this test setup was unsatisfactory for obtaining the early portion of the wall friction-penetration curve. The frictional force developed between the three load cells and the rear face of the wall precluded frictional measurements below a wall friction angle of 5.9 degrees. This disadvantage could be eliminated by inserting several steel bars, which have a knife edge on each end, in between the wall and a bearing plate. The necessary horizontal thrust would be transmitted from the load cells into the bearing plate which would in turn transmit the load to the bars. Structurally, the bars represent steel columns which are pinned at each end.

PHASE II CONCLUSIONS

1. Wall penetration velocities less than 2.667 ips had negligible effects upon the force-penetration characteristics of the sand backfill.
2. Coulomb's theory of passive earth pressure, on the average, predicted the maximum measured earth-pressure factor within 15 per cent for tests conducted on dense backfills. The prediction accuracy was poorer for the tests conducted on loose backfills. On the average, the predicted values for the 12 and 18 in. wall loose-tests were 43.4 and 20.7 per cent respectively, greater than the measured values.
3. Using the average Y/H values listed in Table 13 on p. 120, the wall penetration at which the maximum passive earth pressure occurred may be expressed by $Y = 0.0113H^{1.15}$; this equation is valid only for dense backfill systems.
4. The maximum developed angles of internal friction were on the average approximately 2 degrees higher and 5 degrees lower than the maximum values predicted from triaxial tests on Colorado River sand in its densest and loosest states respectively.
5. The average location of the center pressure, above the bottom of the wall, at failure was 0.33H and approximately 0.39H for dense and loose backfill states respectively.
6. The orientation of the failure surface, β_T, as found from Eq 26 on p. 172 is on the average approximately 5 degrees lower than the measured orientation β_m. The observed orientation of the failure surface is predicted with much better accuracy if the wall is assumed to be smooth thereby making β_T equal to $(45^\circ - \phi/2)$.

PHASE II RECOMMENDATIONS

1. Tests should be performed at greater wall penetration velocities to determine the strain rate effects upon the force-penetration characteristics of the backfill material.
2. Much needed information could be obtained by performing tests using various types of soils. It is also desirable to vary the density of the backfill material to obtain the full range of force-penetration curves for a particular soil type. The roughness of the wall has a great influence upon the magnitude of the developed earth pressures and it is therefore advisable to perform tests using walls of various degrees of roughness.
3. Tests should be performed using several wall heights. This study has shown that the penetration necessary to obtain the maximum developed passive earth pressure is not a linear function of the wall height, as it is normally assumed, and it is therefore suggested that larger wall heights be tested to obtain data that could be used in predicting force-penetration characteristics of larger walls.
4. The test setup did not provide a satisfactory means of obtaining wall friction-penetration curves. The frictional resistance between the horizontal thrust system and the rear face of the wall can be eliminated by using the procedure outlined under the Phase I Recommendations, point 2. The weight of the wall should be counterbalanced by a system which will move horizontally as the wall penetrates into the backfill. The counterbalance system should be instrumented to obtain a measure of the frictional force developed at the soil-wall interface.

PHASE III CONCLUSIONS

1. Model penetration velocities less than 4.0 ips had negligible effects upon the force-penetration characteristics of the sand backfill.
2. The maximum horizontal soil reaction $R_{H(max)}$ on either size of cone or spherical segment was directly proportional to the overburden depth Z squared.
3. The prediction of the maximum resultant vertical soil reaction $R_{v(max)}$ on each model is considerably more complex than the prediction of the $R_{H(max)}$ value. The small model tests on loose backfills indicated that $R_{v(max)}$ is not a function Z. The small model tests on dense backfills indicated that $R_{v(max)}$ is directly proportional to Z. The large model tests on loose backfills showed that $R_{v(max)}$ was directly proportional to Z. The large model tests on dense backfills showed that $R_{v(max)}$ was directly proportional to Z raised to some power greater than one.

PHASE III RECOMMENDATIONS

1. The design of this test setup necessitated the use of a flexible membrane which was used to confine the backfill in a horizontal direction. As the backfill was placed, the membrane deflected under the horizontal forces produced by the weight of the sand. The initial membrane deflection increased rapidly as the depth of overburden was increased. Model penetration caused the portion of the membrane in contact with the model to be pushed inward towards the backfill while the remaining portions of the

PHASE III RECOMMENDATIONS (Continued)

1. (Continued)

   membrane deflected outward under the increased horizontal soil stresses. Hence, localized portions of the backfill were moving in the direction of model penetration and other portions were moving in an opposite direction. The developed vertical and horizontal soil reactions are therefore not solely functions of the model geometry and the properties of the backfill, but are also greatly influenced by the interaction between the backfill and the membrane. This interaction could be eliminated by positioning the model within the backfill. The horizontal thrust shaft would pass through an outer casing which would keep the instrumented thrust-shaft free from the backfill material. It would first be necessary to place the model and shaft housing in the backfill container and then place the sand around the assembly.

2. Valuable information could be obtained by performing tests on several types of soil that had been placed using varying degrees of densification.

3. The relative influence of model geometry could be obtained by using cones, spherical segments, and flat plates. A minimum of three sizes of each model should be tested.

APPENDIX A

COMPUTER PROGRAM PASSIV

Program PASSIV was written to reduce and convert the raw load-cell strain data to a usable form. The program also calculated values of developed passive earth pressure, passive earth-pressure factors, location of center of pressures, orientation of failure surfaces, and developed angles of internal friction and wall friction for each test performed during Phase I.

Calculation of Passive Earth Pressure

The horizontal force required to push the wall into the backfill was measured by Load Cells 1, 2, and 3. A portion of the frictional force developed at the soil-wall interface was measured by Load Cell 4. The developed passive earth pressure may be expressed as

$$P_p = \frac{P_{Horiz}}{\cos \delta} \tag{21}$$

where,

$$P_{Horiz} = P_1 + P_2 + P_3. \tag{22}$$

Figure 89 shows a sketch of the forces necessary to keep the wall in an equilibrium state. Forces P_1, P_2, and P_3 were calculated by

$$P_i = S_i \left[R_i - (R_o)_i \right], \quad i = 1, 2, 3, \tag{23}$$

where,

R_i = Strain recorded for Load Cell i,

$(R_o)_i$ = Zero correction due to cell drift during the test,

S_i = Slope of calibration curve for Load Cell i.

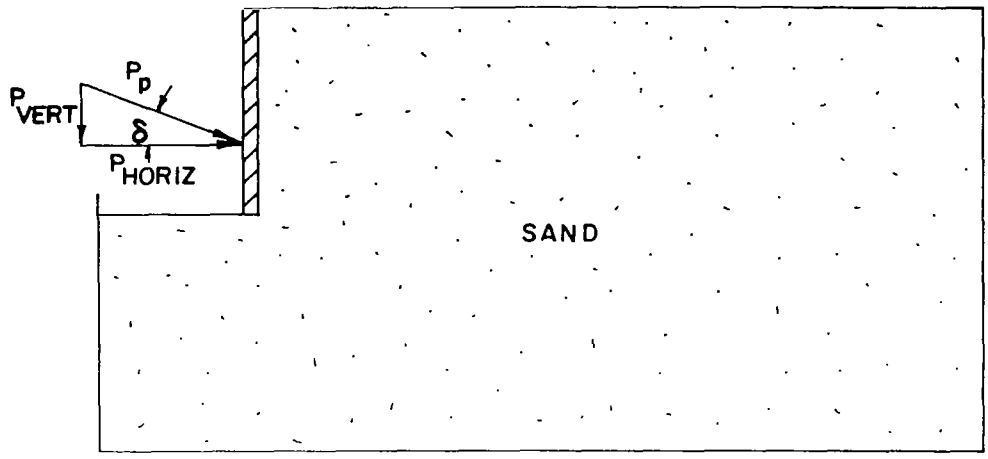

FIG.89 FORCES NECESSARY FOR EQUILIBRIUM OF THE WALL FORMED BY THE STEEL PLATES

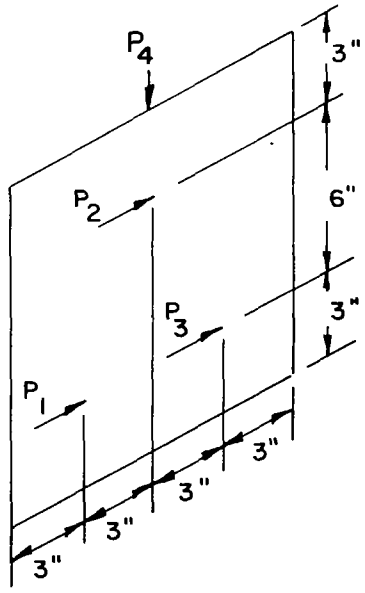

FIG.90 POSITION OF LOAD--CELL REACTIONS ON THE CENTER PLATE

The values of wall friction δ were obtained from the equation which expressed the appropriate portion of the curves shown in Fig. 45 on p. 78. It should be noted that a series of values of passive earth pressure will be obtained for each test, these values being dependent upon the amount of wall penetration.

Calculation of Passive Earth-Pressure Factors

The passive earth-pressure factor was expressed by

$$\frac{K_p}{\cos \delta} = \frac{P_p}{0.5 \gamma H^2} \tag{24}$$

where,

P_p = Passive earth pressure,

γ = Backfill density,

H = Height of wall.

Calculation of the Center of Pressure

The center of pressure was found by summing moments about the lower edge of the center plate. The centroidal distance is expressed by Eq 25 and the constants appearing in the equation are defined in Fig. 90.

$$CD = \frac{3P_1 + 9P_2 + 3P_3}{P_{Horiz}} \tag{25}$$

Calculations Based on Coulomb's Theory

The program contains a general expression that calculates the passive earth pressure based on Coulomb's assumption that the failure surface is plane. The passive earth pressure necessary to keep the failure wedge, shown in Fig. 91, in equilibrium is

$$P_p = \frac{W \sin (\beta + \phi)}{\sin (180^\circ - \delta - \alpha - \beta - \phi)} , \tag{26}$$

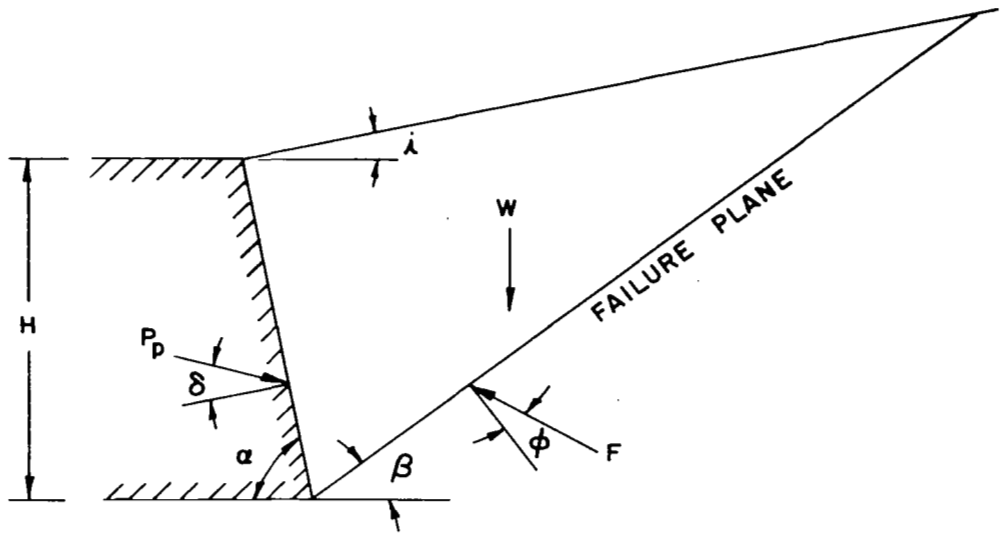

FIG.91 PASSIVE FAILURE WEDGE BEHIND A RETAINING WALL

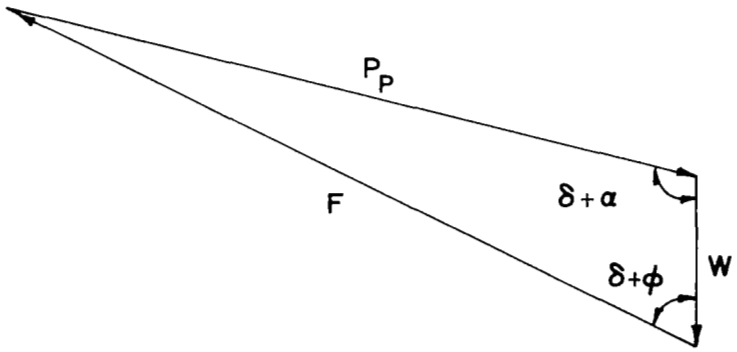

FIG.92 EQUILIBRIUM FORCE POLYGON FOR THE FAILURE WEDGE SHOWN IN FIG.91

where the weight of the failure wedge is

$$W = 1/2\ \gamma\ H^2\ \frac{\text{Sin}\ (\alpha + i)\ \text{sin}\ (180^\circ - \alpha - \beta)}{\text{Sin}\ (\beta - i)\ \text{Sin}^2\ \alpha} \quad . \tag{27}$$

All of the parameters appearing in Eqs 26 and 27 are known except for the angle β. The angle β is varied until the minimum passive earth pressure is found. It should be noted that an expression for P_p can be developed, in which β does not appear and by the direct substitution of known parameters, the maximum value of the passive earth pressure is obtained. However, by expressing the passive earth pressure as shown in Eq 26, one not only obtains the value of earth pressure, but also the orientation of the failure surface. Values of $K_p/\cos\ \delta$ were obtained using Eq 24.

The developed angle of internal friction was calculated using Eq 28.

$$P_p = 1/2\ \gamma\ H^2 \left[\frac{\text{CSC}\ (180^\circ - \alpha)\ \text{Sin}\ (180^\circ + \phi - \alpha)}{\sqrt{\text{Sin}\ (180^\circ - (\alpha + \delta))} - \sqrt{\frac{\text{Sin}\ (\phi + \delta)\ \text{Sin}\ (\phi + i)}{\text{Sin}\ (180^\circ - (\alpha + i))}}} \right]^2 \tag{28}$$

Values of P_p were obtained from Eq 21, and these values along with γ, H, δ, α, and i values were substituted into Eq 28. The developed ϕ values were then found by using a trial and error substitution procedure. Equation 28 reduces to Eq 7 on p. 12 if i is set equal to zero and α is set equal to 90 degrees.

The following pages contain a flow diagram, listing, example data input, discussion of data input, data input form, and example data output for Program PASSIV.

GENERAL FLOW DIAGRAM FOR PROGRAM PASSIV

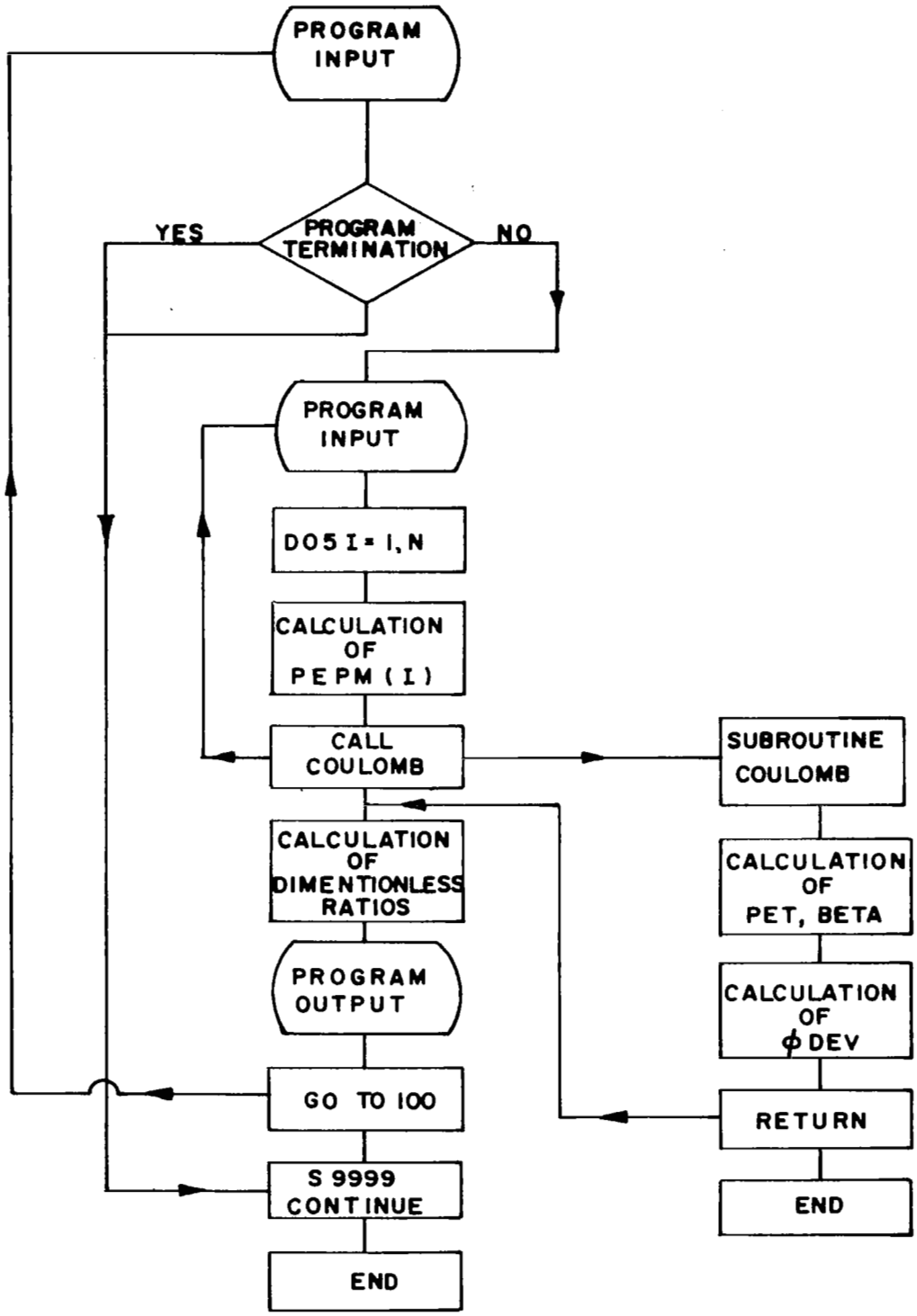

FORTRAN Listing

```
PASSIV,1,100,130000,40.CE694527,HUSTAD.
QXX(RUN,G)
QXX(PASSIV)
-
      PROGRAM PASSIV (INPUT,OUTPUT)
C--- RUN     ---  A VARIABLE USED TO READ AND PRINT PROGRAM IDENTIFICATION
C--- N       ---  THE NO. OF DEFLECTION VALUES INPUT
C--- GAMMA   ---  THE UNIT DENSITY OF THE SOIL            ( PCF   )
C--- DELMAX  ---  THE MAXIMUM VALUE OF FRICTION AT THE SOIL - WALL
C                  INTERFACE                              (DEGREES)
C--- DELTA   ---  THE ANGLE OF FRICTION DEVELOPED AT THE SOIL - WALL
C                  INTERFACE
C--- PHIMAX  ---  THE MAXIMUM VALUE OF INTERNAL FRICTION (DEGREES)
C--- FI      ---  SLOPE OF THE BACKFILL MATERIAL          (DEGREES)
C--- SHI     ---  SLANT HEIGHT OF THE WALL                ( FEET  )
C--- ALPHA   ---  ANGLE BETWEEN THE WALL AND THE HORIZ.   (DEGREES)
C--- SCN     ---  WHERE N VARIES FROM 1 TO 4 . THESE VARIABLES
C                  REPRESENT THE SLOPE OF THE CALIBRATION CURVES
C                  FOR EACH OF THE LOAD CELLS        (LBS. / MICRO-INCH)
C--- CNZERO  ---  WHERE N VARIES FROM 1 TO 4 . THESE VARIBLES
C                  REPRESENT THE ZERO CORRECTION MEASUREMENT
C                  FOR EACH LOAD CELL                    (MICRO-INCHES)
C--- DEFL    ---  HORIZONTAL PENETRATION OF THE WALL      (INCHES)
C--- CELLN   ---  WHERE N VARIES FROM 1 TO 4 . THESE VARIABLES
C                  REPRESENT THE LOAD CELL READINGS      (MICRO-INCHES)
C--- FLOADN  ---  WHERE N VARIES FROM 1 TO 4 . THESE VARIABLES
C                  REPRESENT THE FORCE MEASURED BY EACH LOAD
C                  CELL                                   ( LBS. )
C--- RELOAD  ---  THE RESULTANT HORIZONTAL FORCE         ( LBS. )
C--- PEPM    ---  PASSIVE EARTH PRESSURE OBTAINED FROM TEST MEASUREMENTS
C--- PEPT    --- THE PASSIVE EARTH PRESSURE OBTAINED USING COULOMBS THEORY
C--- BETA    --- ANGLE THAT THE FAILURE PLANE MAKES WITH THE HORIZONTAL
C                  UNITS --- (DEGREES)
C--- PKM     --- COEFFICIENT OF PASSIVE EARTH PRESSURE THAT IS CALCULATED
C                  USING TEST RESULTS
```

```
C--- PKT     --- COEFFICIENT OF PASSIVE EARTH PRESSURE THAT IS CALCULATED
C                USING RESULTS FROM COULOMBS THEORY
C--- DRATIO --- RATIO OF WALL FRICTION DEVELOPED TO THE MAXIMUM WALL FRICT.
C--- PHI     --- THE ANGLE OF INTERNAL FRICTION DEVELOPED
C--- PRATIO --- RATIO OF INTERNAL FRICTION DEVELOPED TO THE MAXIMUM
C                VALUE OF INTERNAL FRICTION
C--- DEFR    --- RATIO OF THE HORIZ. PENETRATION TO THE SLANT HEIGHT OF THE WALL
C                THE WALL
C--- CPM     --- THE EARTH PRESSURE CENTROID AS DETERMINED FROM TEST RESULTS
C                UNITS  --- (INCHES)
C--- ERROR   --- PERCENT DEVIATION OF CPM FROM THE PRESSURE CENTROID
C                CALCULATED BY THEORY
C--- KCASE   --- INDEX USED TO REDUCE THE INCREMENTING OF BETA AND PHI
C--- FINC    --- INCREMENTING VALUE FOR BETA AND PHI
      DIMENSION RUN(10),DEFL(50),CELL1(50),CELL2(50),CELL3(50),
     1          CELL4(50),FLOAD1(50),FLOAD2(50),FLOAD3(50),FLOAD4(50),
     2          RELOAD(50),PEPM(50),PEPT(50),BETA(50),PKM(50),PKT(50),
     3          DRATIO(50),PRATIO(50),DEFR(50),CPM(50),ERROR(50),FE(50),
     4          DEL(50)
      COMMON GAMMA, DELTA, PHI, PHIMAX, FI, SHI, ALPHA, CONV, HEIGHT
C--- READING INPUT DATA ***********************************************
  100    READ 1000, (RUN(I), I=1,10)
         READ 2000, N, GAMMA, DELMAX, PHIMAX, FI, SHI, ALPHA
C--- CHECKING TO SEE IF THE PROGRAM SHOULD BE TERMINATED
         IF(N)99999,99999,200
  200    READ 3000, SC1,SC2,SC3,SC4, C1ZERO, C2ZERO, C3ZERO, C4ZERO
         READ 4000, (DEFL(I), CELL1(I), CELL2(I), CELL3(I), CELL4(I),I=1
     1,N)
C--- END OF INPUT DATA ************************************************
C--- CONVERSION FACTOR (RADIANS / DEGREE)
      CONV       = 3.14159 / 180.0
C--- THEORETICAL COMPUTATION OF THE EARTH PRESSURE CENTROID
      CPT        =  ( SHI * 12.0 ) / 3.0
                 DO 5 I=1,N
C--- COMPUTATION OF THE FORCE MEASURED BY EACH LOAD CELL
      FLOAD1(I) =  ( CELL1(I) - C1ZERO )*SC1
      FLOAD2(I) =  ( CELL2(I) - C2ZERO )*SC2
      FLOAD3(I) =  ( CELL3(I) - C3ZERO )*SC3
```

```
      FLOAD4(I) =  ( CELL4(I) - C4ZERO )*SC4
C--- COMPUTATION OF THE RESULTANT HORIZONTAL LOAD
      RELOAD(I) =  FLOAD1(I) + FLOAD2(I) + FLOAD3(I)
C--- CALCULATING THE COEFFICIENT OF FRICTION DEVELOPED AT THE
C    SOIL - WALL INTERFACE
             IF( PHIMAX - 50.0 )115,120,120
  120        IF( DEFL(I) - 0.63 )135,135,140
  135 DELTA    =  30.0 * DEFL(I) * CONV
             GO TO 105
  140        IF( DEFL(I) - 1.03 )145,145,110
  145 DELTA    =  ( 17.9 +   SQRT ( 240.* DEFL(I) - 147.2 ) /2.0)* CONV
             GO TO 105
  110 DELTA    =  22.9 * CONV
             GO TO 105
  115        IF( DEFL(I) - 3.5 )125,125,130
  125 DELTA    =  4.257 * DEFL(I) * CONV
             GO TO 105
  130 DELTA    =  14.9 * CONV
C--- CALCULATING THE PASSIVE EARTH PRESSURE MEASURED
  105 PEPM(I)  =  RELOAD(I) / COS( DELTA )
C--- CALLING THE SUBROUTINE COULOMB **********************************
             CALL COULOMB( PEPM(I), PEPT(I), BETA(I) )
C--- CALCULATING THE COEFFECIENT OF PASSIVE EARTH PRESSURE
C    USING EXPERIMENTAL RESULTS
      PKM(I)   =  PEPM(I) / ( 0.5 * GAMMA * HEIGHT ** 2 )
C--- CALCULATING THE COEFFECIENT OF PASSIVE EARTH PRESSURE
C    USING THEORETICAL RESULTS
      PKT(I)   =  PEPT(I) / ( 0.5 * GAMMA * HEIGHT ** 2 )
C--- CALCULATING THE RATIO OF WALL FRICTION DEVELOPED TO
C    MAXIMUM WALL FRICTION
      DRATIO(I) =  DELTA / DELMAX
C--- CALCULATING THE RATIO OF INTERNAL FRICTION DEVELOPED TO
C    MAXIMUM INTERNAL FRICTION
      PRATIO(I) =  PHI / PHIMAX
      DEL(I)   =  DELTA
      FE(I)    =  PHI
C--- CALCULATING THE  RATIO OF HORIZ. DEFLECTION TO SLANT
```

```
C     HEIGHT OF THE WALL
       DEFR(I)    =  DEFL(I) / ( SHI * 12.0 )
C---- CALCULATING THE PRESSURE CENTROID
       CPM(I)     =  ( 3.0 * ( FLOAD1(I) + FLOAD3(I) ) + 9.0 * FLOAD2(I) )
      1              / RELOAD(I)
C---- CALCULATING THE PERCENT DEVIATION BETWEEN THE THEORETICAL
C     AND MEASURED PRESSURE CENTROID
       ERROR(I)   =  (( CPT - CPM(I) ) / CPT ) * 100.0
     5 CONTINUE
C---- PRINTOUT OF INPUT DATA ******************************************
          PRINT 1500, (RUN(I), I = 1,10)
          PRINT 2500, N, GAMMA, PHIMAX, DELMAX, FI, ALPHA, SHI
          PRINT 3500, SC1, SC2, SC3, SC4, C1ZERO, C2ZERO, C3ZERO, C4ZERO
          PRINT 4500
          PRINT 5500, ( DEFL(I), CELL1(I), CELL2(I), CELL3(I), CELL4(I) ,
      1 I = 1,N )
C---- PRINTOUT OF RESULTS *********************************************
          PRINT 6500
          PRINT 7500 , (DEFL(I), FLOAD1(I), FLOAD2(I), FLOAD3(I),
      1                  FLOAD4(I), RELOAD(I) , I = 1,N )
          PRINT 8500
          PRINT 9500, (DEFR(I), PEPM(I), PEPT(I), PKM(I), PKT(I), BETA(I)
      1, I = 1,N )
          PRINT 10500
          PRINT 11500, ( DEFR(I), DRATIO(I), PRATIO(I), CPM(I), ERROR(I),
      1I = 1,N )
          PRINT 12500
          PRINT 13500, ( DEFL(I), FE(I), DEL(I) , I = 1,N )
 1000     FORMAT (10A8)
 2000     FORMAT (I10,6E10.3)
 3000     FORMAT (8E10.3)
 4000     FORMAT (5E10.3)
 1500     FORMAT (1H1,1X,10A8 //)
 2500     FORMAT (5X,55H                              DATA INPUT
     1       ,    //,55H     NUMBER  OF  LOAD  CELL  READINGS
     2       , I5 ,/,55H     SOIL  DENSITY  ( LBS. / CUBIC FOOT )
     3       ,E10.3/,55H     ANGLE  OF  INTERNAL  FRICTION  ( DEGREES )
     4       ,E10.3/,55H     MAX. VALUE OF  WALL  FRICTION  ( DEGREES )
     5       ,E10.3/,55H     SLOPE  OF  THE  BACKFILL  ( DEGREES )
```

```
     6      ,E10.3/,55H      ANGLE BETWEEN WALL AND HORIZ. ( DEGREES )
     7      ,E10.3/,55H      SLANT  HEIGHT  OF  THE  WALL  ( FEET )
     8      ,E10.3,//)
 3500    FORMAT (5X,50HSLOPE OF CAL. CURVE FOR CELL NO. 1 (LBS./INCH)
     1      ,E10.3/,55H      SLOPE OF CAL. CURVE FOR CELL NO. 2 (LBS./INC
     2H)    ,E10.3/,55H      SLOPE OF CAL. CURVE FOR CELL NO. 3 (LBS./INC
     3H)    ,E10.3/,55H      SLOPE OF CAL. CURVE FOR CELL NO. 4 (LBS./INC
     4H)    ,E10.3/,55H      ZERO BALANCE CORR.  FOR CELL NO. 1 (MICRO-IN
     5CH)   ,E10.3/,55H      ZERO BALANCE CORR.  FOR CELL NO. 2 (MICRO-IN
     6CH)   ,E10.3/,55H      ZERO BALANCE CORR.  FOR CELL NO. 3 (MICRO-IN
     7CH)   ,E10.3/,55H      ZERO BALANCE CORR.  FOR CELL NO. 4 (MICRO-IN
     8CH)   ,E10.3//)
 4500    FORMAT (60H                  DEFLECTION AND LOAD CELL STRAIN READ
     1INGS    //,65H     DEFLECTION   CELL NO. 1  CELL NO. 2  CELL NO. 3
     2 CELL NO. 4  ,/,65H        INCHES    (--------------- MICRO-INCHES
     3---------------) ,//)
 5500    FORMAT (5X,E10.3,3X,E10.3,2X,E10.3,2X,E10.3,2X,E10.3)
 6500    FORMAT (1H1,//,50H                                   OUTPUT   INFORMATIO
     1N    ,/           ,75H DEFLECTION  CELL NO. 1  CELL NO. 2  CELL NO.
     2 3  CELL NO. 4  RESULTANT     ,/
     3                  75H   INCHES   (--------- --------------- LBS. -
     4------------ ---------  -)    ,//)
 7500    FORMAT (1X,E10.3,5(2X,E10.3))
 8500    FORMAT (///,68H    DEFR         PEPM         PEPT            PKM
     1       PKT      BETA,/,70H  UNITLESS   (   LBS. / LIN. FT.  )  ( -
     2--- UNITLESS ---- )   DEGREES ,//)
 9500    FORMAT (1X,E10.3,5(2X,E10.3))
10500    FORMAT (///,60H    DEFR       DRATIO      PRATIO      CPM
     1   ERROR    ,/,60H   (----*----- UNITLESS ---------)     INCHES
     2  PERCENT   ,//)
11500    FORMAT (1X,E10.3,4(2X,E10.3))
12500    FORMAT (////,72H     DEFLECTION   INTERNAL FRICTION DEVELOPED
     1 WALL FRICTION DEVELOPED  ,/,65        INCHES               DEGREES
     2                         DEGREES   ,//)
13500    FORMAT (5X,E10.3,10X,E10.3,19X,E10.3)
C--- GOING BACK TO READ ANOTHER SET OF DATA
           GO TO 100
99999 CONTINUE
      END
```

```
C--- THIS IS THE END OF THE MAIN PROGRAM ******************************
              SUBROUTINE COULOMB( PEM, PET, BETA )
      COMMON GAMMA, DELTA, PHI, PHIMAX, FI, SHI, ALPHA, CONV, HEIGHT
      KCASE      =  0
      FINC       =  1.0
              IF ( DELTA - 0.314 )85,85,90
C--- GIVING BETA AN INITIAL VALUE  (RANKINE STATE )
   85 BETA       =  ( 45.0 - PHIMAX / 2.0 ) * CONV
              GO TO 95
C--- GIVING BETA AN INITIAL VALUE
   90 BETA       =  10.0 * CONV
C--- CONVERTING ANGLES IN DEGREES TO RADIANS
   95 FI         =  FI * CONV
      PHIMAX     =  PHIMAX * CONV
      ALPHA      = ALPHA * CONV
      HEIGHT     =  SHI * SIN( ALPHA )
      J          =  0
C--- CALCULATING THE LENGTH OF THE FAILURE PLANE (FROM LAW OF SINES)
   10 SLIP       =  SIN( ALPHA + FI ) * SHI / SIN( BETA - FI )
C--- CALCULATING THE VOLUME OF SOIL WITHIN THE FAILURE WEDGE
      VOL        =  0.5 * ( SLIP * SHI * SIN( 180.0 * CONV - ( ALPHA +
     1              BETA)))
      WEIGHT     =  VOL * GAMMA
      THETA      =  DELTA + ALPHA
C--- CALCULATING THE PASSIVE EARTH PRESSURE USING COULOMBS ASSUMPTION
C     OF A PLANE RUPTURE SURFACE
      PET        =  WEIGHT * SIN( BETA + PHIMAX) / SIN( 180.0 * CONV -
     1              (THETA + BETA + PHIMAX))
C--- CHECKING TO SEE IF A PREVIOUS VALUE OF PASSIVE EARTH PRESSURE
C     ( PEPP) HAS BEEN CALCULATED
              IF( J.GT.0)15,20
C--- CHECKING TO SEE IF THIS VALUE OF PASSIVE EARTH PRESSURE IS GREATER
C     THAN THE PREVIOUS VALUE (PEPP)
   15         IF( PET.GT.PEPP )25,20
   20 BETAP      =  BETA
C--- DECREASING BETA BY EITHER 1 OR 0.1 DEGREES
      BETA       =  BETA - FINC * CONV
      PEPP       =  PET
      J          =  1
```

```
                GO TO 10
C--- CHECKING TO SEE IF FINC HAS BEEN REDUCED TO 0.1
   25           IF ( KCASE.GT.0 )35,30
   30 FINC       =  0.1
      BETA       =  BETAP
      KCASE      =  1
                GO TO 10
   35 BETA       =  BETAP / CONV
      PET        =  PEPP
C--- BEGINNING OF CALCULATIONS FOR DEVELOPED INTERNAL FRICTION *******
      KCASE      =  0
      FINC       =  1.0
C--- GIVING PHI AN INITIAL VALUE OF 1 DEGREE
      PHI        =  FINC * CONV
      PIE        =  180.0 * CONV
C--- CALCULATING THE MINIMUM VALUE OF PASSIVE EARTH PRESSURE POSSIBLE
      GAMHI      =  0.5 * GAMMA * HEIGHT ** 2
C--- CHECKING TO SEE IF THE PASSIVE EARTH PRESSURE IS GREATER THAN THE
C    MINIMUM VALUE
                IF ( PEM - GAMHI )70,70,40
C--- CALCULATING PASSIVE EARTH PRESSURE FOR A VALUE OF DEVELOPED
C    INTERNAL FRICTION
   40 FNUM       =  SIN ( PIE + PHI - ALPHA ) / SIN ( PIE - ALPHA )
      FDEN       =  SQRT ( SIN ( PIE - ALPHA - DELTA )) - SQRT ( SIN( PHI
     1              + DELTA ) * SIN ( PHI + FI ) / SIN (PIE - ALPHA -FI))
      P          =  GAMHI * ( FNUM / FDEN ) ** 2
                IF( P - PEM )45,50,50
   45 PHIP       =  PHI
C--- INCREASING PHI BY EITHER 1 OR 0.1 DEGREES
      PHI        =  PHI + FINC * CONV
                GO TO 40
   50           IF( KCASE.GT.0 )60,55
   55 FINC       =  0.1
      PHI        =  PHIP
      KCASE      =  1
                GO TO 40
   70 PHI        =  0.0
                GO TO 80
C--- CONVERTING ANGLES BACK TO DEGREES
```

```
   60 PHI        =  PHIP / CONV
   80 PHIMAX     =  PHIMAX / CONV
      DELTA      =  DELTA / CONV
      FI         =  FI / CONV
      ALPHA      =  ALPHA / CONV
                 RETURN
      END
```

Example Data Input

```
SEPT. 9, 1965 TEST NO. D10 EARTH PRESSURE TEST ON COLORADO RIVER SAND
        16  102.5    28.0      51.7      0.0       1.0       90.0
   0.664    1.275     0.640     0.644     0.0       0.0       0.0       0.0
  0.0       47.       0.        38.       0.
  0.1      190.      88.       200.       0.
  0.2      256.     102.       252.       0.
  0.3      296.      86.       300.       0.
  0.4      365.      67.       356.      26.
  0.5      415.      53.       420.     110.
  0.6      455.      44.       474.     144.
  0.7      472.      33.       450.     153.
  0.8      460.      22.       402.     158.
  0.9      408.      14.       346.     161.
  1.0      363.      18.       306.     163.
  1.2      283.      16.       263.     158.
  1.4      247.      24.       236.     138.
  1.6      228.      27.       218.     134.
  1.8      221.      30.       217.     121.
  2.0      218.      24.       228.      74.
```

Discussion of Data Input

The data input for one problem consists of a minimum of 4 cards and a maximum of 53 cards. The first card is a problem identification having an alphanumeric format of 10A8. The second card contains the number of strain readings input and also physical properties of the soil and wall. This card has an I10, 6E10.3 format. The third card contains slope constants and zero corrections for each load cell, (8E10.3 format). The last card or series of cards consists of deflection and strain readings, (5E10.3 format). This completes a set of data. Any number of problems may be read with only one compilation of the source deck. To terminate the program it is necessary to put two blank cards after the last set of data.

DATA INPUT FORM

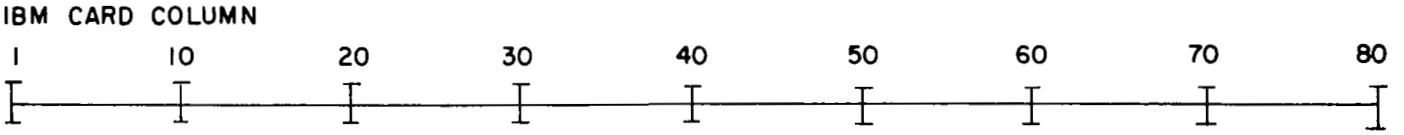

PROBLEM IDENTIFICATION (ONE CARD)

N	GAMMA	DELMAX	PHIMAX	FI	SHI	ALPHA

SC1	SC2	SC3	SC4	C1ZERO	C2ZERO	C3ZERO	C4ZERO

DEFL (I)	CELL1 (I)	CELL2 (I)	CELL3 (I)	CELL4 (I)

← N CARDS PER SET

Example Data Output

SEPT. 9, 1965 TEST NO. 010 EARTH PRESSURE TEST ON COLORADO RIVER SAND

DATA INPUT

NUMBER OF LOAD CELL READINGS	16
SOIL DENSITY (LBS. / CUBIC FOOT)	1.025E+02
ANGLE OF INTERNAL FRICTION (DEGREES)	5.170E+01
MAX. VALUE OF WALL FRICTION (DEGREES)	2.800E+01
SLOPE OF THE BACKFILL (DEGREES)	0.
ANGLE BETWEEN WALL AND HORIZ. (DEGREES)	9.000E+01
SLANT HEIGHT OF THE WALL (FEET)	1.000E+00
SLOPE OF CAL. CURVE FOR CELL NO. 1 (LBS./INCH)	6.640E-01
SLOPE OF CAL. CURVE FOR CELL NO. 2 (LBS./INCH)	1.275E+00
SLOPE OF CAL. CURVE FOR CELL NO. 3 (LBS./INCH)	6.400E-01
SLOPE OF CAL. CURVE FOR CELL NO. 4 (LBS./INCH)	6.440E-01
ZERO BALANCE CORR. FOR CELL NO. 1 (MICRO-INCH)	0.
ZERO BALANCE CORR. FOR CELL NO. 2 (MICRO-INCH)	0.
ZERO BALANCE CORR. FOR CELL NO. 3 (MICRO-INCH)	0.
ZERO BALANCE CORR. FOR CELL NO. 4 (MICRO-INCH)	0.

DEFLECTION AND LOAD CELL STRAIN READINGS

DEFLECTION INCHES	CELL NO. 1	CELL NO. 2	CELL NO. 3	CELL NO. 4
	(---------- MICRO-INCHES ----------)			
0.	4.700E+01	0.	3.800E+01	0.
1.000E-01	1.900E+02	8.800E+01	2.000E+02	0.
2.000E-01	2.560E+02	1.020E+02	2.520E+02	0.

3.000E-01	2.960E+02	8.600E+01	3.000E+02	0.
4.000E-01	3.650E+02	6.700E+01	3.560E+02	2.600E+01
5.000E-01	4.150E+02	5.300E+01	4.200E+02	1.100E+02
6.000E-01	4.550E+02	4.400E+01	4.740E+02	1.440E+02
7.000E-01	4.720E+02	3.300E+01	4.500E+02	1.530E+02
8.000E-01	4.600E+02	2.200E+01	4.020E+02	1.580E+02
9.000E-01	4.080E+02	1.400E+01	3.460E+02	1.610E+02
1.000E+00	3.630E+02	1.800E+01	3.060E+02	1.630E+02
1.200E+00	2.830E+02	1.600E+01	2.630E+02	1.580E+02
1.400E+00	2.470E+02	2.400E+01	2.360E+02	1.380E+02
1.600E+00	2.280E+02	2.700E+01	2.180E+02	1.340E+02
1.800E+00	2.210E+02	3.000E+01	2.170E+02	1.210E+02
2.000E+00	2.180E+02	2.400E+01	2.280E+02	7.400E+01

OUTPUT INFORMATION

DEFLECTION INCHES	CELL NO. 1	CELL NO. 2	CELL NO. 3	CELL NO. 4	RESULTANT
	(---------- LBS. ----------)				
0.	3.121E+01	0.	2.432E+01	0.	5.553E+01
1.000E-01	1.262E+02	1.122E+02	1.280E+02	0.	3.664E+02
2.000E-01	1.700E+02	1.300E+02	1.613E+02	0.	4.613E+02
3.000E-01	1.965E+02	1.096E+02	1.920E+02	0.	4.982E+02
4.000E-01	2.424E+02	8.542E+01	2.278E+02	1.674E+01	5.556E+02
5.000E-01	2.756E+02	6.757E+01	2.688E+02	7.084E+01	6.119E+02
6.000E-01	3.021E+02	5.610E+01	3.034E+02	9.274E+01	6.616E+02
7.000E-01	3.134E+02	4.207E+01	2.880E+02	9.853E+01	6.435E+02
8.000E-01	3.054E+02	2.805E+01	2.573E+02	1.018E+02	5.908E+02
9.000E-01	2.709E+02	1.785E+01	2.214E+02	1.037E+02	5.102E+02
1.000E+00	2.410E+02	2.295E+01	1.958E+02	1.050E+02	4.598E+02
1.200E+00	1.879E+02	2.040E+01	1.683E+02	1.018E+02	3.766E+02
1.400E+00	1.640E+02	3.060E+01	1.510E+02	8.887E+01	3.456E+02
1.600E+00	1.514E+02	3.442E+01	1.395E+02	8.630E+01	3.253E+02
1.800E+00	1.467E+02	3.825E+01	1.389E+02	7.792E+01	3.239E+02
2.000E+00	1.448E+02	3.060E+01	1.459E+02	4.766E+01	3.213E+02

DEFR	PEPM	PEPT	PKM	PKT	BETA
UNITLESS	(LBS. / LIN. FT.)		(---- UNITLESS ----)		DEGREES
0.	5.553E+01	4.250E+02	1.083E+00	8.293E+00	1.915E+01
8.333E-03	3.669E+02	4.972E+02	7.158E+00	9.702E+00	1.715E+01
1.667E-02	4.639E+02	5.891E+02	9.051E+00	1.150E+01	1.585E+01
2.500E-02	5.044E+02	7.098E+02	9.842E+00	1.385E+01	1.415E+01
3.333E-02	5.680E+02	8.722E+02	1.108E+01	1.702E+01	1.275E+01
4.167E-02	6.335E+02	1.099E+03	1.236E+01	2.145E+01	1.115E+01
5.000E-02	6.956E+02	1.431E+03	1.357E+01	2.792E+01	9.800E+00
5.833E-02	6.856E+02	1.779E+03	1.338E+01	3.472E+01	8.800E+00
6.667E-02	6.339E+02	2.001E+03	1.237E+01	3.904E+01	8.000E+00
7.500E-02	5.505E+02	2.193E+03	1.074E+01	4.279E+01	7.900E+00
8.333E-02	4.985E+02	2.378E+03	9.727E+00	4.640E+01	7.500E+00
1.000E-01	4.089E+02	2.441E+03	7.978E+00	4.764E+01	7.000E+00
1.167E-01	3.752E+02	2.441E+03	7.321E+00	4.764E+01	7.000E+00
1.333E-01	3.532E+02	2.441E+03	6.891E+00	4.764E+01	7.000E+00
1.500E-01	3.516E+02	2.441E+03	6.860E+00	4.764E+01	7.000E+00
1.667E-01	3.488E+02	2.441E+03	6.805E+00	4.764E+01	7.000E+00

DEFR	DRATIO	PRATIO	CPM	ERROR
(----------	UNITLESS	---------)	INCHES	PERCENT
0.	0.	4.255E-02	3.000E+00	2.500E+01
8.333E-03	1.071E-01	8.975E-01	4.838E+00	-2.094E+01
1.667E-02	2.143E-01	9.265E-01	4.691E+00	-1.729E+01
2.500E-02	3.214E-01	9.014E-01	4.321E+00	-8.014E+00
3.333E-02	4.286E-01	8.878E-01	3.922E+00	1.938E+00
4.167E-02	5.357E-01	8.665E-01	3.663E+00	8.436E+00
5.000E-02	6.429E-01	8.414E-01	3.509E+00	1.228E+01
5.833E-02	7.207E-01	8.027E-01	3.392E+00	1.519E+01

6.667E-02	7.588E-01	7.660E-01	3.285E+00	1.788E+01
7.500E-02	7.874E-01	7.157E-01	3.210E+00	1.975E+01
8.333E-02	8.113E-01	6.789E-01	3.299E+00	1.751E+01
1.000E-01	8.179E-01	6.209E-01	3.325E+00	1.688E+01
1.167E-01	8.179E-01	5.938E-01	3.531E+00	1.172E+01
1.333E-01	8.179E-01	5.764E-01	3.635E+00	9.128E+00
1.500E-01	8.179E-01	5.745E-01	3.709E+00	7.285E+00
1.667E-01	8.179E-01	5.725E-01	3.571E+00	1.071E+01

DEFLECTION	INTERNAL FRICTION DEVELOPED	WALL FRICTION DEVELOPED
0.	2.200E+00	0.
1.000E-01	4.640E+01	3.000E+00
2.000E-01	4.790E+01	6.000E+00
3.000E-01	4.660E+01	9.000E+00
4.000E-01	4.590E+01	1.200E+01
5.000E-01	4.480E+01	1.500E+01
6.000E-01	4.350E+01	1.800E+01
7.000E-01	4.150E+01	2.018E+01
8.000E-01	3.960E+01	2.125E+01
9.000E-01	3.700E+01	2.205E+01
1.000E+00	3.510E+01	2.272E+01
1.200E+00	3.210E+01	2.290E+01
1.400E+00	3.070E+01	2.290E+01
1.600E+00	2.980E+01	2.290E+01
1.800E+00	2.970E+01	2.290E+01
2.000E+00	2.960E+01	2.290E+01

APPENDIX B

EXPERIMENTAL EXAMPLE DATA

This appendix contains representative plots of experimental data points that were obtained from the Phase III series of tests. The graphs on the following pages represent the development of horizontal forces which acted on the models as they penetrated into sand backfills. The purpose of these graphs is to qualify the average curves presented in Chapter VIII.

As stated in Chapter VIII, tests were performed using three rates of model penetration; the results indicated that for these rates of penetration no measurable difference existed. Since no additional information could be attained by presenting the results from each series of tests, only the results from the 4.0 ips series of tests have been presented in this appendix and Chapter VIII.

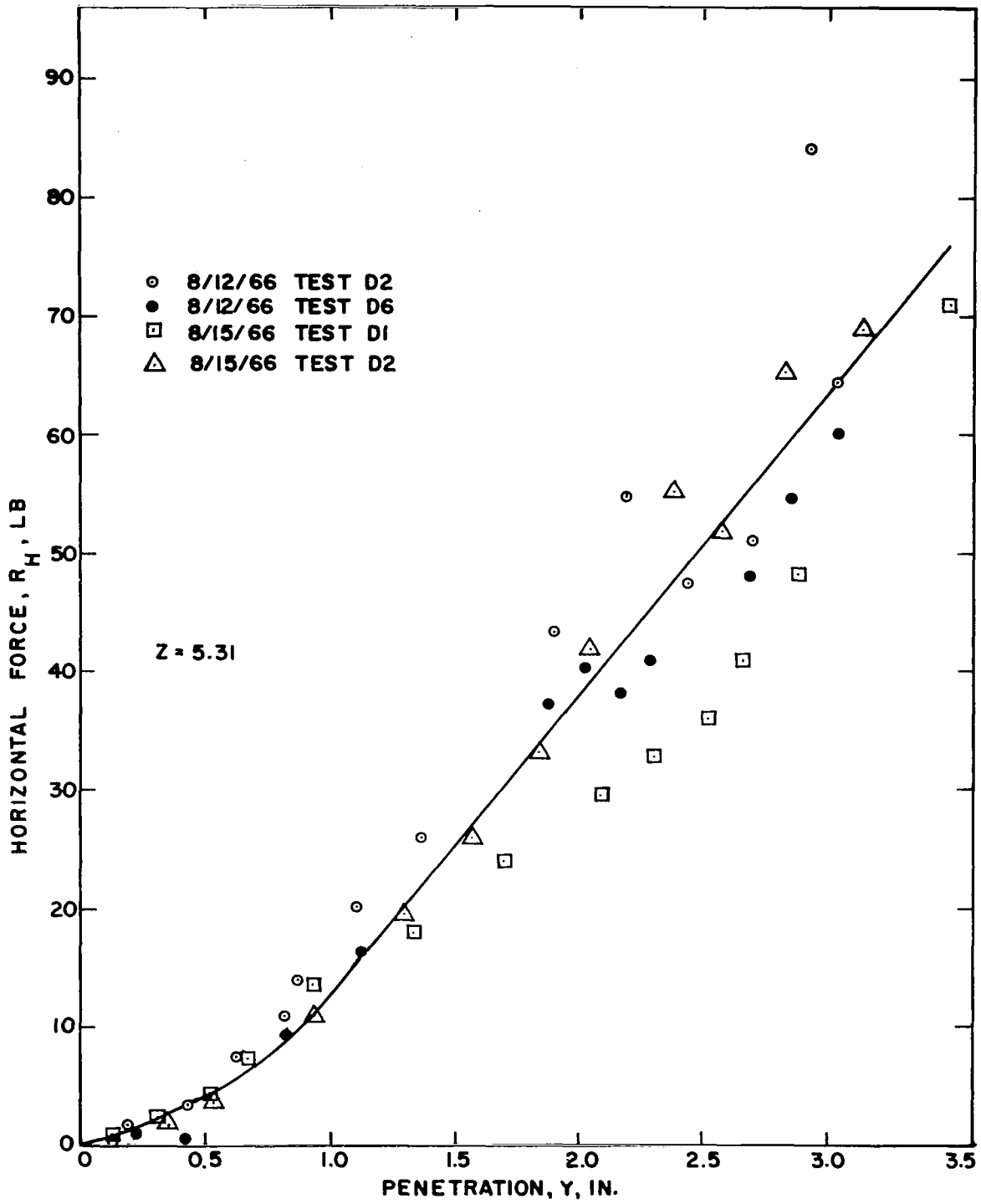

FIG.93 HORIZONTAL FORCE VERSUS PENETRATION – 3.54 IN. DIA CONE, DENSE CASE

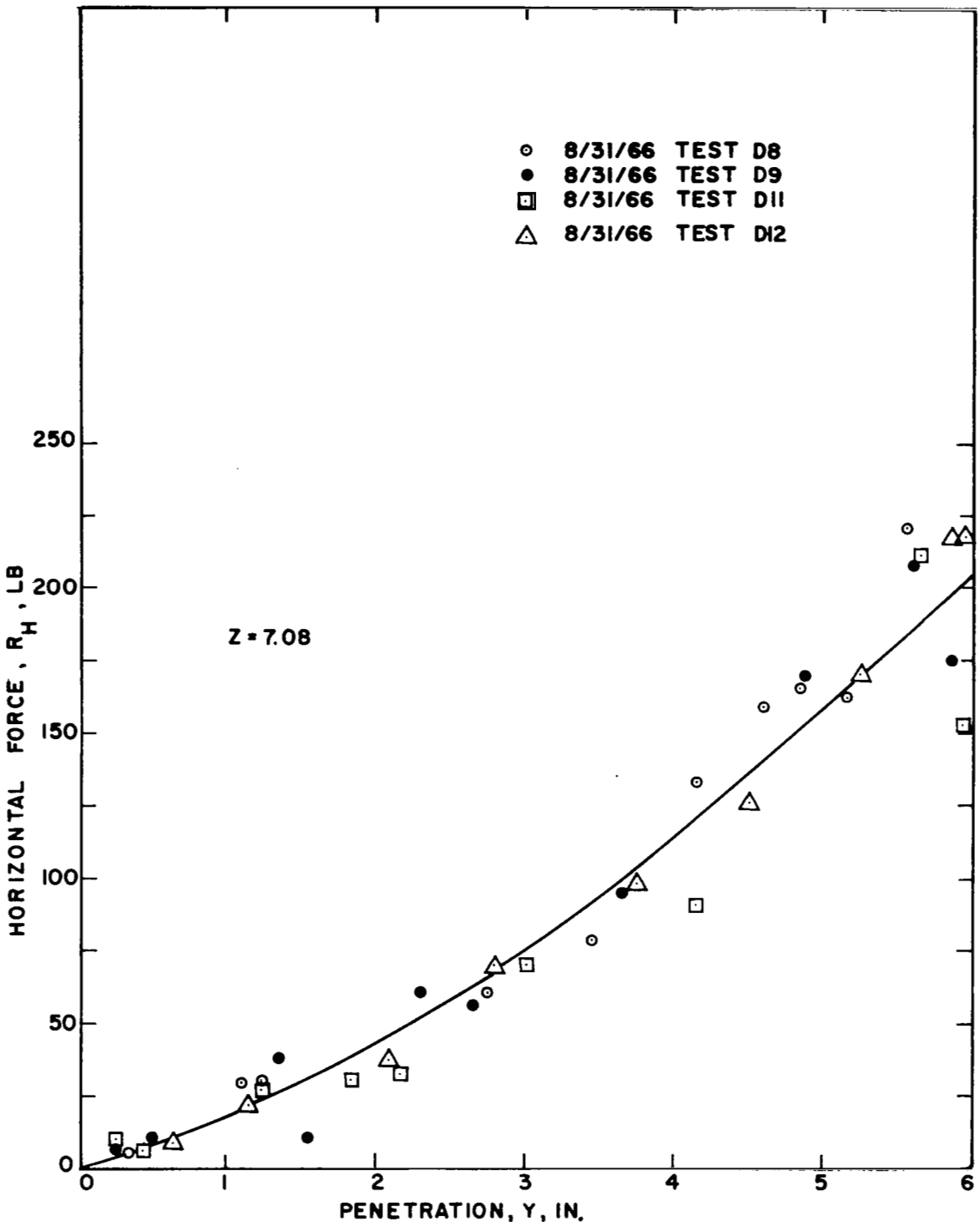

FIG.94 HORIZONTAL FORCE VERSUS PENETRATION - 7.08 IN. DIA CONE, DENSE CASE

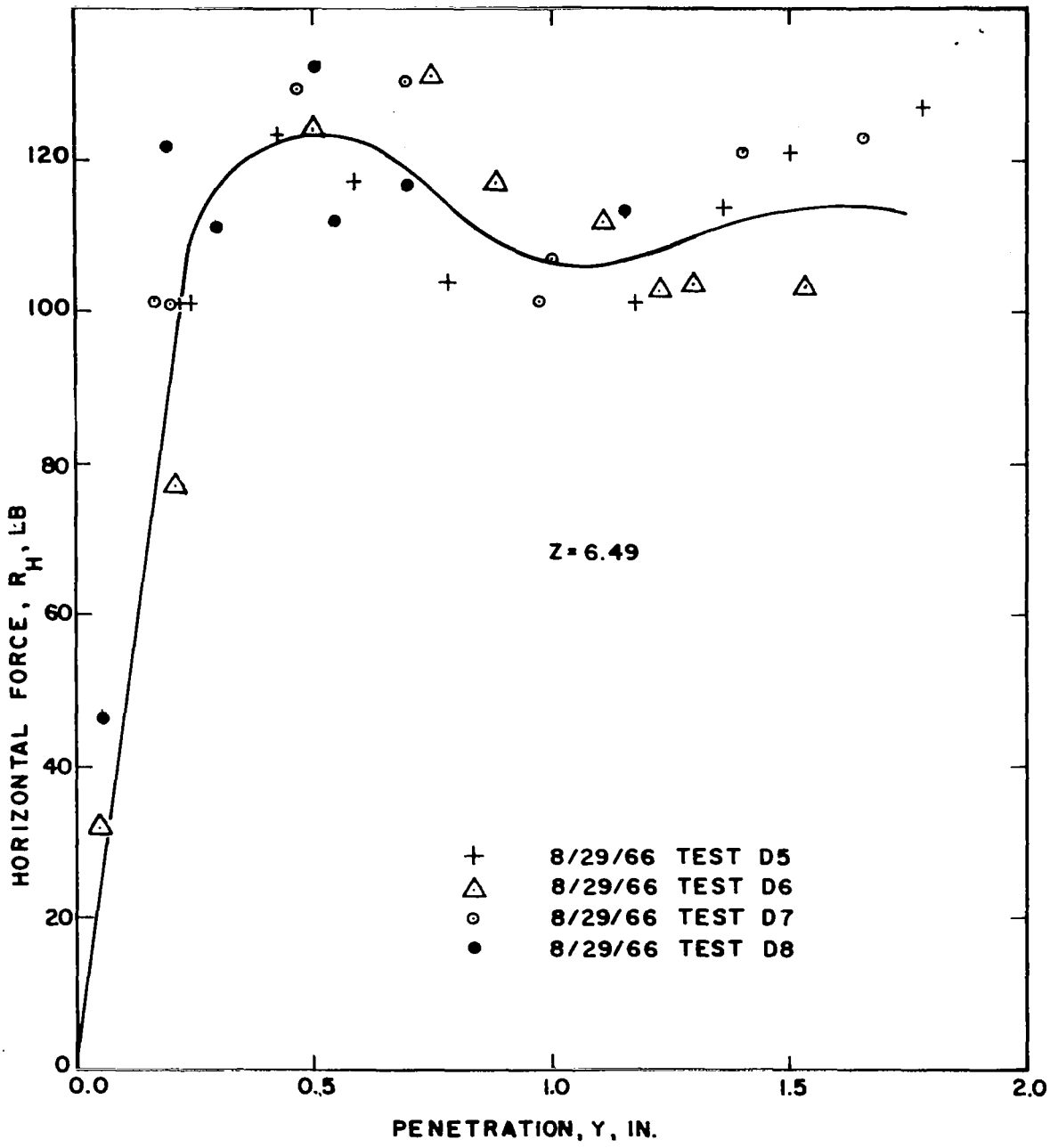

FIG. 95 HORIZONTAL FORCE VERSUS PENETRATION – 4.33 IN. DIA SPHERICAL SEGMENT, DENSE CASE

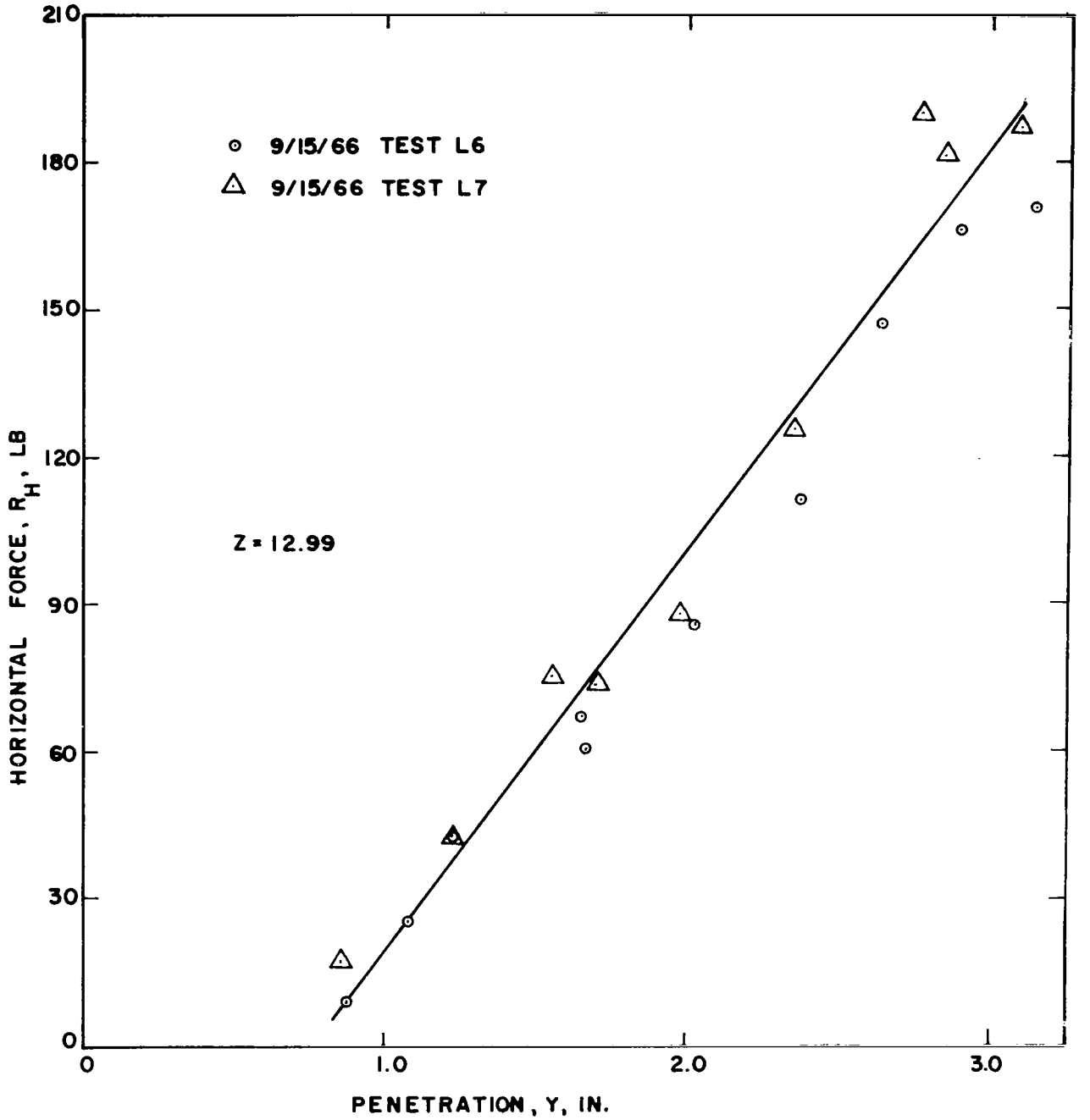

FIG. 96 HORIZONTAL FORCE VERSUS PENETRATION — 8.66 IN. DIA SPHERICAL SEGMENT, DENSE CASE

APPENDIX C

EXPERIMENTAL EXAMPLE DATA

This appendix contains representative plots of experimental data points that were obtained from the Phase III series of tests. The graphs on the following pages represent the development of resultant vertical forces which acted on the models as they penetrated into sand backfills. The purpose of these graphs is to qualify the average curves presented in Chapter VIII.

As stated in Chapter VIII, tests were performed using three rates of model penetration; the results indicated that for these rates of penetration no measurable difference existed. Since no additional information could be attained by presenting the results from each series of tests, only the results from the 4.0 ips series of tests have been presented in this appendix and Chapter VIII.

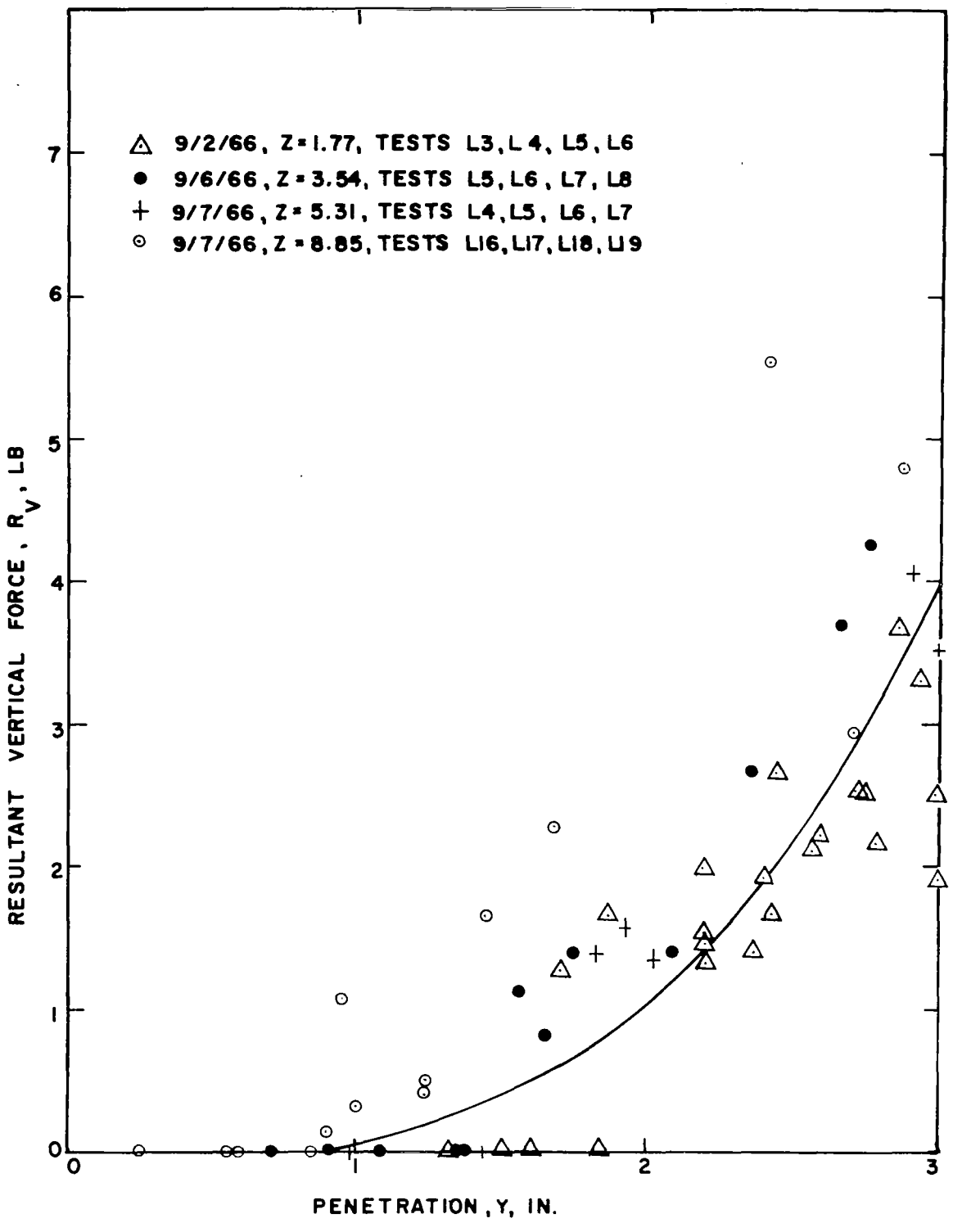

FIG. 97 RESULTANT VERTICAL FORCE VERSUS PENETRATION - 3.54 IN. DIA CONE, LOOSE CASE

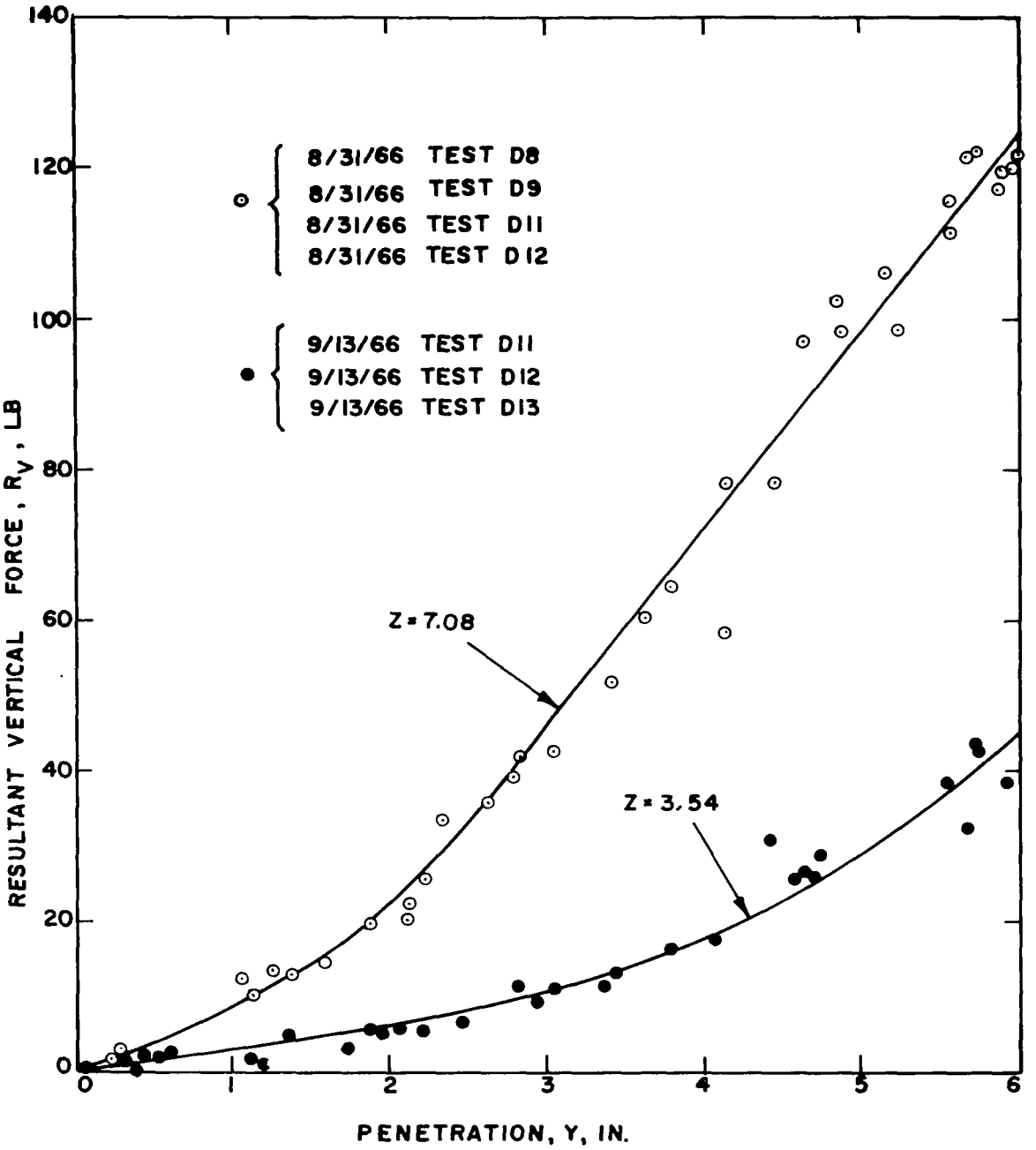

FIG. 98 RESULTANT VERTICAL FORCE VERSUS PENETRATION - 7.08 IN. DIA CONE, DENSE CASE

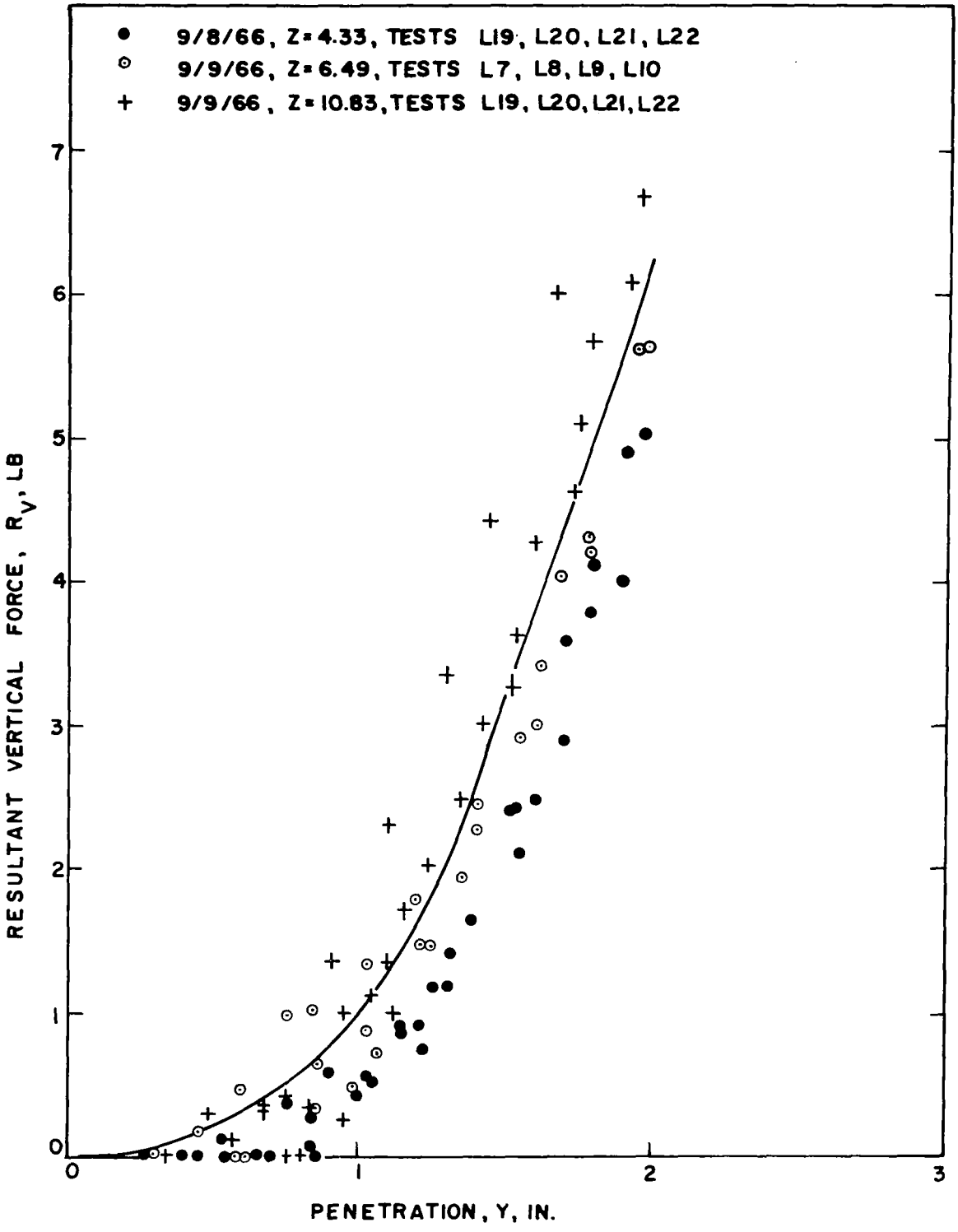

FIG. 99 RESULTANT VERTICAL FORCE VERSUS PENETRATION -4.33 IN. DIA SPHERICAL SEGMENT, LOOSE CASE

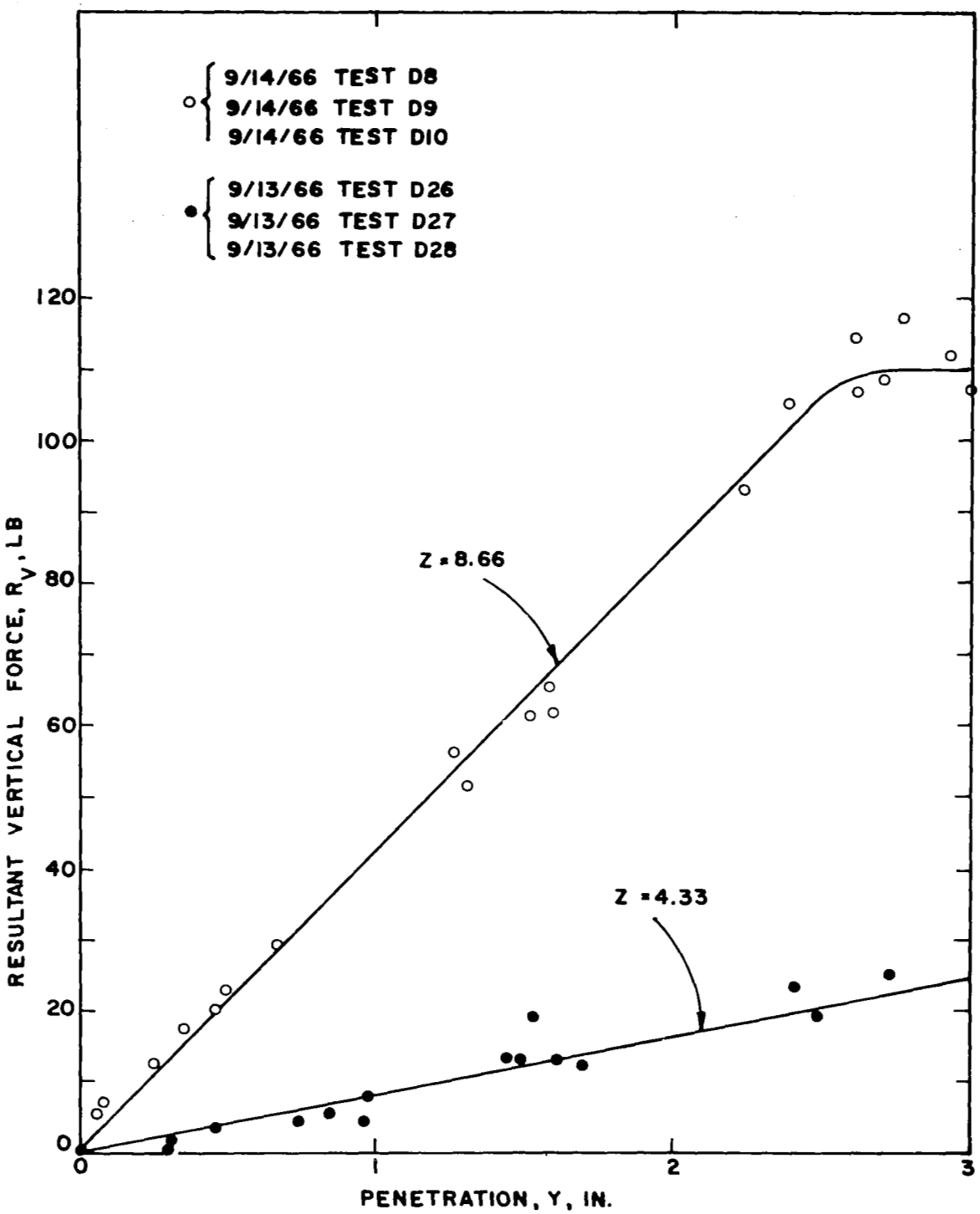

FIG. 100 RESULTANT VERTICAL FORCE VERSUS PENETRATION -8.66 IN. DIA SPHERICAL SEGMENT, DENSE CASE

REFERENCES

1. Bjerrum, L., Casagrande, A., Peck, R. B., and Skempton, A. W., From Theory to Practice in Soil Mechanics, John Wiley & Sons, Inc., New York, 1960.

2. Cornforth, D. H., "Some Experiments on the Influence of Strain Conditions on the Strength of Sand," Geotechnique, London, England, Vol. 14, No. 2, 1964, pp. 143-167.

3. Dawson, R. F., Laboratory Manual in Soil Mechanics, 2nd Ed. Pitman Publishing Co., New York, 1959, pp. 157-162.

4. Ghazzaly, O. I., and Dawson, R. F., "Laboratory Stress-Deformation Characteristics of Soils Under Static Loading," a report from Department of Civil Engineering, The University of Texas, to National Aeronautics and Space Administration, Langley Research Center, Hampton, Virginia, NASA Contractor Report CR-571, October 1966, p.42.

5. Hansen, J. B., Earth Pressure Calculation, The Danish Technical Press, Copenhagen, 1953, p. 26.

6. Rowe, P. W., "Passive Earth Pressure Measurements," Geotechnique, London, England, Vol. 15, No. 1, 1965, pp. 57-78.

7. Taylor, D. W., "A Comparison of Results of Direct Shear and Cylindrical Compression Tests," Symposium on Shear Testing of Soils, Proceedings of the American Society for Testing Materials, 1939, p. 1058.

8. Terzaghi, K., Theoretical Soil Mechanics, John Wiley & Sons, Inc., New York, 1943.

9. Terzaghi, K., "General Wedge Theory of Earth Pressure," Transactions of the American Society of Civil Engineers, Vol. 106, 1941, p. 70.

10. Terzaghi, K., "Old Earth-Pressure Theories and New Test Results," Engineering News-Record, Vol. 85, No. 14, p. 636.

11. Wu, T. H., Soil Mechanics, Allyn & Bacon, Inc., Boston, 1966, p. 277.